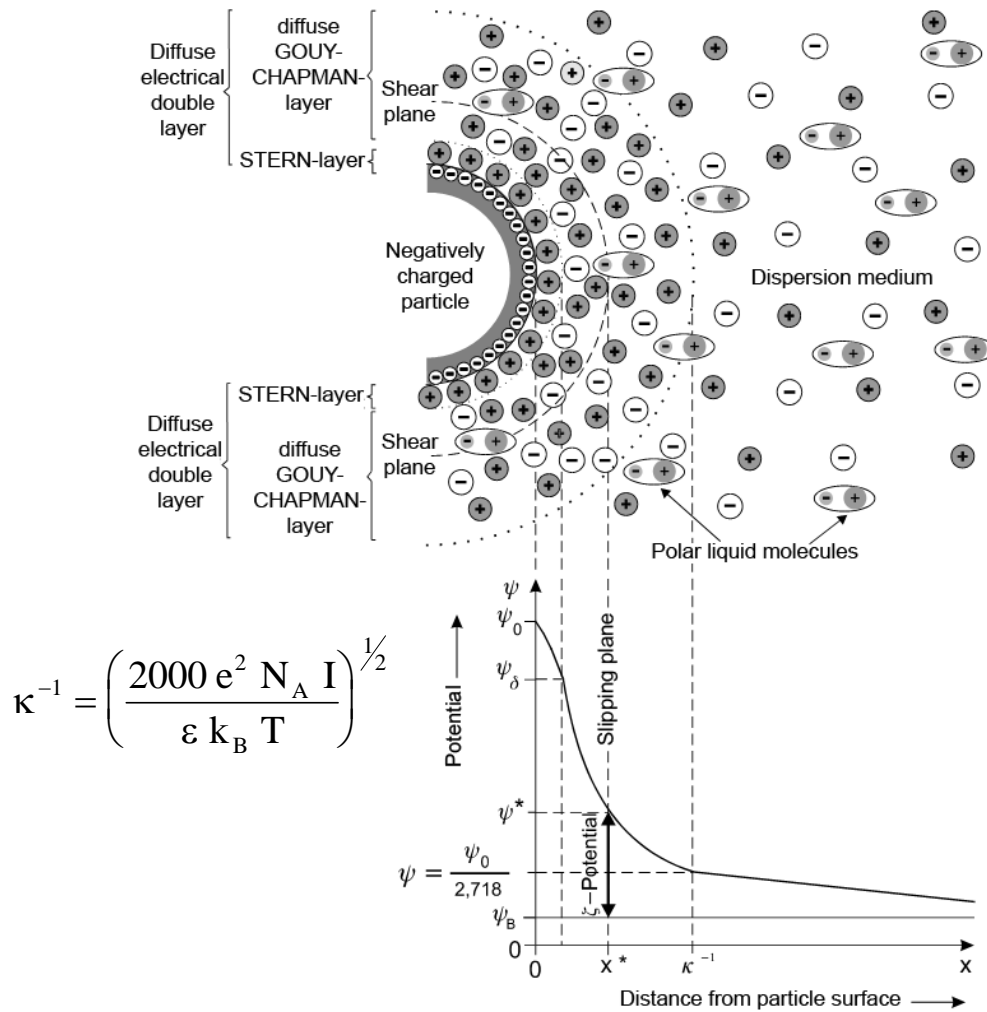


## Introduction to Ceramics Processing

Jürgen G. Heinrich  
Cynthia M. Gomes



## Authors



**Jürgen G. Heinrich** is Professor of Engineering Ceramics at the Institute of Non-metallic Materials at Clausthal University of Technology, Germany. He received a B.Sc. degree in materials engineering from the Johann Friedrich Böttger Institute in Selb, Germany, a M.Sc. and a Ph.D. in materials science both from the Technical University in Berlin, Germany. He joined the faculty of Materials Science at Clausthal University of Technology after several years of research activity at the German Aerospace Center in Cologne and at Hoechst CeramTec AG in Selb, Germany. He was president of the German and the European Ceramic Society and secretary of the International Ceramic Foundation. He is fellow of the American and the European Ceramic Society, editor of the Journal of Ceramic Science and Technology and Senior Visiting Professor of the Chinese Academy of Sciences.



**Cynthia M. Gomes** is research scientist at the BAM, Federal Institute for Materials Research and Testing in Berlin, Germany. She received her Diploma in Materials Science and Engineering from the Federal University of Paraiba, Brazil, with M.Sc. and Ph.D. in Materials Science and Engineering both from the Federal University Santa Catarina, Brazil. After working as guest visitor scientist and a two-year post doctorate at the University of Erlangen-Nuremberg she has joined the BAM. At the Division for Ceramic Processing and Biomaterials she has been working mainly in the field of additive manufacturing of ceramic materials, co-working also on national and international (DIN, ISO) groups for standardization of these technologies.

## **Acknowledgement**

For a better understanding of the theory video clips and computer animations are available in this lecture manuscript. The videos have been shot at different ceramic manufacturers and equipment as well as raw material suppliers by the cameraman of Clausthal University of Technology, Stefan Zimmer. We would like to take the opportunity to thank him for his professional work and excellent performance and the following companies for their assistance:

ARBURG GmbH & Co KG, Loßburg, Germany

BHS tabletop AG, Weiden, Germany

CeramTec GmbH, Marktredwitz, Germany

Engineered Pressure Systems International N.V.

Oost-Vlaanderen, Belgium

Imerys Tableware GmbH, Tirschenreuth, Germany

Riedhammer GmbH, Nürnberg, Germany

Rosenthal GmbH, Selb, Germany

SGL Carbon GmbH, Meitingen, Germany

## **Notes**

*For an optimum presentation of the PDF-file please use the current Adobe Reader version:  
[www.adobe.com/products/reader.html](http://www.adobe.com/products/reader.html)*

*The videoclip are available in different formats (mov, avi and mp4). To watch the videos the Adobe Flash Player ([www.adobe.com/support/flashplayer/downloads.html](http://www.adobe.com/support/flashplayer/downloads.html)) is an appropriate player for the most operating systems. If you cannot open the videos in the lecture manuscript please find them at [video.tu-clausthal.de/film/435.html](http://video.tu-clausthal.de/film/435.html)*

# Contents

<b>1. Introduction</b>	<b>3</b>
<b>2. Raw materials</b>	<b>14</b>
2.1 Structure of the earth	14
2.2 Deposits	24
2.3 Natural ceramic raw materials	31
2.3.1 Kaolins and clays	31
2.3.2 Feldspars	37
2.3.3 Quartzites and sands	39
2.3.4 Binary and ternary silicates, high alumina containing raw materials	44
2.4 Synthetic ceramics raw materials	48
2.4.1 Silicates	48
2.4.2 Oxides	51
2.4.3 Non-oxide materials	54
2.5 Organic raw materials	56
2.6 Raw material preparation	67
<b>3. Body preparation</b>	<b>80</b>
3.1 Grain size modification	80
3.2 Classification	93
<b>4. Forming</b>	<b>100</b>
4.1 Introduction	100
4.2 General principles	100
4.2.1 Characterisation of suspensions	101
4.2.1.1 Particle charging in liquid suspensions	101
4.2.1.2 Electrical double layers on particle surfaces	105
4.2.1.3 Electrokinetic properties and slip stability	107
4.2.1.4 Rheological properties of ceramic suspensions	113
4.2.2 Plasticity of ceramic systems	118
4.2.3 Granulation	122
4.2.3.1 Production of granules	123
4.2.3.2 Characterization of granules	129

4.3	Forming .....	132
4.3.1	Casting processes .....	134
4.3.1.1	Slip casting 美 .....	134
4.3.1.2	Pressure casting .....	137
4.3.1.3	Tape casting 美 .....	139
4.3.2	Plastic deformation forming .....	148
4.3.2.1	Roller tool forming ... 美 .....	148
4.3.2.2	Extrusion 美 .....	150
4.3.2.3	Injection molding ... 美 .....	154
4.3.3	Pressing .....	162
4.3.3.1	Uniaxial dry pressing 美 .....	162
4.3.3.2	Isostatic Pressing 美 美 美 .....	166
4.3.4	New developments 美 .....	169
4.4	Literature list of chapter "Forming" .....	174
<b>5.</b>	<b>Thermal processes .....</b>	<b>180</b>
5.1	Drying .....	180
5.2	Sintering .....	186
5.2.1	Sintering of porcelain, silicate and oxide ceramics 美 美 美 .....	186
5.2.2	Sintering of non-oxide ceramics 美 .....	195
5.2.3	Pressure sintering .....	197
5.2.4	Microwave sintering .....	198
<b>6.</b>	<b>Finishing and post processing .....</b>	<b>201</b>
6.1	Glazing 美 .....	201
6.2	Decoration .....	210
<b>7.</b>	<b>Special technologies .....</b>	<b>214</b>
7.1	Porcelain production .....	214
7.2	Brick production .....	216
7.3	SiC production .....	216
7.4	Piezoceramics production .....	217
7.5	Laser sintering 美 .....	218
<b>8.</b>	<b>Literature .....</b>	<b>219</b>

## 1. Introduction

The term „Ceramics Processing“ describes the process of production of ceramic components from natural to synthetic raw materials as well as their disposal.

Contrary to metals, polymers or glasses, the starting materials for the production of ceramic materials are powders. These powders are brought into shape and the components then are sintered which is a temperature treatment clearly below the melting point. This technique is applied because of the high melting points of ceramic materials which make casting impossible or uneconomical. The starting material can be of oxidic or non-oxidic nature; some care must be taken in order not to sinter both types of materials in the same furnace. Example: silicon nitride would incinerate or combust if sintered in an oxidizing atmosphere. Therefore, furnace technology for non-oxidic materials must be different from the one for oxidic starting materials. This is the reason why this lecture “Ceramics Processing” can only give an overview of the most important materials. The variety of technological procedures is so large that it is not possible to describe everything in detail.

Classification of the most important material groups distinguishes between natural and synthetic materials. Natural raw materials are extracted from earth, and these raw materials must be further processed. They are blast in quarries, i.e., pieces of rock are exploited and worked up to powders (materials) (Fig. 1.1). From these materials pre-products are produced by forming or shaping. Metal components can be formed during the process of reshaping whereas ceramic components can be produced only by a sintering process. The product in later time has to be disposed by recycling or remineralisation.

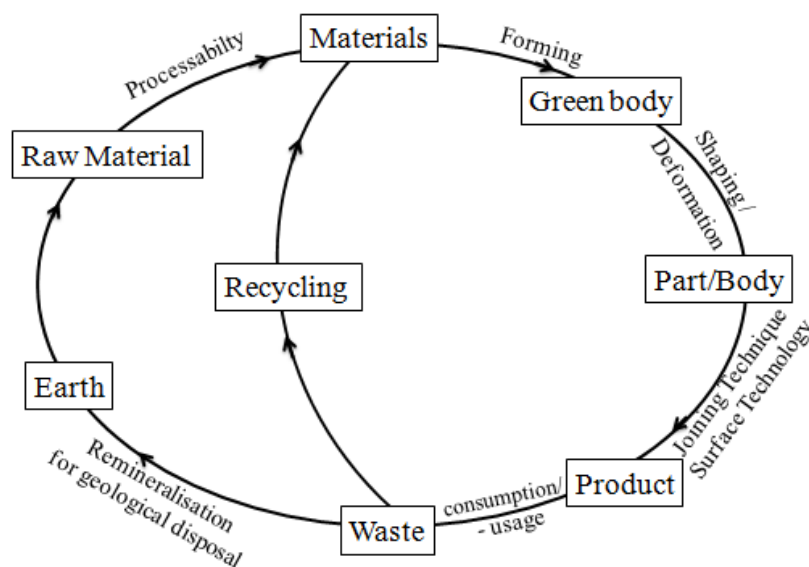


Fig. 1.1: Cycle of materials by Ondracek.

Synthetic materials are classified into non-metallic materials, semiconductors and metallic materials (Fig. 1.2). Non-metallic materials are non-conductors, or insulating materials. Metallic materials have a very high electric conductivity; in semiconductors the electric conductivity can be found in between. Non-metallic materials are divided into inorganic and organic materials. Oxide and non-oxide ceramics as well as glass belong to the group of inorganic materials.

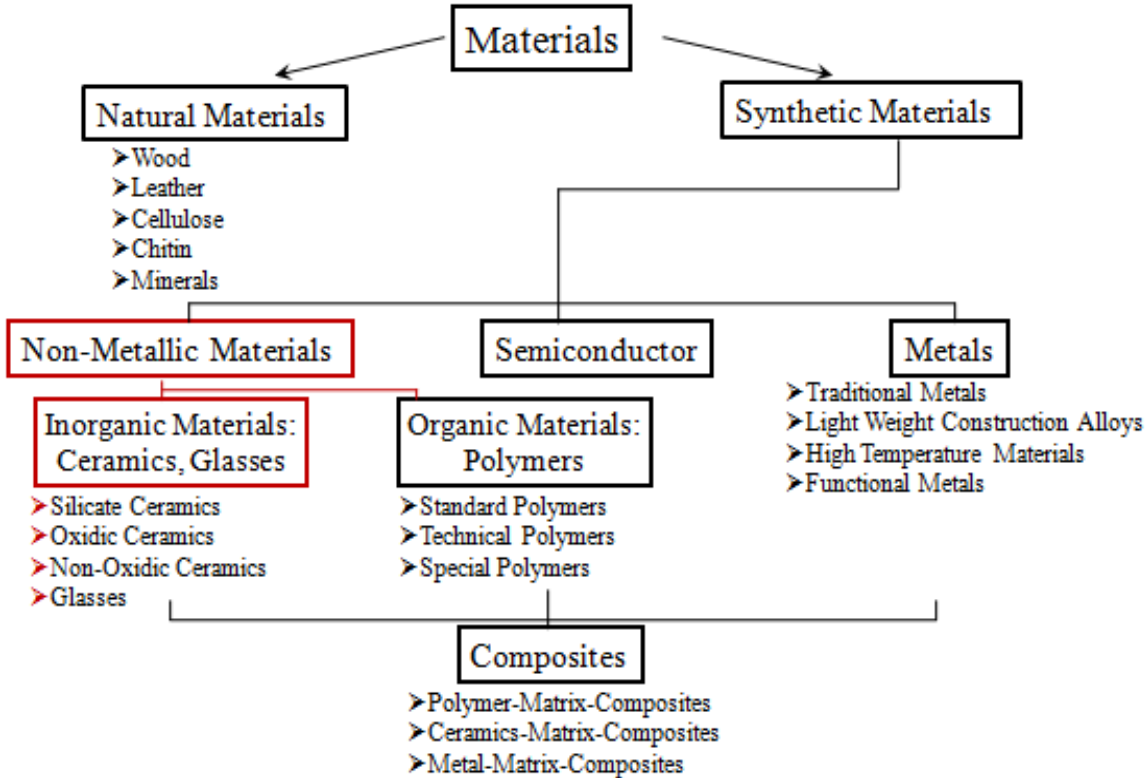


Fig. 1.2: Classification of the main material groups.

To modify their characteristics ceramic materials are often treated together with organic or metallic materials, originating the category of composite materials. From the chemical point of view, ceramic materials can be divided into oxides and non-oxides (Fig.1.3). Oxidic ceramics can be made of natural or synthetic raw materials.

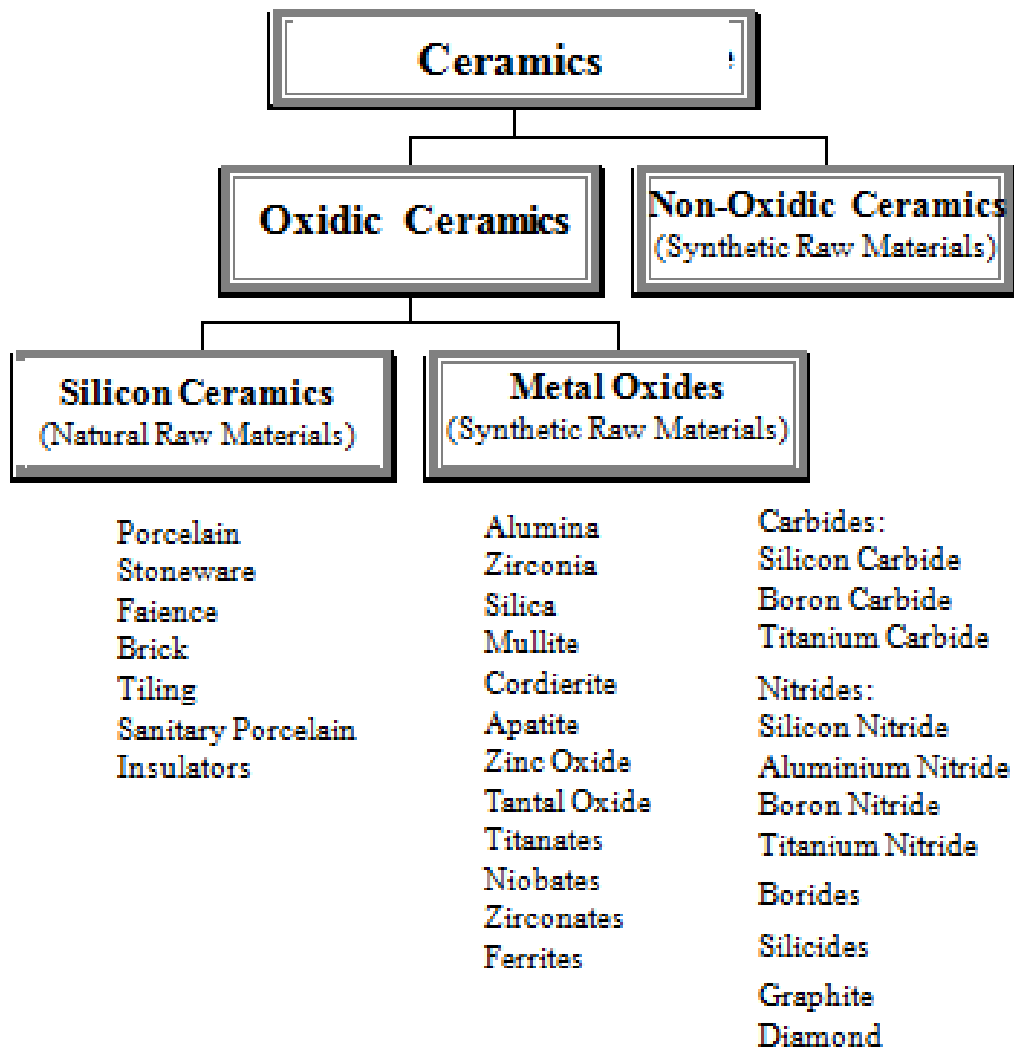


Fig. 1.3: Classification of ceramic materials.

Non-oxide ceramic materials also made of synthetic raw materials are classified into carbides, nitrides, borides, silicides. The complete group of metal oxides within the periodic system belongs to ceramic materials, mostly made from synthetic raw materials. Silicates are made from natural raw materials. In particular within industry, another classification has been established which will be discussed on the next topics.



Silicates are often divided into coarse clay ceramics and fine ceramics, subdivided into their constituents (>1 mm coarse clay ceramics, <1 mm fine ceramics). Further distinction is made between porous and dense materials and, depending on the degree of purity of the raw materials, for example brightly burning porcelain (almost white) and coloured materials such as tiles and bricks (Fig 1.4).

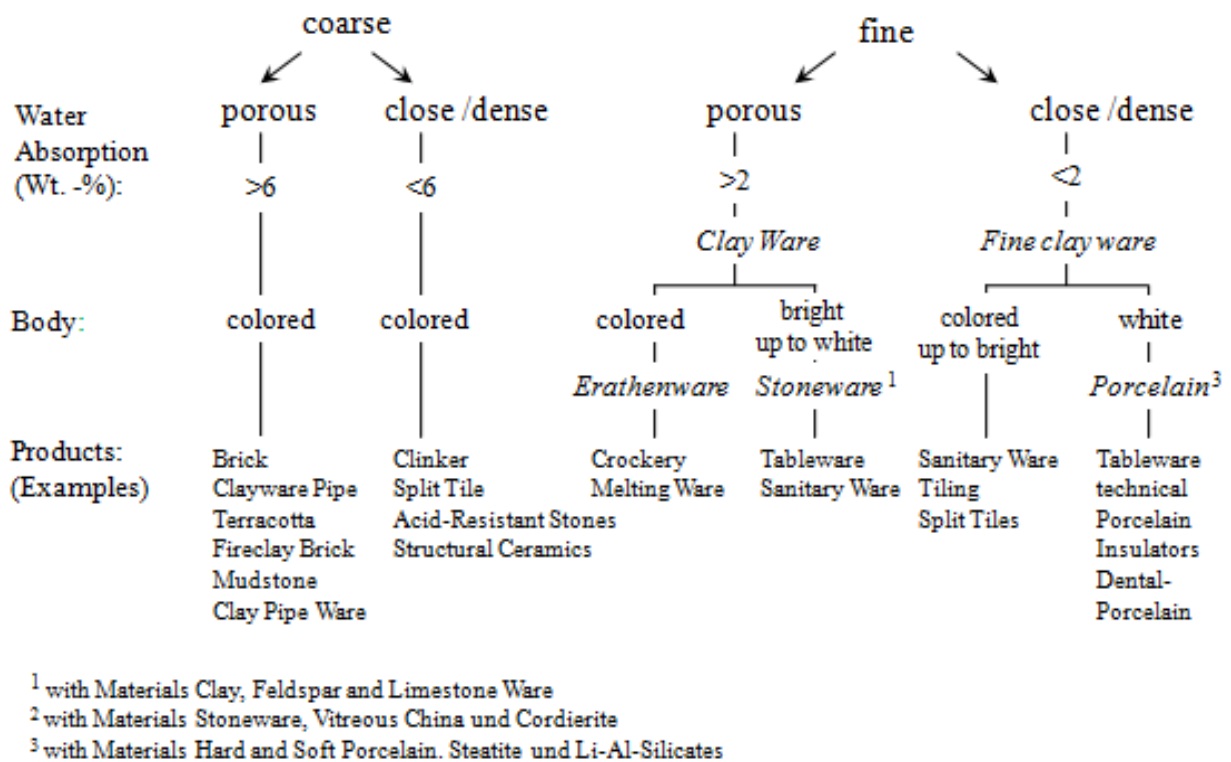
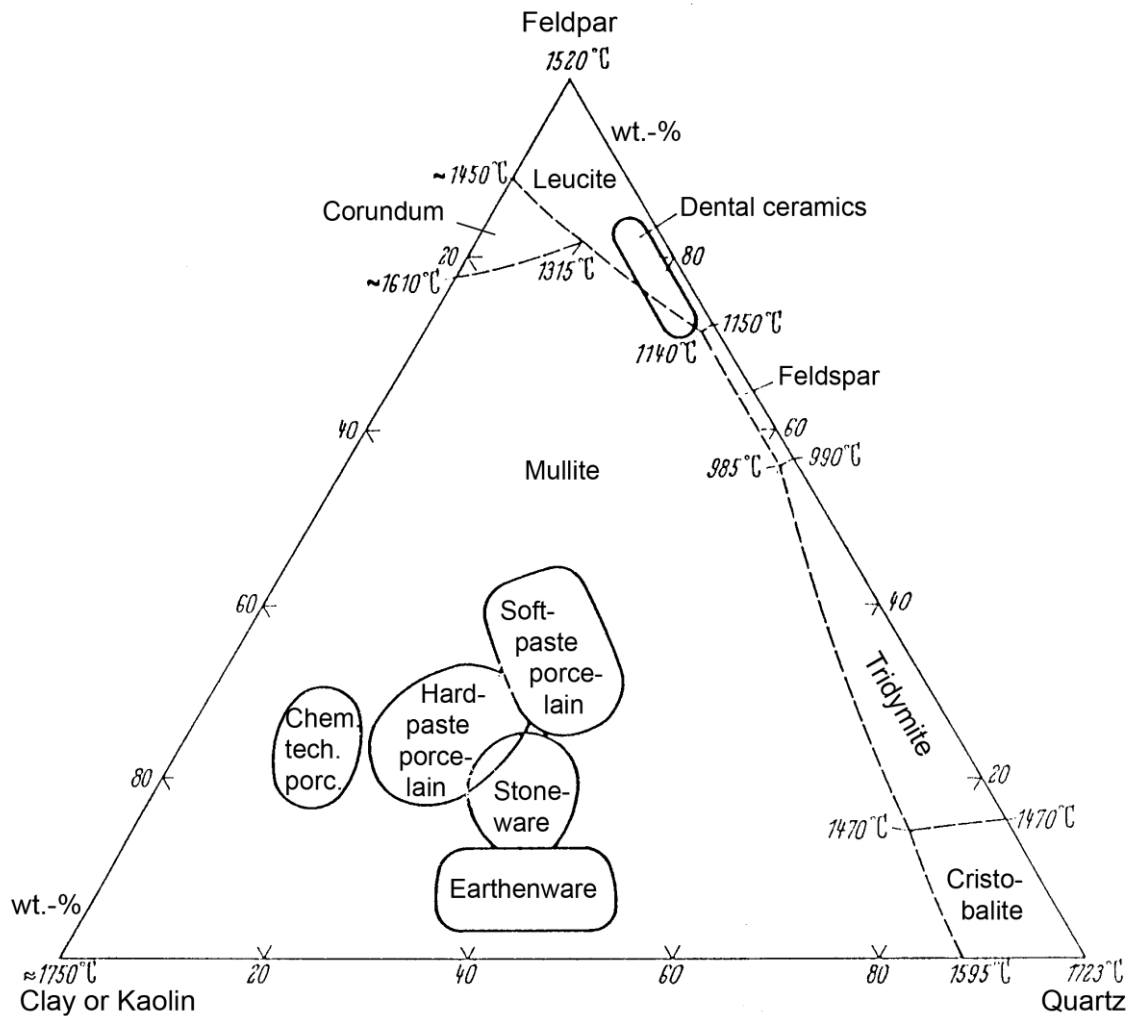


Fig. 1.4: Classification of ceramic materials [1].

Another overview of silicates can be seen from the ternary phase diagram of clay or kaolin, quartz and feldspar (Fig. 1.5). Porcelain is a mixture of kaolin, feldspar and quartz. It is situated approximately in the middle of this diagram. Stoneware and earthenware can also be found here. So, it must have be taken into consideration that a wide range of materials with different technological production processes, therefore various procedures, from the starting powder to the final product is necessary.



**Fig. 1.5:** Diagram with different ceramic compositions from the system clay or caolin-feldspar-quartz in dependence of the temperature [1].

Fig. 1.6 elucidates the reason why ceramic materials are made of powders, which after shaping must undergo a sintering process to achieve the final properties and, unlike metallic materials, cannot be molten and cast in a mould. This is mainly due to the high melting temperatures of these materials, often above 2000°C. Technologically, it is extremely difficult to produce molten masses at such high temperatures and cast them into suitable containers. In Fig. 1.6 another difference of the ceramics with regard to metals can be seen. Due to the nature of the covalent or ionic bonds in the ceramic materials, their electron conductivity is quasi equal to zero. Ionic conductivity is extremely low respectively the specific electric resistance is very high.

Oxide	Density g/cm <sup>3</sup>	Melting Point °C	Resistivity @	
			225 °C	1000 °C
BeO	3,01	2570	10 <sup>14</sup>	10 <sup>8</sup>
MgO	3,57	2840	10 <sup>14</sup>	10 <sup>7</sup>
CaO	3,32	2580	10 <sup>14</sup>	10 <sup>6</sup>
Al <sub>2</sub> O <sub>3</sub>	3,99	2050	10 <sup>14</sup>	10 <sup>8</sup>
Y <sub>2</sub> O <sub>3</sub>	4,50	2450	---	---
ZrO <sub>2</sub>	5,56 mon. 6,10 tetr.	2680	10 <sup>11a</sup>	10 <sup>a</sup>
HfO <sub>2</sub>	9,68 mon. 10,0 tetr.	2900	---	---
ThO <sub>2</sub>	10,05	3220	10 <sup>14</sup>	10 <sup>5</sup>

Fig. 1.6: Properties of high-melting oxides [1].

Uranium compounds with their high density also belong to the ceramic materials (Fig. 1.7). Here again, a particular technology, for example for the production of nuclear fuel rods is required.

Compound	Melting Point	Density	Uranium Density	Thermal Conductivity at
	°C	g/cm <sup>3</sup>	g Uranium/cm <sup>3</sup>	500 °C W/(m ·K)
U	1132	19,05	19,05	42
UO <sub>2</sub>	2800	10,97	9,67	3
UC	2390	13,63	12,97	23
UN	2850 (2,3 bar N <sub>2</sub> )	14,32	13,52	21

Fig. 1.7: Properties of some Uranium compounds [1].

Refractories are another material group (Fig. 1.8). Mixed oxides of silicon oxide, alumina, chromium oxide and magnesium oxide are part of this group as well as refractory bricks and chrome-magnesia stones. Refractories present a very high temperature resistivity and a very good corrosion resistance and are used in steel, binder or glass industry for kiln lining, thermal insulators.

Stone Type	$t_a$ -Point
Fireclay Brick	1300 – 1550 °C
Chrome-Magnesia Stone	> 1550 °C
Chromite Stone	> 1600 °C
Zirconium Silicate Stone	> 1600 °C
Corundum Brick	1600 – 1750 °C
Silica Brick	> 1660 °C
Chrome-Magnesia High-Fired Stone	> 1700 °C
Dolomite Brick	> 1700 °C
Mullite Stone	> 1750 °C
Magnesia Brick (low iron and C <sub>2</sub> S-bounded)	> 1750 °C
Zirconia Stone	> 1750 °C

Fig.1.8: Softening temperature of some refractories under load [1].

Non-oxidic ceramic materials (Fig. 1.9) have extremely high melting temperatures (over 3000°C) and a very low density. Today, these materials are used for machinery construction or electronics, for example, when the emphasis is to achieve low thermal conductivity and low specific weight. Movable and abrasion-resistant components are increasingly applied for automobile fabrication or aerospace industry where high temperature-resistant materials with low specific weight and therefore low inertia masses are needed.

Substance		Crystal System	Melting Point °C	Density at 20 °C g/cm <sup>3</sup>	Resistivity bei 20 °C Ω·cm
Carbon	Diamond	cubic	3800 <sup>a</sup>	3,52	10 <sup>12</sup>
	Graphite	hexagonal	3800 <sup>a</sup>	2,26	0,5 · 10 <sup>-4</sup> ; 1 <sup>h</sup>
Carbides	Be <sub>2</sub> C	cubic	2150	2,26	10 <sup>-3</sup>
	B <sub>4</sub> C	rhombohedral	2450	2,52	400
	SiC	hexagonal	2300 <sup>a</sup>	3,21	>5
	TiC	cubic	3140	4,93	7 · 10 <sup>-5</sup>
	ZrC	cubic	3420	6,6	6 · 10 <sup>-5</sup>
	HfC	cubic	3890	12,3	4 · 10 <sup>-5</sup>
	TaC	cubic	3880	14,5	3 · 10 <sup>-5</sup>
	WC	hexagonal	2780	15,7	2 · 10 <sup>-5</sup>
Nitrides	BN	hexagonal	3000 <sup>a</sup>	2,25	10 <sup>9</sup>
	AlN	hexagonal	2300 <sup>a</sup>	3,25	10 <sup>5</sup>
	Si <sub>3</sub> N <sub>4</sub>	hexagonal	1900 <sup>a</sup>	3,2	10 <sup>12</sup>
	TiN	cubic	2950	5,4	3 · 10 <sup>-5</sup>
	ZrN		2980	7,3	2 · 10 <sup>-5</sup>
Borides	TiB <sub>2</sub>	hexagonal	2900	4,5	10 <sup>-5</sup>
	ZrB <sub>2</sub>	hexagonal	2990	6,1	10 <sup>-5</sup>
Silicides	MoSi <sub>2</sub>	tetragonal	2030	6,2	2 · 10 <sup>-5</sup>
	Ti <sub>3</sub> Si <sub>3</sub>	hexagonal	2120	4,3	5 · 10 <sup>-5</sup>
Sulfides	BaS	cubic	>2200	4,3	10 <sup>6</sup>
	CeS	cubic	2450	5,9	6 · 10 <sup>-5</sup>
	ThS	cubic	>2200	9,5	2 · 10 <sup>-5</sup>
Fluorides	CaF <sub>2</sub>	cubic	1360	3,18	> 10 <sup>15</sup>

a) sublimation

Fig. 1.9: Properties of some non-oxidic substances [1].

Fig. 1.9 presents some materials which are not classified among ceramics, for example, titanium carbide, zirconium carbide, and titanium nitride or zirconium boride. Despite the fact they are produced like ceramics, they show metallic bonds, which means electron conductivity.

Composite materials with different matrixes and reinforcement components have been developed in order to combine the advantages of the different material categories (Fig.1.10).

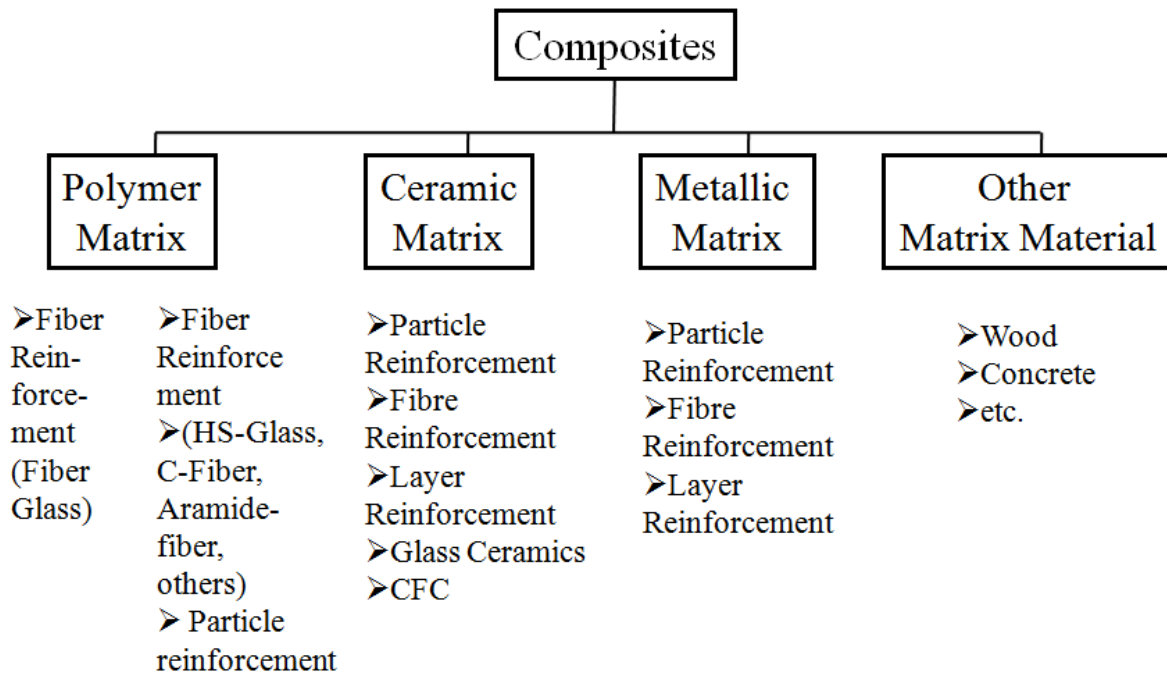


Fig. 1.10: Classification of composites.

This variety of materials requires various production technologies. Using the example of a carbon brake disc assembled in some classy cars, the following video clip shows how complex production technology may be.

*Videoclip: Processing of carbon brake discs*

Carbon fibres mixed with carbon powder and organic additives are the starting material for the production of ceramic brake disks. This fibre-powder-mixture is first put into shape. The shaping procedure used here is called uniaxial dry pressing. It is difficult to automate processing of fibre materials, therefore production is mostly manually: A plastic model is placed into the mould. This will be later burned out; the plastic model geometry then generates the cooling channels for the brake disk. Uniaxial pressing is made at slightly increased temperatures in order to liquefy the polymer material and facilitate consolidation. This almost manual production process makes also clear why brake disks have such a high price. A set for the Porsche Carrera costs about 7,500 Euro. The organic additives have to be burned out after mould release. This is made in an inert gas atmosphere where the plastic materials are cracked and the carbon relicts remain in the structure.

Burning out of the organic additives has to be made very carefully so that no cracks are formed, because it is related to volume expansion. Gas feeding and gas evacuation must be extremely well-controlled in order to keep atmosphere constant. After this, the carbon brake disk presents a machineable state – like e.g. graphite. However, it is porous and has not yet the resistance needed for use in a car.

This condition is perfect for conventional treatment like boring a hole, cutting, combining the cooling channels. After this green machining the carbon disk is infiltrated with silicon (element). For this purpose, the disks lying on Si powder are put into a vacuum furnace. Temperature is set above the silicon's melting point – to about 1,500°C, when silicon enters the pore channels. Part of the silicon reacts with the carbon to build SiC; part of it remains as silicon. So the brake disk consists of carbon fibre, silicon carbide and free silicon.

The technological processes of porcelain production or fabrication of alumina substrates for electronics are different. Therefore it will not be possible to describe in this lecture every procedural step, but the most important procedures in ceramic production can be demonstrated.

This brings us to this lecture's outline:

We will first take a look on natural raw materials, later on synthetic and organic materials needed for shaping. The structure of earth elements and deposits will be discussed in the context with natural raw materials.

Ceramic raw materials have to be prepared for further processing. When quarried out from a mine they often appear as pieces of rocks. These have to be milled to a desirable grain size. We will talk about this in chapter "Processing of raw materials". After milling, separating and fractionating the raw materials get normally mixed into masses which are no longer subject to natural fluctuations, but show uniquely defined profile properties.

Once the raw materials or masses are accordingly prepared, this must be shaped. 95 % of the ceramic powders get in contact with water during shaping. As a start, we will therefore concentrate on basic theories, dedicating to the question what happens if powder is dispersed in water. What happens on the particles' surface and how can we modify this surface? The intention is reduction of the water content of such suspensions (ceramicists call it slurry), because the water has to be removed before sintering starts, and every kilogram of water which has to be evaporated, costs money.

We will then discuss different forming technologies and differentiate, in particular, fluid, malleable and dry procedures.

Shape forming will be followed by thermal treatment. Water is evaporated during the drying process; furthermore organic additives will be burned out. The following sintering process is related to a treatment temperature below their melting temperature. We will first talk about theoretical basics and then specifically about the silicate ceramic's firing, about sintering of oxide and non-oxide ceramic materials and sintering at elevated pressure.

At the end of this lecture we will discuss finishing processes and further treatment of ceramic materials. With regard to silicate ceramic materials (e.g. porcelain) this means glazing and decoration. As for technical ceramic materials cutting, polishing or coating is concerned. At the end of these lectures I will once again pick up some typical examples regarding this variety of particular technologies and compare procedures at porcelain and brick factories or the production of piezoceramics and silicon carbide.



## 2. Raw materials

### 2.1 Structure of the earth

We first have to learn where the rocks come from which are the basis of ceramic raw materials. Then we can understand why these raw materials' chemical composition is fluctuating and what we can do to stop those fluctuations during preparation.

Fig. 2.1.1 shows schematically the sectional view through the terrestrial body. The inner section consists of an iron-nickel core with a radius of 3,500 km. This section is called barysphere with a specific weight of  $9.6 \text{ g/cm}^3$ . The oxide-sulphide interlayer has a thickness of 1,700 km. We call this layer chalkosphere with a specific weight of  $6.4 \text{ g/cm}^3$ . Lithosphere has a thickness of 1,200 km with a specific weight of  $3.4 \text{ g/cm}^3$ . The crust of the earth with just a few kilometres thickness has a specific weight of  $2.7 \text{ g/cm}^3$ .

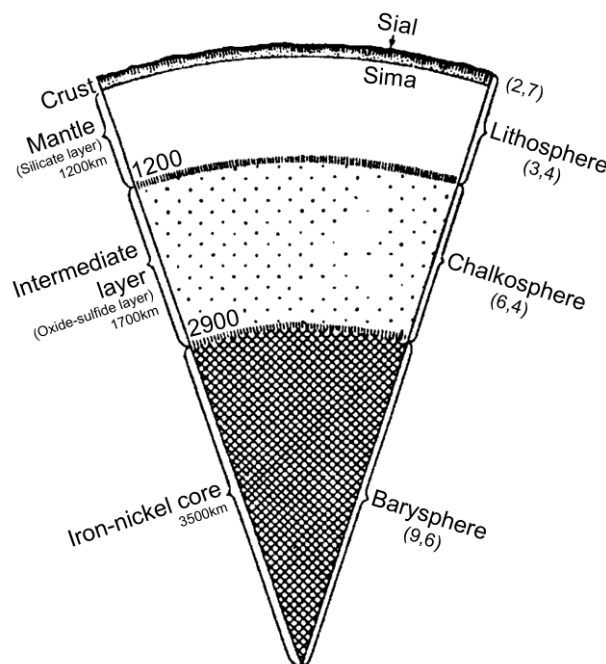


Fig. 2.1.1: Schematic cross section through earth by Suess-Wiechert [2].

The chemical composition of this earth crust (Fig. 2.1.2) is important for the raw materials' chemical composition. The earth crust consists mostly of oxides. The most important ones are  $\text{SiO}_2$  and  $\text{Al}_2\text{O}_3$ . Iron oxide is often regarded as a contamination in the raw materials, which are commonly undesired once it gives the end product a strong red colour. Magnesium oxide, calcium oxide, sodium and potassium oxides are other important components in natural raw materials used for the preparation of ceramic products.

SiO <sub>2</sub>	59,07	CO <sub>2</sub>	0,35	V <sub>2</sub> O <sub>5</sub>	0,03
Al <sub>2</sub> O <sub>3</sub>	15,22	TiO <sub>2</sub>	1,03	MnO	0,11
Fe <sub>2</sub> O <sub>3</sub>	3,10	ZrO <sub>2</sub>	0,04	NiO	0,03
FeO	3,71	P <sub>2</sub> O <sub>5</sub>	0,30	BaO	0,05
MgO	3,45	Cl	0,05	SrO	0,02
CaO	5,10	F	0,03	Li <sub>2</sub> O	0,01
Na <sub>2</sub> O	3,71	S	0,06	Cu	0,01
K <sub>2</sub> O	3,11	(Ce, Y) <sub>2</sub> O <sub>3</sub>	0,02	C	0,04
H <sub>2</sub> O	1,30	Cr <sub>2</sub> O <sub>3</sub>	0,05		

Fig. 2.1.2: Average Chemical Composition of Earth Crust up to 16 km Depth from Barth, Correns, Eskola [2].

The interior of the earth consists of liquid magma. When it approaches the surface of the earth the magma solidifies. Igneous rocks have a so-called calcium-alkaline line and the so-called sodium and potassium alkaline earth lines. With regard to slow solidification we talk about plutonic rocks, such as granite. If magma erupts from a volcano and solidifies very quickly, we talk, for example, about quartz porphyries, basalt or diabase, according to their chemical composition (Fig. 2.1.3).

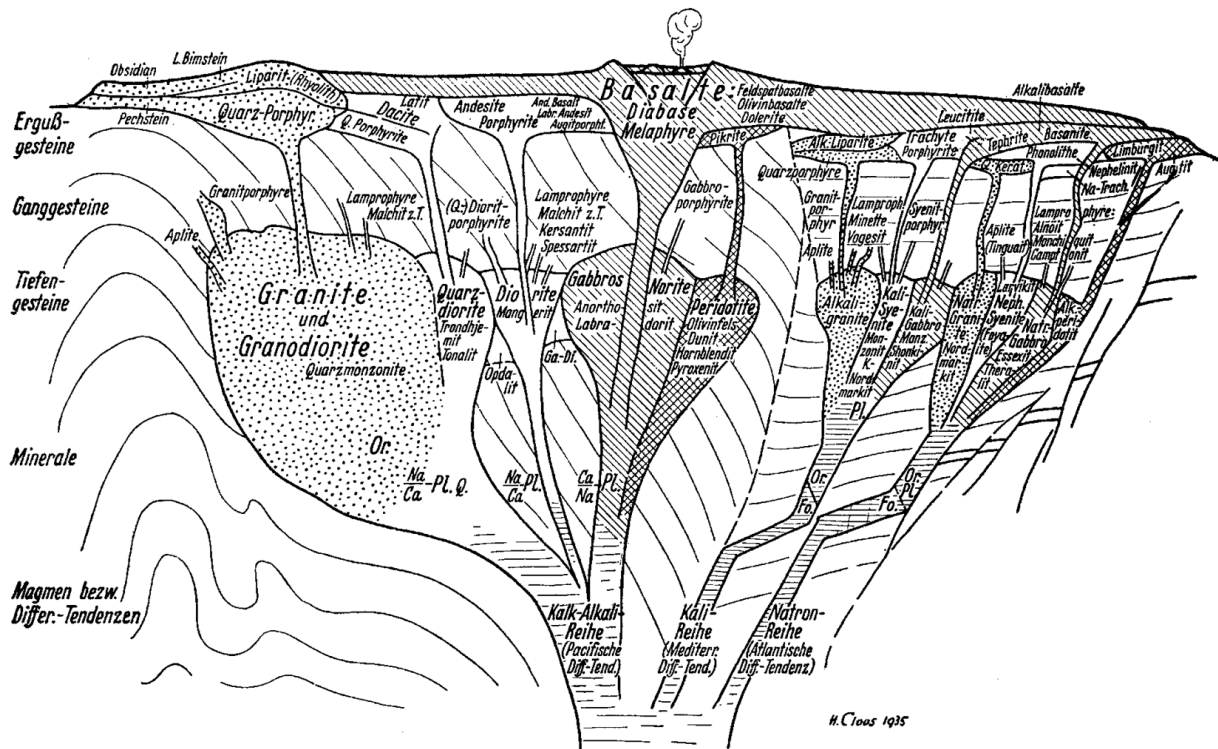


Fig. 2.1.3: Geological Tree of volcanic Rocks by Cloos [2].

Chemical composition for example of granite and quartz porphyry is the same, their crystallite size is different. Deep inside earth, granite had a long time to crystallise out (big grain size), however, quartz porphyry quickly petrified on the surface (small grain size). In between there are the so-called dyke rocks, like e.g. quartz. Fig. 2.1.4 describes the types of rocks and their mineralogical composition. Chemical composition for typical rocks can be found in Fig. 2.1.5.

Rocks					Minerals						
	basic (silica-poor)	←————→		acidic (silica-rich)							
Surface rocks	young	Basalt	Andesite	Trachyte	Olivine	Brightness	Hardness	Fissility			
	old	Diabase	Porphyrite	Porphyry							
Plutonic rock				Liparite	(Mg, Fe) <sub>2</sub> [SiO <sub>4</sub> ]	dark	light				
				Quartz-porphry	Ca (Mg, Fe) [Si <sub>2</sub> O <sub>6</sub> ]				~ 7	-	
					Hornblende				(OH) <sub>2</sub> Ca <sub>2</sub> (Mg, Fe) <sub>2</sub> [Si <sub>5</sub> O <sub>22</sub> ]	6-7	+
					Biotite				K(OH) <sub>2</sub> (Mg, Fe) <sub>3</sub> [Si <sub>3</sub> AlO <sub>10</sub> ]	5-6	+
					Muscovite				K(OH) <sub>2</sub> Al <sub>2</sub> [Si <sub>3</sub> AlO <sub>10</sub> ]	~ 3	+
					Plagioclase				(Na, Ca) [(Si, Al) <sub>4</sub> O <sub>8</sub> ]	~ 2	+
					K Feldspar				K [Si <sub>3</sub> AlO <sub>8</sub> ]	~ 6	+
					Quartz				SiO <sub>2</sub>	6	+
										7	-
		Gabbro	Diorite	Syenite	Granite						

Fig. 2.1.4: System of magmatic stones with their mineral composition.

	Granite (acidic)	Quartz-diorite (intermediate)	Plateau basalt (basic)
SiO <sub>2</sub>	70,18	61,59	48,80
TiO <sub>2</sub>	0,39	0,66	2,19
Al <sub>2</sub> O <sub>3</sub>	14,47	16,21	13,98
Fe <sub>2</sub> O <sub>3</sub>	1,57	2,54	3,59
FeO	1,78	3,77	9,78
MnO	0,12	0,10	0,17
MgO	0,88	2,80	6,70
CaO	1,99	5,38	9,38
Na <sub>2</sub> O	3,48	3,37	2,59
K <sub>2</sub> O	4,11	2,10	0,69
H <sub>2</sub> O	0,84	1,22	1,80
P <sub>2</sub> O <sub>5</sub>	0,19	0,26	0,33
Sum	100	100	100

Fig. 2.1.5: Chemical composition of stones [2].

Fig. 2.1.6 shows the formation of volcanites. Liquid magma is brought very quickly to the earth's surface, crystallising into very fine grains. There is no significant change in its chemical composition. Secondary sites can develop from these primary ones. Rocks can mechanically weather or chemically change (Fig. 2.1.7), producing chemical or biogenic sediments. Mechanical weathering brings water into the rocks, which freezes during winter. Stresses occur and the material weathers (Fig. 2.1.8). A rock unit may also weather when mineral grains are removed in saline solutions (Fig. 2.1.9). Mechanical sediments are formed following mechanical weathering and transport by water or air, chemical or biogenic sediments follow chemical weathering (Fig. 2.1.7). This weathered rock in Southern Taiwan clearly shows that the processes schematically outlined in nature really occur (Fig. 2.1.10).

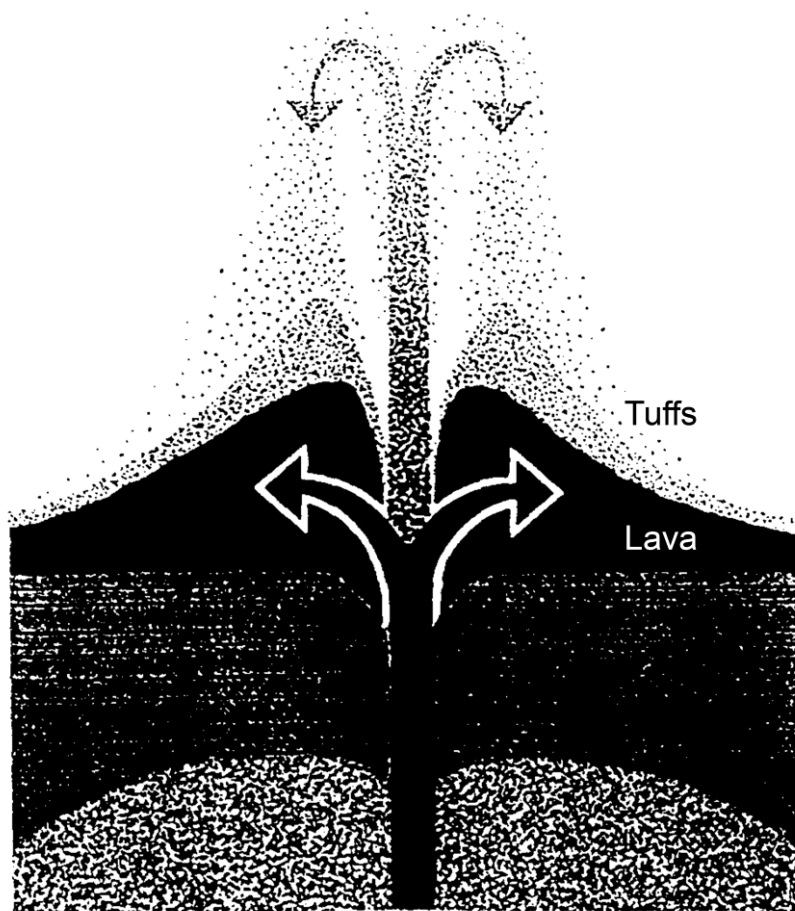


Fig. 2.1.6: Formation of Vulcanite.

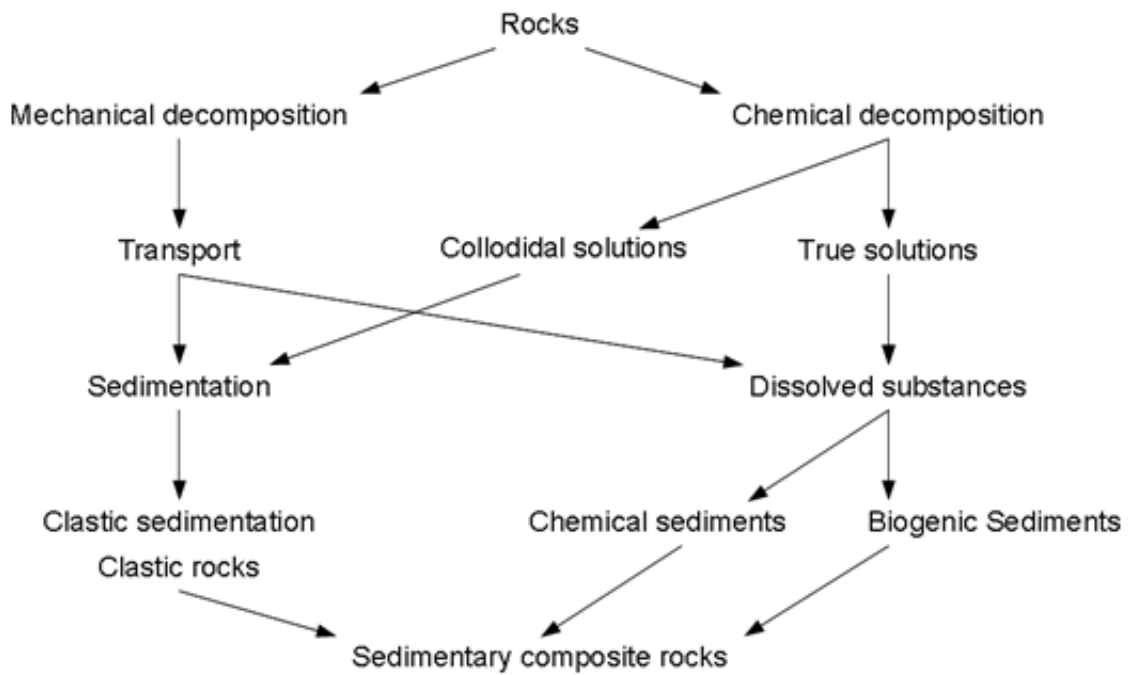


Fig. 2.1.7: Scheme of rock metamorphism via alteration [1].

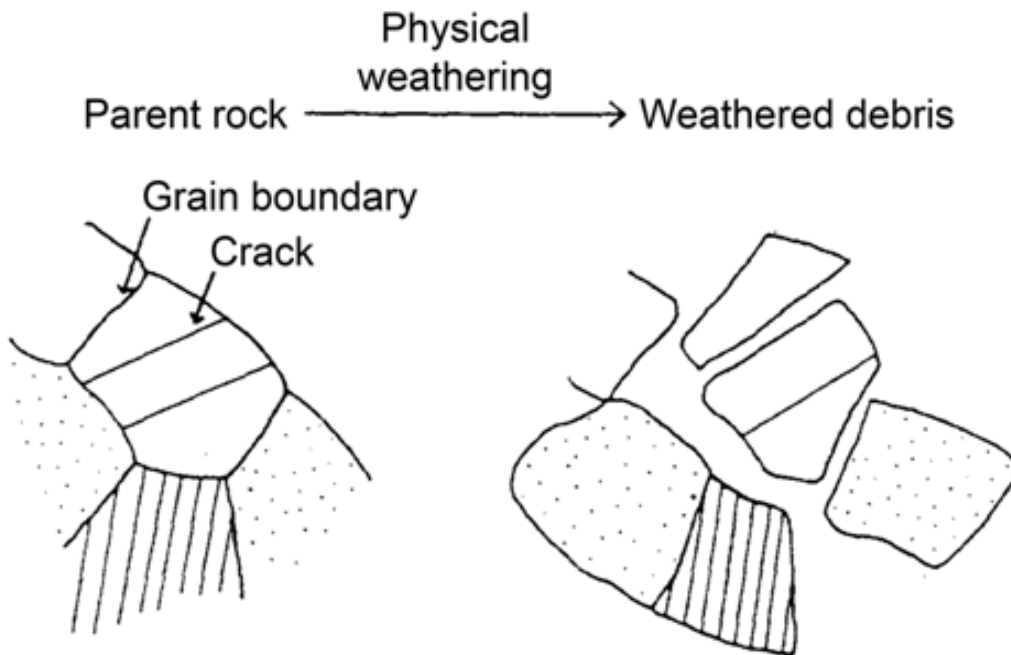


Fig. 2.1.8: Schematic representation of physical weathering of rocks with multi-mineral components.

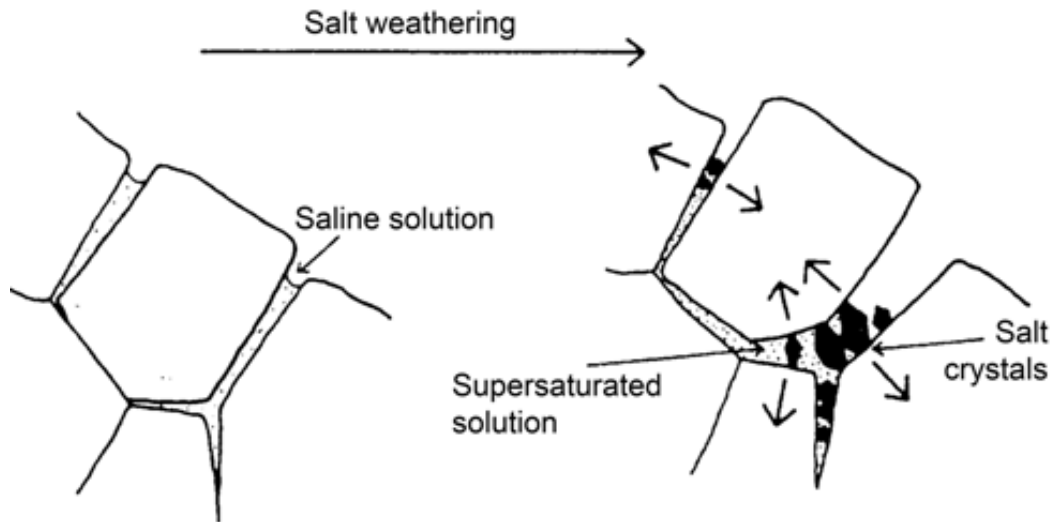


Fig. 2.1.9: Dissolution of mineral grains from rock formation via salt weathering.



Fig. 2.1.10: Dissolution of mineral grain from rock formation (South Taiwan, Nov. 2007).

Kaolin develops as a result of weathering of feldspar. Feldspar is a potassium-aluminium-silicate. There are two different possibilities of weathering: The so-called allitic weathering means removal of some of the components from the feldspar structure during millions of years, with aluminium hydroxide remaining. Siallitic decomposition means that  $K_2O$  and water leave the system and mineral remains which we call kaolin (Fig. 2.1.11). Weathering products can be transported to secondary mineral deposits by water or air (Fig. 2.1.12 and

2.1.13). When kaolin is transported and found on secondary deposits, we call it clay. Clay is much finer than kaolin, because due to the transport the coarse crystals remain further up, the fine ones further down. However, it is more contaminated since in this way metal and organic contaminations increase. Transport to the secondary deposits may cause different sediment structures (Fig. 2.1.14). When sediments are transported by earth faults into deeper regions and come again under pressure, we get, for example, mudstone (Fig 2.1.15), lime stone (Fig. 2.1.16), marble or quartzite (Fig. 2.1.17). This hardening is called diagenesis, which may also cause chemical changes (Fig. 2.1.15 left). Fig 2.1.18 recapitulates the formation of rocks.

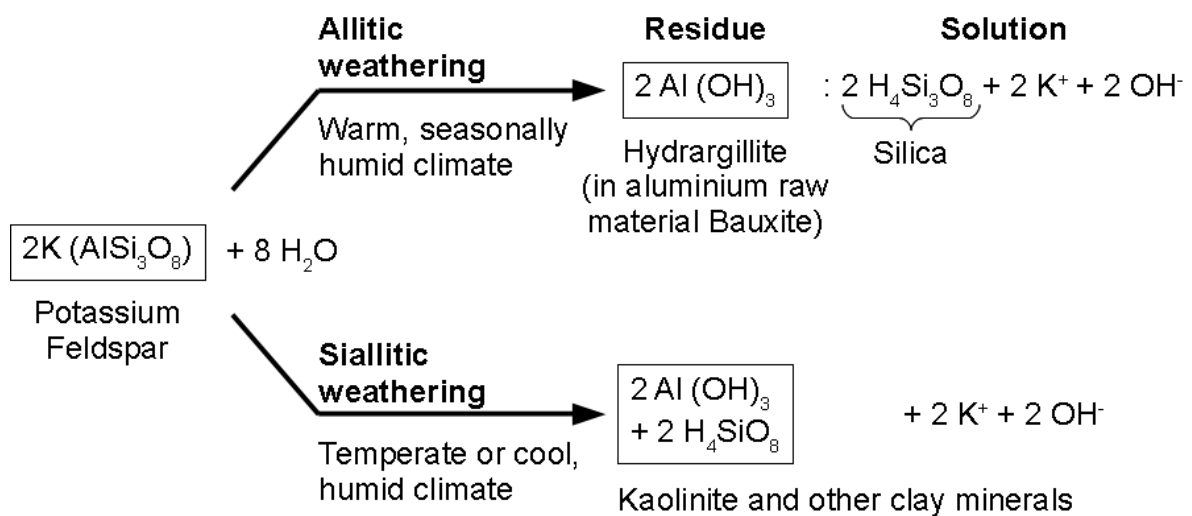


Fig. 2.1.11: Allitic and siallitic weathering of potassic feldspar.

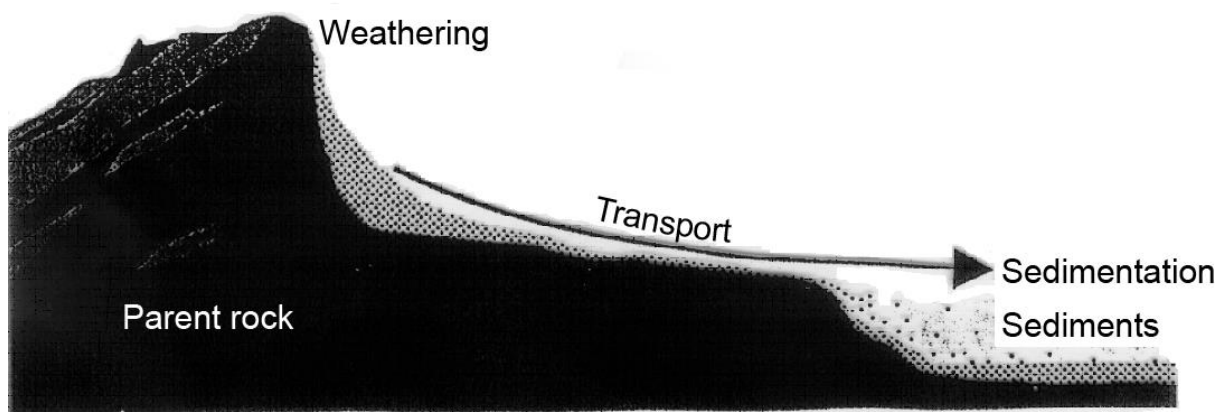


Fig. 2.1.12: Formation of sediments.

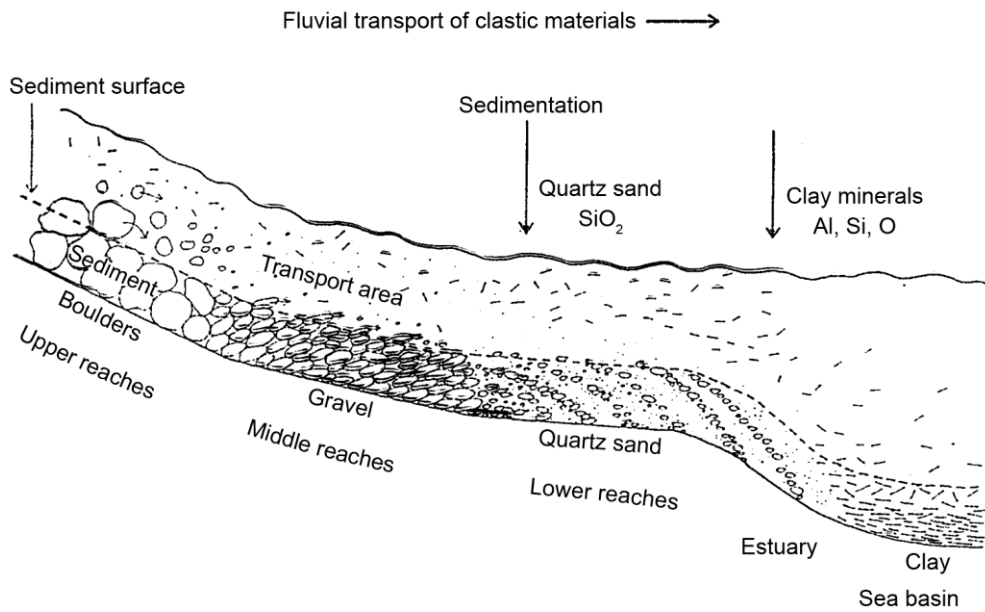


Fig. 2.1.13: Transport and deposition of clastic material.

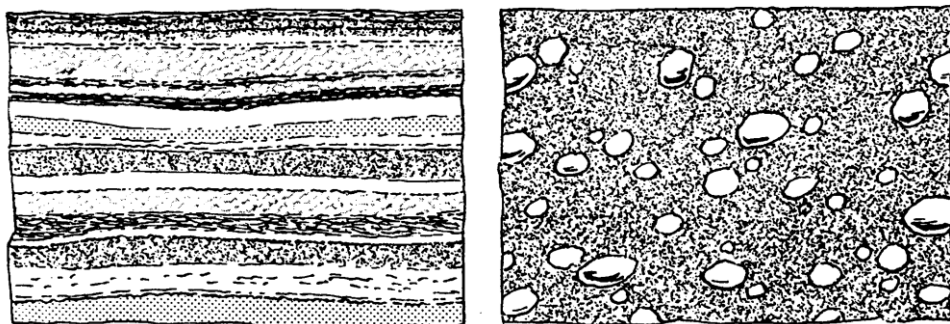


Fig. 2.1.14: Type of sediments: (left) sediments in water – layered -; (right) sediments in glacier [Moraine] – unlayered.

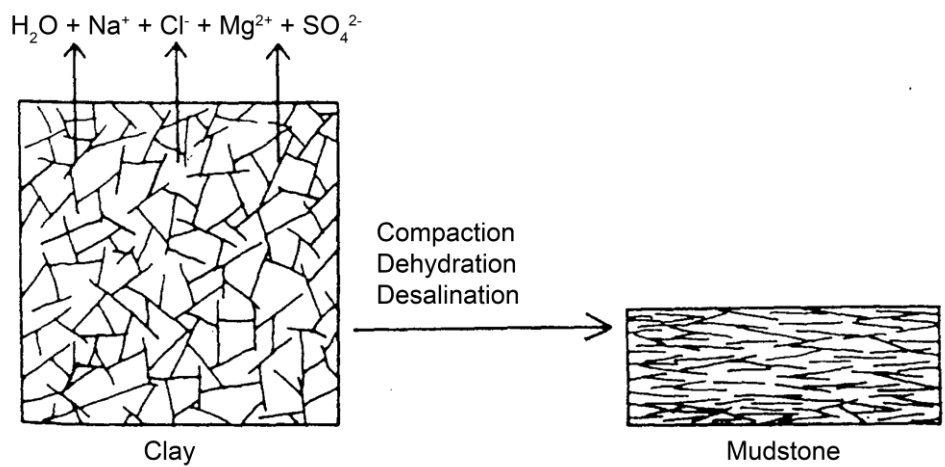
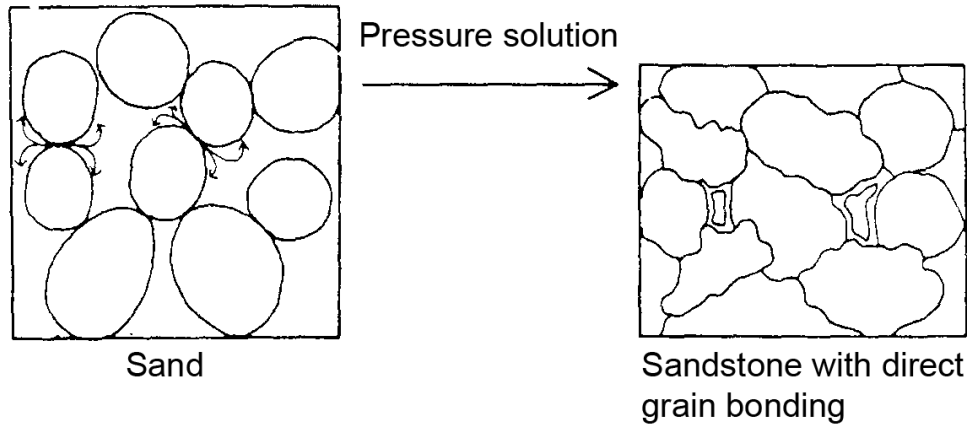
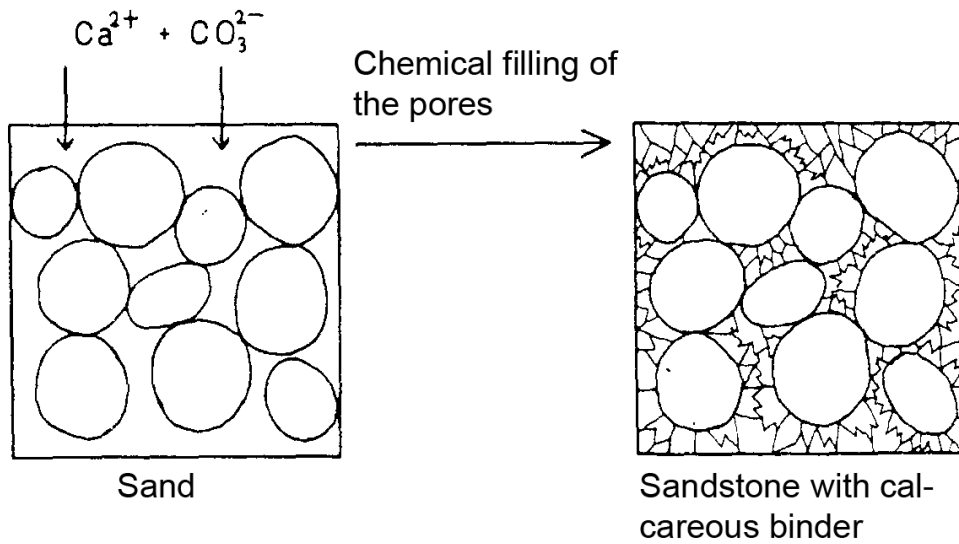


Fig. 2.1.15: Diagenesis of clay into clay stone.

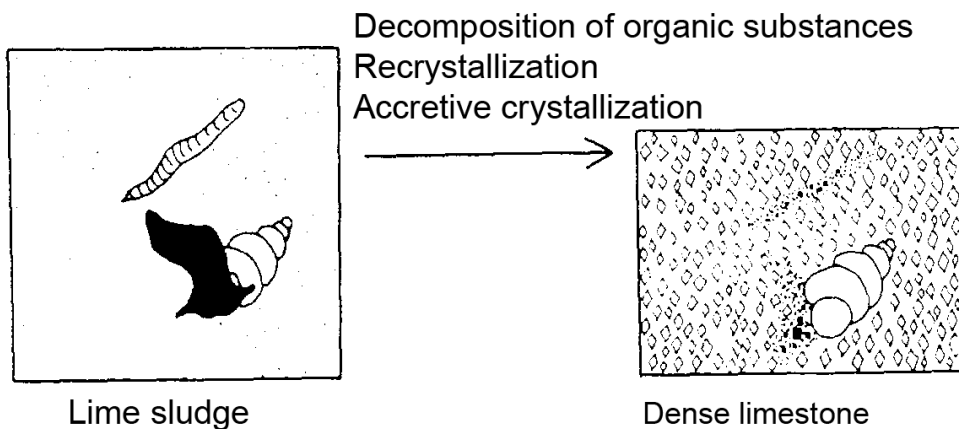




Diagenesis of sand to sandstone with direct grain bonding in a pressure solution

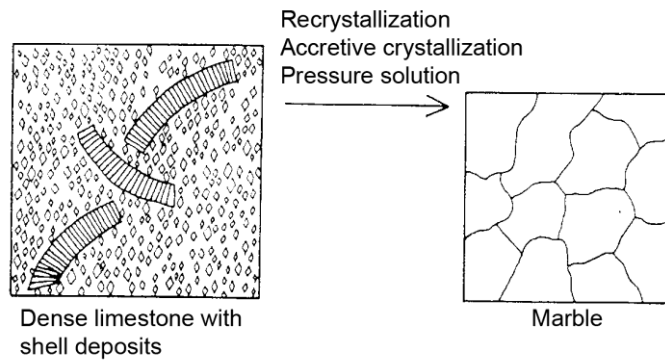


Diagenesis of sand to sandstone with a calcareous binder by chemical filling of the pores

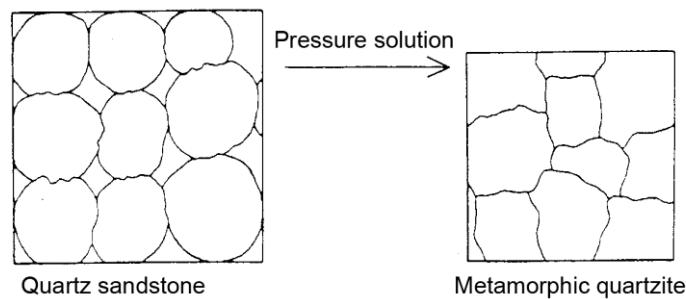


Diagenesis of lime sludge to dense limestone

Fig. 2.1.16: Diagenesis of sand and lime slurry.



Metamorphosis of limestone into marble



Metamorphosis of Quartz sandstone into metamorphic quartzite

Fig. 2.1.17: Metamorphosis of lime stone into silica sandstone.

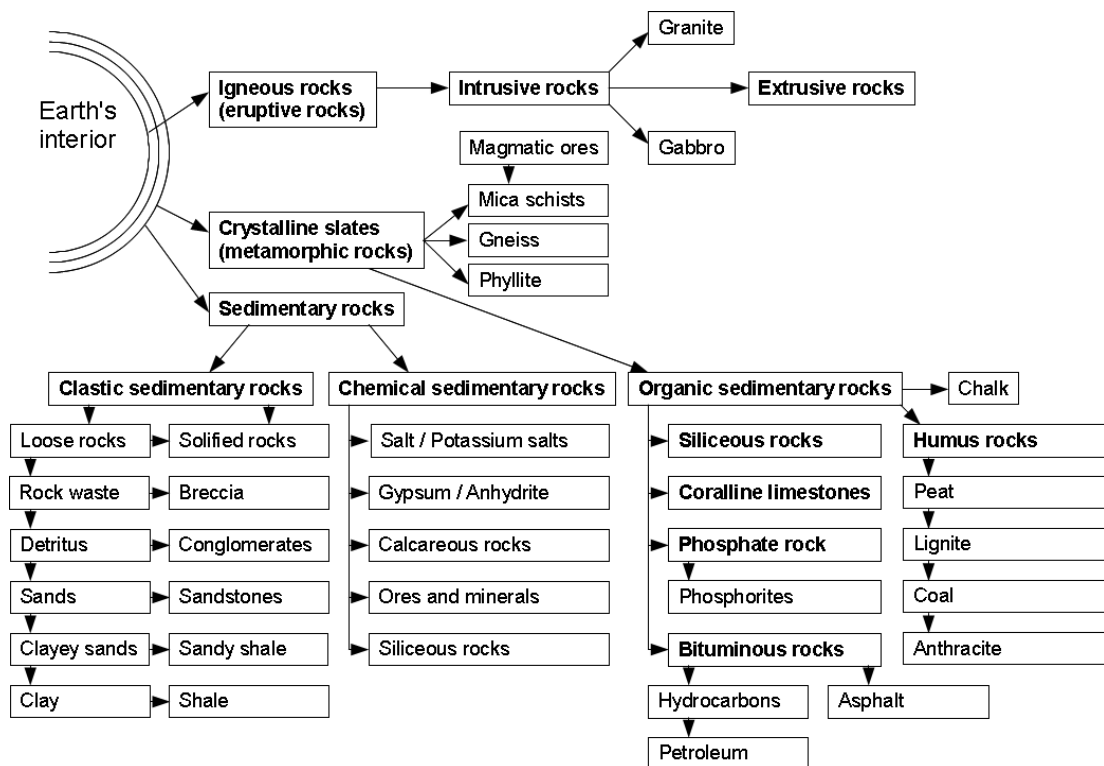


Fig. 2.1.18: Simplified scheme of rock formation by Kukuk [2].

## 2.2 Deposits

The feldspar deposit from Fig. 2.2.1 shows besides clear feldspar sections a quartz stock and pegmatite sections. The mining waste has to be removed first before exploitation can start. Feldspars exist in three pure forms: potassic feldspar, albites and anorthite. In nature there are no mixed deposits of anorthites and potassic feldspars. But deposits of albites and anorthites, as well of sodium and potassic feldspar can naturally occur (Fig. 2.2.2).

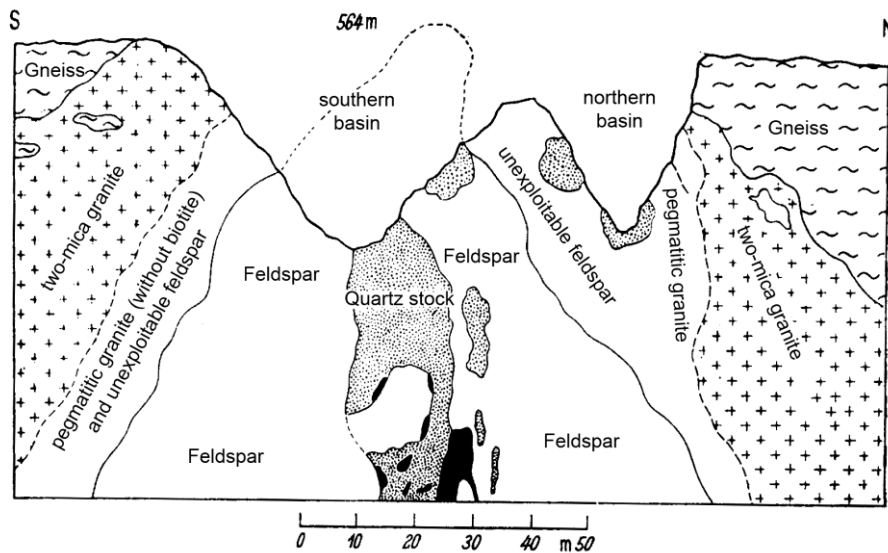


Fig. 2.2.1: Pegmatit from Hagendorf (Oberpfalz) [2].

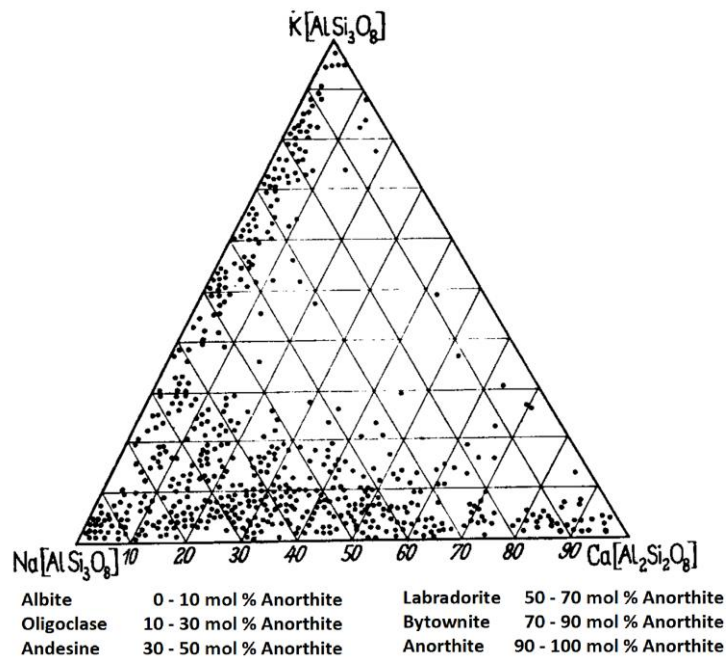


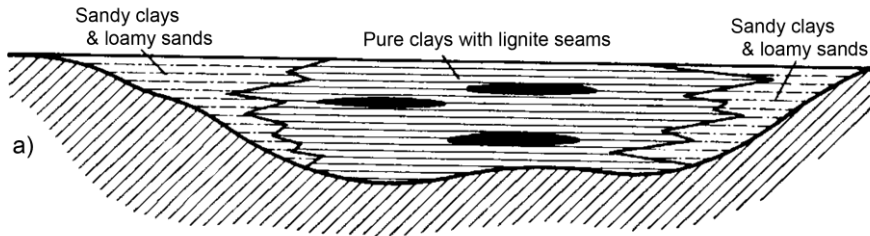
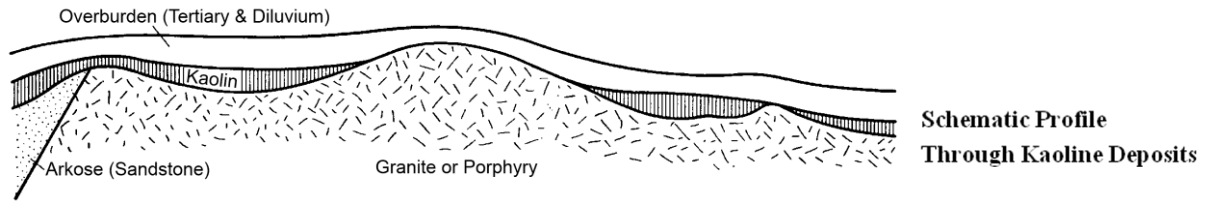
Fig. 2.2.2: Triangular phase diagram (ternary system) Orthoclase – Albite – Anorthite; Variations in the chemical composition of natural feldspars (according to Betehtin).

No.	Origin	SiO <sub>2</sub>	Al <sub>2</sub> O <sub>3</sub>	TiO <sub>2</sub>	Fe <sub>2</sub> O <sub>3</sub>	CaO	MgO	Loss on ignition	SK (PCE)
		%	%	%	%	%	%	%	
1	<b>Germany</b> <i>Siebengebirge</i> Wintermühlenhof	97,46	0,46		1,00	traces	traces	1,13	--
2	<i>Westerwald</i> Herschbach	97,94	0,92		0,19	traces	traces	0,18	>34
3	<i>Vogelsberg</i> Rainrod	98,42	0,58		0,19	0,20	0,19	0,50	34
4	<i>Hessische Senke</i> Marienrode	97,30	0,65	0,84	0,45	traces	traces	0,39	>34
5	<i>Süd-Hannover</i> Kattenbühl	98,30	0,17	0,64	0,69	0,07	traces	0,15	>34
6	<i>Sachsen</i> Glossen	98,39	0,64		0,32	0,20	traces	0,25	34
7	<b>Italy</b>	97,90	0,36	0,64	0,06	traces	traces	0,85	--
8	<b>South Africa</b>	94,20	0,29	1,72	0,76	2,01	traces	--	--

Fig. 2.2.3: Analysis of different concrete quartzites.

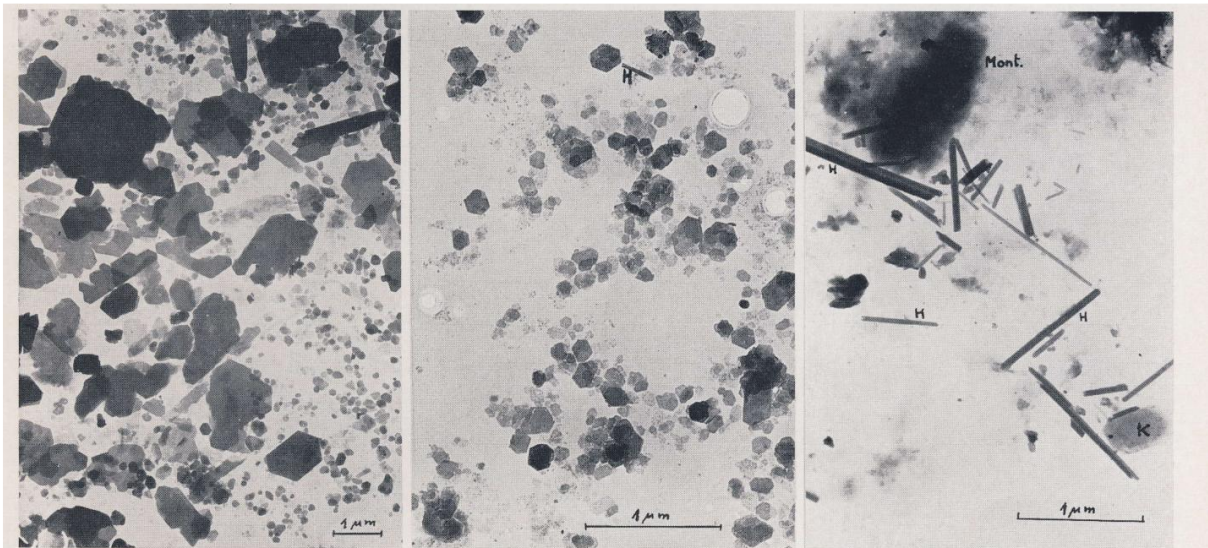
Quartz is won in quartz dikes. This raw material, as for feldspars, requires intensive milling. Quartz deposits have a relatively high purity (Fig. 2.2.3), as there are quartz deposits with a SiO<sub>2</sub> content >99%. Such raw materials are especially used for the production of glass where pure SiO<sub>2</sub> grades are particularly demanded.

Fig. 2.2.4 shows schematically a typical profile of a kaolin deposit. Kaolins developed during weathering are normally not much pure. Clays are often found on secondary deposits together with brown coal beds. Faults of earth occurred during millions of years cause problems to the exploitation of raw materials. Due to earth faults, layers with different chemical compositions lay next to each other. Therefore, much care has to be taken with regard to the preparation of such raw materials in order to either compensate these differences in chemical compositions by mixing or separate them from each other.



**Schematic profile through clay deposits:**  
a) undisturbed  
b) disturbed by fault

**Fig. 2.2.4: Deposit profiles [3].**



Kalonite (Hirschau), finely elutriated,  
el. opt. magn.: 7200:1

Disordered kaolinite (Beaujard clay) < 2μm  
idiomorphic down to the finest fractions,  
el. opt. magn.: 15000:1

Halloysite (clay from Bavaria) < 2μm  
el. opt. magn.: 15000:1

**Fig. 2.2.5: SEM (Scanning Electron Microscopy) of clay minerals [2].**

Grain size of weathered kaolin is extremely small (Fig. 2.2.5). So this raw material does not have to be further crushed. But it has to be dispersed, suspended into water.

Halloysite has a kaolin structure with increased water content. This mineral shows small hexagonal kaolinite plates composed of different layers, which curls, since the size of the layers varies and chemical bonds between the layers are only possible following geometric deformation. This means that the raw material cannot be used for the processing of components because its transport in tubes for fully automated industrial facilities is extremely difficult.

The chemical composition of pure kaolin is: 46.6 weight percent (wt. %)  $\text{SiO}_2$  – 39.5 wt. %  $\text{Al}_2\text{O}_3$  and 13 wt. % water (Fig. 2.2.6). Its water content can be noticed in Fig. 2.2.6 as loss of ignition, which happens when kaolin undergoes thermal treatment, also see detailed reviewed in section “Sintering”.

	$\text{SiO}_2$ %	$\text{Al}_2\text{O}_3$ %	$\text{TiO}_2$ %	$\text{Fe}_2\text{O}_3$ %	$\text{CaO}$ %	$\text{MgO}$ %	Alkalis %	LOI. %	SK (PCE)
pure kaolinite prime quality	46,6 46,25	39,50 39,28	0,14	0,64	0,14	traces	0,15	13,9 13,40	36
Kaolin from Seilitz	56,49	30,66		0,57	0,25	0,30	0,96	10,84	--
Kaolin from Kemmlitz	56,47	30,58		0,81	0,11	0,06	0,64	11,39	34
Kaolin from Gösen	52,95	32,65		1,27	0,09	0,61	1,55	10,96	34
Schnaittenbach's raw kaolin	84,58	11,32		0,52	--	--	0,24	3,34	33/34

Fig. 2.2.6: Chemical analysis of some kaolins.

As already mentioned clay is more contaminated than kaolin due to transport on secondary deposits (Fig. 2.2.7). With regard to sintered products the high content of iron-oxide causes massive red coloration (clay bricks).

	SiO <sub>2</sub> %	Al <sub>2</sub> O <sub>3</sub> %	TiO <sub>2</sub> %	Fe <sub>2</sub> O <sub>3</sub> %	CaO %	MgO %	Alkalis %	LOI. %	SK (PCE)
Blue clay from Saarau	47,9	36,4		1,8	0,8	0,4	n. b.	12,3	34
Blue clay from Rauske	50,4	34,8		2,1	0,6	0,5	n. b.	11,4	34/35
Pot clay from Wiesau	51,3	33,7		1,8	0,9	0,5	2,2	9,7	32
Premium clay from Zinzendorf	47,6	36,8		1,8	0,03	Spur	0,3	13,4	34
Clay from Groß-Saubernitz	57,0	28,0		3,5	--	0,6	1,9	9,2	31
Clay from Schwepnitz	48,8	35,3		1,9	0,03	--	1,0	12,9	34
Premium clay from Hohenbocka	48,8	34,0		1,3	0,15	0,3	1,8	13,6	33
Fat clay from Großalmerode	48,1	35,1	1,4	2,2	--	--	n.b.	12,3	33

Fig. 2.2.7: Analysis of some selesian, middle German and hessian clays.

With regard to the shifting of rocks the sectional drawing of a magnesite deposit (Fig. 2.2.8) makes clear how many efforts are required to exploit these raw materials. Magnesite is used for the production of refractory materials for the steel, cement or the glass industry.

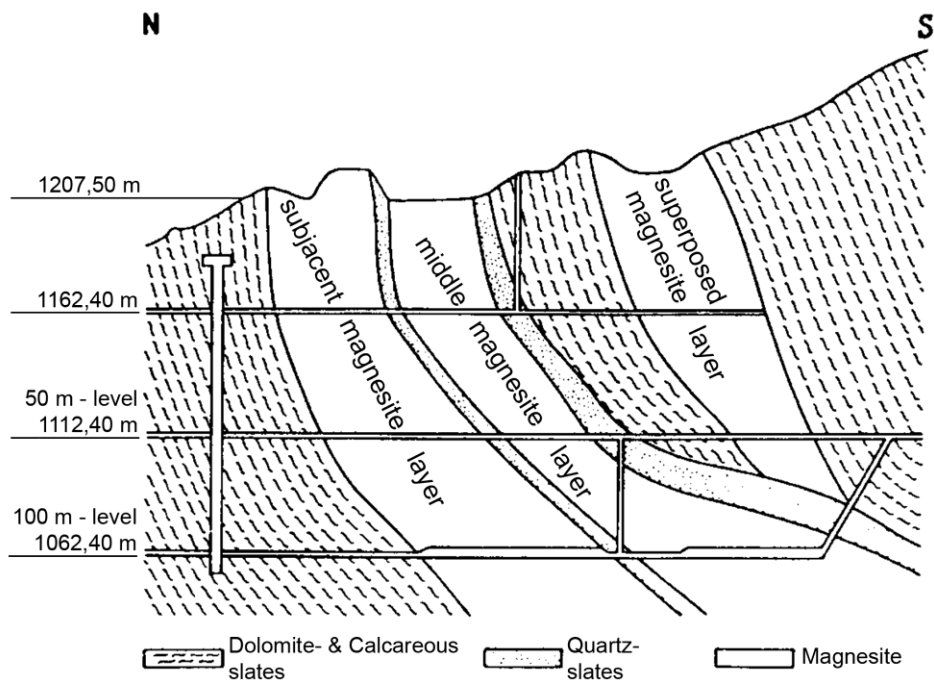


Fig. 2.2.8: Geological Profile through magnesite deposit [3].

Zirconium is a natural zirconium silicate, so a solid solution from zirconium oxide and  $\text{SiO}_2$ .

	$\text{SiO}_2$ %	$\text{ZrO}_2$ %	$\text{Al}_2\text{O}_3$ %	$\text{TiO}_2$ %	$\text{Fe}_2\text{O}_3$ %	CaO %	MgO %	Alkalis %	LOI. %
Zircon from Madagascar	33	66	1						-
Zircon from Ceylon	33,86	64,25	-	-	1,08	-	-	-	-
Sand from Florida, cleaned	98,5		1,5			-	-	-	-
Brazilian Baddeleyite	0,70	96,52	0,43	-	0,41	0,55	0,10	0,42	0,39
Zircon-favas	0,48	97,19	0,40	0,48	0,92	Spur	-	-	0,38
Zircon-favas, light brown	15,35	81,64	0,90	0,51	1,10	-	-	-	0,63

Fig. 2.2.9: Analysis of some zirconium raw materials [3].

Raw materials with a high percentage of high alumina are highly attractive materials for the production of ceramic components for the electronics and mechanical engineering industries and will therefore be separately considered (Fig. 2.2.10).



	SiO <sub>2</sub> %	Al <sub>2</sub> O <sub>3</sub> %	TiO <sub>2</sub> %	Fe <sub>2</sub> O <sub>3</sub> %	CaO %	MgO %	Alkalis %	LOI. %
South African sillimanite	14,43	82,97	--	0,52	0,38	0,16	--	1,35
Indian sillimanite	35,13	62,00	--	0,95	0,17	0,12	--	1,30
Indian Cyanite, pre-fired	31,61	67,68	--	0,35	0,14	0,13	--	0,05
French bauxite	16,50	73,00	--	1,5	--	--	--	9,00 (H <sub>2</sub> O)
Upper Hessian bauxite	3,20	50,60	3,0	16,4	--	--	--	27,10
Bauxite from Belje Poljjane	24,7	55,7		3,7	0,30	0,40	--	14,80
Sintered bauxite from Guayana	4,76	89,72	4,27	0,99	0,05	0,04	0,08	0,29
Bauxite from Katni, Jubbulpure / India	1,85	59,22	6,46	2,32	0,46	0,05	0,22	29,55
Diaspore from Missouri	6,56	72,72	3,65	2,37	--	--	1,00	13,88
Natural corundum	bis 3	93-98	--	bis 1	--	--	--	--

Fig. 2.2.10: Analysis of some high-alumina containing raw materials.

This video clip taken at a raw material mine which belongs to the Imerys Group, gives you an impression about the size of such a mine. You will see an excavator vehicle collecting material from various places in the mine. The mine is a secondary deposit, in other words, the material has been already crushed by weathering.



*Videoclip: Deposits*

In the background you see earth-source with various shades of colours. These are raw materials with different chemical compositions. The decision for the material's mixture has already to be taken in the mine, in order to get a reasonably constant composition of the raw materials to be delivered to the customers.

## 2.3 Natural ceramic raw materials

### 2.3.1 Kaolins and clays

Silicates play an important role within natural materials and therefore their structure and characteristics are discussed first.

Kaolin and clays are essentially composed of  $\text{SiO}_4$  tetrahedra. Four-free-valence silicon in a  $\text{SiO}_4$  tetrahedron is surrounded by four oxygen ions (Fig. 2.3.1.1). The silicon ion shows a positively 4-valence. Eight negative charges show the 4 oxygen ions, meaning that this  $\text{SiO}_4$  tetrahedron has, in all, 4-valences negatively charged. For neutralisation, it has either to connect to other tetrahedron or saturate these charges with cations. Fig. 2.3.1.1 demonstrates how these  $\text{SiO}_4$  tetrahedra can be linked together to form, for example, island, ring or chain silicates. If two  $\text{SiO}_4$  tetrahedra are combined by a corner, which means, by an oxygen ion, this construct contains two silicon ions and seven oxygen ions. Consequently, this 2-valence-free tetrahedron has a charge of 6-. When a ring is formed, we get the chemical formula  $\text{Si}_3\text{O}_9$  with also six negative charges. Chain silicates have the formula  $[\text{SiO}_3]^{2-}$ . If negative charges are saturated by cations, we get minerals which we find in nature.

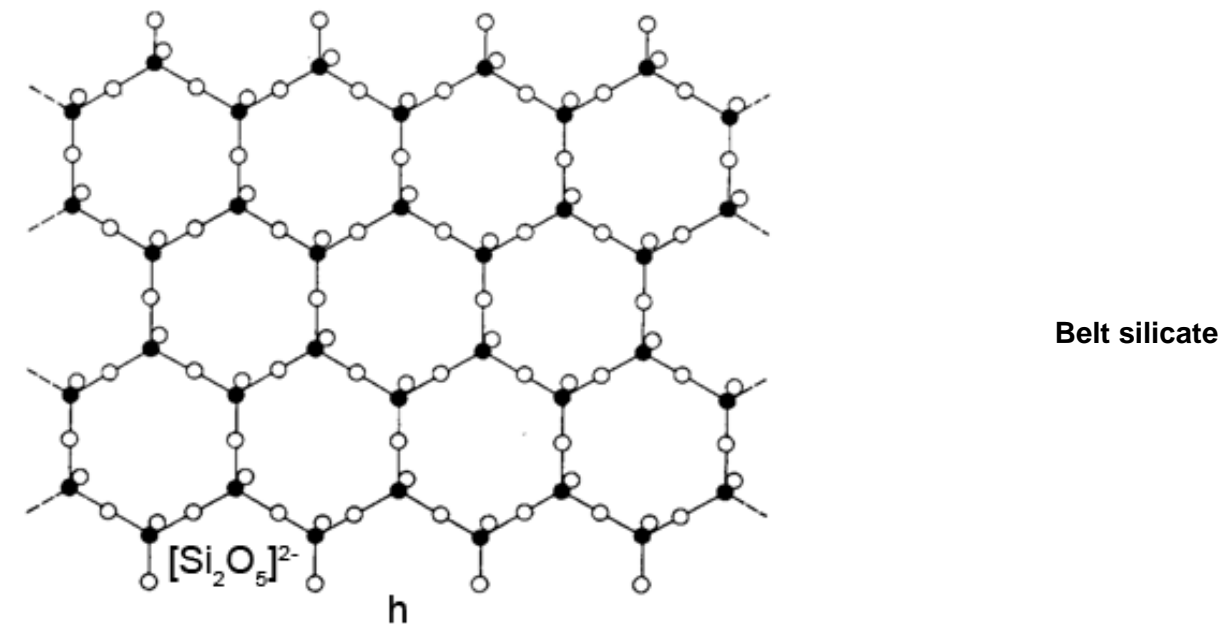
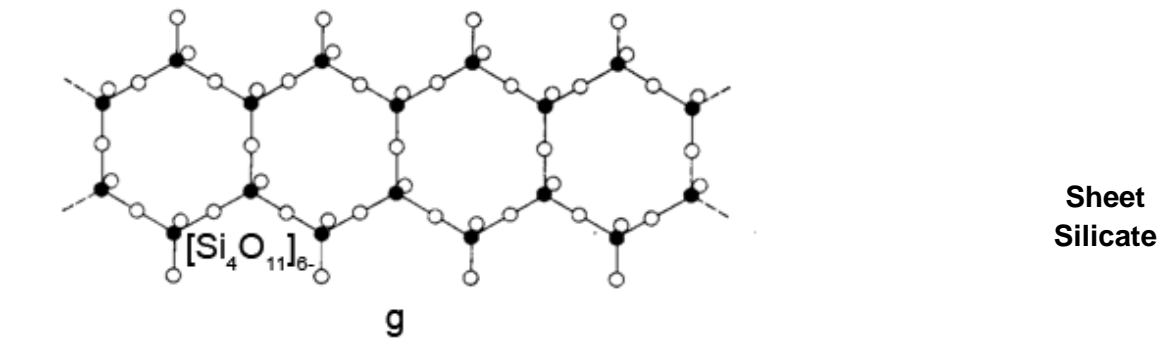
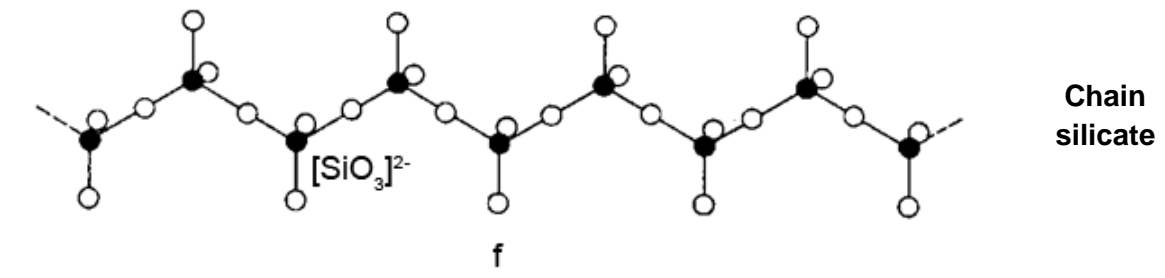
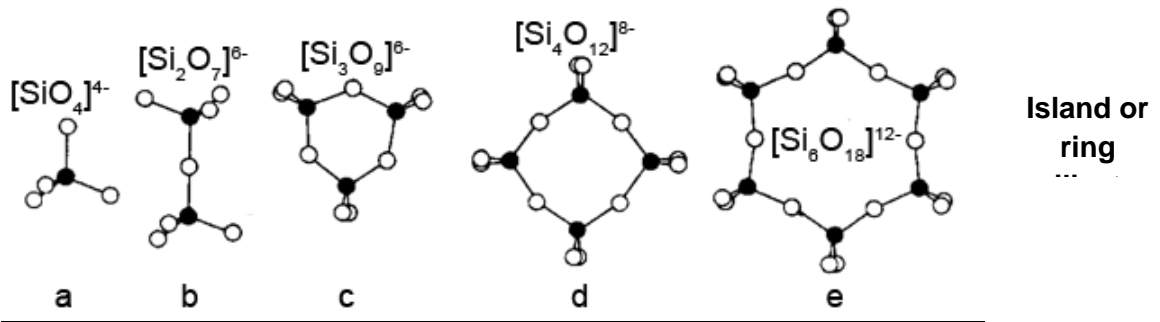


Fig. 2.3.1.1: Linkage of  $[\text{SiO}_4]^{4-}$  tetrahedra ( $\bullet = \text{Si}^{4+}$ ,  $\circ = \text{O}^{2-}$ ) [1].

$[\text{Si}_4\text{O}_{11}]^{6-}$  or  $[\text{Si}_2\text{O}_5]^{2-}$  structures are formed, if the  $\text{SiO}_4$  tetrahedra are linked to sheet or belt silicates. They also have negative charges (Fig. 2.3.1.1). To become electrically neutral, cations or other positively charged structural components have to attach. Layer silicates, for example, show this effect (Fig. 2.3.1.2), when a tetrahedron layer links to an octahedron layer consisting of Al, O and OH groups. This construct is called double-single layer, because within stacking sequence every third layer shows the same geometric array as the first layer. In the lower section, where the three oxygen ions are situated, the tetrahedron layer has a negative excess charge, and in the upper section, where just one oxygen ion above the 4-valence-free silicon ion is found, a positive excess charge. These positive excess charges in the upper part of the  $\text{SiO}_4$  tetrahedron are saturated as the octahedron layer with negative excess charge attaches to the  $\text{SiO}_4$  tetrahedron.

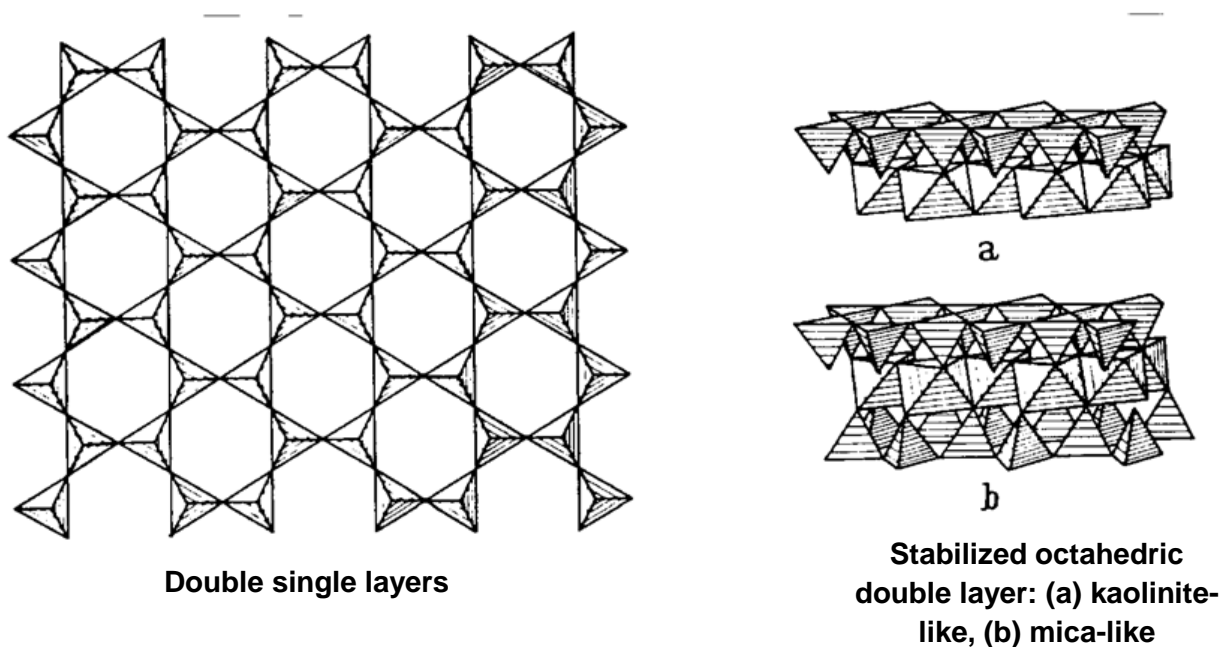


Fig. 2.3.1.2: Double layered silicates [1].

With regard to three-layer minerals a tetrahedron layer attaches to both, the top and the bottom of an octahedron layer. These layered minerals form the basis for kaolin and clays which in the following are reviewed in detail.

Water molecules can intercalate between the layers (Fig. 2.3.1.3). This intercalation of water molecules influences enormously the processing properties of clays and kaolins. Water molecules are attached by hydrogen bonds to the oxygen ions or OH groups of each layer. In case of shear stress, this slight bond causes the layers' shifting against each other. And this leads to a certain plasticity (not related to the plasticity of metals) used for plastic forming (see chapter forming).

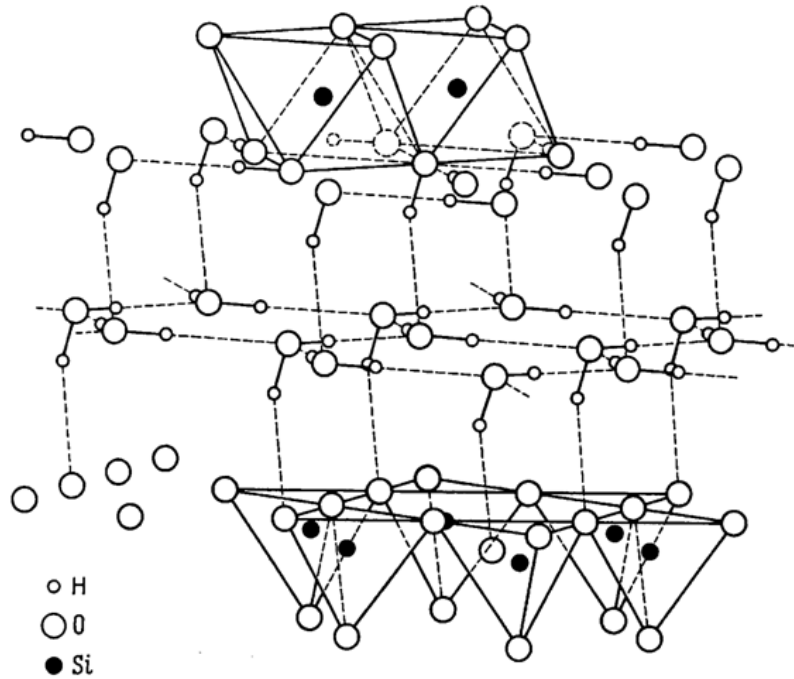


Fig. 2.3.1.3: Orientated layer of water in halloysite [3]. Bottom: Tetrahedra layer; top: Octahedra layer from the further unit.

Exchange of silicon atoms in tetrahedron layers or aluminium atoms in octahedron layers brings about a variety of minerals. If a 4-valence free silicon ion is replaced by a 3-valence-free aluminium ion, a cation in the interlayer ensures valence equalisation. This cation is highly flexible in the liquid layer and can very easily be exchanged. Here, we talk about ion exchange capability (Fig. 2.3.1.4). This exchange capability can, for example, be used for water softening, as we will see later on. Anions can also be laid in or be exchanged, if the 4-valence free silicon ion is replaced by a 5-valence free ion.

Clay mineral	Exchange capacity [mval/100 g]	
	cationic	anionic
Kaolinite	0 - 15	7 - 20
Halloysite	5 - 50	80
Montmorillonite	60 - 150	20 - 30
Vermiculite	100 - 150	4
Chlorite	3 - 40	
Illite	3 - 40	

Fig. 2.3.1.4: Ion exchange in clay minerals [1].

In addition, the number of water molecules can be varied in the inter-layers. If air humidity changes from 90 % to over 96 % to 99 % (Fig. 2.3.1.5), the clay minerals absorb more water. Water content increases from 0.4 gram water per gram dry substance at 90 % relative humidity up to 1g water/g dry substance at a relative humidity of 99 %. If humidity increases, the layer distance also increases (from 9.6 Å to 16.2 Å, and up to 19.5 Å), what leads to a change of the processing properties of these materials.

Relative moisture [%]	Total adsorption in $g_{\text{water}}$ per $g_{\text{dry solids}}$	Average distance $d$ [Å] between layer packages	Intermediate layer water (mean number of layers)	Water amount on surface of primary particles in g per $g_{\text{dry solids}}$	Observed bulking
I. 0	0	9,6	0	0	no bulking of the film
90	0,40	16,2	2,2	0,18	
II. 96	0,60	18,5	3	0,30	beginning of bulking and deformation about 30 % of bulking
99	1,00	19,5	3,3	0,80	
III. Adsorption in contact with water	about 5	The layer distance remains between 19,4 and 20 Å, whereas the (00l)-reflections disappear  (00l)-reflections disappear entirely			bulking increases up to 20 times the original film thickness

Fig. 2.3.1.5: Adsorbed water film between Na-montmorillonite layers with increasing the humidity [3].

As already mentioned, free cations are often exchanged in tetrahedra or octahedral, silicon ions in tetrahedron layers, aluminium ions in octahedron layers. The variety of minerals which can be found in nature is systematically summarised in Fig. 2.3.1.6. Mixtures of all these minerals can also be found in the nature, making their analysis quite complicated. If 3-valence free aluminium atoms occupy two octahedra each and the third octahedron remains empty, this layer succession is called dioctahedral. If 3-valence free aluminium ions in the octahedra are replaced by 2-valence-free magnesium ions, there is a magnesium ion in each octahedron and we call this trioctahedral occupation. Then we get the mineral antigorite. If

additional water is given to the interlayers, receive the mineral is called halloysite. The simplest three-layer mineral is pyrophyllite. If here the aluminium ions are again replaced by magnesium ions, we get saponite. If water is added to pyrophyllite, we have montmorillonite.

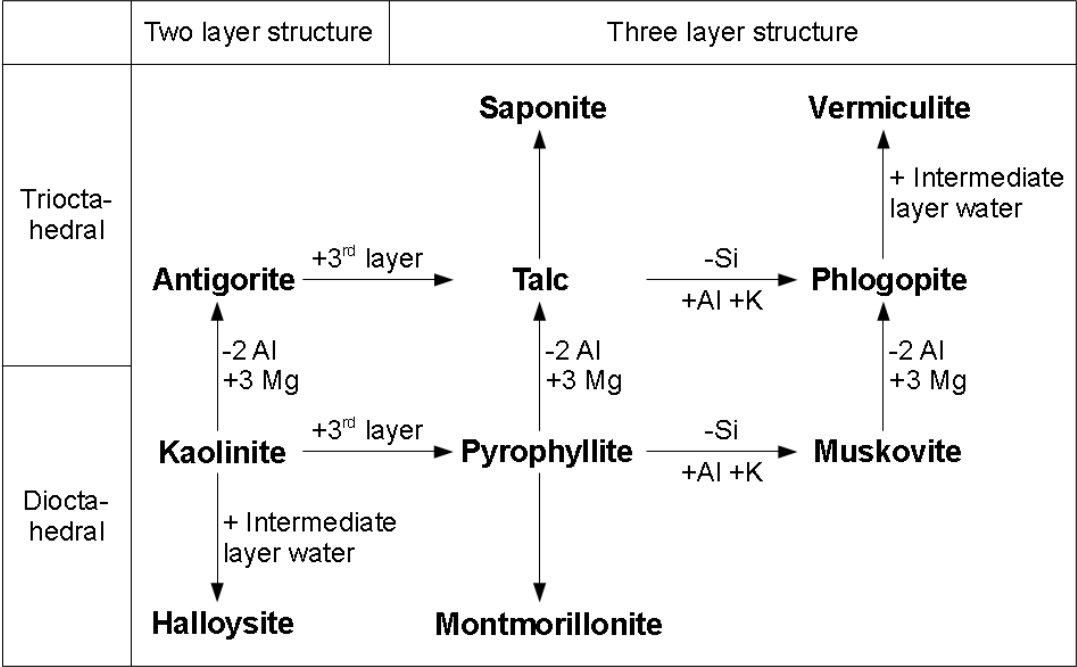


Fig. 2.3.1.6: Structural dependence of most important silicate minerals with layered structures [1].

If in pyrophyllite in the tetrahedron layer the 4-valence-free silicon ions are replaced by 3-valence-free aluminium ions, we find 1-valence-free cation in the interlayer for valence adjustment (muscovite etc.). On a macroscopic level, this layer structure results in flaky minerals (Fig. 2.3.1.7). Geological changes by torsion of these platelets result in minerals like nakrite or “fireclay”. At this point you can already imagine that the properties of such raw materials during transport in a pipeline are different from spherical powder particles. Clays and kaolins are very finely grained and normally further grinding is not necessary. They are just suspended in water.

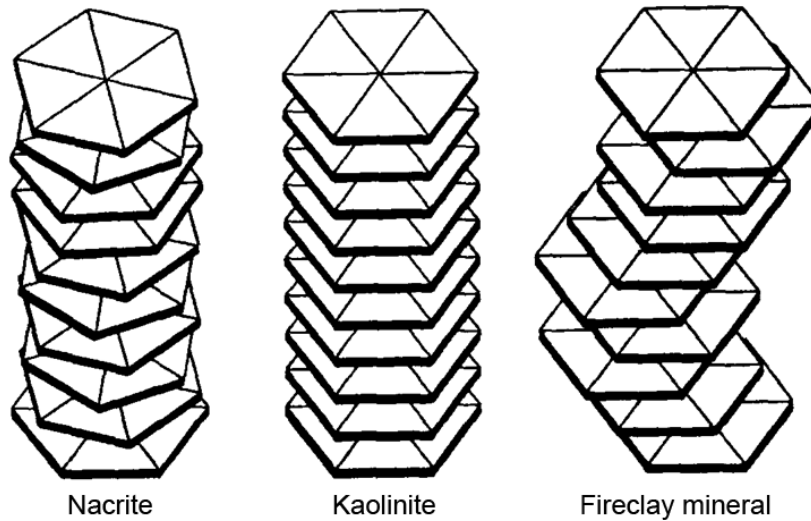


Fig. 2.3.1.7: Order and disorder in minerals of kaolinite group [3].

### 2.3.2 Feldspars

In tectosilicates the  $\text{SiO}_4$  tetrahedra are interconnected in a three-dimensional way (Fig.2.3.2.1). If 2-, 3- or 4-valence-free chains are linked to the tetrahedra's corners, corresponding networks occur. If in the  $\text{SiO}_4$  tetrahedra silicon ions are replaced by aluminium ions, electrical neutrality is re-established by incorporation of alkali or alkaline earth ions on interstitials, and this results in feldspar.

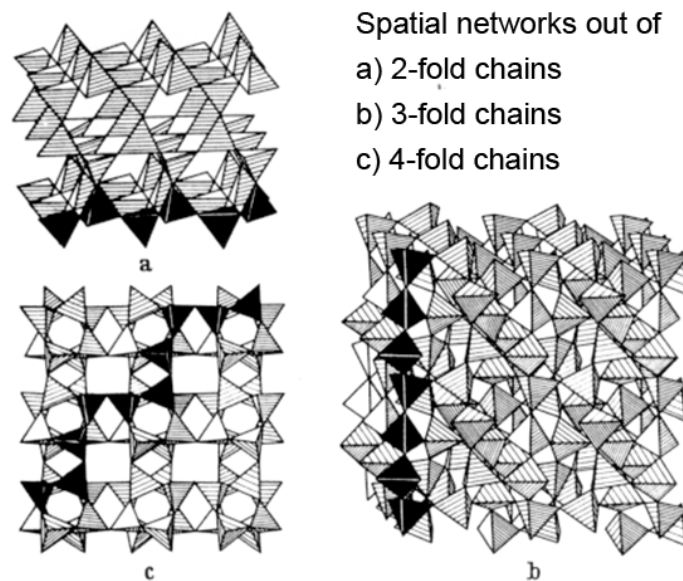


Fig.2.3.2.1: Some types of tetrahedral arrangements [1].



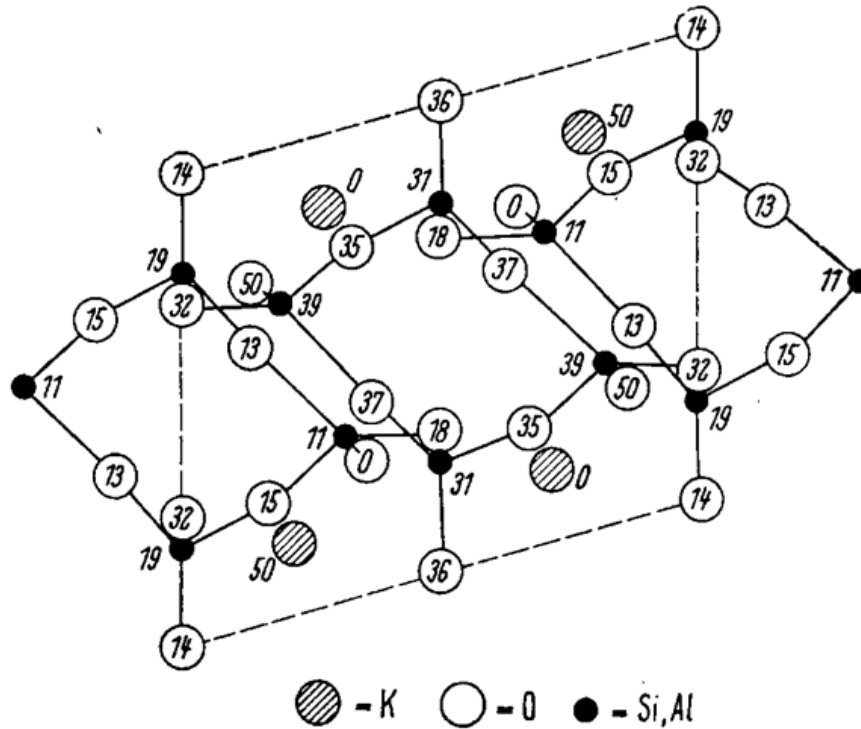


Fig.2.3.2.2: Half unit cell of lime feldspar projected on (010) [1].

The lattice structure projected on the base level is demonstrated in Fig. 2.3.2.2. The figures in this chart are multipliers with the distance from the respective oxygen or silicon ion in the basic level. Contrary to the layer minerals on interstitials, the potassium atoms are here firmly bound into the structure.

A selection of feldspars found in nature is summarised in Fig. 2.3.2.3. In microcline a silicon ion was replaced in the  $\text{SiO}_4$  tetrahedron by an alumina ion. A potassium ion ensures valence adjustment (potassic feldspar). Its varying crystal modifications have different volumes, which may cause cracks during sintering of ceramic masses, as feldspar is used. If valence is adjusted with sodium ions or calcium ions, albite (sodium feldspar) and anorthite (calcium feldspar), which can also crystallise in different modifications, is formed.

Mineral	Chemical formula	Crystal system	Lattice constants		Density (20 °C) [g/cm <sup>3</sup> ]	Refractive index n <sub>α</sub> n <sub>β</sub> n <sub>γ</sub>	Annotations
			a b c [Å]	α β γ			
Microcline	K[AlSi <sub>3</sub> O <sub>8</sub> ]	triclinic	8,57 12,98 7,22	90° 41' 115° 59' 87° 30'	2,57	1,514 1,518 1,521	Stable low-temperature modification, ordered
Sanidine	K[AlSi <sub>3</sub> O <sub>8</sub> ]	monoclinic	8,56 13,03 7,18	– 115° 59' –	2,57	1,521 1,527 1,527	
Albite	Na[AlSi <sub>3</sub> O <sub>8</sub> ]	triclinic	8,14 12,79 7,16	94° 19' 116° 34' 87° 39'	2,62	1,528 1,532 1,538	Stable low-temperature modification, ordered
Analbite	Na[AlSi <sub>3</sub> O <sub>8</sub> ]	triclinic	8,23 13,00 7,25	94° 03' 116° 20' 88° 09'	2,62	1,527 1,532 1,534	
Monalbite	Na[AlSi <sub>3</sub> O <sub>8</sub> ]	monoclinic	7,25 12,98 6,41	– 116° 07' –		1,523 1,528 1,529	Instable modification, unordered
Anorthite	Ca[Al <sub>2</sub> Si <sub>2</sub> O <sub>8</sub> ]	triclinic	8,18 12,88 14,17	93° 10' 115° 51' 91° 13'	2,77	1,576 1,583 1,589	
Celsian	Ba[Al <sub>2</sub> Si <sub>2</sub> O <sub>8</sub> ]	monoclinic	8,65 13,13 14,60	– 115° 02' –	3,8	1,587 1,593 1,600	ordered

Fig. 2.3.2.3: Properties of some feldspars [1].

### 2.3.3 Quartzite and sands

Quartz also originates from a three-dimensional linkage of SiO<sub>4</sub> tetrahedra. The figures shown in Fig. 2.3.3.1 describe again the distance from the base level, for example, c axis by a factor of 0.33. The SiO<sub>4</sub> tetrahedra unscrew themselves spirally from the base level.

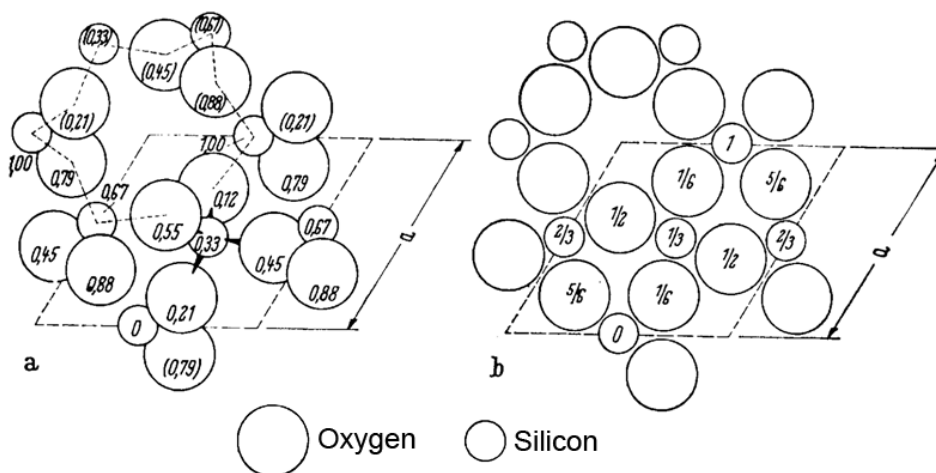


Fig. 2.3.3.1: Unit cells of low quartz (a) and high quartz (b) projected on the plan (0001) [1].

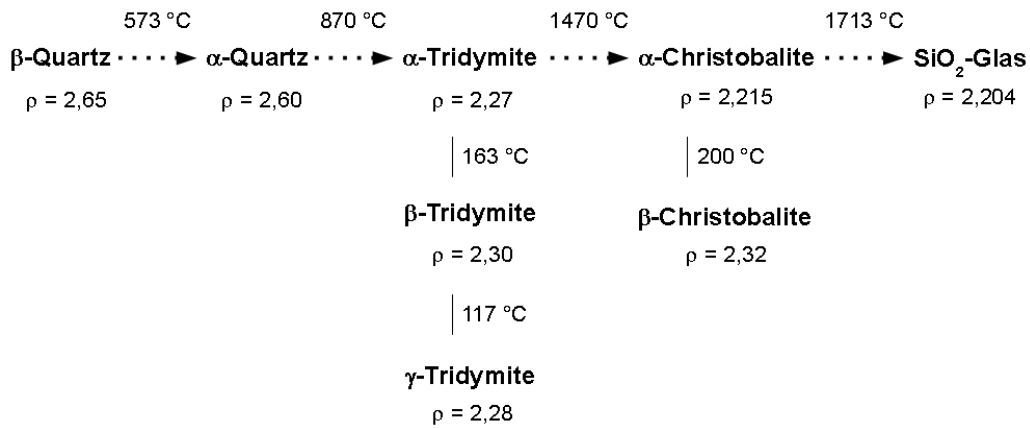


Fig. 2.3.3.2: Phase transformation of SiO<sub>2</sub> with temperature.

SiO<sub>2</sub> can be found in different crystallographic modifications (Fig. 2.3.3.2). Low temperature modification of quartz (β-quartz) into α-quartz takes place at a temperature of 573° C. Here just a marginal shift of silicon and oxygen ions can be observed. The temperature of 870°C is known as the high temperature modification of quartz to tridymite. In this case, new bonds are formed. Therefore this transformation does not happen very quickly, while the transformation from α-quartz into β-quartz is quick and unavoidable. Reconversion of tridymite into quartz can be prevented, if it is cooled very quickly, leaving no time for the structure to reconvert. Further transformations are related to α-cristobalite at 1,470°C, and SiO<sub>2</sub> melting at 1,713°C. Such transformations cause tremendous problems for the sintering of ceramic products, because they are partly combined with major volume changes. Quartz inversion at 573°C leads to a volume expansion of 0.8 %. This expansion of the volume may indeed cause cracks in the porcelain during the cooling stages, after sintering. This problem is accentuated during the quartz transformation into cristobalite or tridymite. This is accompanied by a volume expansion of more than 15 % (Fig.2.3.3.3), which after sintering causes stresses in the structure and destructs the components during cooling.

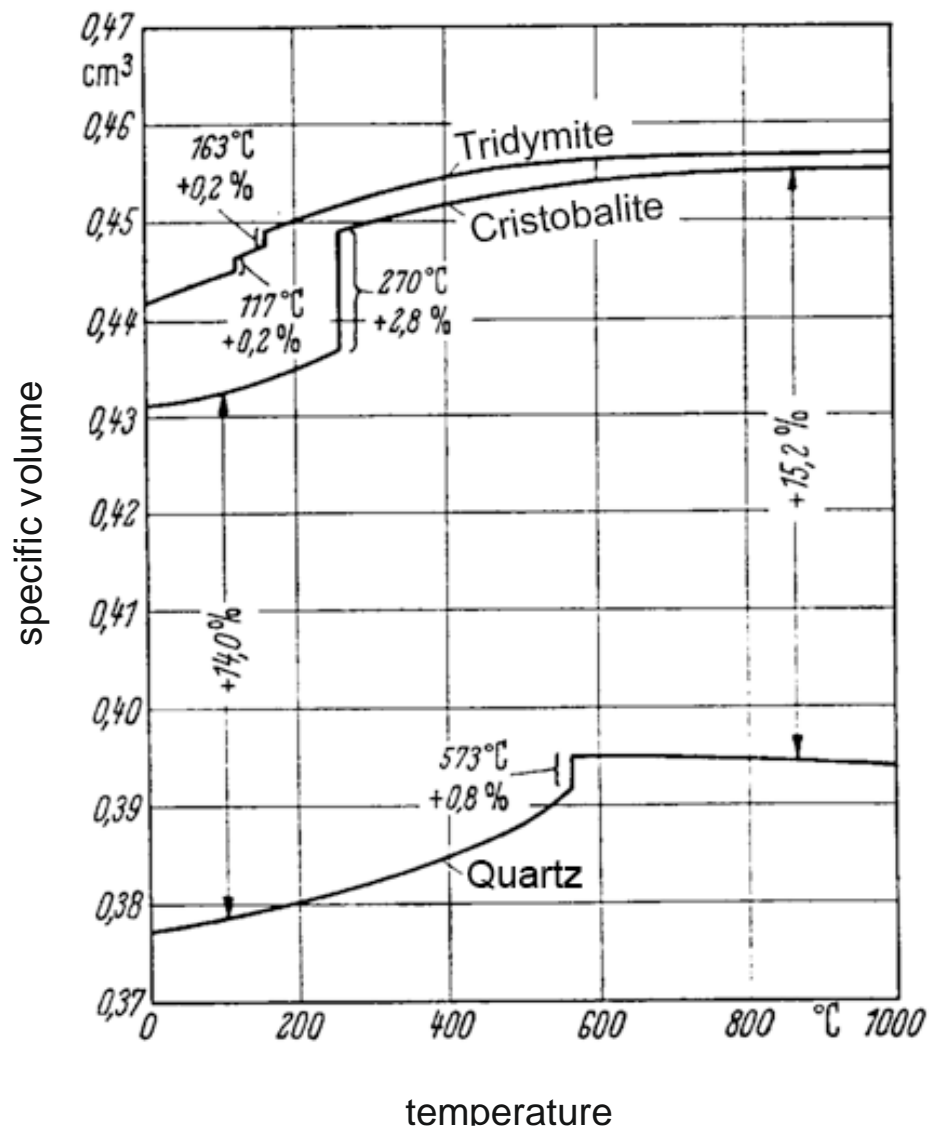


Fig. 2.3.3.3: Dependence of the specific volume on the temperature for quartz, cristobalite and tridymite [1].

Transformation temperature may change as chemical impurities are added or when the order varies (Fig. 2.3.3.4).

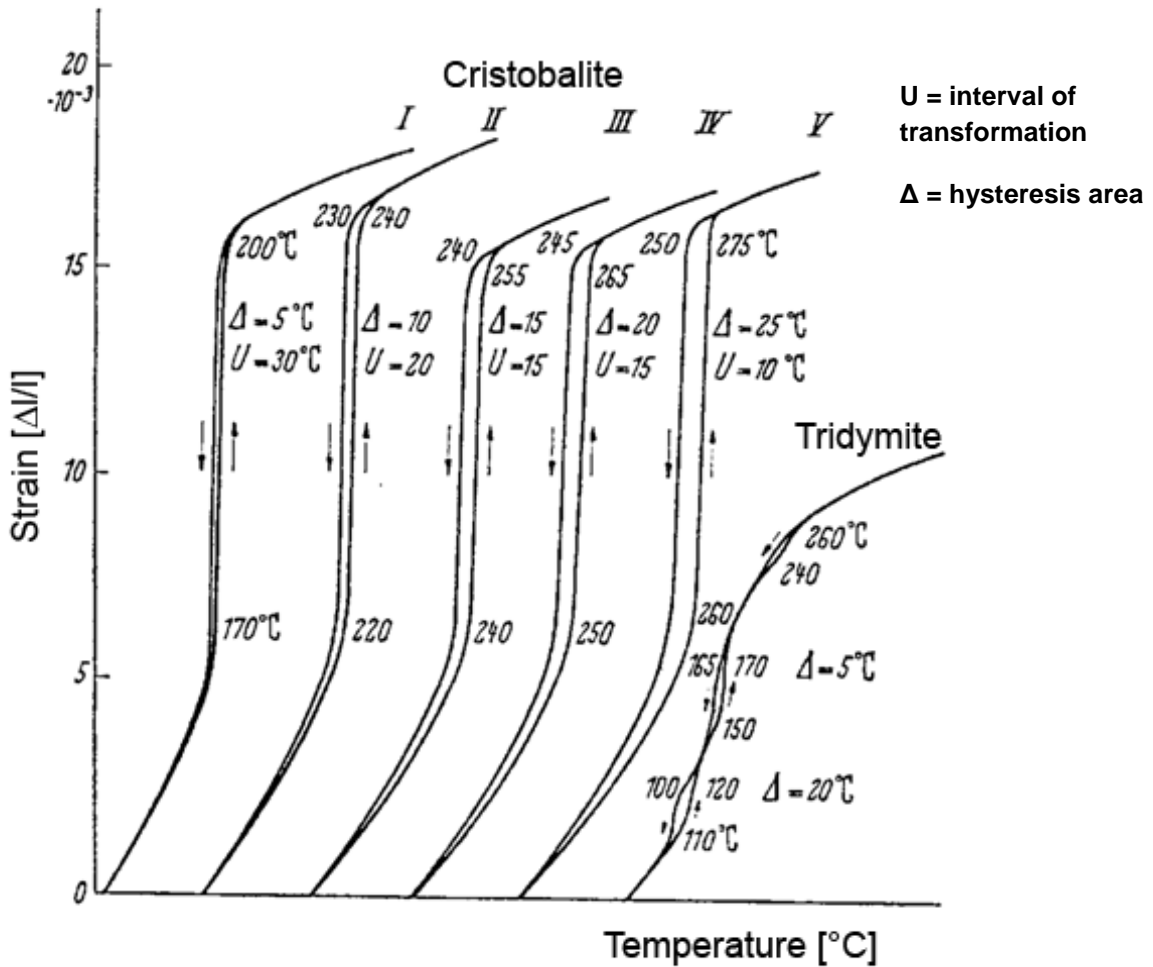


Fig. 2.3.3.4: Dilatometer curves of cristobalite with distinct degree of orientation in comparison to well-oriented tridymite [1].

If quartz after adding 5 weight % of feldspar is exposed to a temperature treatment of 1,300 $^{\circ}\text{C}$  and a holding time of 14 hours, a structure which consists of 40 % cristobalite and 60 % quartz (Fig. 2.3.3.5) can be obtained. If 2wt% CaO is added, at 1,300 $^{\circ}\text{C}$  and 14 hours holding time, almost 100% of quartz can be found in the sintered product. At 1,400 $^{\circ}\text{C}$  and a very short holding time, tridymite is formed, and at a slightly higher temperature also cristobalite. The situation changes even further if sodium is added. This means that the transformation temperature changes depending on the raw material used and their level of chemical contamination. Transformation velocities can be influenced by appropriate temperature time curves (holding times), so that stresses during cooling can be avoided.



### 2.3.4 Binary and ternary silicates, high alumina containing raw materials

Some characteristics of binary silicates are described in Fig. 2.3.4.1. Negative charges of SiO<sub>4</sub> tetrahedra can be saturated, for example, by magnesium ions (forsterite), iron ions (fayalite) or by zirconium ions (zircon). The formation of enstatite takes place if, for example, two SiO<sub>4</sub> tetrahedra are combined with each other and valence adjustment is made by magnesium ions. If silicon ions are replaced by aluminium ions and valence adjustment is made with aluminium ions, sillimanite or andalusite/mullite is formed. The systematic formation of silicates is presented in Fig. 2.3.4.2.

Mineral	Chemical formula	Crystal system	Lattice constants			Density (20 °C) [g/cm <sup>3</sup> ]	Refractive index n <sub>α</sub> n <sub>β</sub> n <sub>γ</sub>	Linear coefficient of expansion [10 <sup>-6</sup> K <sup>-1</sup> ]
			a b c	α β γ	pm			
Forsterite	Mg <sub>2</sub> [SiO <sub>4</sub> ]	orthorhombic	598 478 1025			3,21	1,636 1,651 1,669	20/1000: 11
Fayalite	Fe <sub>2</sub> [SiO <sub>4</sub> ]	orthorhombic	617 481 1061			4,35	1,824 1,864 1,875	
Zircon	Zr[SiO <sub>4</sub> ]	tetragonal	659 – 594			4,6	1,94 1,99	20/1000: 4,5
Enstatite	Mg <sub>2</sub> [SiO <sub>6</sub> ]	orthorhombic	1822 881 520			3,18	1,650 1,653 1,658	
Protoenstatite	Mg <sub>2</sub> [SiO <sub>6</sub> ]	orthorhombic	925 874 532			3,10	similar to Enstatite	20/1000: 11
Clinoenstatite	Mg <sub>2</sub> [SiO <sub>6</sub> ]	monoclinic	961 882 520	71° 40'		3,18	1,651 1,654 1,660	20/600: 8,9
Wollastonite	Ca <sub>3</sub> [Si <sub>3</sub> O <sub>9</sub> ]	triclinic	794 732 707	90° 02' 95° 22' 103° 26'		2,92	1,620 1,632 1,634	20/800: 12
Sillimanite	Al[AlSiO <sub>5</sub> ]	orthorhombic	748 767 577			3,25	1,657 1,658 1,677	25/300: 3,2 25/600: 4,6 25/900: 6,0
Andalusite	Al <sub>2</sub> [O/SiO <sub>4</sub> ]	orthorhombic	779 790 556			3,14	1,632 1,638 1,643	25/300: 8,7 25/600: 10,6 25/900: 11,9
Kyanite	Al <sub>2</sub> [O/SiO <sub>4</sub> ]	triclinic	710 774 557			3,67	1,717 1,722 1,729	25/300: 8,8 25/600: 9,2 25/900: 9,2
Mullite (3:2)	Al[Al <sub>1,25</sub> Si <sub>0,75</sub> O <sub>4,875</sub> ]	orthorhombic	754 767 283			3,16	1,642 1,644 1,654	25/1000: 4,5
Mullite (2:1)	Al[Al <sub>1,4</sub> Si <sub>0,6</sub> O <sub>4,8</sub> ]	orthorhombic	757 768 289			3,17	1,650 – 1,663	

Fig. 2.3.4.1: Properties of some binary silicates [1].

Type	Shape	Dimensionality	Silicate anion	O/Si ratio	Example	
					Name	Chemical formula
Tetrahedrons	single	0	[SiO <sub>4</sub> ] <sup>4-</sup>	4,0	Forsterite	Mg <sub>2</sub> [SiO <sub>4</sub> ]
	double	0	[Si <sub>2</sub> O <sub>7</sub> ] <sup>6-</sup>	3,5	Rankinite	Ca <sub>3</sub> [Si <sub>2</sub> O <sub>7</sub> ]
Rings	3-fold ring, single	0	[Si <sub>3</sub> O <sub>9</sub> ] <sup>6-</sup>	3,0	Benitoite	BaTi[Si <sub>3</sub> O <sub>9</sub> ]
	6-fold ring, single	0	[Si <sub>6</sub> O <sub>18</sub> ] <sup>12-</sup>	3,0	Beryllite	Al <sub>2</sub> Be <sub>3</sub> [Si <sub>6</sub> O <sub>18</sub> ]
	6-fold ring, double	0	[Si <sub>12</sub> O <sub>30</sub> ] <sup>12-</sup>	2,5	Milarite	KCa <sub>2</sub> AlBe <sub>2</sub> [Si <sub>12</sub> O <sub>30</sub> ]• ½ H <sub>2</sub> O
Chains	single	1	[SiO <sub>3</sub> ] <sup>2-</sup>	3,0	Enstatite	Mg[SiO <sub>3</sub> ]
	double	1	[Si <sub>4</sub> O <sub>11</sub> ] <sup>6-</sup>	2,75	Tremolite	Ca <sub>2</sub> Mg <sub>5</sub> [Si <sub>4</sub> O <sub>11</sub> ] <sub>2</sub> (OH) <sub>2</sub>
Sheets	single	2	[Si <sub>4</sub> O <sub>10</sub> ] <sup>4-</sup>	2,5	Kaolinite	Al <sub>4</sub> [Si <sub>4</sub> O <sub>10</sub> ](OH) <sub>8</sub>
Frameworks	–	3	[SiO <sub>2</sub> ]	2,0	Quartz	SiO <sub>2</sub>

Fig. 2.3.4.2: Systematic formation of silicates [1].

Mineral	Chemical formula	Crystal system	Lattice constants		Density (20 °C) [g/cm <sup>3</sup> ]	Refractive index n <sub>α</sub> n <sub>β</sub> n <sub>γ</sub>	Annotations
			a b [pm] c	β			
Low nepheline	Na[AlSiO <sub>4</sub> ]	hexagonal	1001 841		2,62	1,533 1,537	at 850 °C → high temperature modification at 1254 °C → high carnegieite at 690 °C → high temperature modification
High nepheline	Na[AlSiO <sub>4</sub> ]	orthorhombic	1020 1760 850		2,47		
Low carnegieite	Na[AlSiO <sub>4</sub> ]	triclinic			2,51	1,509 1,514 1,514	
High carnegieite	Na[AlSiO <sub>4</sub> ]	cubic	732		2,34	1,510	
Low leucite	K[AlSi <sub>2</sub> O <sub>6</sub> ]	tetragonal	1304 1385		2,47	1,508 1,509	at 620 °C → high temperature modification
High leucite Kaliophillite	K[AlSi <sub>2</sub> O <sub>6</sub> ] K[AlSiO <sub>4</sub> ]	cubic hexagonal	1343 2706 861		2,47 2,60	1,509 1,532 1,527	
Kalsilite	K[AlSiO <sub>4</sub> ]	hexagonal	518 869		2,59	1,542 1,539	metastable
synthetic	K[AlSiO <sub>4</sub> ]	orthorhombic	901 1567 857		2,60	1,528 1,536 1,537	stable
Petalite	Li[AlSi <sub>4</sub> O <sub>10</sub> ]	monoclinic	1176 514 752	112° 24'	2,42	1,504 1,510 1,516	stable only < 900 °C
Low spodumene	Li[AlSi <sub>2</sub> O <sub>6</sub> ]	monoclinic	952 832 525	110° 28'	3,15	≈ 1,72	at 700 °C → high temperature modification
High spodumene	Li[AlSi <sub>2</sub> O <sub>6</sub> ]	orthorhombic	1838 1061 1068		2,44	≈ 1,52	
Low eucryptite	Li[AlSiO <sub>4</sub> ]	trigonal	1353 904		2,67	1,572 1,587	at 970 °C → high temperature modification
High eucryptite	Li[AlSiO <sub>4</sub> ]	hexagonal	524 1113		2,33	1,524 1,520	

Fig. 2.3.4.3: Properties of some ternary aluminium silicates [1].



In ternary aluminum silicates the silicon atom within  $\text{SiO}_4$  tetrahedron is replaced by an aluminum atom. Valence adjustment occurs by alkali or alkaline earth ions like, for example, sodium ions (nepheline) or potassium ions (leucite) etc. (Fig. 2.3.4.3). The feldspars already mentioned belong to this group of materials.

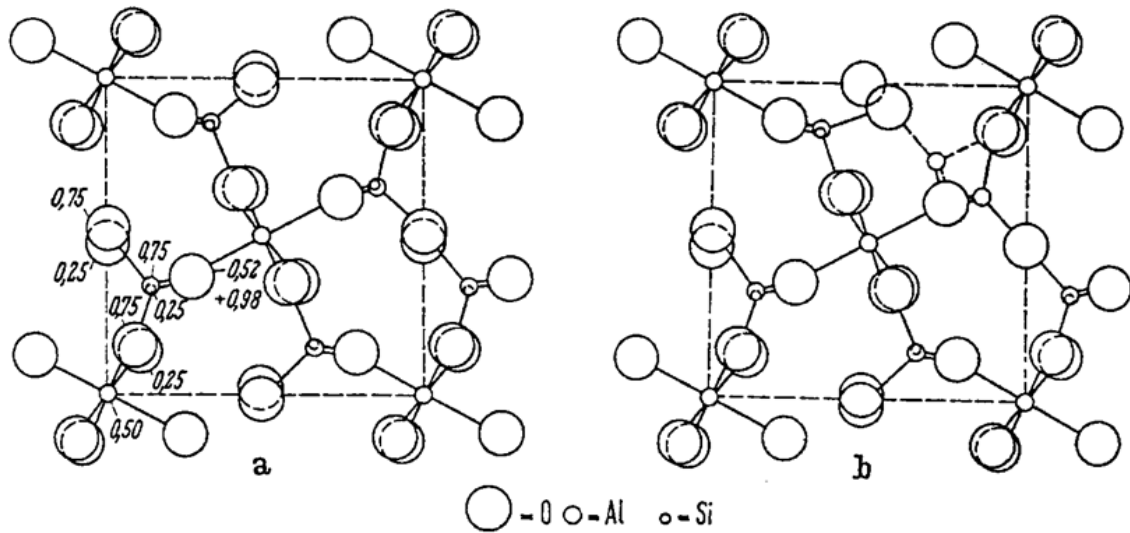


Fig. 2.3.4.4: Unit cells of sillimanite (a) and (b) mullite projected on (001) [1].

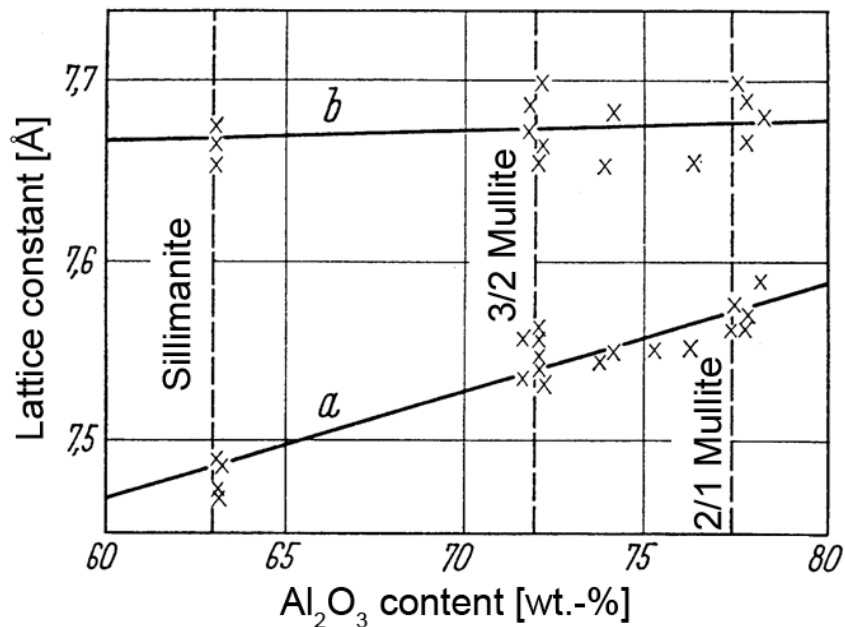


Fig. 2.3.4.5: Dependence of lattice constants  $a$  and  $b$  of sillimanite and mullite from  $\text{Al}_2\text{O}_3$ -content [1].

Sillimanite and mullite (Fig. 2.3.4.4) are  $\text{Al}_2\text{O}_3\text{-SiO}_2$  mixed crystals which are characterized by slight shifts of the lattice spacing in the crystal structure. In Fig. 2.3.4.4 tetrahedral coordinated Si atoms and Al ions in octahedral coordination can be found. So that, aluminum ions are surrounded by six oxygen ions while Si ions by four. The lattice constant changes depending on the content of alumina (Fig. 2.3.4.5).

Mineral	Crystal system	Specific weight before firing	Increase in Volume [%]	Initial temperature of mullite-crystallization [°C]
Cyanite	triclinic	3,5 to 3,6	16 to 18	1325
Andalusite	rhombic	3,1 to 3,2	3 to 6	1350
Sillimanite	rhombic	3,23 to 3,25	7 to 8	1530

Fig. 2.3.4.6: Transformation of sillimanite group materials into mullite via heating [3].

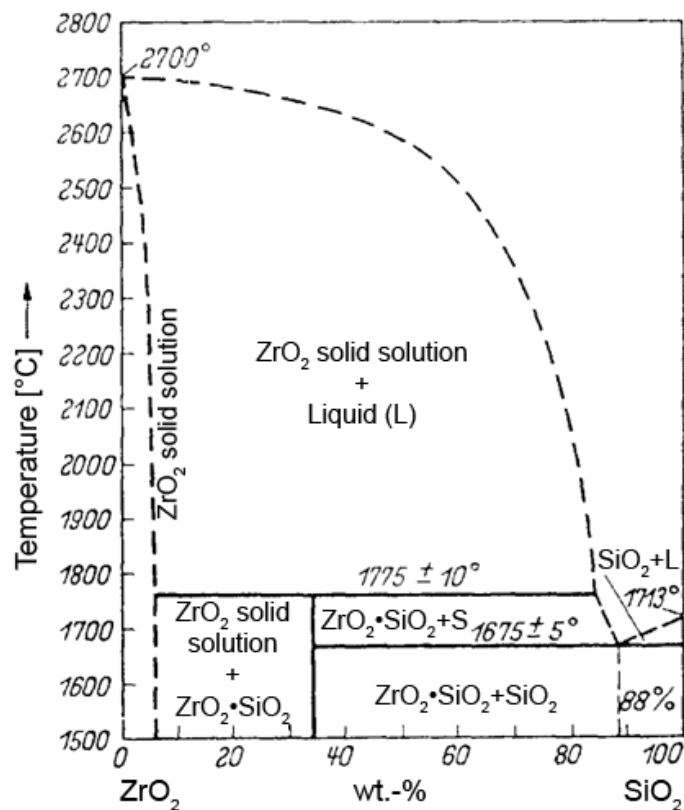


Fig. 2.3.4.7: Phase diagram for the system  $\text{SiO}_2\text{-ZrO}_2$  [adapted from R.F. Geller and S.M. Lang].

Further minerals of the sillimanite group are cyanite, andalusite and sillimanite (Fig. 2.3.4.6). Zirconia and silica form a peritectic melting compound in zirconium silicate (Fig. 2.3.4.7). Peritectic melting point means that above 1,775°C there is equilibrium between a melt and solid solutions, in which the melt portion increases by increasing the temperature. Above 2,600°C the solid solution is completely melted.

Name	Chemical formula	Amount of Al <sub>2</sub> O <sub>3</sub> (theoretical) [%]	Amount of water (theoretical) [%]	Specific weight	Shrinkage [%]	Transformation temperature [°C]	transforms into
Diaspor	$\alpha\text{-Al}_2\text{O}_3 \cdot \text{H}_2\text{O}$	85,0	15	3,36	–	450	$\alpha\text{-Al}_2\text{O}_3$
Boehmite	$\gamma\text{-Al}_2\text{O}_3 \cdot \text{H}_2\text{O}$	85,0	15	3,01	33	280	$\gamma\text{-Al}_2\text{O}_3$
Hydrargillite (Gibbsite)	$\gamma\text{-Al}_2\text{O}_3 \cdot 3 \text{H}_2\text{O}$	64,5	34,6	2,3 bis 2,4	60	150	Boehmite
Bayerite	$\text{Al}_2\text{O}_3 \cdot 3 \text{H}_2\text{O}$	64,5	34,6	–	60	150	Boehmite

Fig. 2.3.4.8: Properties and heating behavior of hydrated alumina [3].

Diaspor, boehmite, hydrargillite und bayerite (Fig. 2.3.4.8) belong to these high alumina containing raw materials. Al<sub>2</sub>O<sub>3</sub> can be produced from such Al-hydroxides by calcination.

## 2.4 Synthetic ceramic raw materials

### 2.4.1 Silicates

Depending on the charge, natural raw materials may show slightly differing chemical compositions or different grain size distributions. This makes processing in manufacturing plants occasionally difficult. And this is the reason for experiments to produce silicates synthetically.

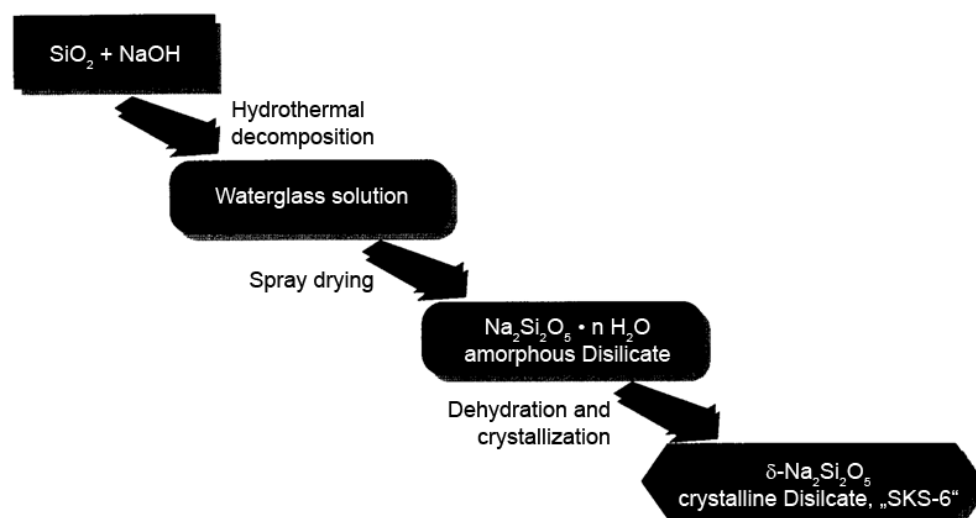


Fig. 2.4.1.1: Production of synthetic, amorphous and crystalline sodium disilicates.

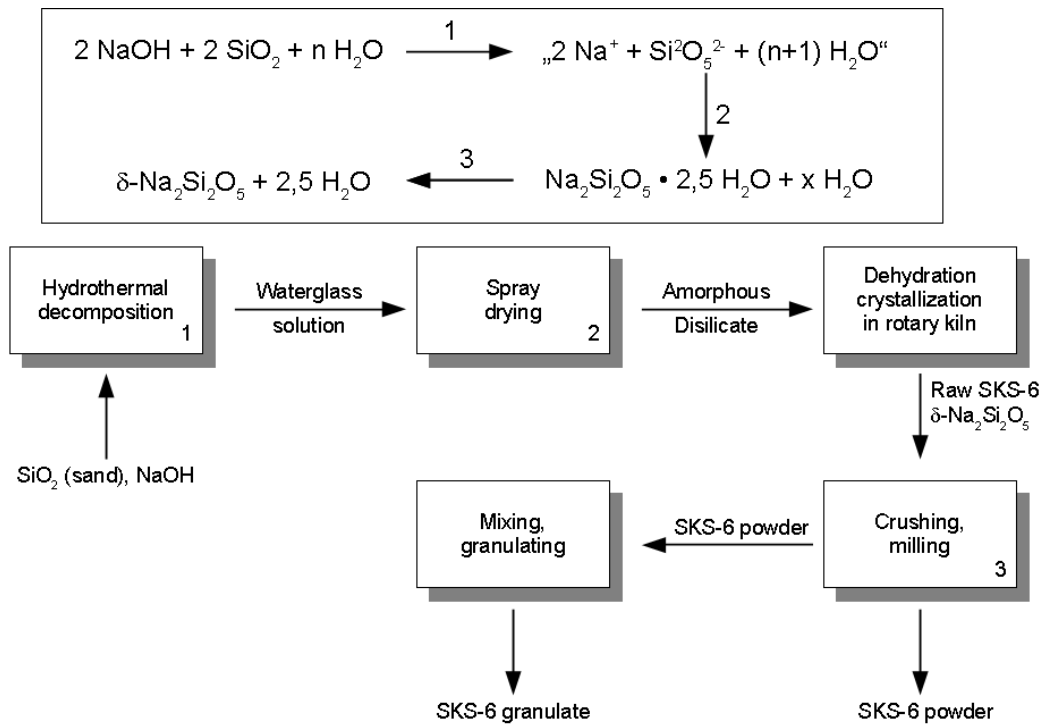


Fig. 2.4.1.2: Production of SKS-6 and SKS-6-Co- Granulate at Hoechst.

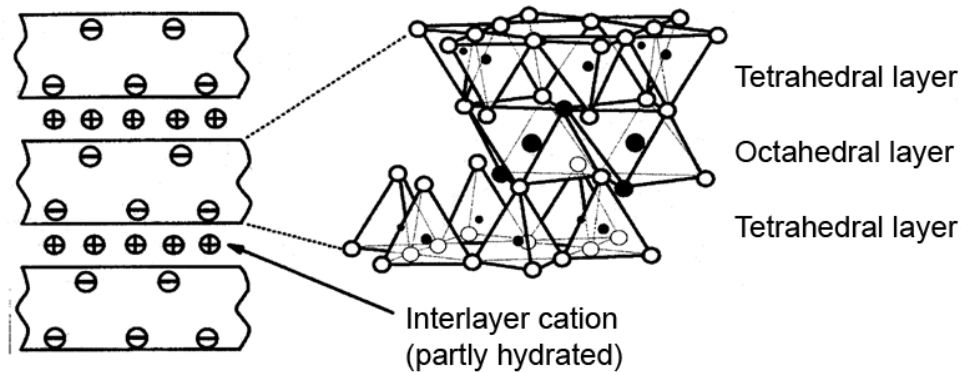
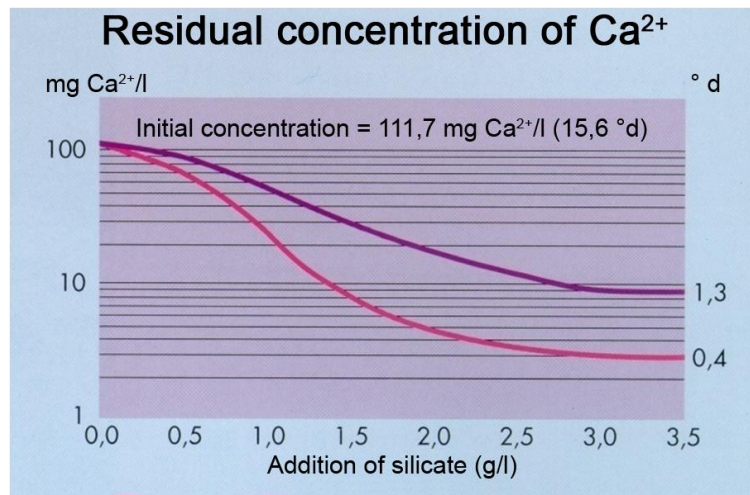


Fig. 2.4.1.3: Structure from amorphous and crystalline synthetic sodium-disilicate (Hoechst).

For the production of synthetic silicates SiO<sub>2</sub> is hydrothermally solubilised with caustic soda (Fig. 2.4.1.1 and Fig.2.4.1.2). This leads to an aqueous water-glass solution which is spray dried. The result is an amorphous disilicate which after further dewatering is transformed to a crystalline disilicate. The crystal structures consist of tetrahedron and octahedron layers with water in the interlayers, just like the natural layer silicates (Fig. 2.4.1.3).

As these synthetic silicates are stirred in water, calcium ions from the water get integrated into the interlayers and the water is softened (Fig.2.4.1.4). Compared to natural layer silicates, the pureness of these synthetic materials is an advantage (fig.2.4.1.6). The content of alumina and silica is comparable. But there are clear differences with regard to the iron content which is particularly responsible for the raw materials' discoloration. Synthetic kaolins could never establish in ceramic industries because of their high production costs. But they are used, for example, for water softening within detergents industries.



Besides the type of water softening element, the effectiveness of the builder in removing these elements is also important. Here, the difference in effectiveness especially at higher additions of amorphous or crystalline di-silicates.

Fig. 2.4.1.4: Different properties form SKS-6 (Hoechst).

Elements	Natural	Synthetic
Al <sub>2</sub> O <sub>3</sub>	30,1%	31,7%
SiO <sub>2</sub>	47,7%	48,1%
Na <sub>2</sub> O	0,08%	0,3%
K <sub>2</sub> O	1,2%	0,01%
MgO	-	0,03%
Fe <sub>2</sub> O <sub>3</sub>	0,76%	0,03%
H <sub>2</sub> O (110°C)	n.d.	5,6%
Weight loss	14,4%	17,6%

Fig. 2.4.1.5: Chemical composition of synthetic and natural kaolins.

### 2.4.2 Oxides

All oxides of the periodic table elements belong to ceramic materials. Fig. 2.4.2.1 shows a small selection of the most important oxides which are very attractive due to their field of application. Among them we find beryllium oxide, magnesium oxide, calcium oxide, alumina, yttria, zirconia as well as hafnium and thorium oxide, which have extremely high melting temperatures. Ceramic oxide materials are characterized by their ionic bond and therefore show no electronic conductivity. This explains the high specific electrical resistance.

Oxide	Density [g / cm <sup>3</sup> ]	Melting point [°C]	Coefficient of expansion $\alpha_{20/1000}$ 10 <sup>-6</sup> / K	Thermal conductivity		Young's modulus at 25 °C GN / m <sup>2</sup>	Specific electrical resistance at	
				100 °C W / (m · K)	1000 °C W / (m · K)		225 °C $\Omega \cdot \text{cm}$	1000 °C $\Omega \cdot \text{cm}$
BeO	3.01	2570	8,9	210	20	390	10 <sup>14</sup>	10 <sup>8</sup>
MgO	3.57	2840	14,0	35	7	310	10 <sup>14</sup>	10 <sup>7</sup>
CaO	3.32	2580	13,0	14	7	–	10 <sup>14</sup>	10 <sup>6</sup>
Al <sub>2</sub> O <sub>3</sub>	3.99	2050	8,3	25	6	410	10 <sup>14</sup>	10 <sup>8</sup>
Y <sub>2</sub> O <sub>3</sub>	4.50	2450	8,0	14	3	180	–	–
ZrO <sub>2</sub>	5.56	2680	10,0 <sup>a</sup>	2 <sup>a</sup>	2 <sup>a</sup>	240 <sup>a</sup>	10 <sup>11a</sup>	10 <sup>a</sup>
	mon. 6.10							
	tetr.							
HfO <sub>2</sub>	9.68	2900	10,0 <sup>a</sup>	–	–	–	–	–
	mon. 10.0							
	tetr.							
ThO <sub>2</sub>	10.05	3220	9,0	10	3	240	10 <sup>14</sup>	10 <sup>5</sup>

<sup>a</sup> stabilized, only for support

Fig. 2.4.2.1: Properties of high-melting oxides [1].

**Bauxite** = mixture of different aluminum oxide hydrates, with traces of iron hydroxide, silicate and Ti

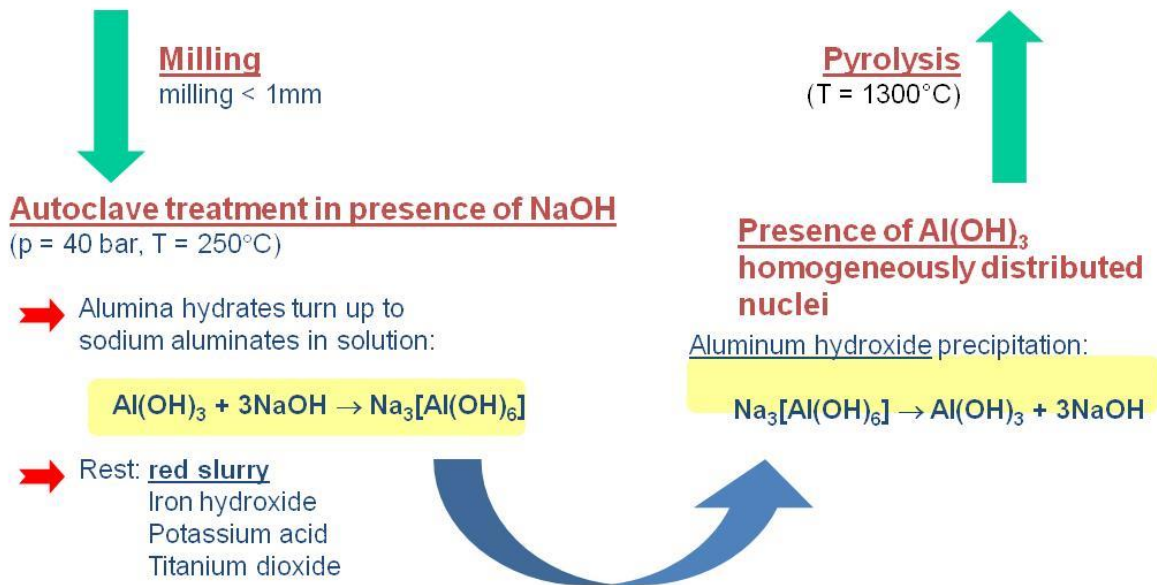


**Fig. 2.4.2.2:** Illustration of production of Al<sub>2</sub>O<sub>3</sub> from bauxite according to the Bayer process.

Exemplary for alumina, Fig. 2.4.2.2 shows how this synthetic oxide is made from natural raw materials. Bauxite as a natural raw material is the basic material for the production of aluminum oxide. Bauxite is a mixture of different aluminum hydroxides, contaminated with iron hydroxides, silicates and titanium oxides. First the raw materials are grinded to a grain size of < 1 mm. Then they are processed with sodium hydroxide in an autoclave at a pressure of 40 bars and a temperature of about 250°C. A sodium aluminate solution is formed dissolving the alumina hydrates as aluminates. Iron oxide, titanium oxide and SiO<sub>2</sub> remain undissolved. This so-called red mud (red coloration caused by iron hydroxide) can be separated by filtration from the sodium aluminate. Aluminum hydroxide seed crystals are now dispersed in the aluminate solution and aluminum hydroxide again crystallizes and can be separated by filtration from the sodium hydroxide. This aluminum hydroxide is transformed into aluminum oxide by a thermal treatment in a rotary kiln. Because of the sodium hydroxide and the high temperatures this is a relatively crucial production process, if aluminum oxide is produced in ton sizes.

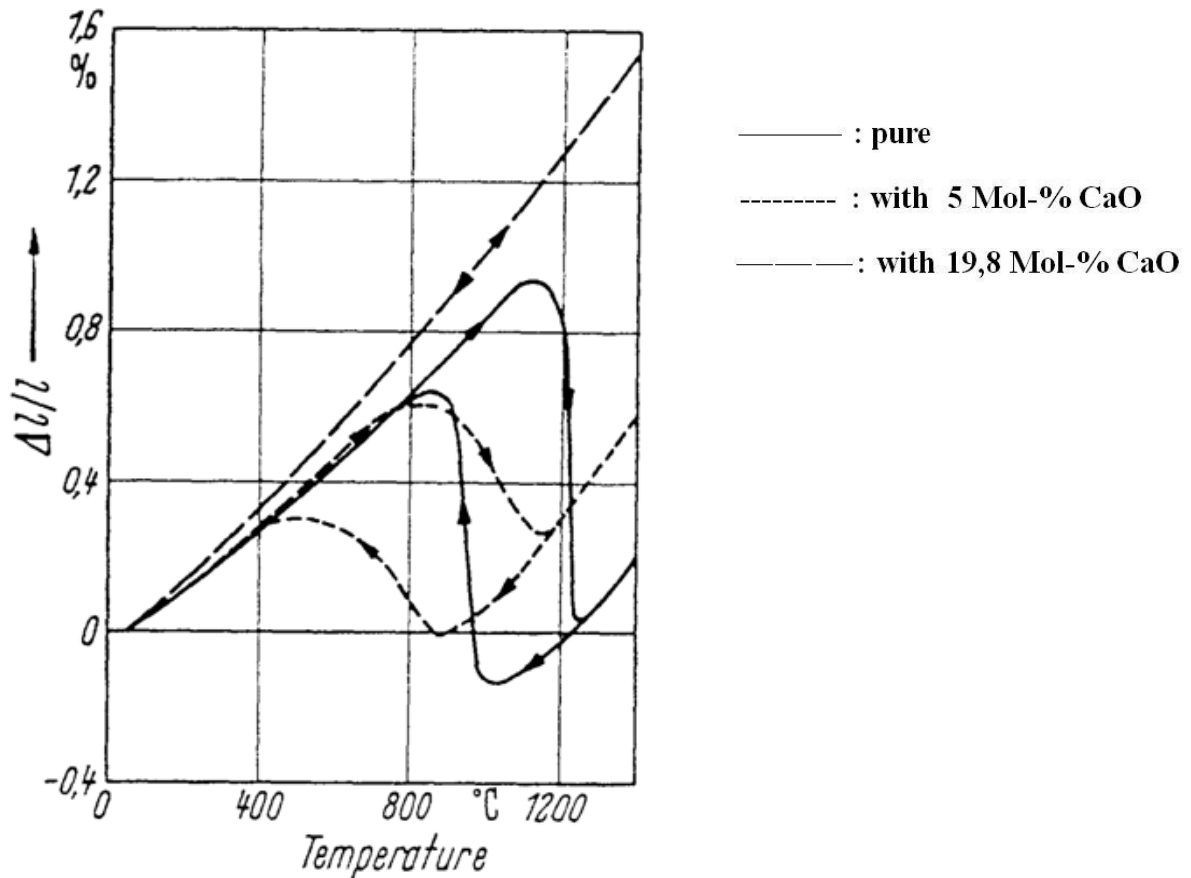


Fig. 2.4.2.3: Dilatometer curve of ZrO<sub>2</sub> [1].

Zirconia is another interesting oxide. ZrO<sub>2</sub> shows particularly problematic properties. Depending on temperature, it changes to various crystal modifications, partly causing big volume changes (Fig. 2.4.2.3). At slightly above 1,000°C the low temperature modification of ZrO<sub>2</sub> changes to high temperature modification. This may, for instance, occur during sintering. Reconversion happens during cooling. Normally this occurs at slightly lower temperatures, and a hysteresis loop is shown. Broadness of the hysteresis loop depends on the cooling rate. The enormous volume changes cause stresses and cracks, and this is the reason why components cannot be made of pure ZrO<sub>2</sub>. This crystal transformation can be prevented, if almost 20 mol% calcium are added, which causes a solid solution formation. Such volume transformations occur in many ceramic materials and have to be considered for the production of ceramic products. To achieve a product free from cracks, these crystal transformations must be avoided.



### 2.4.3 Non-oxide materials

Non-oxide ceramic materials comprise the elements silicon, nitrogen, carbon, boron and aluminium. The chemical compounds herein are: BN, Si<sub>3</sub>N<sub>4</sub>, AlN, SiC, B<sub>4</sub>C, SiB<sub>4(6)</sub>. The elements of which the mentioned compounds result, stand within the periodic table all relatively far to the right. This means that their electronic configuration in the outer orbital has been already relatively completed. Therefore, the different elements provide each other with electrons for covalent bonds without electronic conductivity, what is a typical characteristic of the ceramic materials. Further left on the periodic table, the elements like titanium, hafnium or zircon which also form carbides with carbon or nitrides with nitrogen can be found. Due to the presence of metallic bonds and their electronic conductivity, they are no far considered as ceramics.

Process	Reaction
<p><b>Synthesis from Components</b></p> <p>a) via Melting</p> <p>b) via Sintering</p> <p>Carburization with gases containing carbon</p> <p>Precipitation from gaseous phase</p> <p>Conversion into metal melt</p> <p>Chemical isolation of carbides and polycrystalline carbide</p> <p>fused-salt electrolysis</p>	$\text{Me(H)} + \text{C} \rightarrow \text{MeC} + (\text{H}_2)$ $\text{MeO} + \text{C} \rightarrow \text{MeC} + (\text{CO}_2)$ $\text{Me} + \text{C}_x\text{H}_y \rightarrow \text{MeC} + (\text{H}_2)$ $\text{Me} + \text{CO} \rightarrow \text{MeC} + (\text{CO}_2)$ $\text{Me-halogenide} + \text{C}_x\text{H}_y + \text{H}_2 \rightarrow \text{MeC} + (\text{hydrogen}) + \text{C}_m\text{H}_n + (\text{H}_2)$ $\text{Me-Carbonyl} + \text{H}_2 \rightarrow \text{MeC} + (\text{CO}, \text{CO}_2, \text{H}_2, \text{H}_2\text{O})$ $(\text{Fe}) + \text{Me} + \text{C} \rightarrow \text{MeC} + (\text{Fe})$ $(\text{Ni}) + \text{Me}_1 + \text{Me}_2 + \text{C} \rightarrow (\text{Me}_1, \text{Me}_2)\text{C} + (\text{Ni})$ $\text{MeO} + \text{Alkalikarbonat} + \text{Alkali borate} + \text{Alkali-Fluoride} \rightarrow \text{MeC} + (\text{Alkali-Bor-Fluor-Mixture}) + (\text{O}_2)$

Fig. 2.4.3.1: Production of carbides.

The raw materials necessary for the production of these ceramic materials are not found in nature, but made synthetically. Fig. 2.4.3.1 shows carbides as an example for these synthesis pathways. Carbides can be made from the elements, by carbothermal reduction or by chemical vapour deposition. With regard to the elements, silicon reacts at appropriate temperatures with carbon to SiC. Such production of silicon carbide in ton sizes is too expensive. Far more often, SiC is produced by a carbothermal reduction in which quartz

powder (sand) reacts with carbon to SiC and CO<sub>2</sub>. SiC can be then produced in large-scale productions. If for scientific purposes there is a need to use high-purity SiC, the SiC should be produced from the gas phase by allowing, for example, silicon tetrachloride to react with CH<sub>4</sub> to SiC and HCl.

Process	Reaction
<p><b>Nitration of metal oxides in presence of carbon</b></p> <p><b>Nitration of Metals and Hydrides</b></p> <p><b>Conversion of metal chlorides and metal oxychlorides with NH<sub>3</sub></b></p> <p><b>Decomposition of Ammonium-compounds</b></p> <p><b>Conversion of oxides with calcium nitride</b></p> <p><b>Precipitation from Gaseous Phase</b></p>	<p><math>\text{MeO} + \text{N}_2 (\text{NH}_3) + \text{C} \rightarrow \text{MeN} + (\text{CO} + \text{H}_2\text{O} + \text{H}_2)</math></p> <p><math>\text{Me} + \text{N}_2 (\text{NH}_3) \rightarrow \text{MeN} + (\text{H}_2)</math></p> <p><math>\text{MeH} + \text{N}_2 (\text{NH}_3) \rightarrow \text{MeN} + (\text{H}_2)</math></p> <p><math>\text{MeCl}_4 + \text{NH}_3 \rightarrow \text{MeN} + (\text{HCl})</math></p> <p><math>\text{MeOCl}_3 + \text{NH}_3 \rightarrow \text{MeN} + (\text{HCl} + \text{H}_2\text{O} + \text{H}_2)</math></p> <p><math>\text{NH}_4\text{MeO}_3 + \text{NH}_3 \rightarrow \text{MeN} + (\text{H}_2\text{O} + \text{H}_2)</math></p> <p><math>\text{MeO} + \text{Ca}_3\text{N}_2 \rightarrow \text{MeN} + (\text{CaO})</math></p> <p><math>\text{Me-Halogenide} + \text{N}_2 + \text{H}_2 \rightarrow \text{MeN} + (\text{H})</math></p>

Fig. 2.4.3.2: Production of nitrides.

Production of nitrides can be made similarly (Fig. 2.4.3.2): via the elements, by carbothermal reduction and from the gas phase. Via the elements: silicon reacts with nitrogen to Si<sub>3</sub>N<sub>4</sub>. Via carbothermal reduction: quartz powder reacts with ammonia to Si<sub>3</sub>N<sub>4</sub> and H<sub>2</sub>. From the gas phase: silicon tetrachloride reacts with NH<sub>3</sub> to silicon nitride and hydrochloric acid (SiCl<sub>4</sub>+NH<sub>3</sub>-Si<sub>3</sub>N<sub>4</sub>+HCl). The same applies for borides and silicides. For shaping processes these synthetic materials have to be grinded and crushed, purified and mixed to ceramic masses.

## 2.5 Organic raw materials

Fig. 2.5.1 shows the mechanism of action of different organic additives in ceramic masses. More than 95 % of the ceramic materials are processed as suspensions either during their preparation or during shaping. In many cases the required solvent is water, but organic solvents can be also used. Binders, wetting agent, defoaming or conservation agents are normally added to the suspensions. Binders increase the body's green strength often necessary for the transport of the parts after shaping to the kilns. The binders can be modified by adding plasticizers or softeners. Releasing and anti-blocking agents reduce the friction in compression moulds and increase the powder consolidation. So, normally ceramic masses consist of ceramic powders and a large number of organic additives.

<i>Components</i>	<i>Function</i>
<b>Ceramic Powder</b>	<b>Matrix</b>
<b>Sintering Additives</b>	<b>Consolidation agent</b>
<b>Solvent</b>	<b>Dispersion</b>
<b>Deflocculant</b>	<b>Control of surface charge and pH-Value, dispersion</b>
<b>Dispersant/Surfactant</b>	<b>De-Agglomeration</b>
<b>Wetting agent</b>	<b>Reduction of the surface tension</b>
<b>Anti-foaming</b>	<b>Reduction/Elimination of foaming</b>
<b>Conserving agents</b>	<b>Prevention from bacteria or algae formation</b>
<b>Binder</b>	<b>Mechanical strength of the green body</b>
<b>Plasticizer</b>	<b>Flexibility</b>
<b>Softener</b>	<b>Flexibility</b>
<b>Lubricant</b>	<b>Reduction of attrition with matrix/moulds</b>

Fig. 2.5.1: Function of the different components in ceramic masses.

In Fig. 2.5.2 the variety of organic additives for different shaping processes is shown. Prior to the sinter, the additives must be burn out or must be regained by condensation.

Dry Pressing	Polyacrylates, huminates	Dispersants
	Polyvinyl alcohols, tyloses, waxes	Binder
	Polyethylene glycols	Flow agent
Slip Casting	Polyacrylates, fish oil	Dispersants
	Polyvinyl alcohols, modified	Binder
	Polysaccharides, polyvinyl butyrals	
	Water, trichlor ethylene, ethanol	Dispersing agents
Tape Casting	Oleates, polyacrylates, Fish oil,	Dispersants
	Phosphoric acid ester	
	Polyvinyl butyrals, polyvinyl alcohols,	Binder
	Acrylic resin, plastic dispersions	
	Phthalates, polyethylene glycols,	Softener
	Phosphoric acid ester	
Injection moulding	Toluol, trichloroethylene, methanol,	Dispersion agents
	Ethanol, methyl isobutyl ketone, water	
Extrusion	Oleates, polyacrylates	Dispersants
	Polyethylene, polystyrene, waxes	Binder (Dispersants)
	Polyethylene glycols	Flow agents
	Caster Oil	Porosity inducing agents

Fig. 2.5.2: Function of organic additives in dependence of the processing technology.

Fig. 2.5.3 shows additives for aqueous and non-aqueous tape casting. There are different binders, plasticizers, condensers and wetting agents depending on the nature of the solvent, if organic solvents and water based solvents.

Solvents	Binders	Plasticizers	Deflocculants	Wetting agents
Non-aqueous				
Acetone	Celluloseacetate	Butylbenzylphtalate	Fatty acids (Glyceryl-tri-oleate)	Alkylaryl polyether alcohol
Ethyl alcohol	Butyrate resin	Butylstearate	Natural Fish oils (Menhaden)	Polyethyleneglycol-thylether
Benzole	Nitrocellulose	Dibutylphtalate	Synthetics (Benzene sulfonic acids)	Athylphenylglycol
Bromochloromethane	Petroleum resin	Dimethylphtalate		Polyoxyethylenacetate
Butanol	Polyethylene	Methylabietate		Polyoxethylenester
Diacetone	Polyacrylate ester	Mixed Phtalate esters (Hexal-, octyldecylalcohol)		
Ethanol	Polymethylmethacrylate	Polyethyleneglycol		
Isopropanol	Polyvinyl-alcohol	Polyalkylenglycol		
Methylic isobutylketone	Polyvinyl-butyril resin	Polyalkylenglycol derivates (Triethyleneglycol-hexoat)		
Toluol	Polyvinyl-chloride	Trikresylphosphate		
Trichlorethylene				
Xylol				
Aqueous				
Water (with antifoaming agents based on resins)	Acrylic polymer Acrylic polymer emulsion Ethylenoxide polymer Hydroxyethylencellulose Methylcellulose Polyvinylalcohol TRIS. Isocyanate Resin based sliding additives	Butylbenzylphtalate Ethyltoluolsulfonamide Glycerine Polyalcyleneglycol Triethyleneglycol Tri-N-butylphosphate	Complex vitreous phosphates Condensed arylc sulfoic acid Natural sodium salt	Non-ionic octylphenoxyethanol

**Fig. 2.5.3:** Additives for tape casting of aqueous and non-aqueous slurries.

Generally, binders or plasticizers are used to increase the interval of ignition and avoid crack formation during burn out. This makes the whole system very complex and the understanding of the ignition products is extremely difficult.

To understand the coupling behaviour of organic additives on surfaces of oxidic ceramic particles, we observe the surface of an aluminium oxide particle (Fig. 2.5.4). Ceramic powders normally have a high specific surface and show electric charges in aqueous suspensions. Such electric charges may be explained as follows: oxides show unsaturated valences at their surface due to the incomplete coordination of atoms. When this oxide surface gets in contact with water the surface becomes hydrated. Once these particles are linked to air humidity their surfaces hydrate. The number of the developing -OH groups at the surface depends on the number of oxygen atoms at the surface, and this in turn depends on the crystal structure. With regard to aluminium oxide the oxygen ions are saturated with hydrogen at a pH value of 9, this means that at this pH value the particles are electrically neutral.

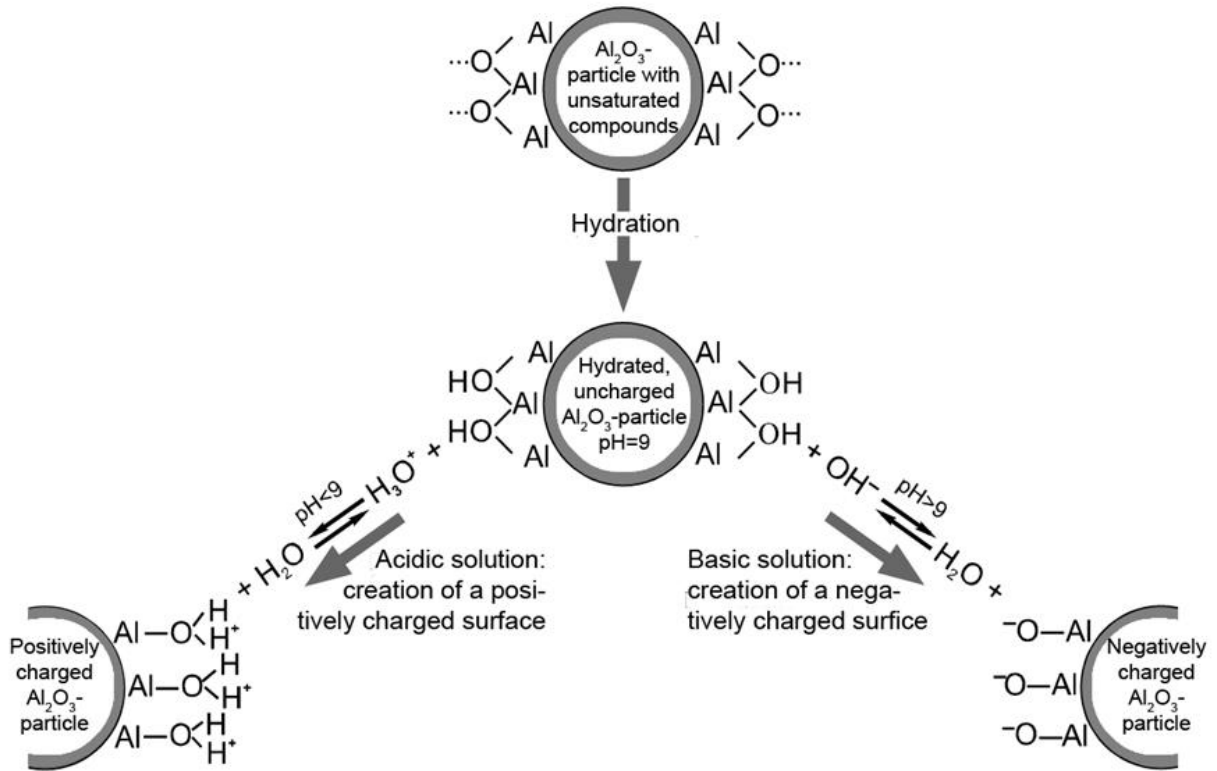


Fig. 2.5.4: Creation of a hydrated Al<sub>2</sub>O<sub>3</sub> particle surface and its reaction in acidic and basic solutions (schematic).

As the pH value is shifted to an alkaline value (by adding -OH) an OH group combines with a hydrogen ion, adsorbs water and a negatively charged surface. When H<sub>3</sub>O<sup>+</sup> is added, water regenerates and an additional proton adsorbs onto the surface, therefore a positively charged surface is formed. According to the pH value ceramic particles' surfaces can be charged positively or negatively. Organic molecules can be coupled to these positively or negatively charged surfaces. In Fig. 2.5.5 oleates adsorbed into an aluminium oxide particle surface is shown. These long-chain molecules prevent particles to agglomerate into a suspension. This is called steric stabilisation. Fig 2.5.6 shows schematically the steric constraint of the powder particles' approach to a suspension by adsorbing long-chain molecules.

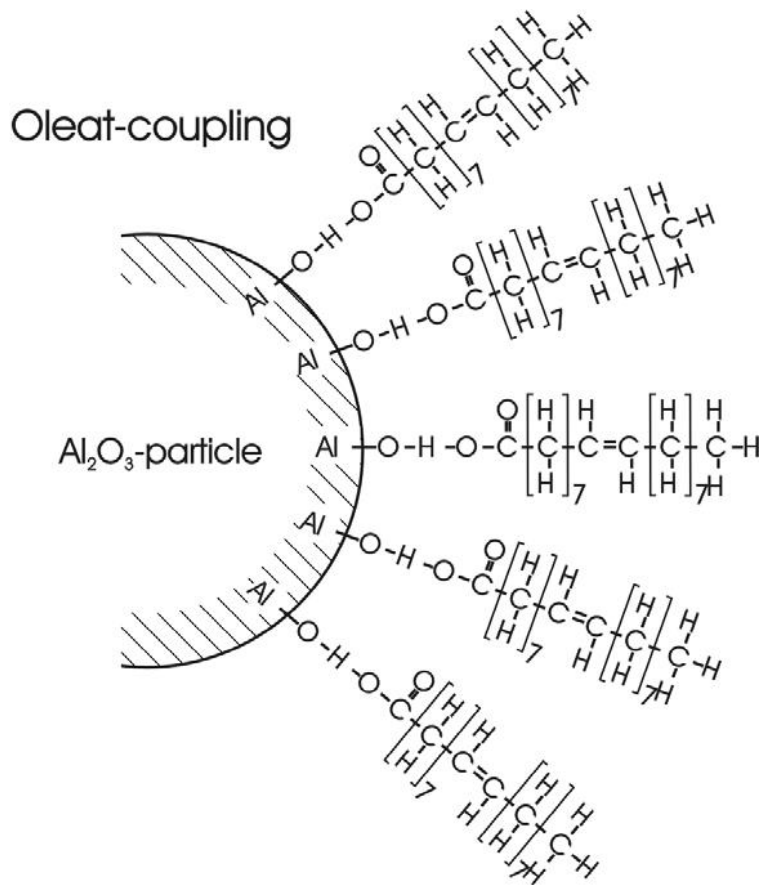


Fig. 2.5.5: Oleate coupling to  $\text{Al}_2\text{O}_3$  surface (schematic).

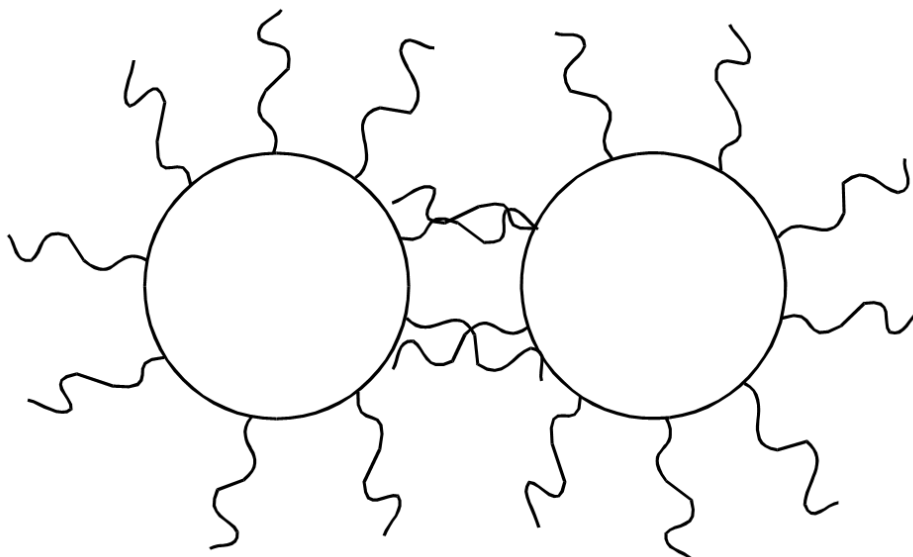


Fig.2.5.6: Steric hindrance due to the approach of powder particles in a suspension by long-chain molecules settled down (schematic).

When negatively or positively charged, surfaces reject each other. It is referred to as electrostatic stabilisation (Fig. 2.5.7). Ceramic particles do not sediment in well dispersed ceramic suspensions, the so-called stabilized suspension.

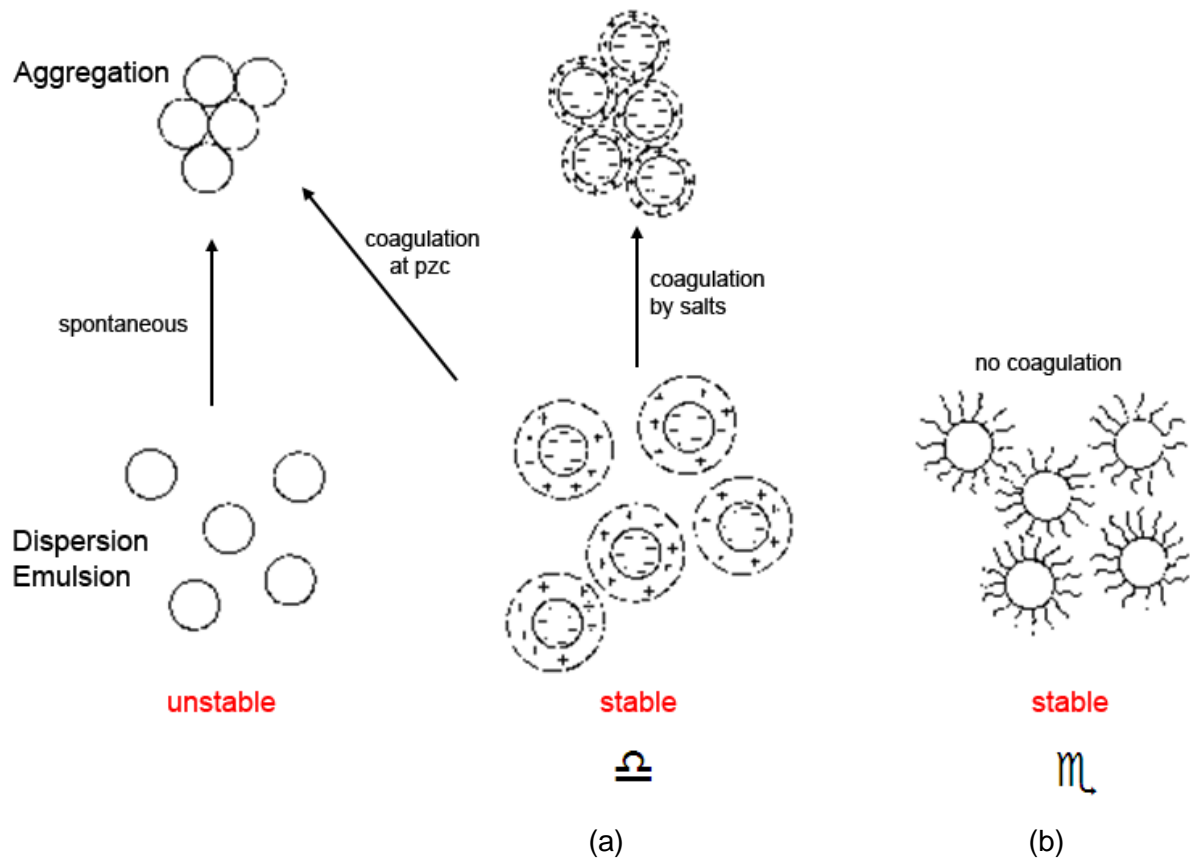


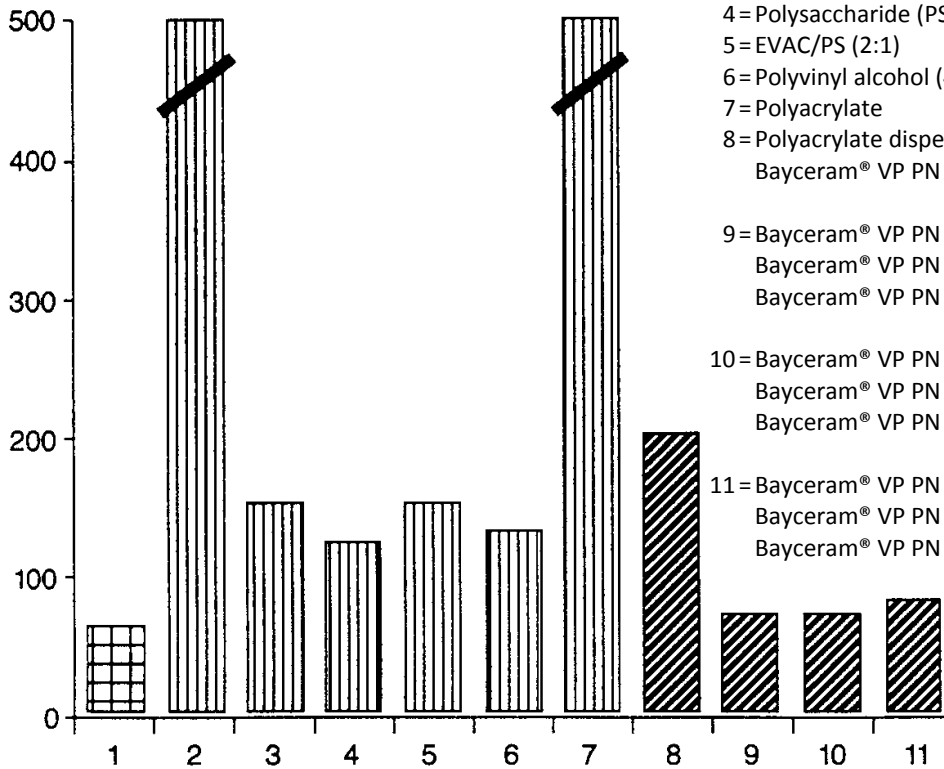
Fig. 2.5.7: Electrostatic (a) and steric (b) stabilisation of colloid dispersions and emulsions [G. Lagaly, Universität Kiel].

In most cases, organic additives are not an exactly defined chemical product. They often show a broad distribution of their molecule chain's length. This can lead to changes during processing. Therefore, the so-called di-block copolymers were developed (Fig. 2.5.8); the length of the adherent and the stabiliser blocks can be variable and then the characteristics could be systematically investigated. Attempts have also been made to understand which crack products occur if these additives are burned out under inert gas or oxygen atmosphere.





Viscosity  
at 440 1/s  
[mPa•s]



Concentration of additive: 0,7 % (solid/solid), Liquifier: 0,3 % polyacrylic acid salt



**Fig. 2.5.9:** Change in viscosities of 64.4% commercial available slurries of porcelain mass due to the presence of different additives.

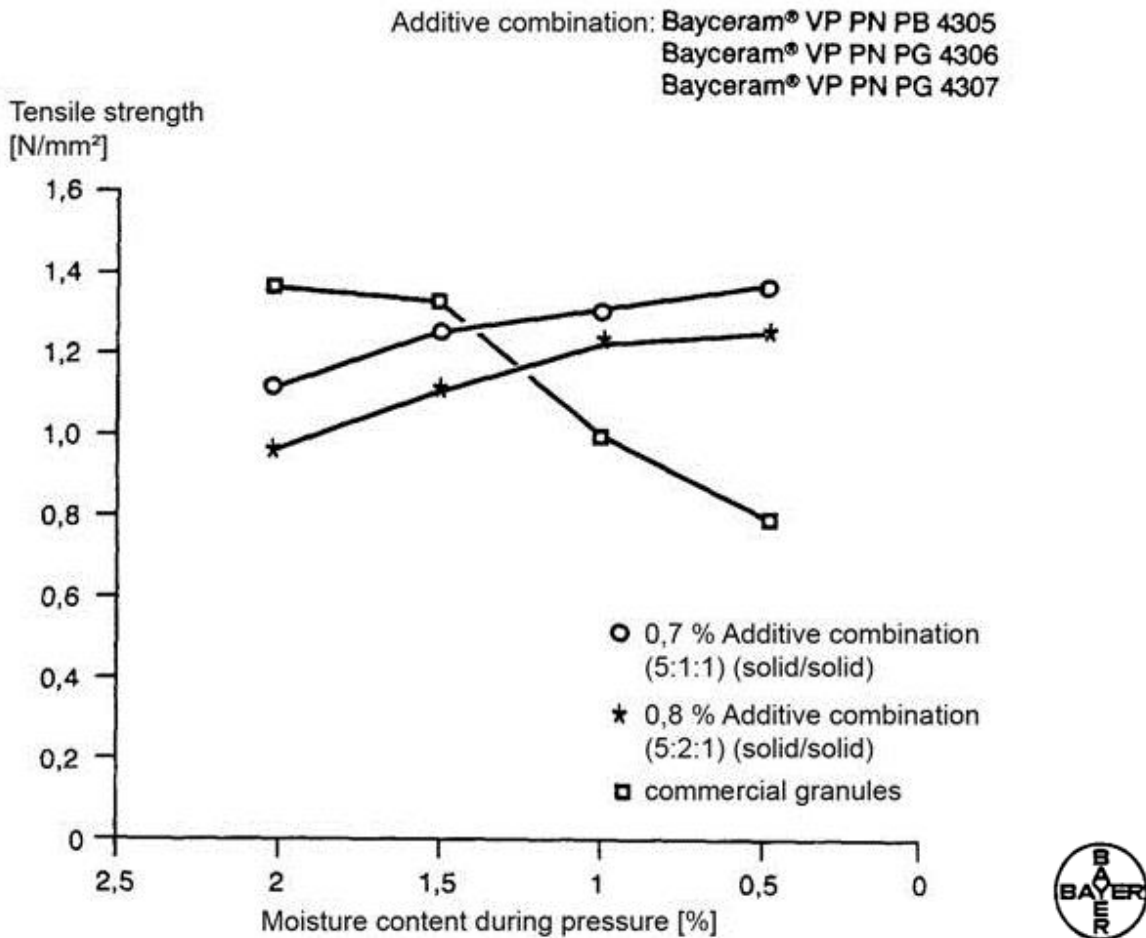


**Fig. 2.5.10:** Influence of the humidity content on the green strength of spray dried granulates due to the addition of Bayceram®.

Fig 2.5.11 shows a typical curve of the mass loss of organic additives depending on the temperature. Maximal burn out rate can range up to temperatures of 800°C and sometimes even beyond that. If just one binding agent would be used, and if this burns away at, for example, exactly 500 °C, burning-out at this temperature would happen very quickly.

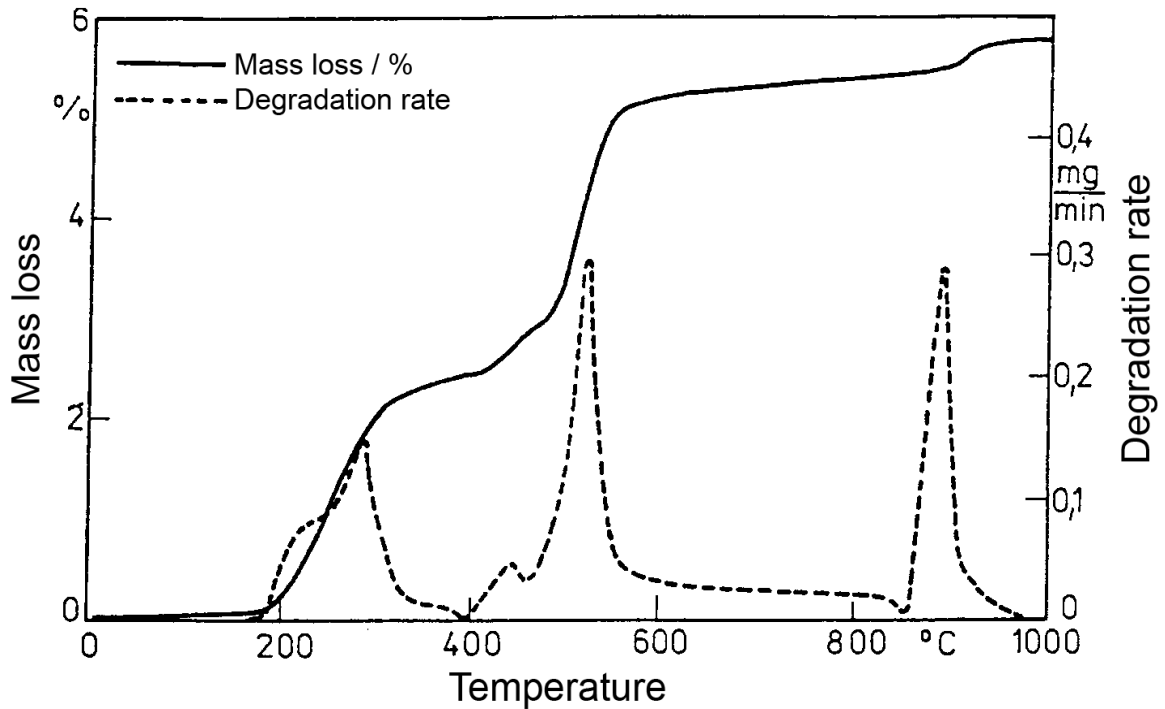


Fig. 2.5.11: Dependence of the mass loss of organic additives with the temperature.

During the solid-liquid-gaseous transition, high volume changes occur, what could lead to crack formation in the components. Therefore different organic additives are mixed in order to conduct to different burning-out temperatures.

The burn-out of additives added to oxide ceramic materials can take place in air, while in non-oxide materials some oxidation at temperatures between 800°C and 900°C can take place. Therefore binders are sometimes burned-out in inert gas atmosphere which can be observed through a displacement in their burning-out curves. In Fig. 2.5.12, for example, polyvinylbutiral, PVB, a binder used for tape casting was burned-out under air and under nitrogen. The maximum burn-out rate shifts from about 300°C to about 330°C. In practice, holding times are taken at such temperatures to reduce the burning-out velocity.

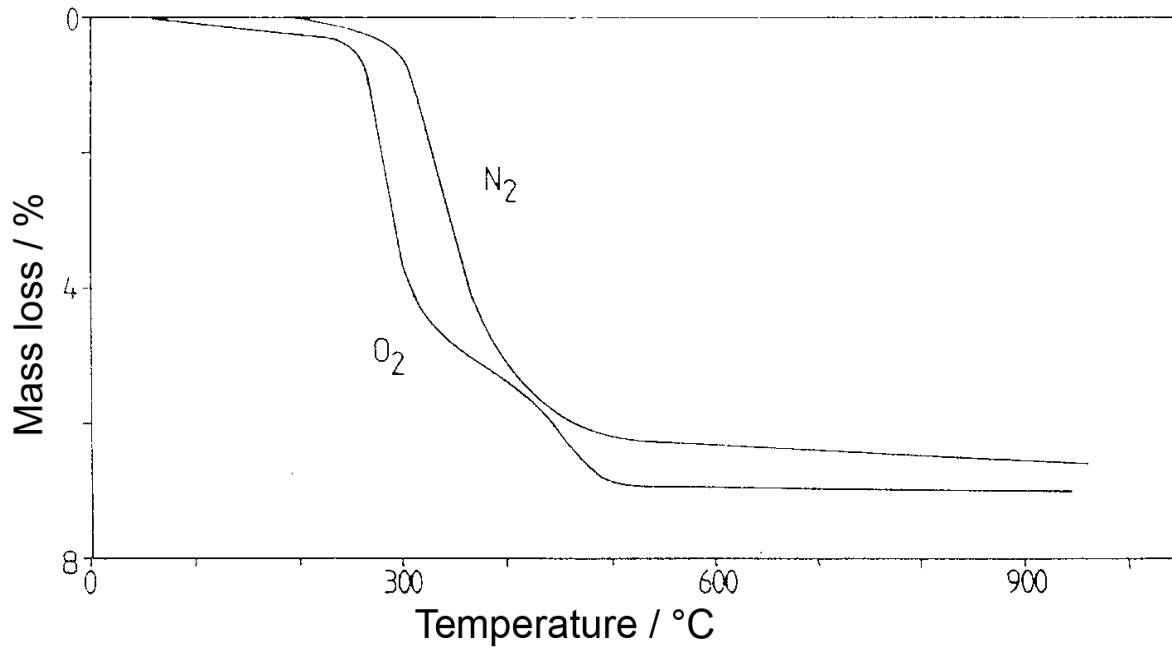


Fig. 2.5.12: Weight loss of polyvinylbutiral during heating under air and nitrogen atmosphere [E.Wessely, FH Nürnberg].

The number and amount of additives to be added varies according to the shaping procedure. If for dry pressing the bodies contain 1 vol.% to 10 vol.% of organic additives, injection moulding masses contain about 40 vol.% of organic additives.

A dry pressing article with an organic content of 5 vol.% can be burned-out within a few hours. This is often carried out in the aggregates where sintering also takes place. Burning-out of an injection moulded article with an organic content of 40 vol.% can last up to two weeks, depending on the component's complexity and thickness of its body, and is carried out in separate burning-out aggregates (Fig. 2.5.13).

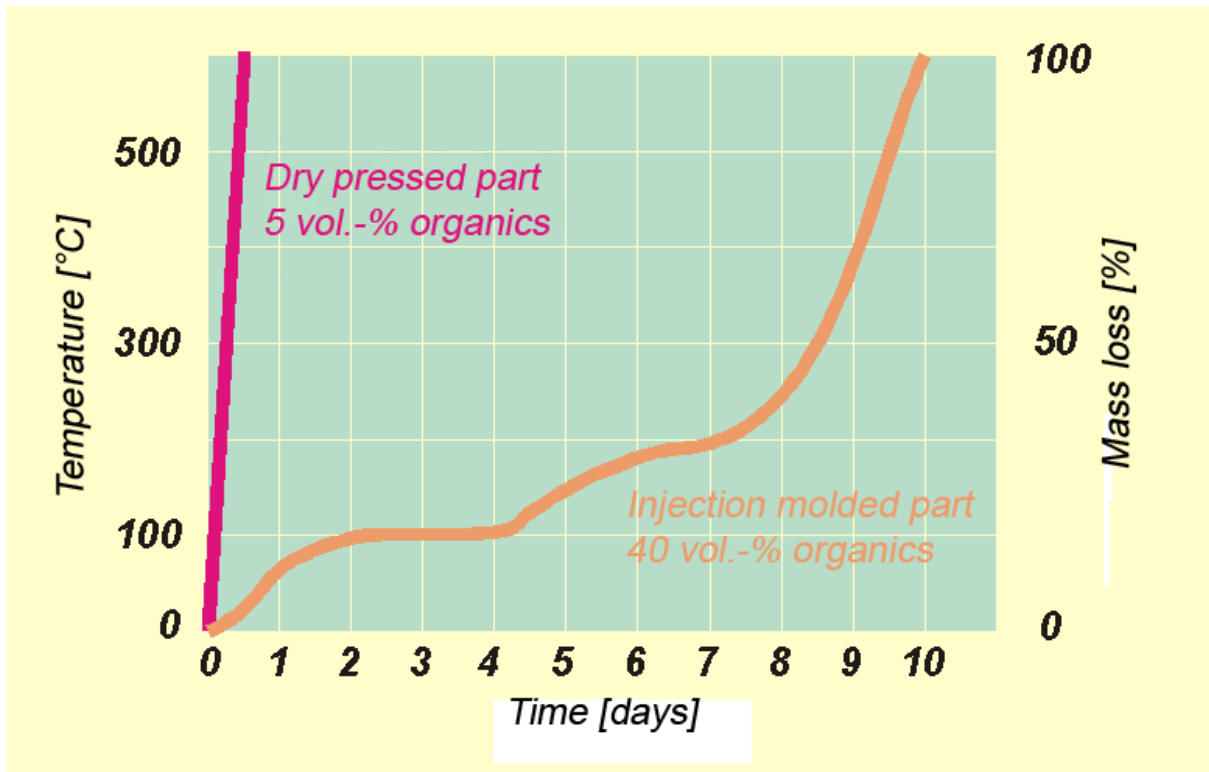


Fig. 2.5.13: Weight loss during burn out of organics in dry pressed and injection moulded bodies.

## 2.6 Raw material preparation

In nature, natural raw materials are not found within a narrow spectrum of grain size and only on rare occasions occur as a pure mineral. Grain size distributions are often represented as shown in Fig. 2.6.1. In this case, the sum of residues is plotted as a function of the grain size. The grain size distribution of kaolin, feldspar and quartz can overlap, showing kaolin the most fine grain size, quartz with the coarser grain size and feldspar in between. In case of such mixtures, the raw materials have to be separated from each other. In case you succeed to separate the grain mixture at about 60  $\mu\text{m}$ , you will get a kaolin and feldspar mixture as well as a feldspar and quartz powder mixture.

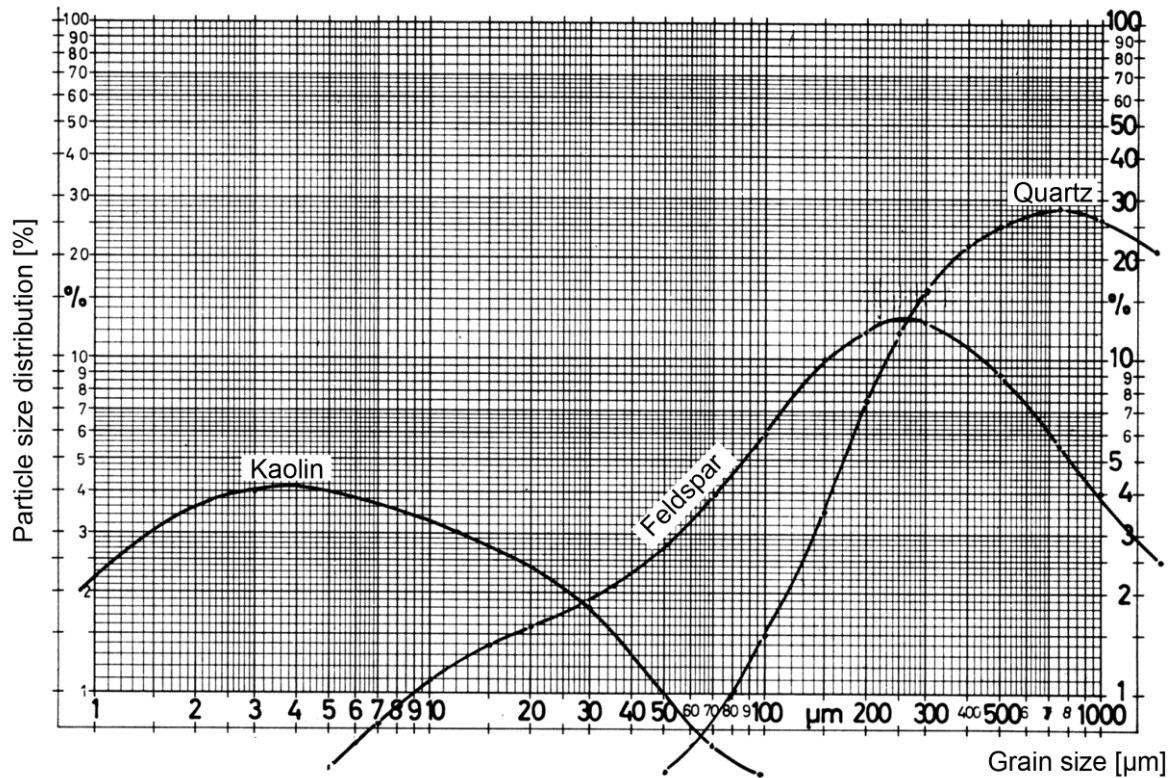


Fig. 2.6.1: Grain distribution of kaolin, feldspar and quartz [2].

Fig. 2.6.2 shows schematically the selective classing of the ternary mixture kaolin, feldspar and quartz powder which can be very often found in nature. The mixture is suspended and first separated at 100-200μm. Now we have a mixture of kaolin and feldspar at the left side and at the right side a mixture of feldspar and quartz. For the separation of the kaolin-feldspar mixture we sieve at 20-40 μm. The coarse fraction contains feldspar; the fine fraction on this sieve is kaolin. In practice, the mixture usually passes through several stages of separation. Feldspar and quartz are separated at 2-4 mm and later again at 200 μm. The coarse fraction is quartz sand. The fine fraction is again separated into fine quartz powder and a fraction of feldspar.

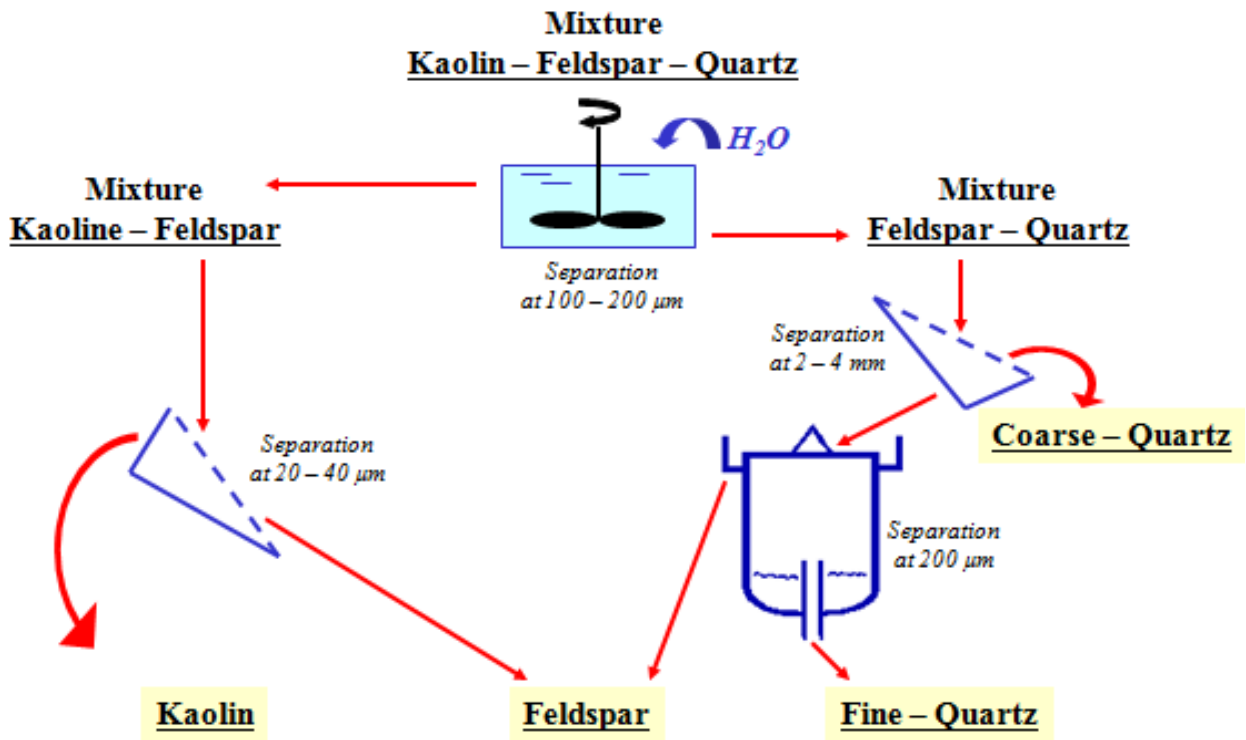


Fig. 2.6.2: Separation of three products via selective separation/ grinding [2].

Fig. 2.6.3 shows schematically a complete preparation of kaolin. The raw materials are charged to the grinding mills and larger stones with diameters within centimetre area are separated from the residual material. The screenings are homogenised with water by adding dispersants in order to charge the particles' surface and reduce the water content during processing. Coarse fractions are separated from the fine ones in log washers and washing mills.



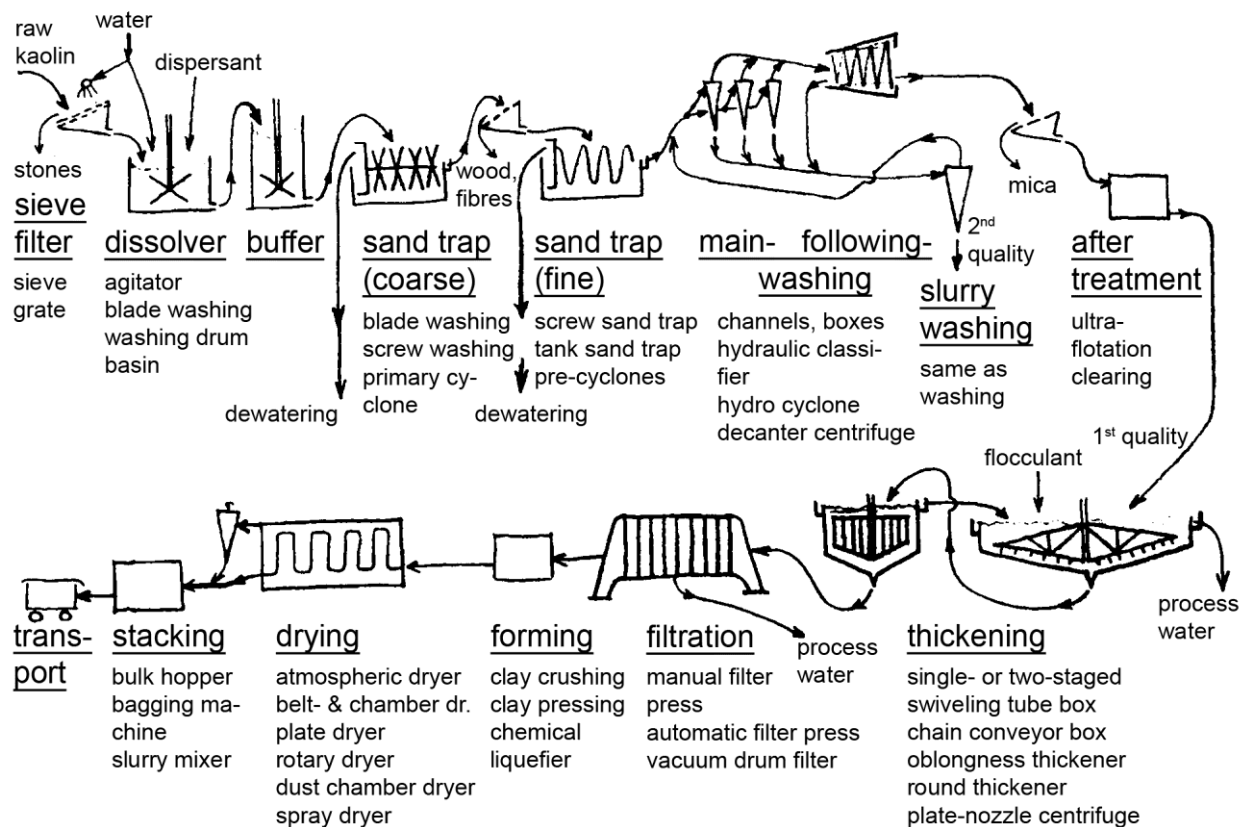


Fig. 2.6.3: Kaolin preparation, flowchart of a general wet process [2].

The fine content is further processed in hydro-cyclones at different stages. Separation grain size is about 20-40  $\mu\text{m}$ . Fig. 2.6.4 shows how a hydro cyclone works. This hydro cyclone is loaded in radial direction with a suspension. Two flow cycles are formed due to the special geometry: the inner flow which in the underflow takes up the coarse fraction and the external spiral which discharges the fine fraction at the top. The cyclone's geometry effects separation within a certain grain size area. The more exact grain separation is required, the more hydro cyclone series have to be operated in succession.

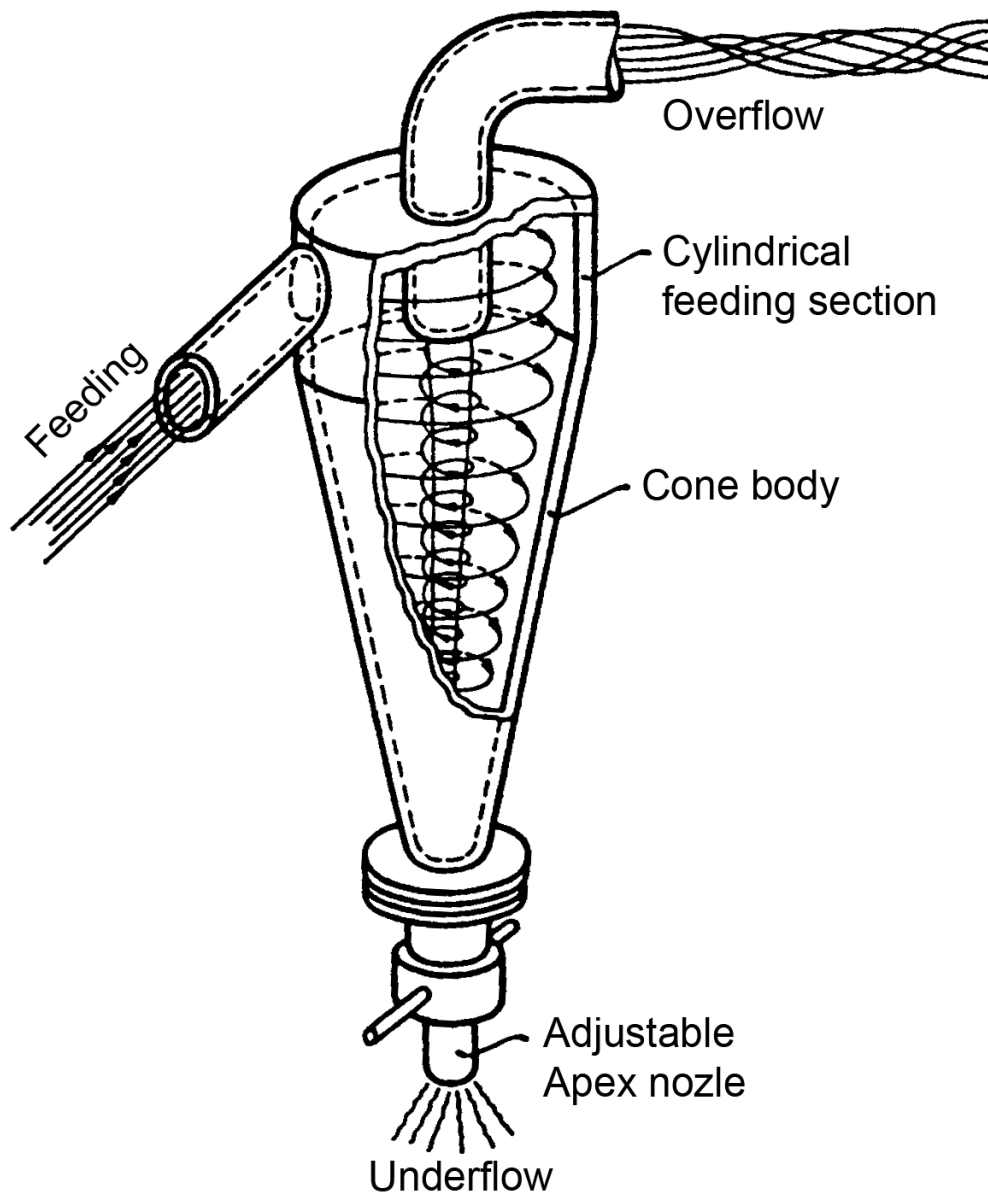


Fig. 2.6.4: Functional scheme of a hydrocyclone [2].

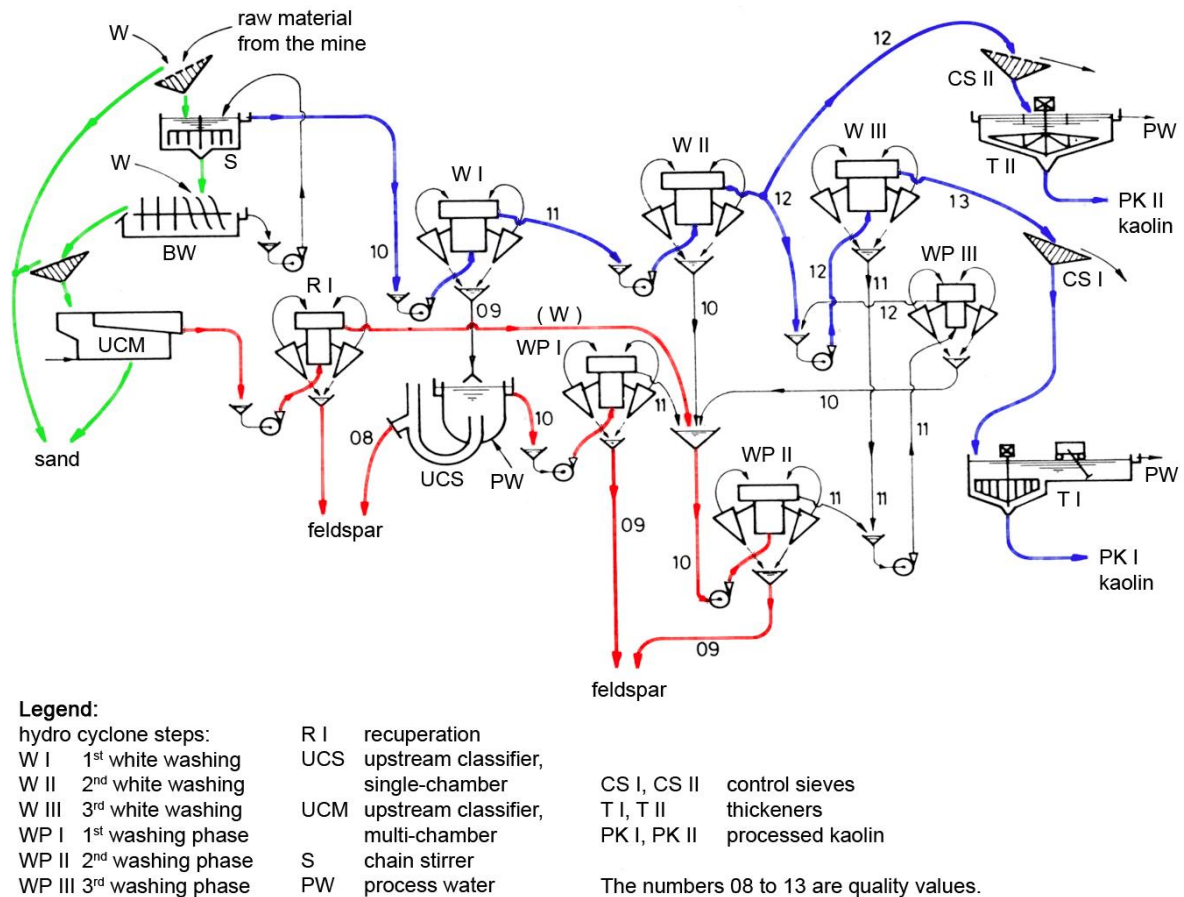


Fig. 2.6.5: Flowchart of a Kaolin preparation plant [2].

Fig. 2.6.5 demonstrates schematically the multi-stage cyclone separation in a kaolin preparation plant. The fines sediment in large slurry tanks, a procedure which we know from sewage works. After sedimentation and filtration the material is dried in drying aggregates and stored in silos or transported in bags to the customers.



Videoclip: Raw material preparation

„The material is transported on conveyors from the mine to a preparation hall. The first log washer separates the coarse grains from the fine ones. The coarse material sediments on the bottom and is transported by bowls to the next step of separation. The fine suspension is separated at the other side of the log washer and transported to these cyclones. Before, the mixture is cleaned in sieves and the fines are separated from the coarsest grains. In the background you see the multi-staged cyclone steps. The coarse material is carried on to bunkers and later-on in another video we will pick up the material to get it crushed. But first it has to undergo several sieve levels and log washers where the coarse fraction is again separated from the finer one.”

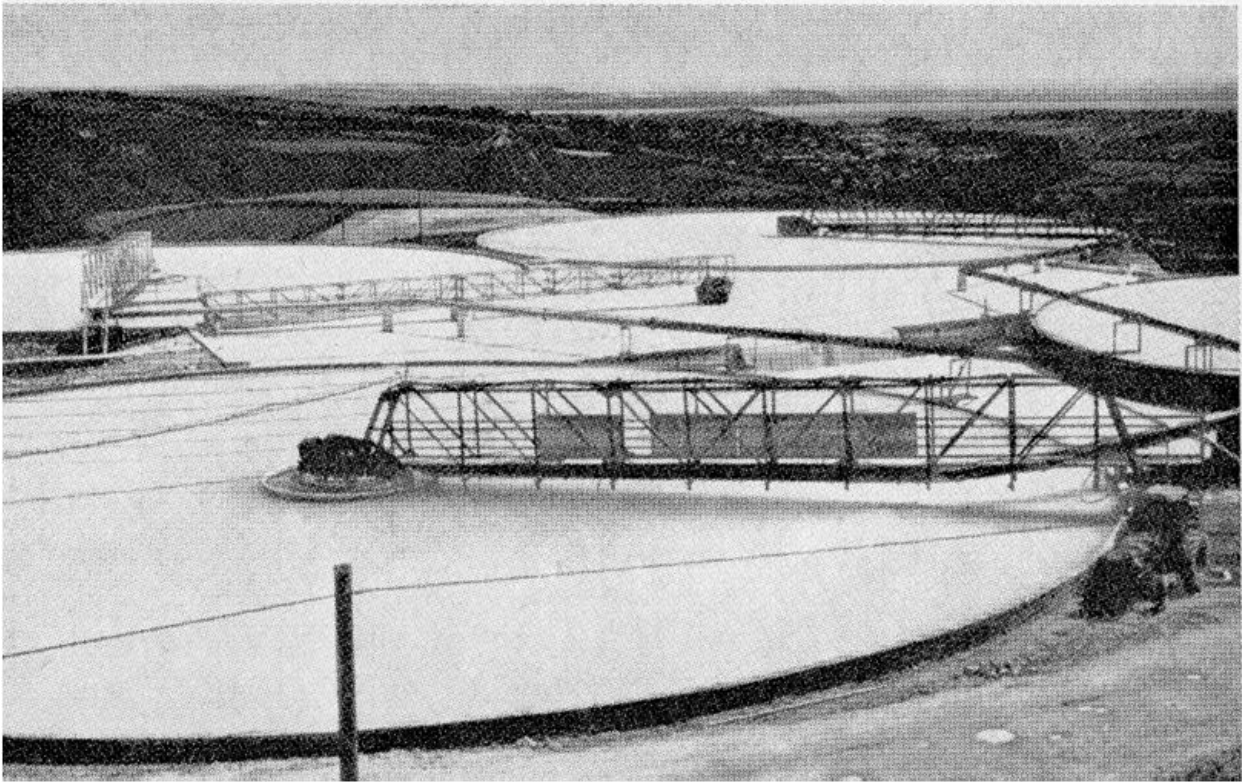


Fig. 2.6.6: Hydro-separator (classifier and concentrator) [2]. English china clay lovering, Pochin&Co.Ltd., Cornwall.

After leaving the hydro cyclones the water has to be separated from the solids. This is made in large slurry tanks (Fig. 2.6.6). The coarse fraction mostly consists of a feldspar-quartz-mixture.

Feldspar and quartz can be separated in electrostatic drum cobbars. For this, the feldspar and quartz surfaces have to be charged. Chemical reagents are added attaching to the surface. The charging process of feldspar and quartz surface is varyingly strong (Fig. 2.6.7).

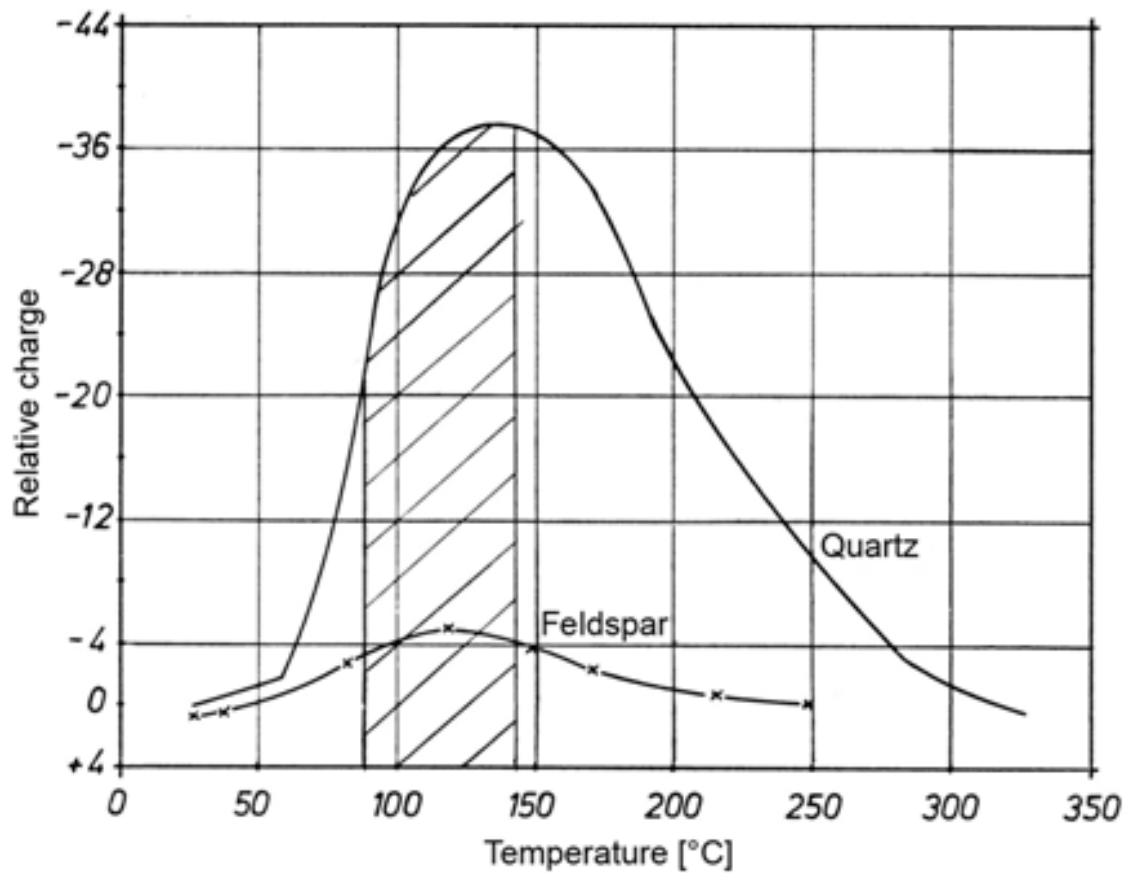


Fig. 2.6.7: Electric charging of quartz and feldspar versus temperature [2].

The distinct electrostatic surface charges are used to separate the material, for example, in a drum cobbler. An electric field is set up on a turning roll. Highly charged material will be higher deflected, while less strong charged material will be less deflected. And in this way with these drum cobbler quartz and feldspar can be separated. In praxis this separation is made in fully automated plants (Fig. 2.6.8). First a sand mixture of feldspar and quartz runs into a preheated drum. The surfaces of feldspar and quartz are charged varyingly strong by a treatment in HF and the raw materials are separated in multi-staged drum cobbler.

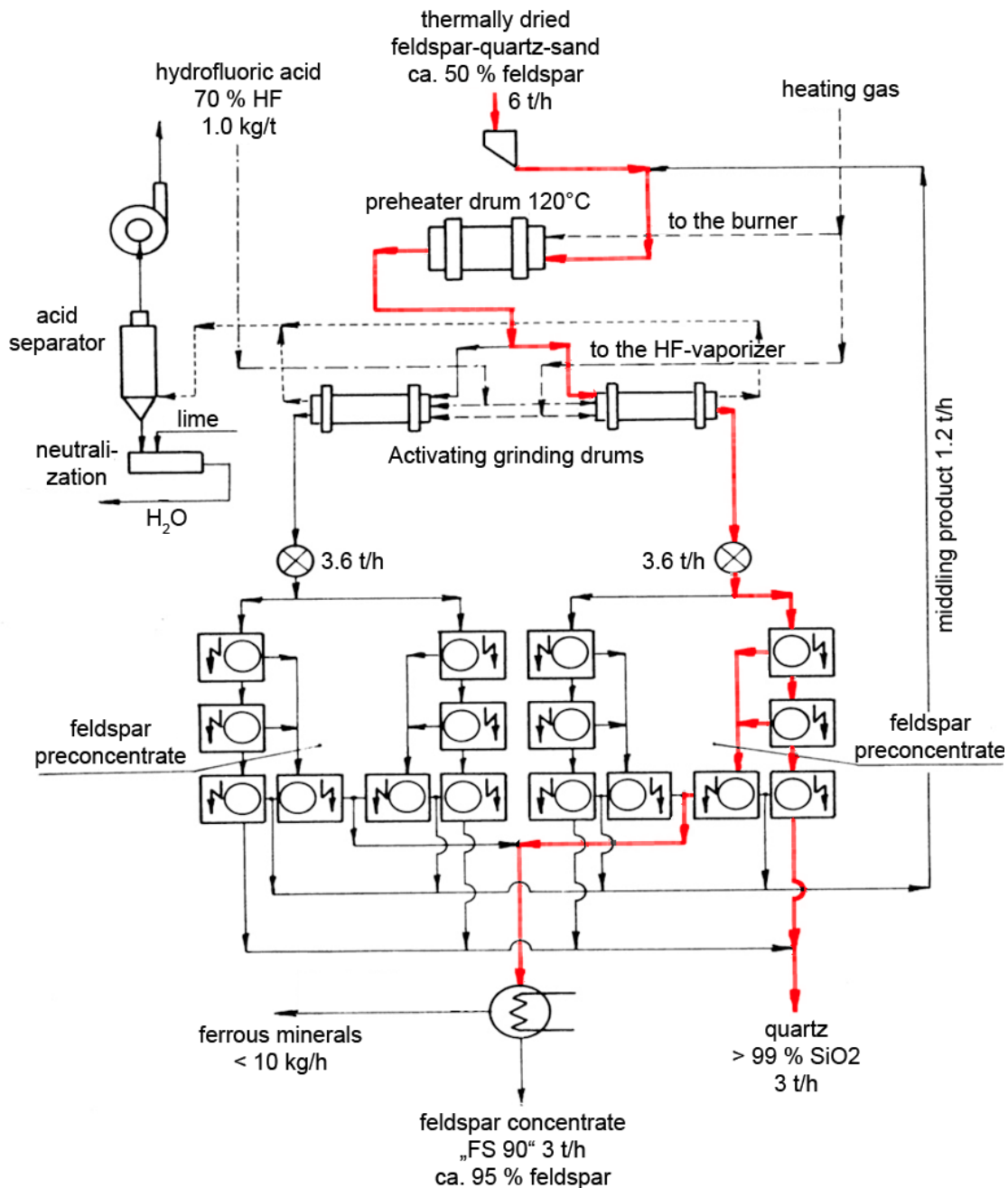


Fig. 2.6.8: Flowchart of electrostatic separation of quartz and feldspar [2].

Flotation is another possibility for material separation. As already discussed, long-chain molecules can be docked onto charged surfaces. Docking behaviour varies because the materials' crystal structure is different. This means, for instance, that particles with a higher addition of organic additives in a water barrel can be dragged-out to the top. As for quartz, for example, relatively few long-chain molecules attach to the surface, but much more with regard to orthoclase (Fig. 2.6.9). When a quartz-feldspar mixture is dispersed in water, the feldspar particles float towards the top and can be taken off, while the quartz particles sediment to the bottom.

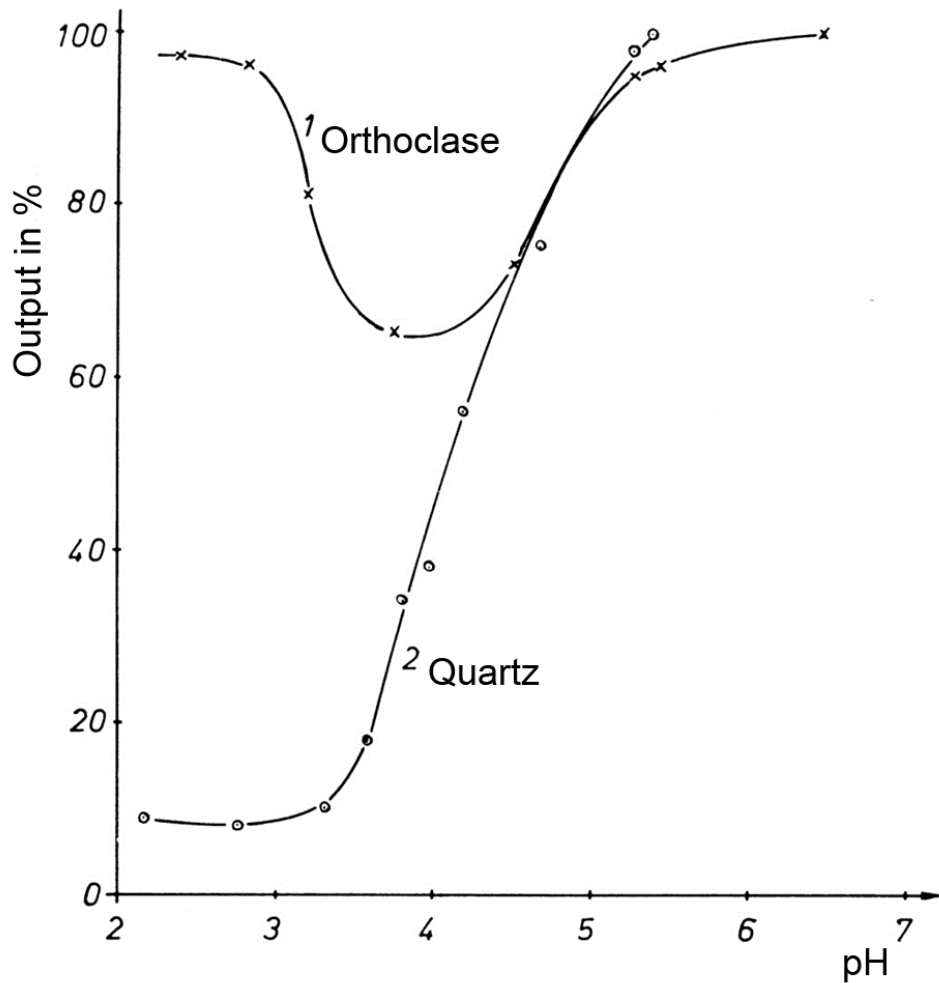


Fig. 2.6.9: Flotation behaviour of quartz and orthoclase as a function of the pH in HF-acidic suspension with Dodecylammonium chloride (500g/t) [2].

Upward current classification is another possibility for material separation (Fig. 2.6.10). The material to be classified is led to a case filled with a liquid and with water streaming in from the bottom. A soft water movement from the bottom to the top appears. The coarse particles sediment downward and are collected in the first bunker. The fine particles stay longer in the suspension phase and sediment in the rear tanks. Prior to further processing the suspensions respectively sediments have to be separated into solids and liquids.

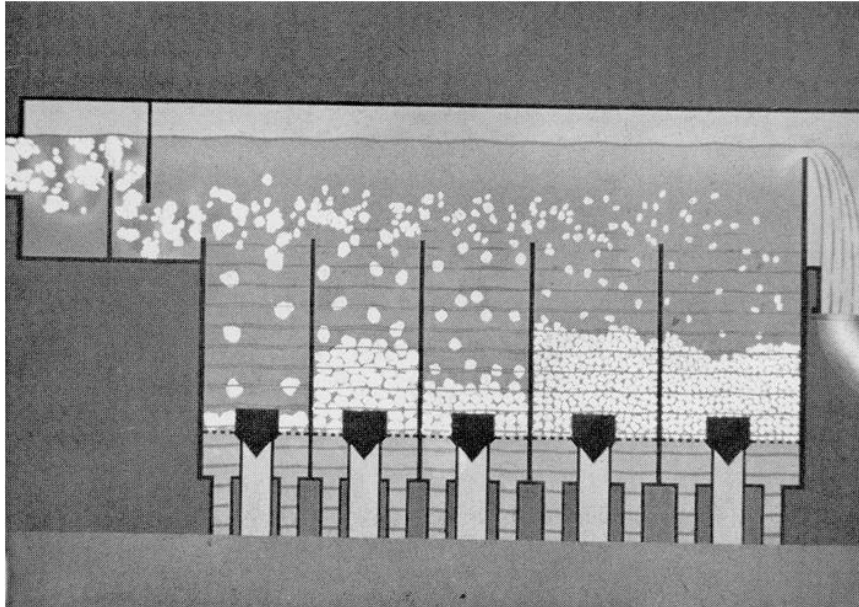


Fig. 2.6.10: Working principle of multi-chamber upward classifiers (schematic) [2].

This can be done in different appliances. Planar filters (Fig. 2.6.11), for example, consist of a filtration level and an extruding screw which extrudes the material sedimenting on this filtration level. The filtrate can be removed from the bottom. Separation of powder and water can also be made in so-called rotary dryers where the material is given into a turning drum with a slight down-grade (Fig. 2.6.12). The material rotates at a turning drum motion to the left, while in the opposite direction hot air is applied to the material which has to be dried.

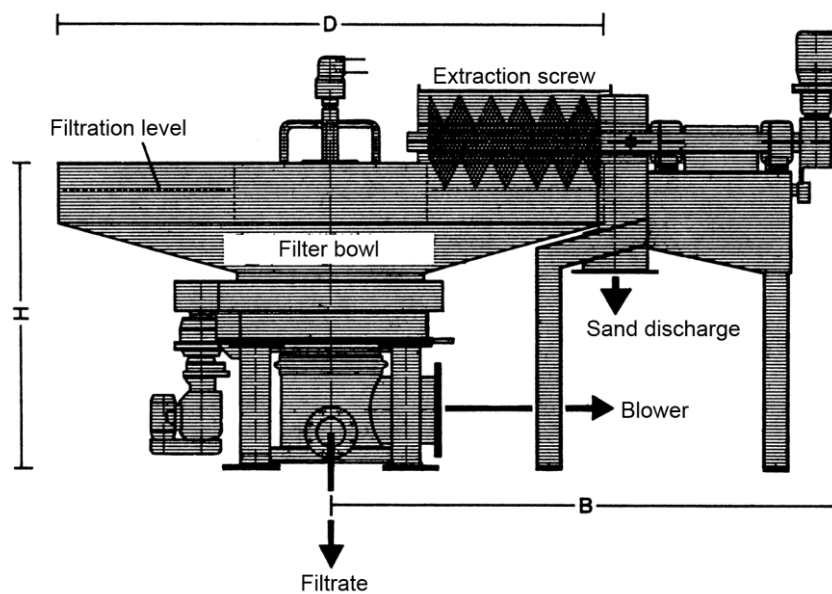


Fig. 2.6.11: Cross-section of a planar filter for quartz-sand dehydration [2].



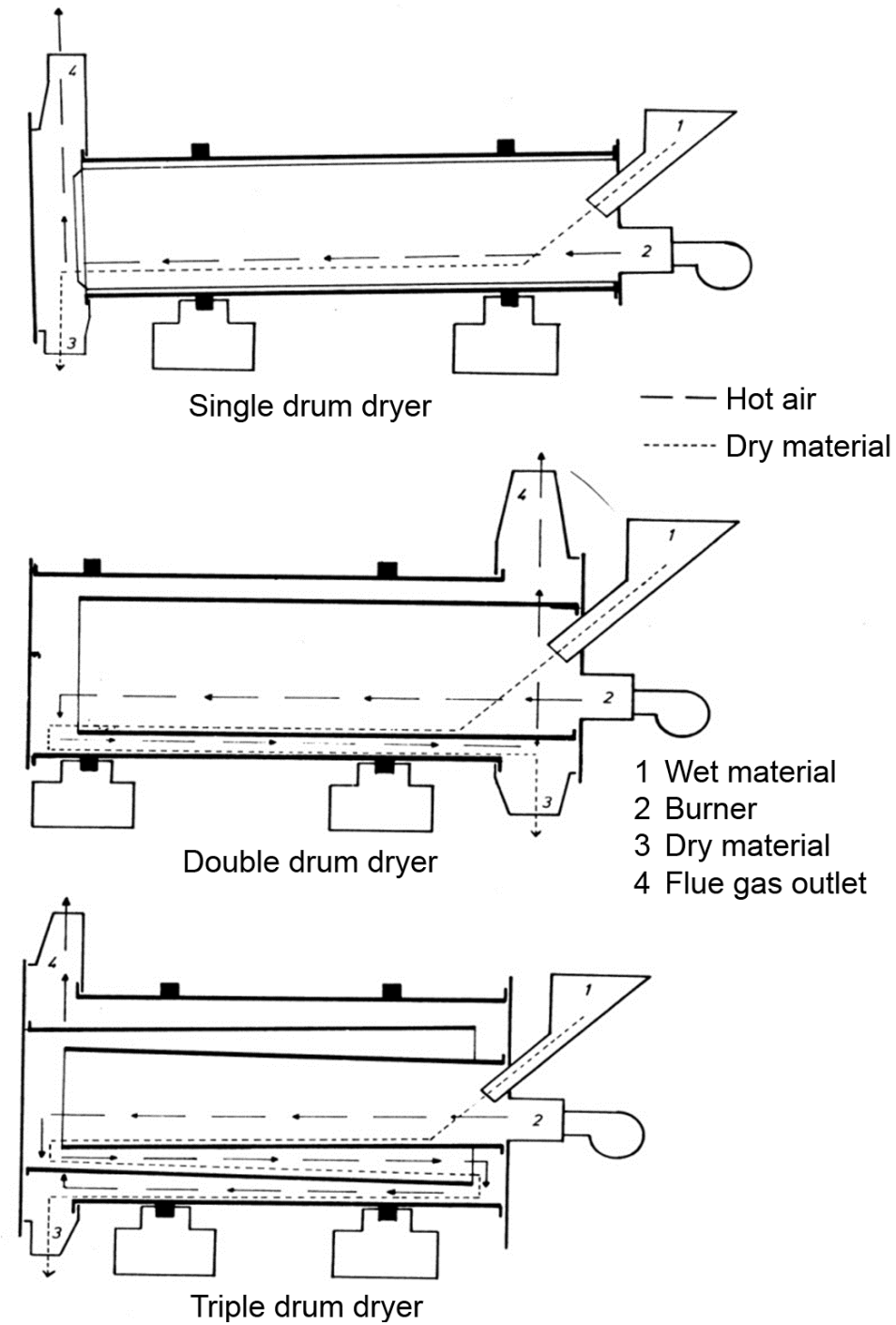


Fig. 2.6.12: Rotary dryer [2].

Another variation is the water jet dryer (Fig. 2.6.13). The compound being charged can first be led to a crushing appliance and is then injected into a hot gas path. The fines are bunkered in a silo while the coarse fraction falls on a conveyor belt and is again supplied to the circulation.

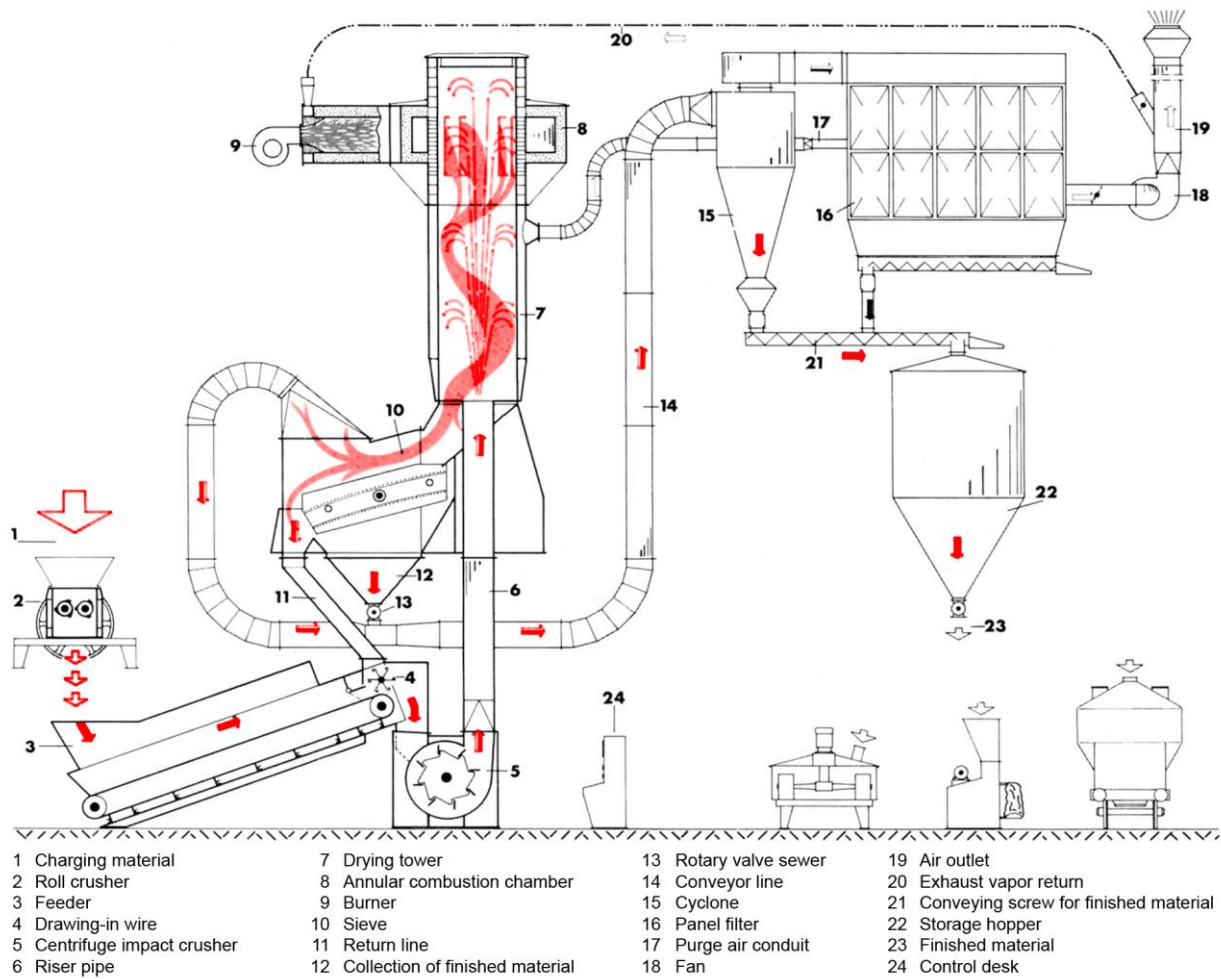


Fig. 2.6.13: Water jet dryer [2].

### 3. Body preparation

#### 3.1 Grain size modification

After the preparation, the raw materials are in many cases still too coarse. Grain sizes within micrometer range are required for ceramic components produced by sintering processes, because then the number of contact points between the particles during sintering is considerably larger. So the raw materials have to be milled, this means that the grain-size distribution curve has to be moved towards smaller grain sizes (Fig. 3.1.1). Depending on the starting grain size different aggregates are available for milling.

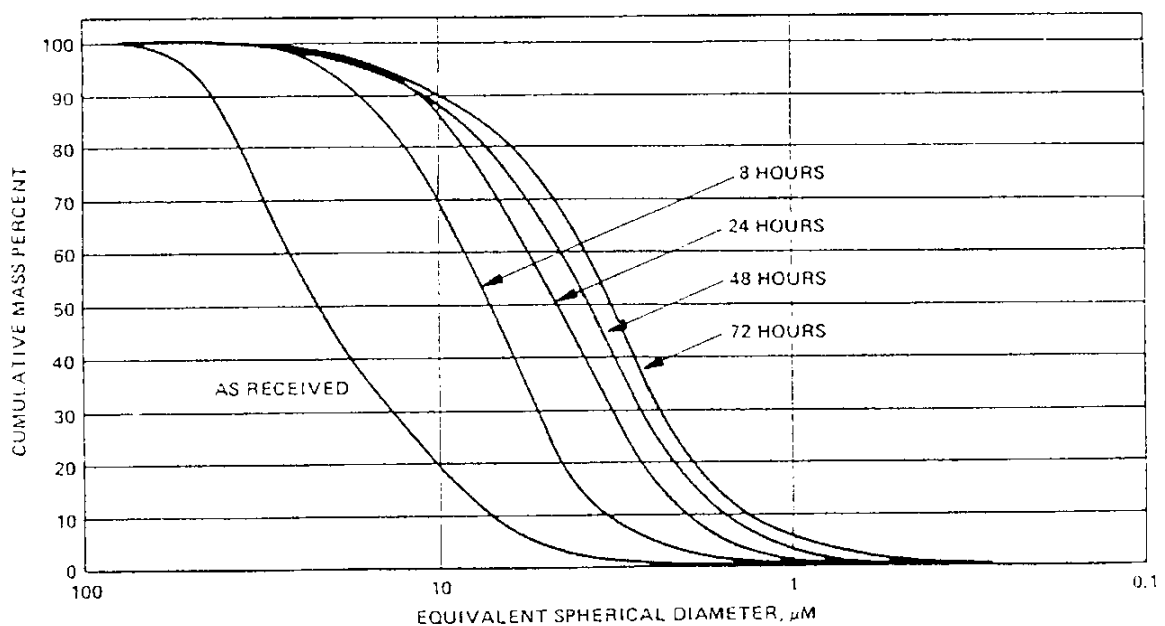


Fig. 3.1.1: Grain size distribution of silica powder as a function of the grinding duration.

Pieces of rock within centimetre range are milled by jaw breakers (Fig.3.1.2). The jaw breaker's left side is fixed while the right side moves oscillating. The desired grain size is defined by the gap width which can be adjusted at the jaw breaker. Another variation for milling coarse material is the so-called cone crusher (Fig. 3.1.3).

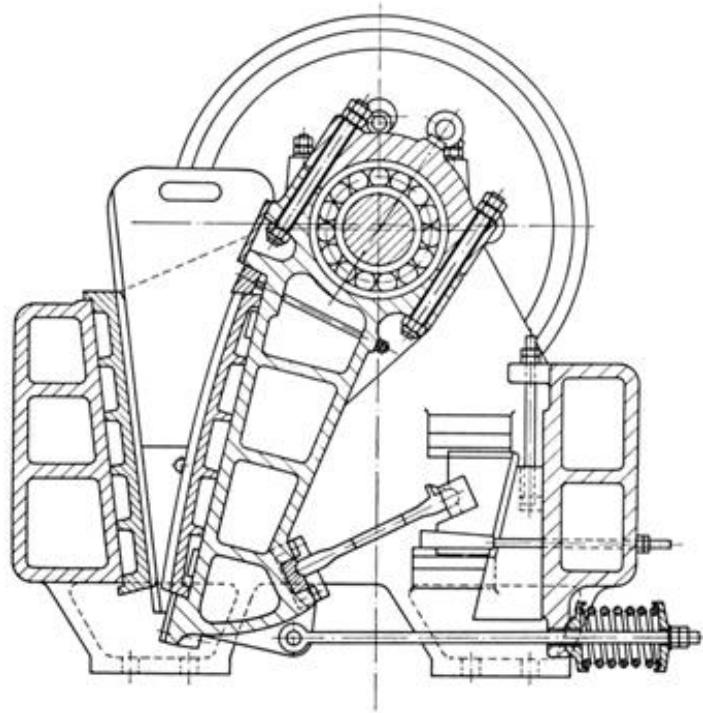


Fig. 3.1.2: Jaw breaker [2].

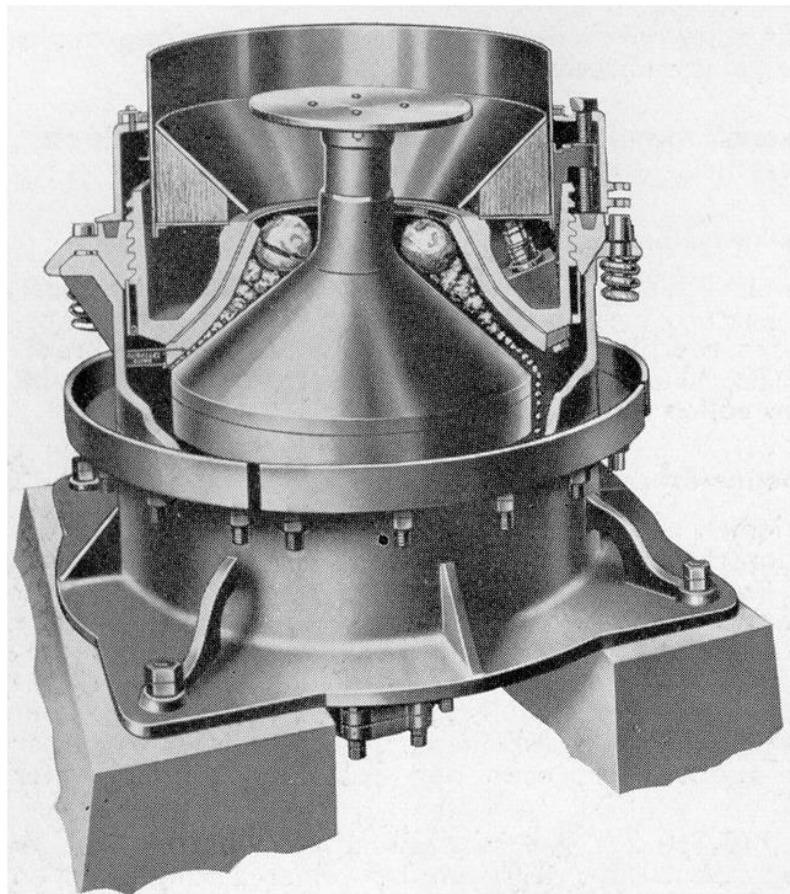


Fig. 3.1.3: Cone crusher [2].

A turning cone crushes the charging material, and here too, grain sizes lie within centimetre range. The roller crusher with blades (Fig. 3.1.4) has rollers equipped with fly cutters which turn against each other. The coarse material is filled at the top and the crushing result is defined by the gap width, which is the distance between the rollers.

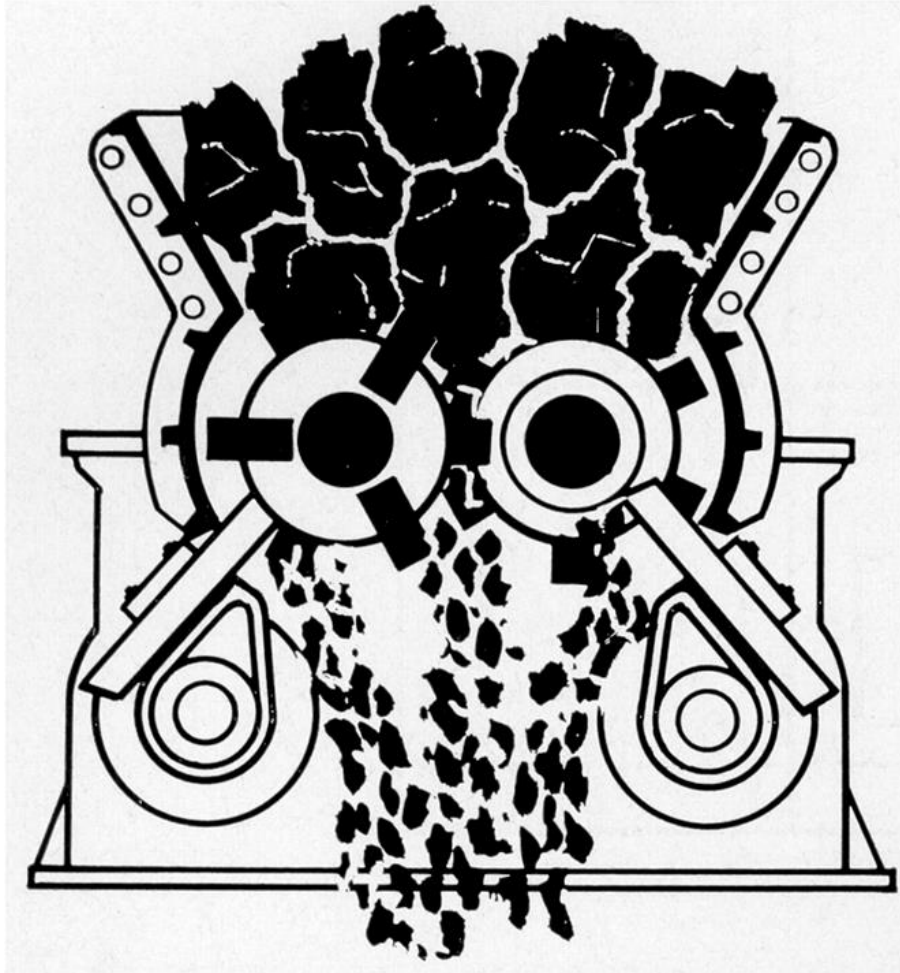


Fig. 3.1.4: Roller crusher with blades [2].

The width of the gap cannot be of any small size, since the effectiveness of this milling process may get lost. Cam roller mills/crushers look quite similar to roller cutter with blades (Fig. 3.1.5). Here too, cam-equipped rollers run in opposite direction and the crushing result is defined by the rollers' gap.

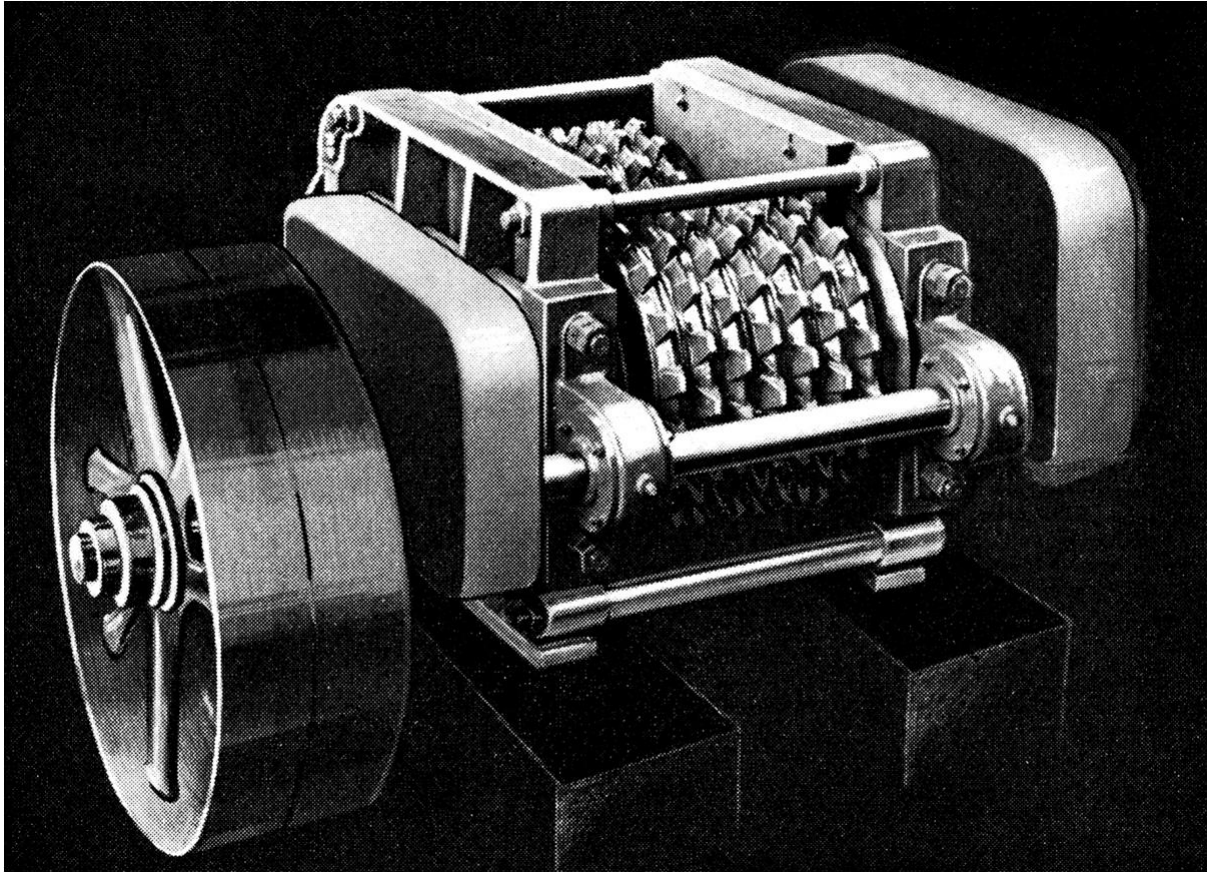


Fig. 3.1.5: Cam roller crusher [2].

Impact disc mills (Fig 3.1.6) are typically used at laboratories. In this mill pins get into each other, turn and grind, pulverise and smash the material to be crushed. Abrasion of these pins is relatively high. Another crushing aggregate for coarse grain ranges is the hammer crusher (Fig. 3.1.7). The material to be crushed is filled in at the top and impact crushing is caused by a roll's rotation respectively conjunction with hammers. The so-called Loesche mill (Fig. 3.1.8) already grinds up to the millimetre range. The material to be crushed is put under big granite rollers moving in a circle and the mill material is grinded.

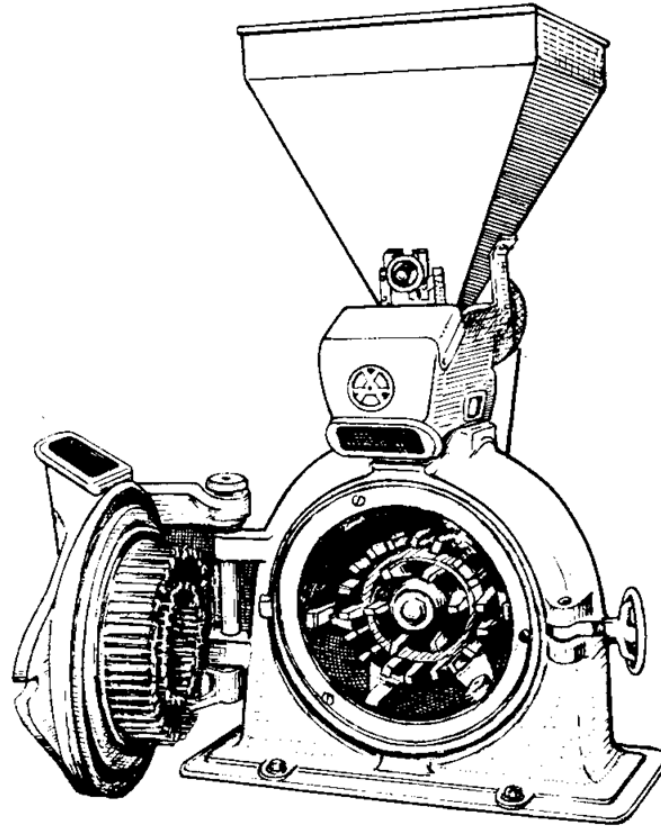


Fig. 3.1.6: Impact disc mill [2].

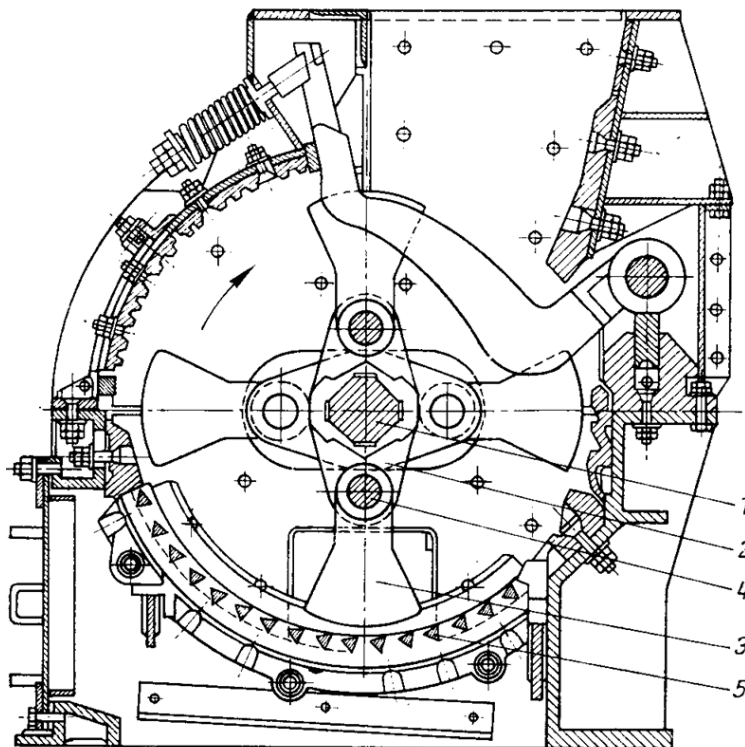


Fig. 3.1.7: Hammer crusher with sieve and scapular inflow [2]. (1) wave; (2) motor; (3) hammer; (4) pins; (5) grid.

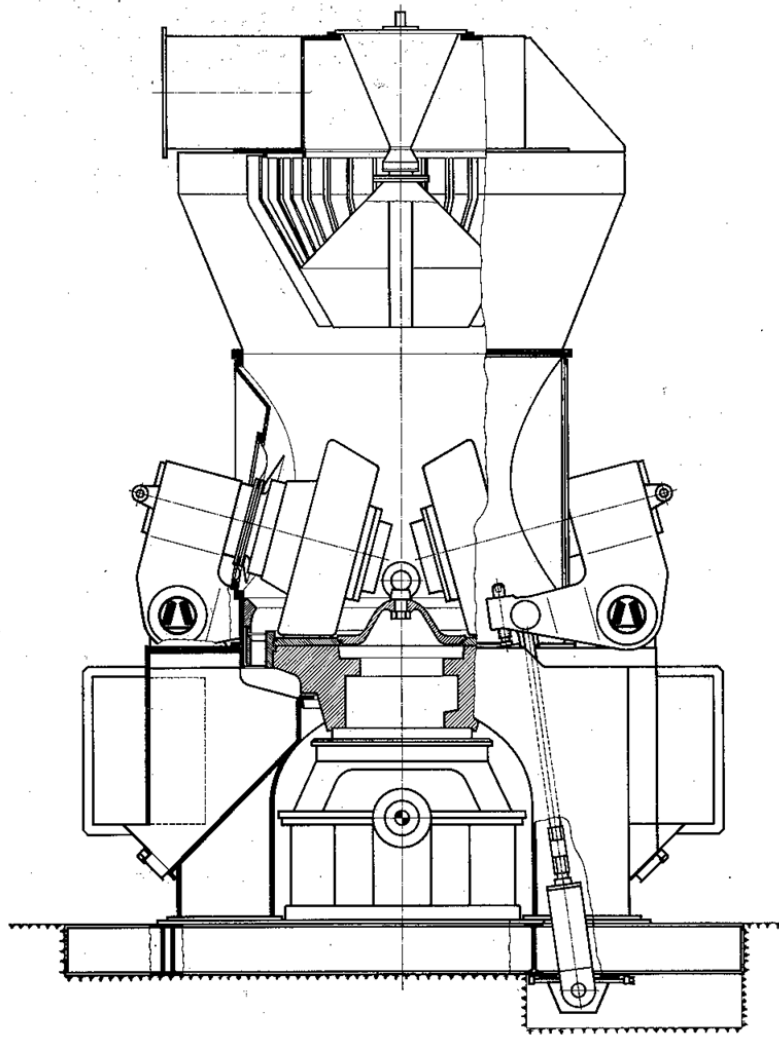


Fig. 3.1.8: Schematic of a Loesche Mill with hydrocyclone [2].

Grinding within micrometer range can be made in rotary tumbling millers. The containers are filled with milling stones, water and grinding material. The material is crushed or grinded between the milling stones. When the mill rotates relatively quickly, the grinding bodies are also moved upwards. They drop back to the grinding area and crush the mill material. If rotary motion is reduced, a sliding and rubbing movement comes up and the material is grinded (Fig. 3.1.9). The ball movement influences the shape of the grain. A splintery grain is normally formed during grinding. Rubbing grinding in the majority of cases forms a round grain.



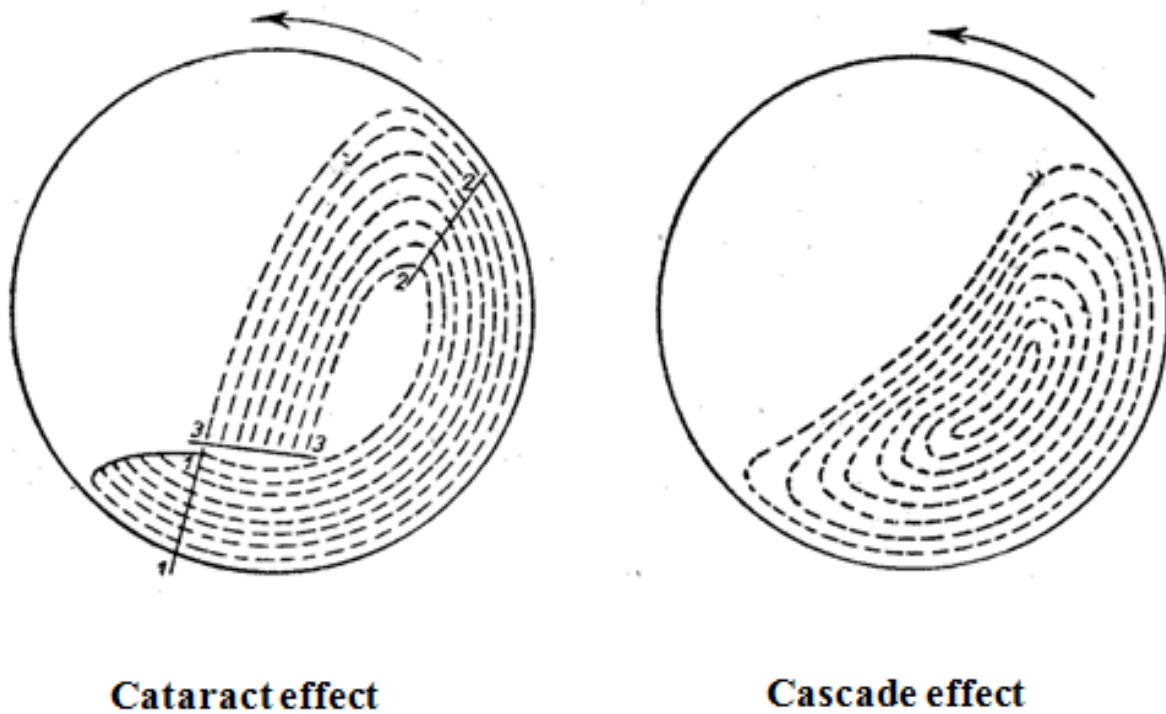


Fig. 3.1.9: Illustration of the milling aid action in the tumbling mills [2].



Videoclip: Comminution in ball mills

„We now pick up a feldspar and quartz mixture which has been stocked in this bunker and transport it to a ball mill. These ball mills have a capacity for several tons. Their diameter has an average up to 2 metres and they are filled with flint pebbles ( $\text{SiO}_2$ ). Knowing the machine's input capacity you can make a prediction on the grinding result (see below). The diameter of the grinding balls depends on the mill's size and the grain size you want to achieve.”

If powder of about  $100 \mu\text{m}$  has to be grinded into the 1-5 micrometer range, an attritor mill should be used (fig. 3.1.10). Such mills are filled with about 1/3 of grinding bodies, 1/3 of mill material to be grinded and 1/3 of water. There are various geometries for these mill types (fig. 3.1.11 and 3.1.12). Application of energy can be determined through the input power of stirring ball mills and a prediction of the grinding result can be made.

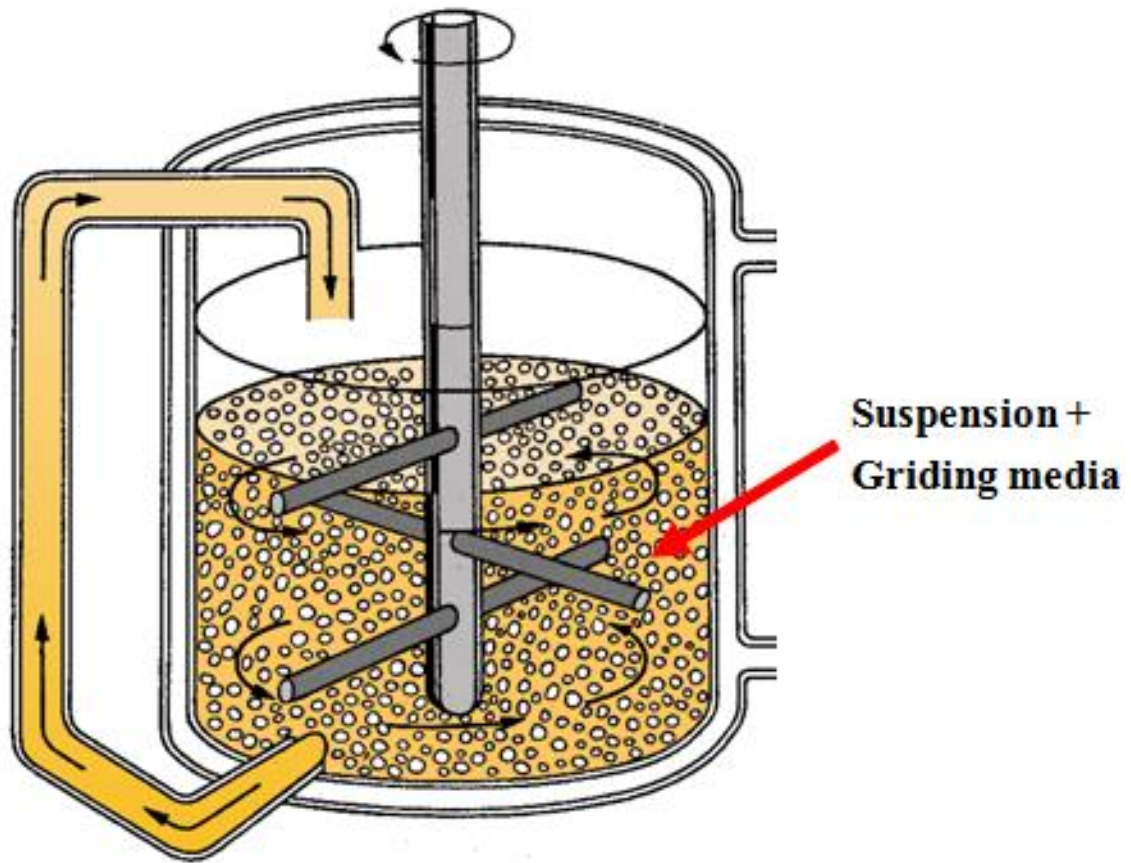


Fig.3.1.10: Attritor (schematic).

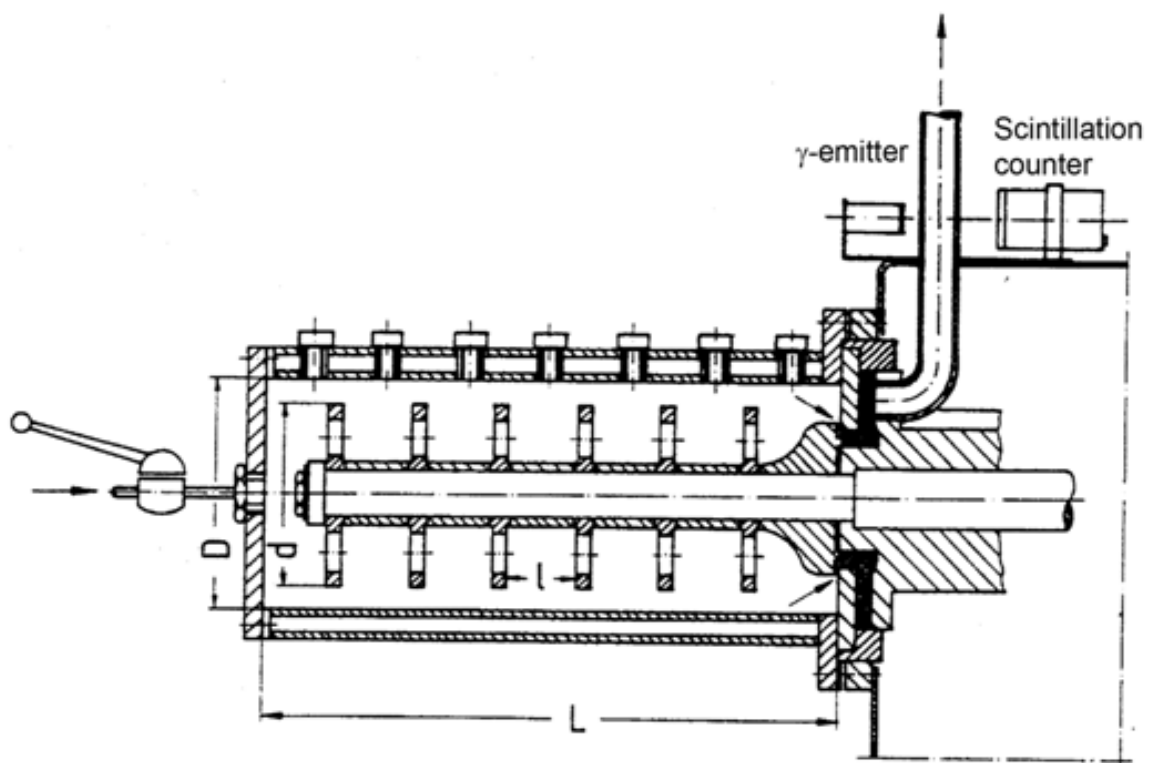
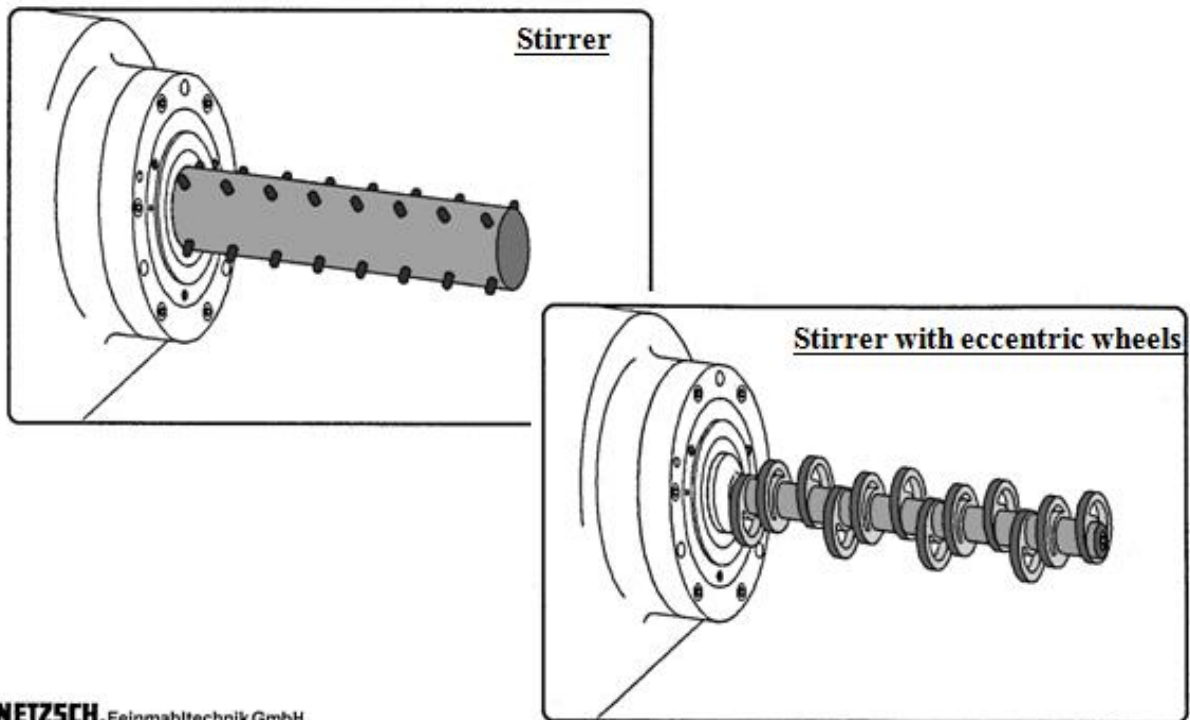


Fig. 3.1.11: Simplified representation of the grinding chambers in an agitator bead mill (Schwedes, TU Braunschweig, 1985).



**NETZSCH** Feinmahltechnik GmbH  
 .....

Fig. 3.1.12: Stirrer and stirrer with eccentric wheels in the agitator bead mill.

Fig. 3.1.13 shows the grinding result by varying circumferential speed  $V_u$  and solid concentration  $C_v$ . Circumferential speed in m/sec varies between 6.4 and 14.4 m/sec. The slip's solid concentration varies at constant milling time between 10 and 30 %. With this variation the medium grain size could be reduced from about 50  $\mu\text{m}$  to about 2  $\mu\text{m}$ . The medium specific energy of a mill can be calculated by measuring turning moment, time, solid concentration and circumferential speed (Fig. 3.1.14). This curve demonstrates that with the material used in this case the application of energy of  $10^3 \text{ Jcm}^{-3}$  causes a particle size reduction to circa of 2  $\mu\text{m}$ . This result is also transferable to a whole series of larger mills. It means that laboratory results can be transferred to production aggregates.

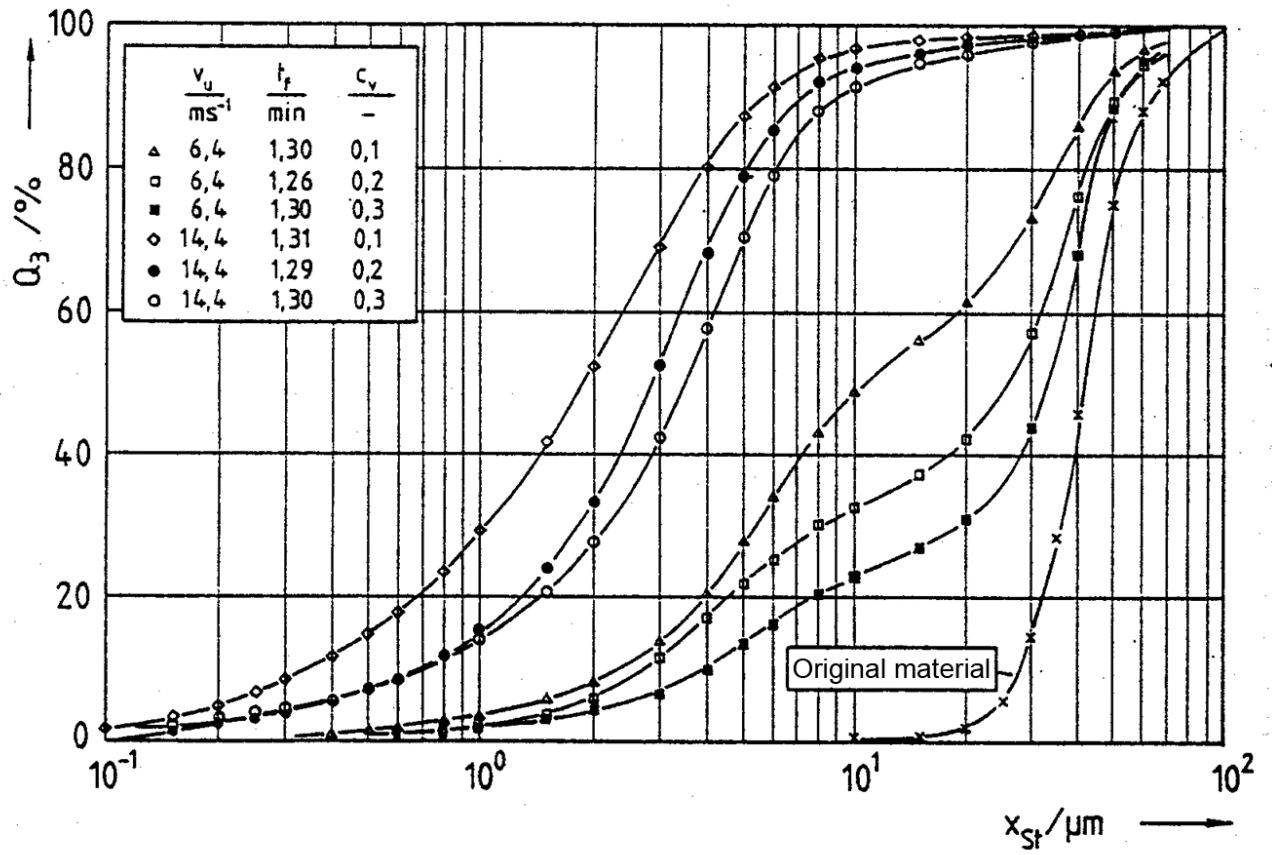


Fig. 3.1.13: Cumulative distribution  $Q_3$  versus Stokes diameter  $x_{st}$  for different velocities  $v_u$  and solid concentration  $c_v$  (Schwedes, TU Braunschweig, 1985).

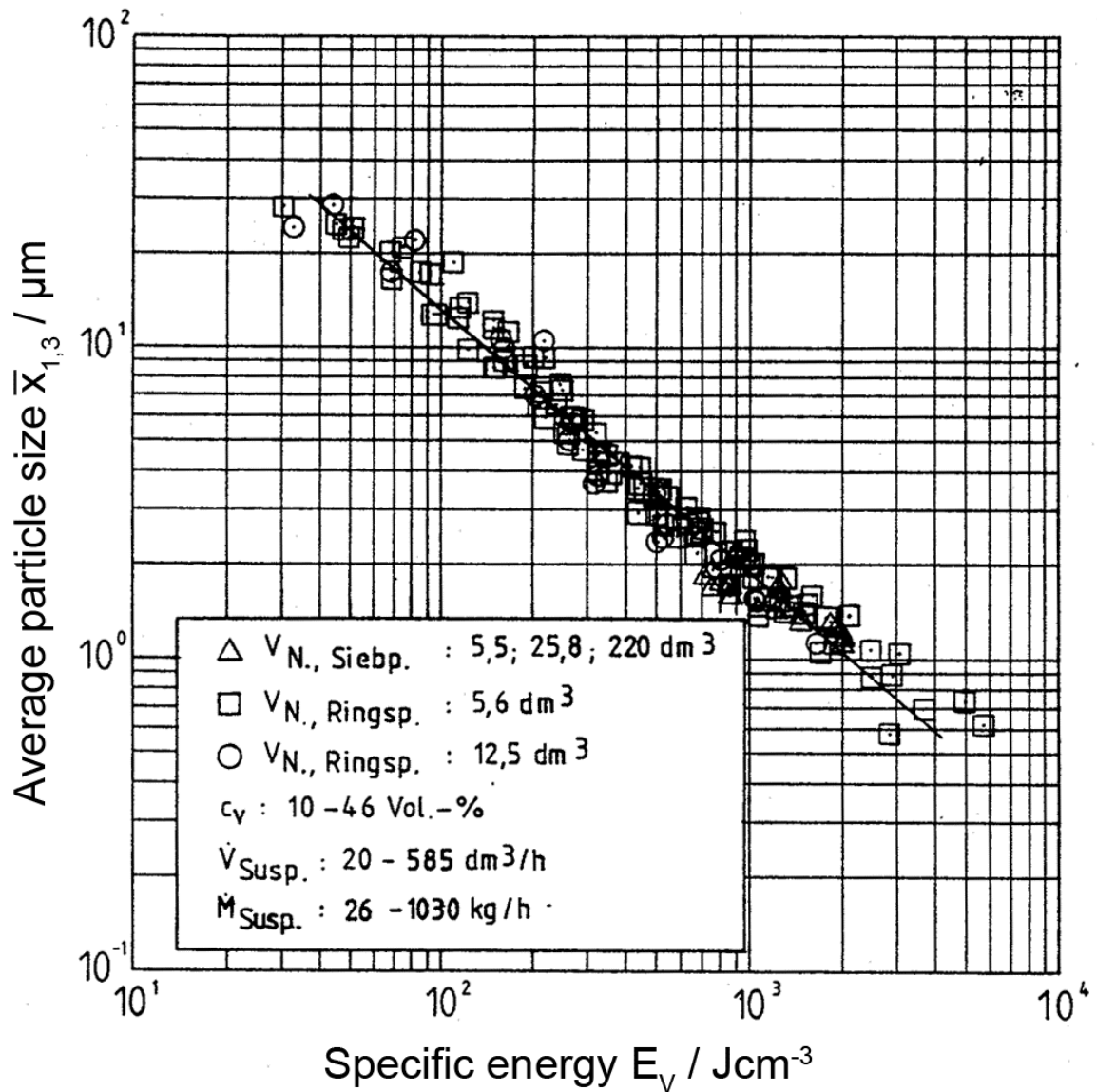


Fig. 3.1.14: Average particle size  $x_{1,3}$  versus specific energy  $E_v$  for different geometries, with variation of processing parameters (Schwedde, TU Braunschweig, 1985).

Fig. 3.1.15 shows that different energy inputs are required depending on the ceramic material to be milled. Considerably more energy input is necessary for SiC with a high covalent amount of bond compared to ionic bonded  $Al_2O_3$  or  $ZrSiO_4$ .

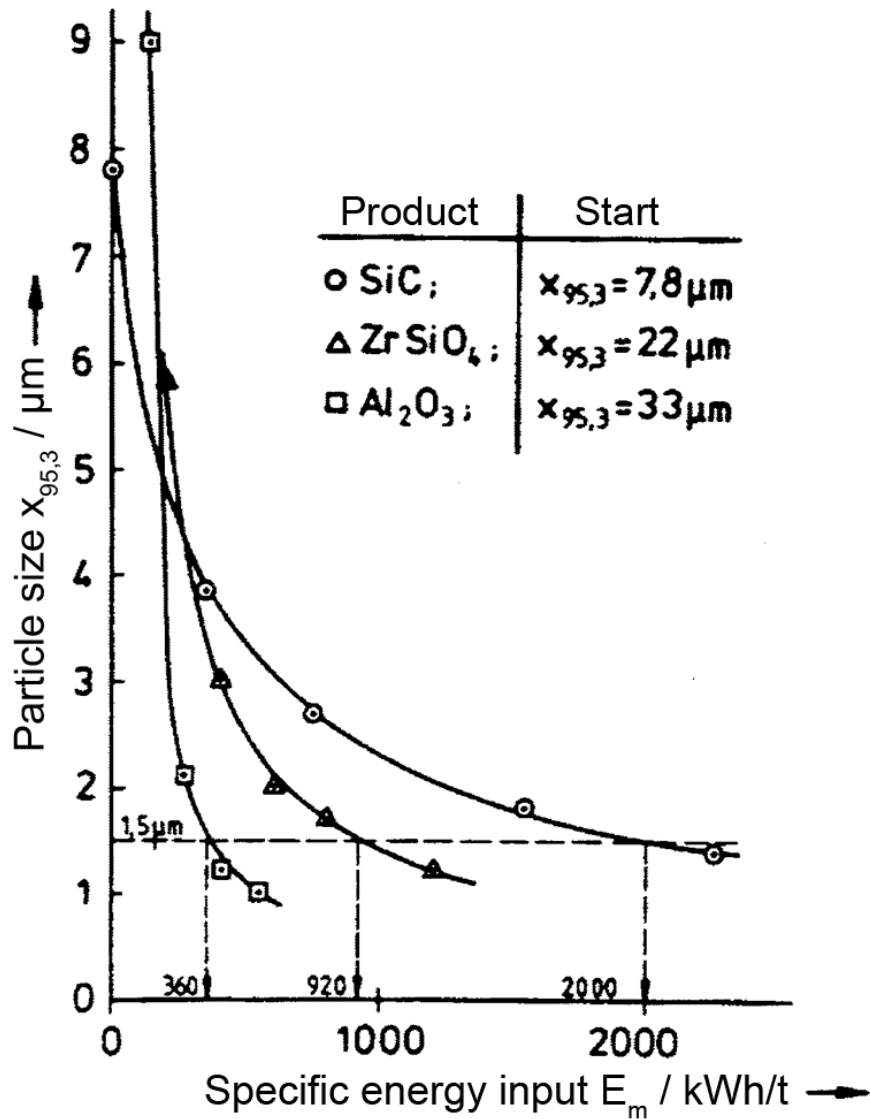


Fig. 3.1.15: Specific mass energy required for the milling of different ceramic materials (Stehr, Draiswerke Mannheim, 1985).

Fig 3.1.16 shows the impact of the grinding ball size on the grinding result. With a grinding body grain size of 1-1.4 mm, the required particle size of 80% < 2 μm is achieved after 315 min. If after 90 min. the grinding media is replace for a size of 0.6 to 0.8 mm diameter, the same particle size is already achieved after 150 min.. Well, it is obvious that in production you cannot empty a mill, separate the mill medium from the grinding stock and then restart the mill. But you can connect two mill types in series and in this way optimise the grinding result.

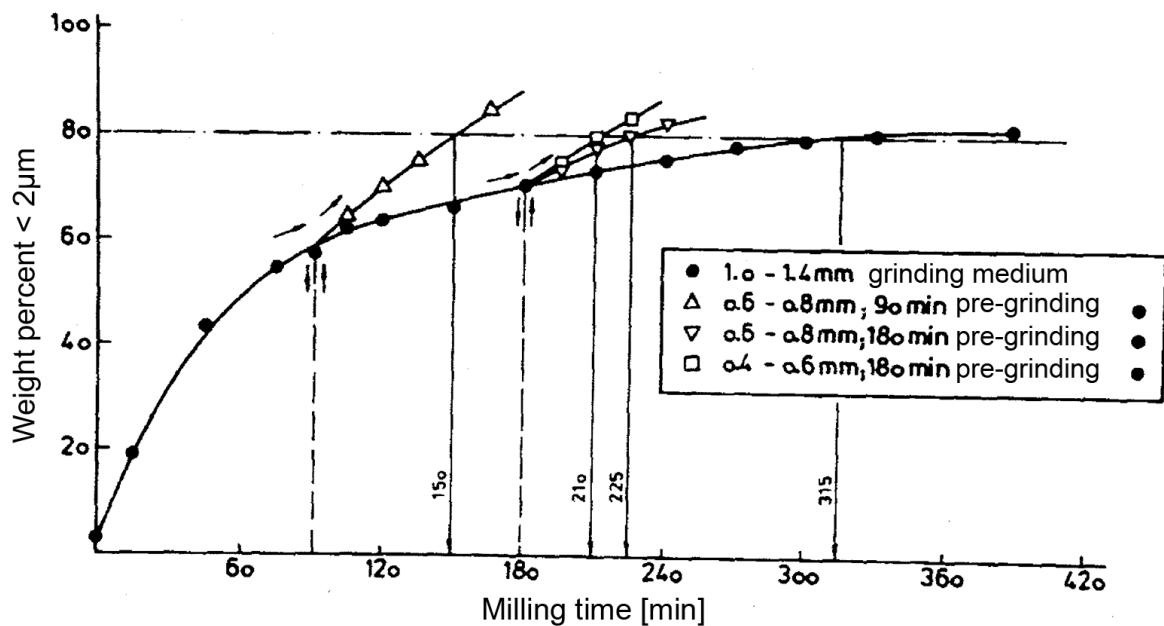


Fig. 3.1.16: Influence of the size of the milling agent on the grinding duration for a desired average particle size finer than  $x_{80.3}=2\mu\text{m}$  (Stehr, Draiswerke Mannheim, 1985).

All these grinding aggregates have the disadvantage that abrasion of the balls with each other as the balls with the mills' boards are relatively high. Therefore the mill media used for stirred media mills is often composed of the same material as the material to be grinded. In laboratory scale this is no problem. But as powders are prepared within ton scale, inexpensive steel balls or flint pebbles ( $\text{SiO}_2$  stones) are frequently used. The alternatives are to either accept the impurities or to separate the contaminants afterwards by a chemical treatment. Abrasion is avoidable in the so-called impact mill where the grinding material is accelerated with air and very high pressure and the accelerated particles are shot against one another (Fig. 3.1.17). The particles are virtually grinding themselves without leaving impurities. However, in this case the shape of the grain is not round like in a ball mill, but splintery, because the particles just burst. Compared to round grains such grain morphology may influence transport in tubes in a negative way.

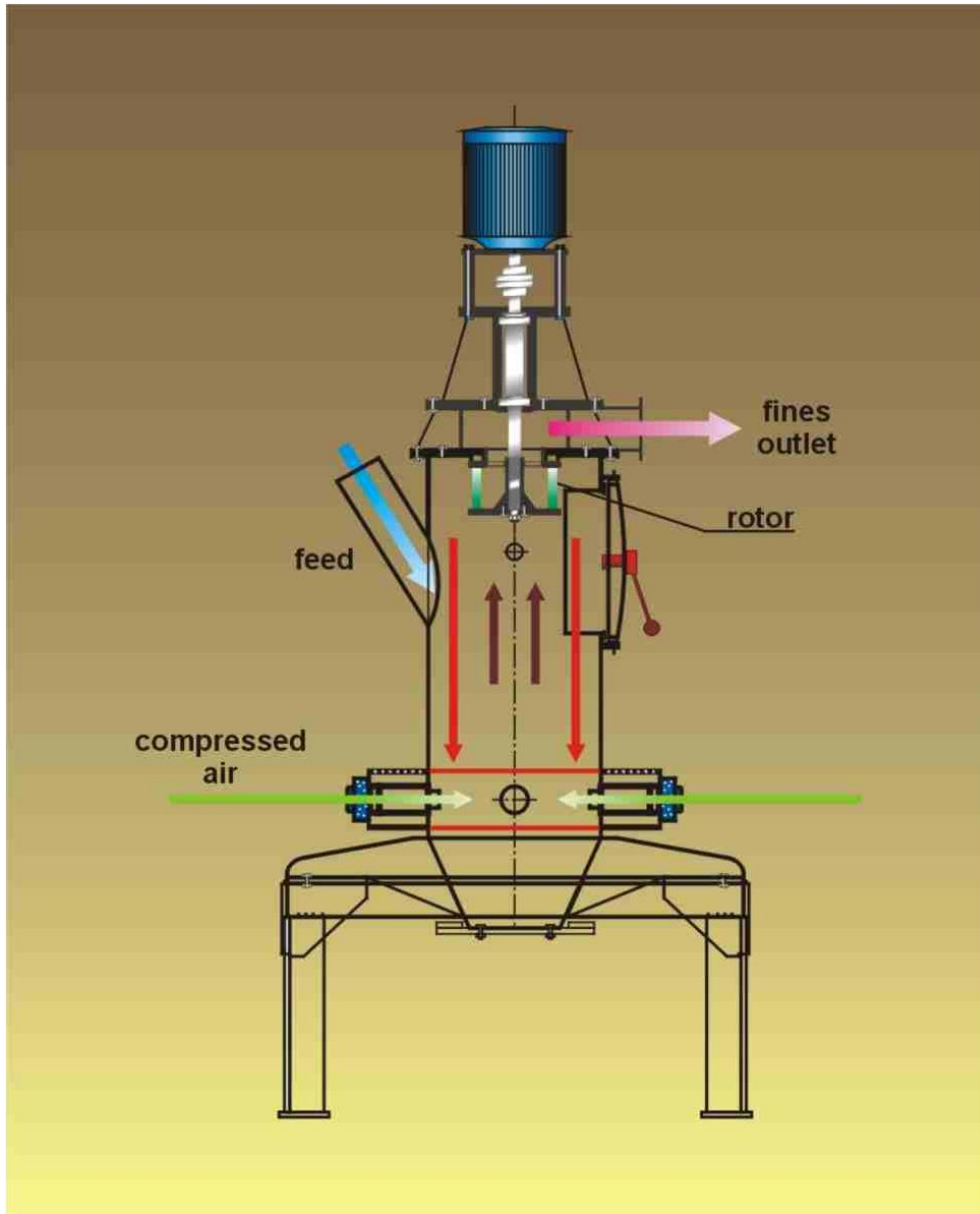


Fig. 3.1.17: Illustration of an impact mill (schematic).

### 3.2 Classification

After milling, a very wide grain size distribution of the powders is normally available. But in order to achieve the defined characteristics for ceramic components after sintering, an exact classification of the powder fractions is necessary.

The easiest procedure for classifying is to sieve (see video clip powder preparation). Depending on the mesh size of each sieve, distinct powder fractions can be separated into coarser and finer (Fig. 3.2.1).



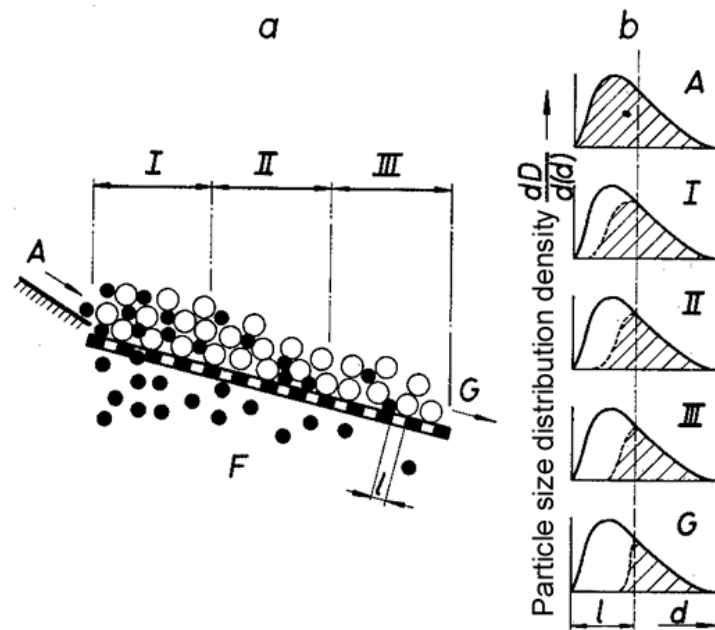


Fig. 3.2.1: Process of sieving [14].

Different kinds of sieves are compiled in Fig. 3.2.2, as compact sieves or grates, drum sieves, throw sieves, flat sieves. The grain sizes which can be classified with sieves lie between 50 and 100  $\mu\text{m}$ , since production of the sieve meshes are mechanically limited and sieves may be blocked by bridging.

1. Fixed sieves and grates



2. Screening machines

2.1 Grates



2.2 Rotary sieves



2.3 Throw sieves



2.4 Flat sieves



Fig. 3.2.2: Overview of equipments and machines used on the classification by sieving according to the type of sieve used [14].

Finer fractions are separated in so-called air classifiers or air separators (Fig. 3.2.3), in which the powder is feed from the top, trickling downwards against an air flow. Following the Stoke's law, finer particles with a certain weight are carried upwards and the coarse fraction falls downwards. With this equipment, exact grain sizes cannot be achieved, but various series have to be connected to get a reasonably sharp separation.

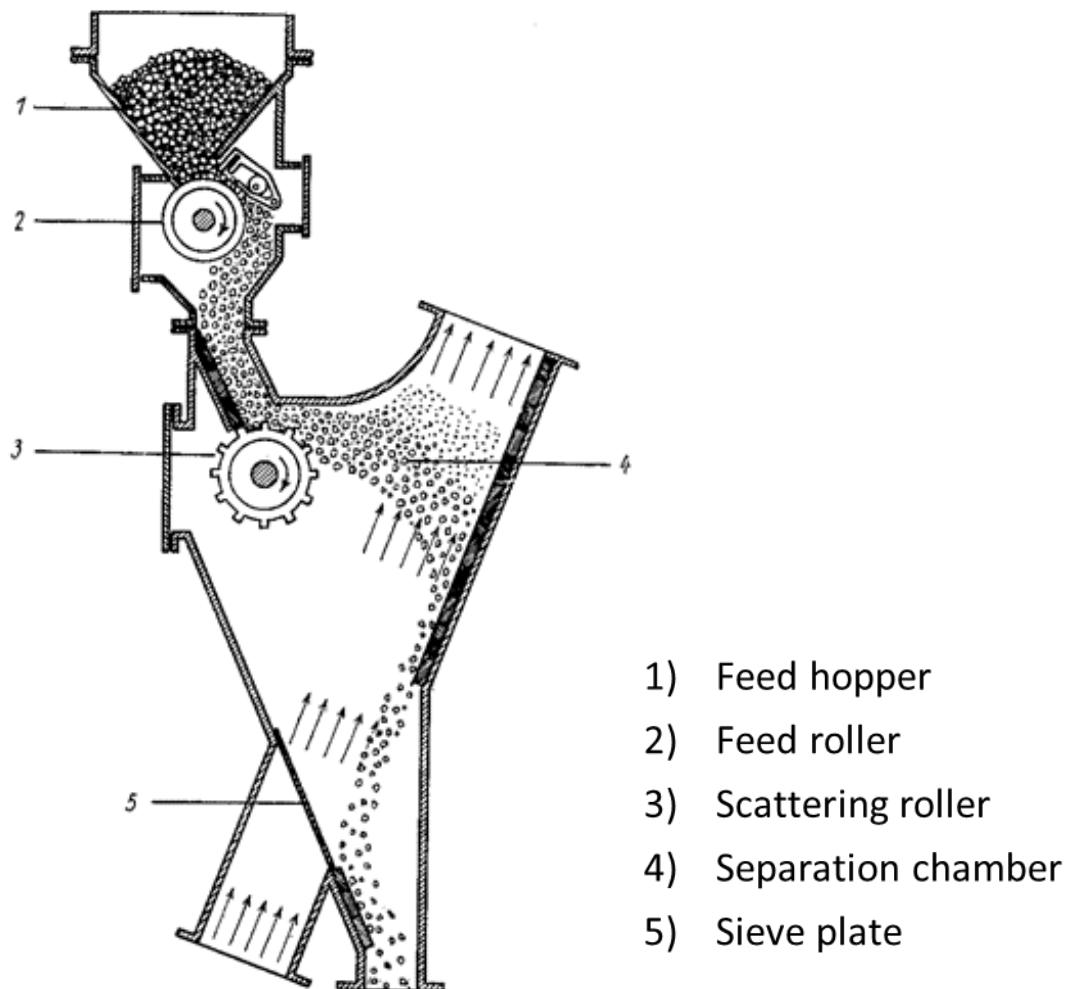
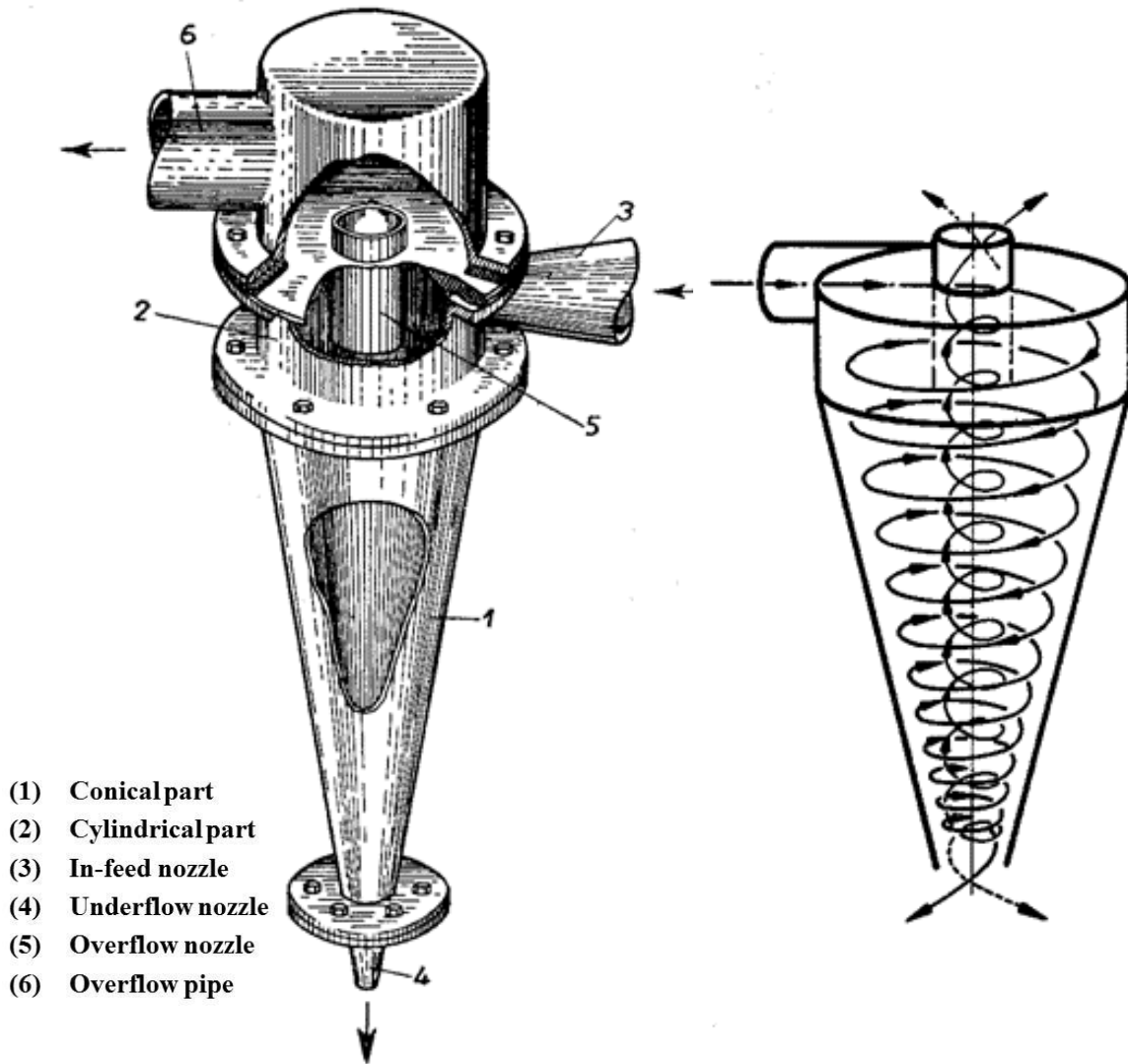


Fig. 3.2.3: Air classifier [14].

If separation cannot be performed at dry conditions, but suspensions must be used, the so-called hydro-cyclones can be used. A suspension is injected into the conic part of the cyclone (Fig. 3.2.4). Two different air cyclones occur, moving downward and upward, respectively. The downward cyclone picks up the coarse fraction; while the upward cyclone the fine ones. Separation effect in a hydro-cyclone is also not exact. Therefore various cyclone series with different geometry and thus different separation effects have to be connected.



**Fig. 3.2.4:** Schematic illustration and principle of operation of a hydro-cyclone [14].

Magnetic particles are stronger deflected by rotary motion in a drum cobber than un-magnetic ones (Fig. 3.2.5) and can be classified in the magnetic field.

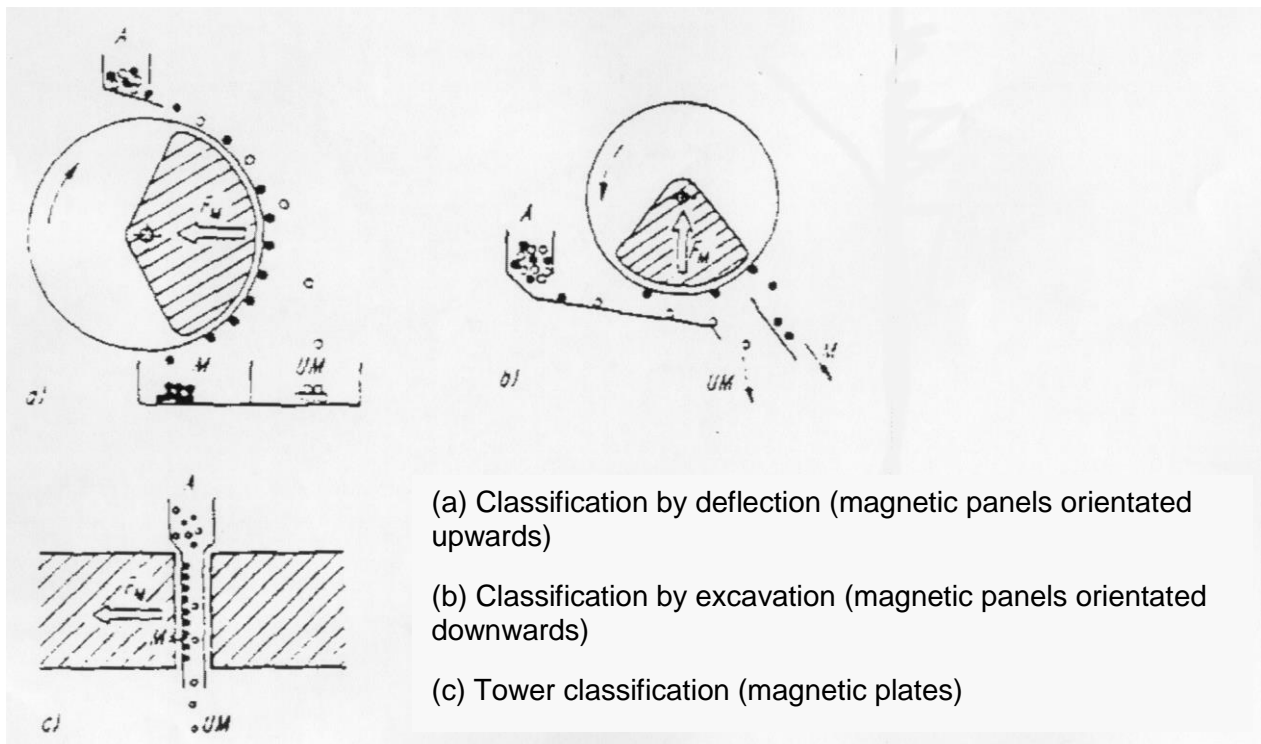
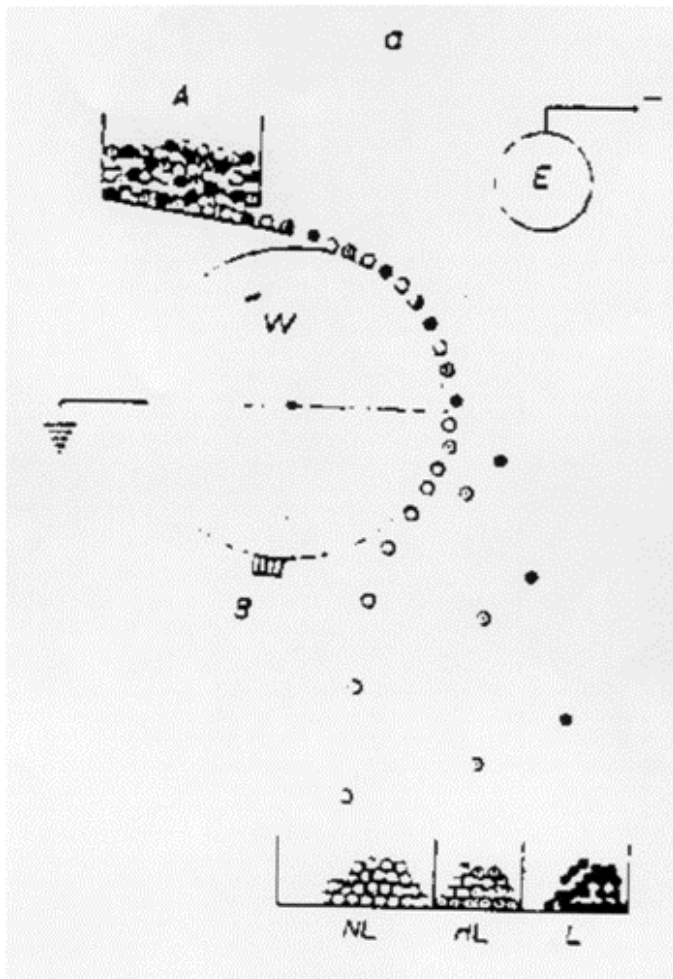


Fig. 3.2.5: Principle of operation on a magnetic panel [14].

Powder surfaces can be electrostatically charged and this effect can be amplified by using different chemical media (Fig. 2.5.4). An electric field is set up through an earthed roller and a backing electrode. Depending on the charge of the powder particles' surface, the particles can be deflected strongly or not by the roller's movement (Fig. 3.2.6).



- A: feed
- W: earthed roller electrode
- B: Brush
- E: Contra electrode
- L: Conductive
- HL: Semi-conductive
- NL: Non-conductive

Fig. 3.2.6: Separation model at a electrostatic roller separator [14].

Another possibility of material separation is flotation. Long-chain molecules can attach at the surface of the particles conducting to a float when in a suspension (Fig. 3.2.7). Particles with long-chained molecules at the surface float at the top and can be discharged. Particles with minor addition or short-chained molecules do sediment downwards.

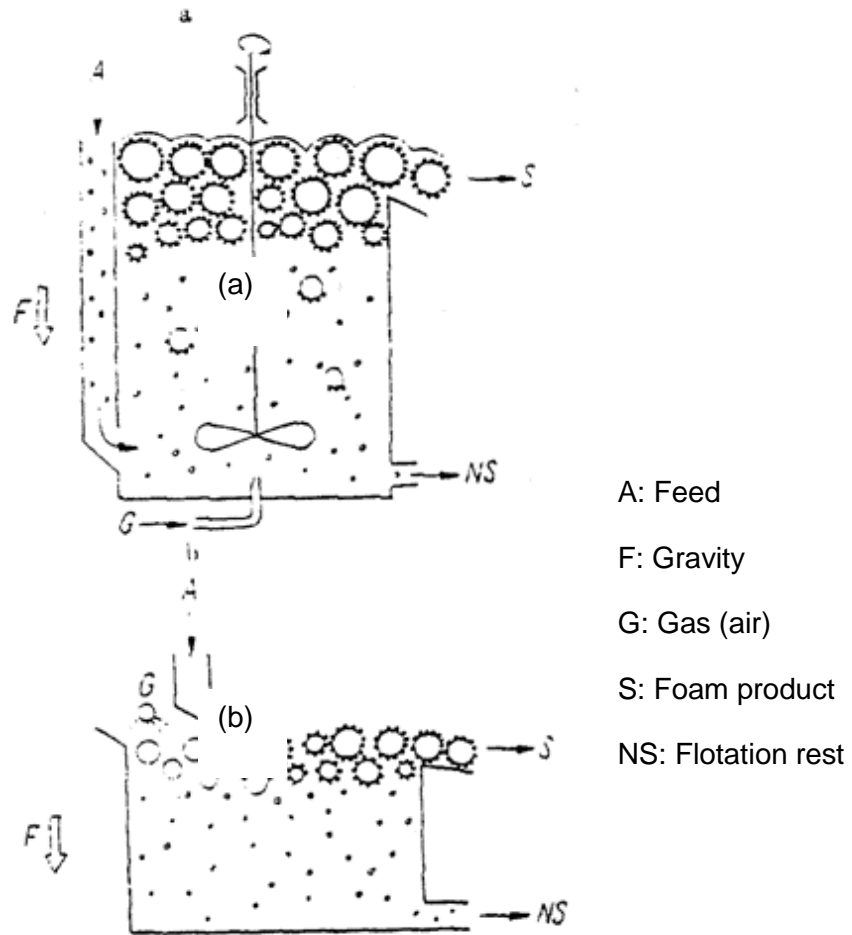


**Fig. 3.2.7:** Operation principle of the heterogeneous coagulation (a) foam flotation (b) foam separation.

After milling and sieving, further steps of the powders' processing is often difficult due to their high specific surface. Moreover the high specific surface can hinder or limit the flowability of ceramic powders. In order to facilitate transport of powders, for instance, in moulding machines, finest powders have to be granulated.

## 4. Forming

This text corresponds to e-book "Introduction to the Principles of Ceramic Forming", ISBN 3-87264-016-X [4].

### 4.1 Introduction

With the exception of some new developments nearly all ceramic forming processes may be classified by three groups, i.e. „casting“, „plastic forming“ or „pressing“.

In such processes the starting powders are prepared in aqueous or organic solvents in the beginning. In case of casting these suspensions are directly processed while plastic forming requires partly dewatered feeds and almost completely dry granules are used in the pressing process.

To produce stable suspensions both the surface condition of the powder particles and the interaction with the suspension media are of utmost importance. That is why the first chapter deals with general principles on this subject and describes the plasticity of ceramic systems and the production of granules from suspensions.

In the second part the individual forming processes will be discussed, laying special stress on theoretic principles. Chapter two closes with the description of some new developments whose suitability in practical applications is still pending to some extent. Not everyone looking for practical help in this introduction will find it. May be this paper serves only as basic information for engineers to continue elaborating their own solutions for special problems that may arise in practical application.

### 4.2 General principles

In almost all forming processes applied for manufacturing ceramic products basically powders are dispersed, mixed and homogenized in water or organic solvents. For the further treatment of these suspensions it is essential to understand the reactions at the surface of the powder particles.

## 4.2.1 Characterisation of suspensions

### 4.2.1.1 Particle charging in liquid suspensions

Ceramic powders normally have a high specific surface to show electric charges in aqueous suspensions. Such electric charges may be explained as follows: oxides show unsaturation at their surface due to the incomplete coordination of atoms. When these oxide surfaces get in contact with water the surface becomes hydrated [1].

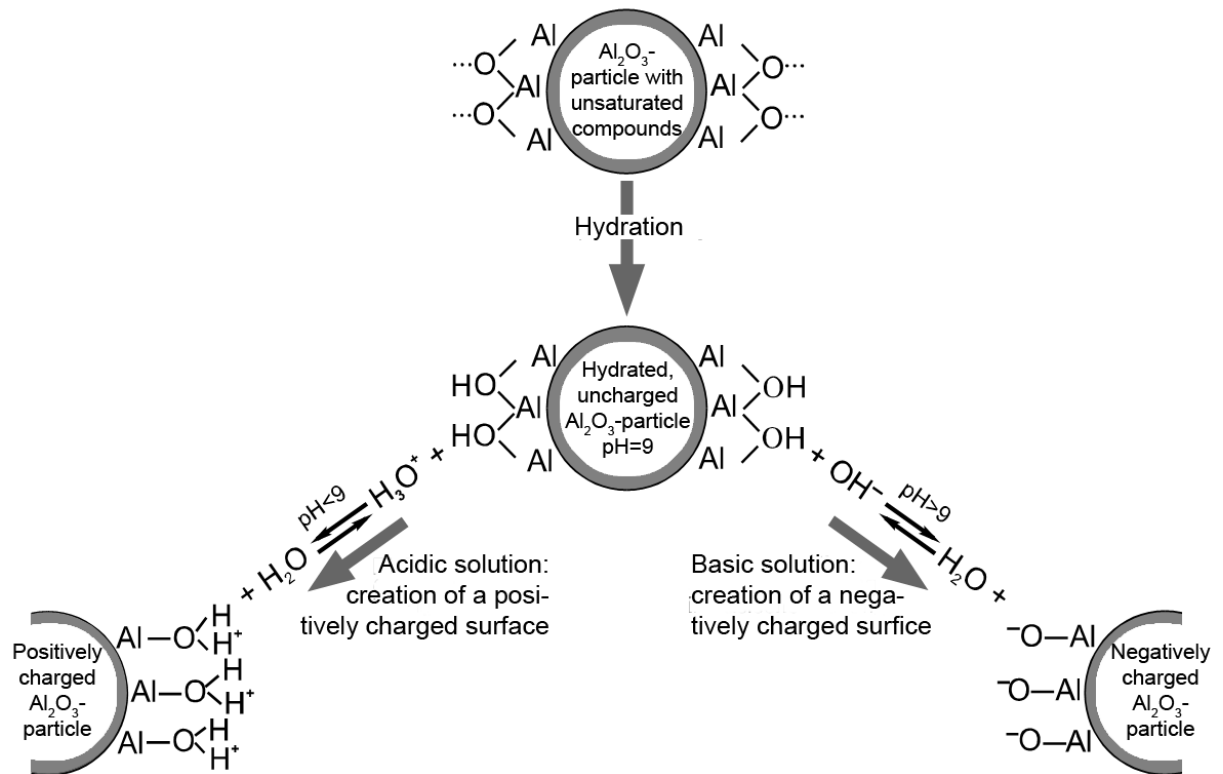
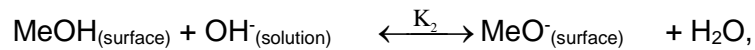
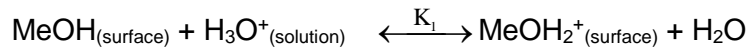


Fig. 4.2.1.1.1: Creation of a hydrated  $\text{Al}_2\text{O}_3$  particle surface and their reaction in acidic and basic solutions (schematic).

In this process protons from the liquid phase are added to surface oxygen ions and create a neutral particle with OH groups at the surface. The surface charges are created subject to the pH of the suspension either by absorbing  $\text{H}^+$  or  $\text{OH}^-$  ions or by dissociating the surface charged OH groups. This mechanism can be seen from fig. 4.2.1.1.1.

The processes appearing at the hydrated surface of an oxide are therefore determined by the chemical reactions





where Me is a metal ion at the surface, i.e.  $\text{Ba}^{2+}$ ,  $\text{Al}^{3+}$  or  $\text{Si}^{4+}$ . By adding  $\text{H}_3\text{O}^+$  ions the pH will be reduced as the uncharged surface absorbs protons and thus becomes positively charged. The addition of  $\text{OH}^-$  ions separates hydrogen from the surface and produces a negative surface charge with pH values that are higher than the point of zero charge (PZC) at the surface.

The point of zero charge – frequently also called isoelectric point (IEP) – of the surface reflecting the acid-base character is given by the two pKs of the above reactions [2].

$$\text{PZC} = \frac{\text{pK}_1 + \text{pK}_2}{2}.$$

According to the valence of the cation and the coordination of the oxygen ions the number of surface charges will vary and the point of zero charge will be shifted.

For pure aluminium oxide the PZC lies at pH= 9. For other oxides with varying crystalline structures the pH values for the point of zero charge will be different (Fig. 4.2.1.1.2).

The creation of surface charges in layer minerals like kaolinite has other reasons. In the tetrahedral di-silicate layer four-valence silicon ions may be replaced by trivalent aluminium ions, in the octahedral gibbsite layer aluminium ions may be replaced by bivalent magnesium ions or by other ions of equal valence by incorporating alkali or earth alkali ions into the lattice for valence compensation. In case of incomplete valence compensation charges will appear at the surface of the kaolinite particles. Moreover, the relatively dissolute alkali or earth alkali ions that are incorporated in the intermediate layers of the kaolinite structures may be absorbed in aqueous media and create additional negative surface charges (Fig. 4.2.1.1.3).

Material	Chemical composition	IEP
Muscovite	$KAl_3Si_3O_{11} \cdot H_2O$	1
Quartz	$SiO_2$	2
$\delta$ -Manganese oxide	$MnO_2$	2
Soda lime silica glass	$1,00 Na_2O \cdot 0,58 CaO \cdot 3,70 SiO_2$	2-3
Albite	$Na_2O \cdot Al_2O_3 \cdot 6 SiO_2$	2
Orthoclase	$K_2O \cdot Al_2O_3 \cdot 6 SiO_2$	3-5
Silica (amorphous)	$SiO_2$	3-4
Zirconia	$ZrO_2$	4-5
Rutile	$TiO_2$	4-5
Tin oxide	$SnO_2$	4-7
Apatite	$10 CaO \cdot 6 PO_2 \cdot 2 H_2O$	4-6
Zircon	$SiO_2 \cdot ZrO_2$	5-6
Anatase	$TiO_2$	6
Magnetite	$Fe_3O_4$	6-7
Haematite	$\alpha\text{-}Fe_2O_3$	6-9
Goethite	$FeOOH$	6-7
$\gamma$ -Iron oxide	$\gamma\text{-}Fe_2O_3$	6-7
Kaolin (edges)	$Al_2O_3 \cdot SiO_2 \cdot 2 H_2O$	6-7
Chromium oxide	$\alpha\text{-}Cr_2O_3$	6-7
Mullite	$3 Al_2O_3 \cdot 2 SiO_2$	7-8
$\gamma$ -Alumina	$\gamma\text{-}Al_2O_3$	7-9
$\alpha$ -Alumina	$\alpha\text{-}Al_2O_3$	9-9,5
Alumina (Bayer process)	$Al_2O_3$	7-9,5
Zinc oxide	$ZnO$	9
Copper oxide	$CuO$	9
Barium carbonate	$BaCO_3$	10-11
Yttria	$Y_2O_3$	11
Lanthanum oxide	$La_2O_3$	10-12
Silver oxide	$Ag_2O$	11-12
Magnesa	$MgO$	12-13

Fig. 4.2.1.1.2: Point of zero charge (IEP) of different oxides in watery suspensions [2].

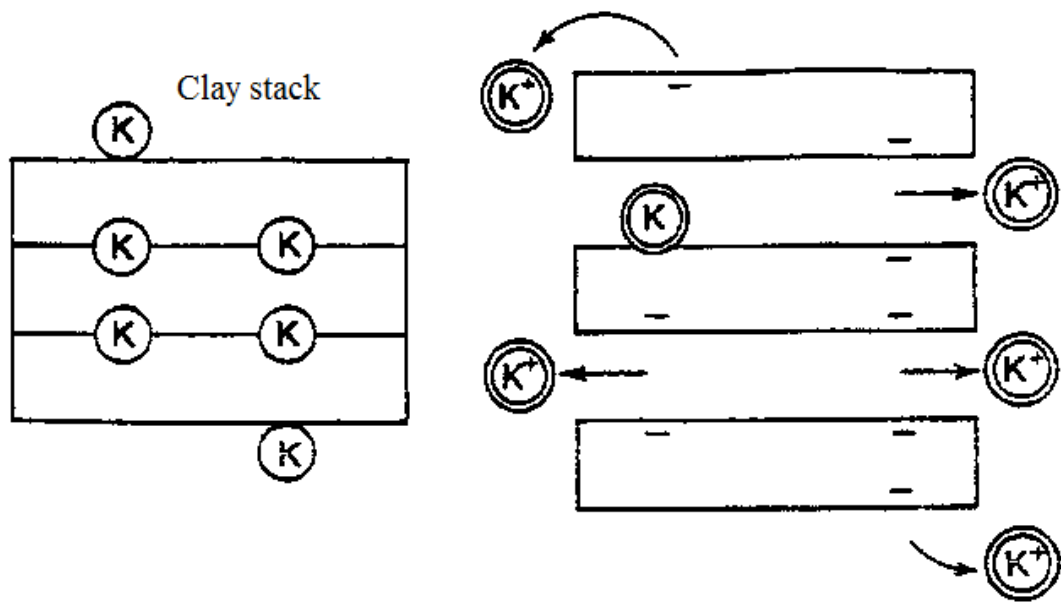


Fig. 4.2.1.1.3: Formation of surface charges at clay stacks by liberating alkali ions from the intermediate layers (schematic) [2].

Apart from the cation exchange capacity there is also an anion exchange capacity available at the edges of the kaolin particles that give rise to positively charged surfaces. This was made visible in an electron-microscope by Thiessen [3] upon the adsorption of negatively charged colloidal gold particles (Fig. 4.2.1.1.4).

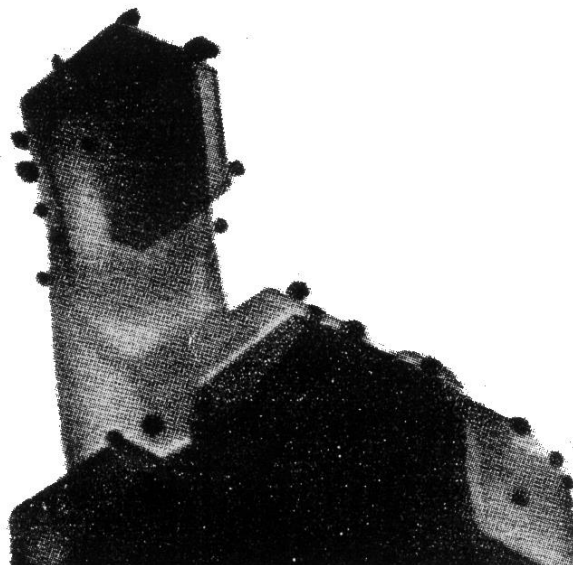


Fig. 4.2.1.1.4: Adsorption of a negatively charged gold colloid on kaolin particles [3].

#### 4.2.1.2 Electrical double layers on particle surfaces

In ceramic slurries particles with charged surfaces are surrounded by ions and polar molecules. Equally charged ions are repulsed due to the Coulomb force while oppositely charged ions and polar molecules are attracted. That is why the concentration of counter ions increases at the particle surface and an electric potential is created between the surface and the suspension (Fig. 4.2.1.2.1).

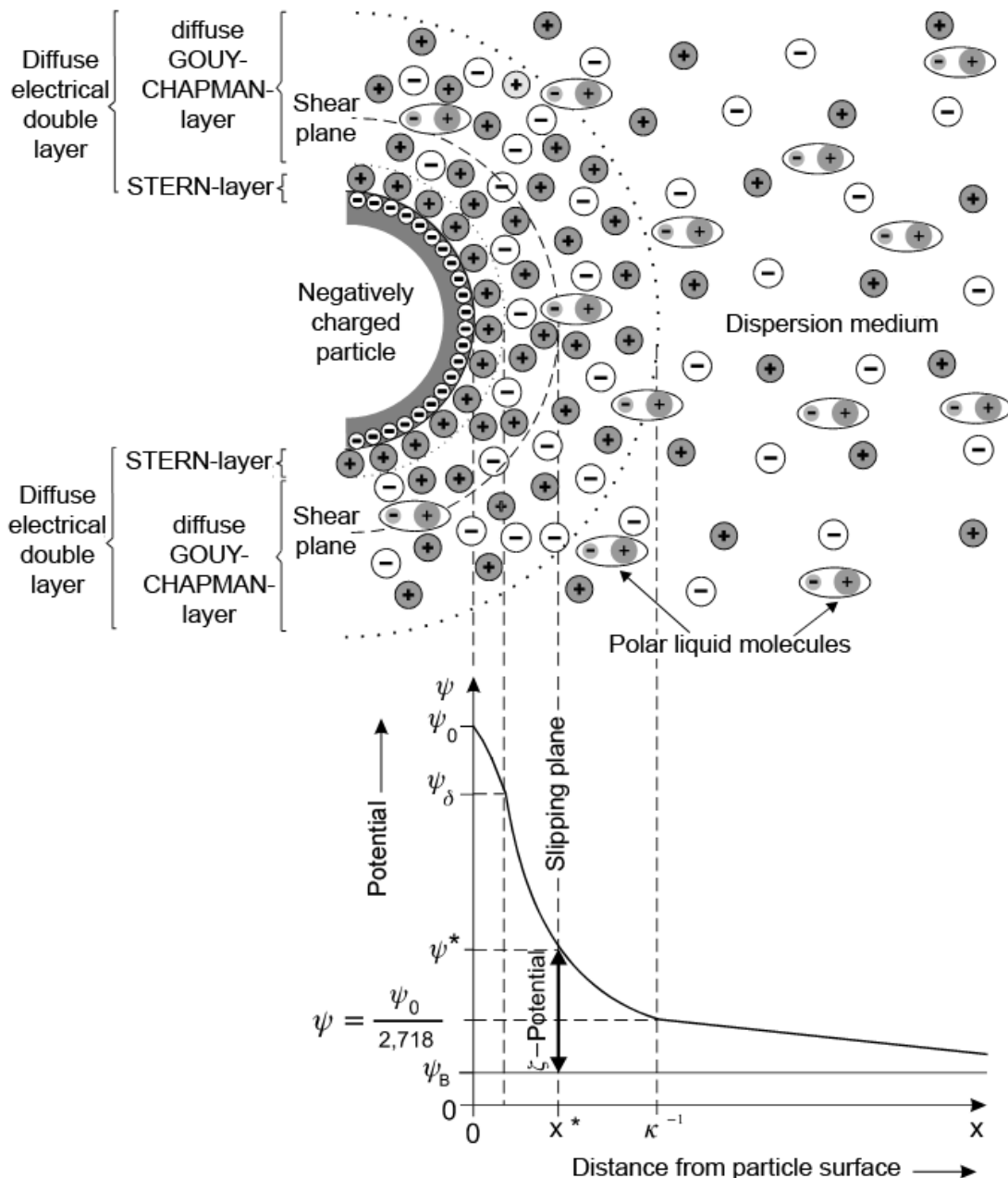


Fig. 4.2.1.2.1: Diffuse electric double layer at a solid particle surface in aqueous suspension and potential gradient between particle surface and suspension (schematic).

At the interface between powder particles and dispersion medium the solid particles are surrounded by a layer of absorbed ions that fit relatively tight to the particle surface. Helmholtz [4] implied that every negative charge of the particle was saturated by a counter ion, but for steric reasons the counter ions will not, as a rule. That is why in the farer surroundings of the powder particles a so-called diffuse electric double layer is built up by a concentration gradient of counter ions and polar molecules of the liquid (fig. 4.2.1.2.1). The potential gradient is no sharp line, as a diffusion of counter ions will be caused by the thermic movement of molecules.

The built-up of this diffuse electrical double layer has been discussed and modified by Stern [5] as well as by Gouy [6] and by Chapman [7]. The potential gradient of the diffuse interfacial layer can be calculated accordingly both for a continuously charged surface and a solution with continuous dielectric constant  $\epsilon_r$  and point charges. Assuming that the charge distribution can be described by the Boltzmann equation the result is the concentration of counter ions  $N_i$  in the diffuse layer compared to the concentration of ions in the solution  $N_i^0$ .

$$N_i = N_i^0 \exp\left(-\frac{U_i}{k_B T}\right).$$

The potential energy of the ions  $U_i$  is a function of the valence  $z_i$  of the ion, the electron charge  $e$  and the electric potential  $\psi$  at the respective position

$$U_i = z_i e \psi.$$

For a surface potential  $\psi_0 \leq 100$  mV is

$$\psi = \psi_0 \exp(-\kappa x)$$

where  $x$  is the distance from the particle surface and the Debye constant

$$\kappa = \left( \frac{e^2 \sum N_i^0 z_i^2}{\epsilon k_B T} \right)^{1/2}.$$

The surface potential thus decreases exponentially in the first approximation with the distance from the particle surface. When  $x = \kappa^{-1}$  is  $\psi = \psi_0/2,718$  (see fig. 4.2.1.2.1). From the ionic strength  $I = \frac{1}{2} \sum c_i z_i^2$  ( $c_i$  = ionic concentration in mol/l) results the thickness of the diffuse electric double layer as

$$\kappa^{-1} = \left( \frac{2000e^2 N_A I}{\epsilon k_B T} \right)^{1/2},$$

where  $N_A$  is the Avogadro's number. For water of 25 °C a thickness of the diffuse electric double layer of 9,6 nm is calculated for a 0,001 molar 1:1 electrolytic solution according to Horn [8].

By modifying the concentration or the valence of the counter ions and by varying the dielectric constant  $\epsilon_r$  and the temperature of the liquid the thickness of the diffuse electric double layer may be varied which is of decisive importance for the stabilization of ceramic slurries.

#### 4.2.1.3 Electrokinetic properties and slip stability

In an electric field electrically charged particles move with a certain speed, the so-called electrophoretic velocity. A part of the diffuse electric double layer passes with the particles through the liquid. So a slippage plane is built up within the diffuse electric double layer to transport the surface ions or polar molecules through the liquid. In figure 4.2.1.2.1  $\psi_0$  is the potential of the particle surface,  $\psi_B$  the potential of the surrounding liquid,  $\psi_S$  the potential of the Stern layer and  $\psi^*$  the potential of the hypothetical slippage plane. The potential difference between the potential  $\psi^*$  of the slippage plane and the potential  $\psi_B$  of the surrounding liquid is called electrokinetic potential or zeta potential. The zeta potential can be calculated as follows according to Reed [2].

$$\zeta = \frac{f_H \eta v_e}{\epsilon_r \epsilon_0 E},$$

where  $\eta$  is the viscosity of the electrolyte and  $v_e$  is the electrophoretic velocity for an imposed electric field  $E$ . The ratio  $v_e/E$  is the electrophoretic mobility.

The Henry constant  $f_H$  is equal to 1, when the product of the particle diameter  $d$  and the Debye constant  $\kappa$  is greater than 100 and  $3/2$  when  $d \cdot \kappa$  is less than 1.

The size of the zeta potential depends on the thickness of the double layer  $D$  as well as on the total charge of the ions settled down on the particle surface. The addition of electrolyte to a slip of constant water content leads first to an increase in thickness of the double layer and to an increase of the total charge, i.e. the zeta potential grows.

When the double layer is at it's optimum the zeta potential will decrease again, as only the potential of the aqueous solution  $\psi_B$  will be increased (Fig. 4.2.1.2.1). This appearance is to be observed both at negatively and at positively charged particle surfaces. The pH with a zeta potential of 0 is called the isoelectric point (IEP). The schematic course of the zeta potential as a function of the pH is to be seen from fig. 4.2.1.3.1.

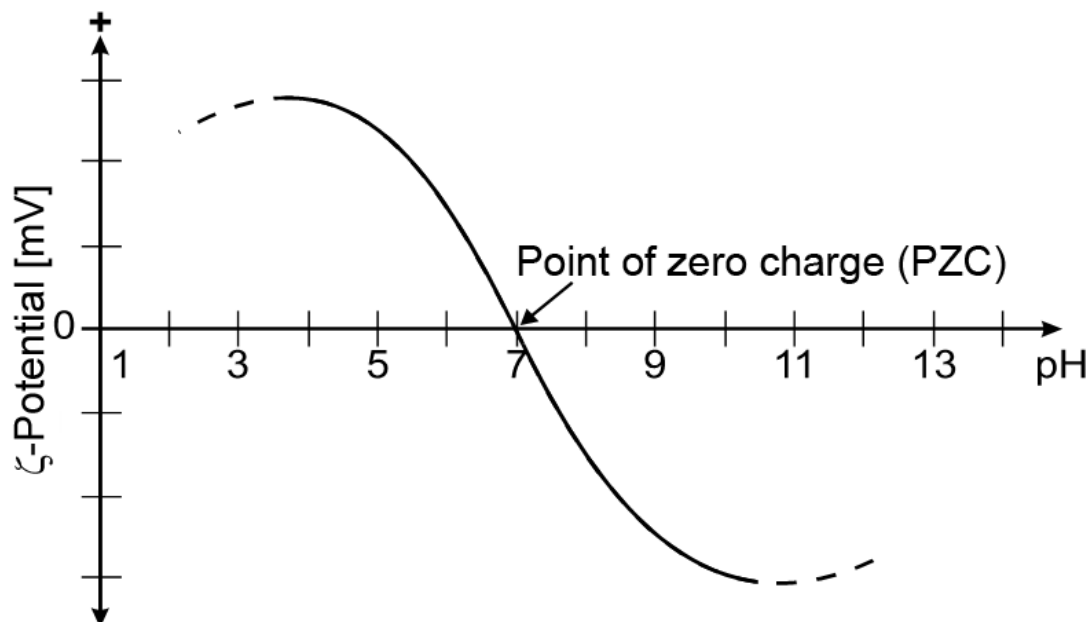


**Fig. 4.2.1.3.1:** Zeta potential as a function of the pH of the solution (schematic).

The increase of the zeta potential both at positively and negatively charged particle surfaces corresponds to the increase in thickness of the diffuse electric double layer.

The interaction of two particles with the same surface charge is described in the so-called DLVO theory both by Derjaguin and Landau [9] and by Verwey und Overbeek [10]. Van-der-Waals attractive forces are the driving force for the coagulation of the particles. For small particle diameters  $d$  and the distance of the particle surfaces  $h$  the potential energy for the attraction is obtained by the equation

$$U_{\text{anziehend}} = \frac{(\sqrt{A_2} - \sqrt{A_1})^2 \cdot d}{24 \cdot h}, \quad \text{attractive}$$

where  $A_1$  and  $A_2$  are the Hamaker constants for particles and dispersion medium.

In order to avoid an agglomeration repulsive forces have to react against the particle attraction. These repulsive forces may result from the interaction between electric double layers. They depend on the size and shape of the particles, the distance  $h$  between their surfaces, the thickness of the double layer  $\kappa^{-1}$  and the dielectric constant  $\epsilon_r$  of the liquid medium. According to the Coulomb law the potential energy of the repulsive forces is calculated as follows for values of  $d/\kappa^{-1} \ll 1$ , i.e. for small particles with relatively large double layer

$$U_{\text{abstoßend}} = \frac{\epsilon_r \cdot d^2 \cdot \psi_0^2}{4(h+d)} \cdot \exp\left(-\frac{h}{\kappa^{-1}}\right). \quad \text{repulsive}$$

When the particle diameter is much bigger than the electric double layer, as this is normally the case for ceramic powder particles in aqueous suspension, i.e. for  $d/\kappa^{-1} \gg 1$ , the following equation is applicable

$$U_{\text{abstoßend}} = \frac{\epsilon_r \cdot d \cdot \psi_0^2}{4} \cdot \ln \left[ 1 + \exp\left(-\frac{h}{\kappa^{-1}}\right) \right]. \quad \text{repulsive}$$

The total potential energy is obtained from the sum of the attracting van-der-Waals potential energy and the repulsive potential energy as per

$$U_{\text{total}} = U_{\text{attracting}} + U_{\text{repulsive}}$$

If the attracting forces between the powder particles prevail in a suspension (Fig. 4.2.1.3.2), the particles will coagulate.

If the repulsive forces prevail because of the formation of electric double layers, suspensions may be stabilised as may be seen from Fig. 4.2.1.3.2.



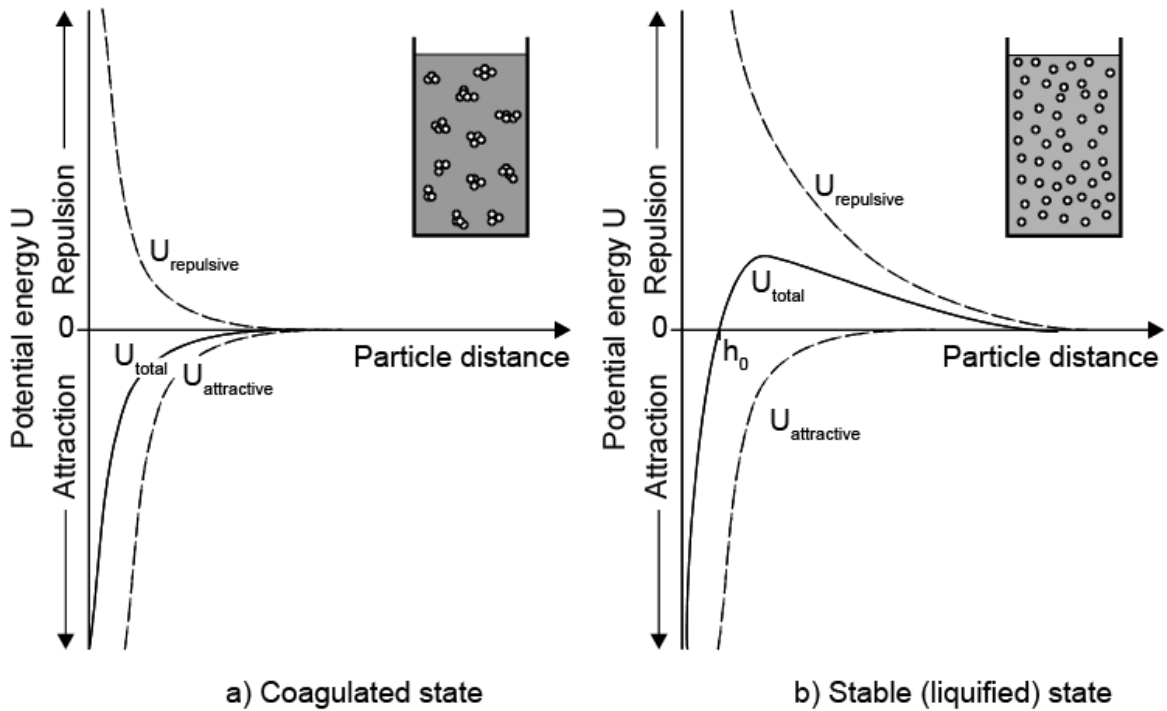


Fig. 4.2.1.3.2: Slip stability and potential energy as a result of the surface condition of particles in an aqueous suspension.

The addition of longer-chain molecules to a charged particle will moreover result in a steric hindrance of the approach of individual particles (Fig. 4.2.1.3.3).

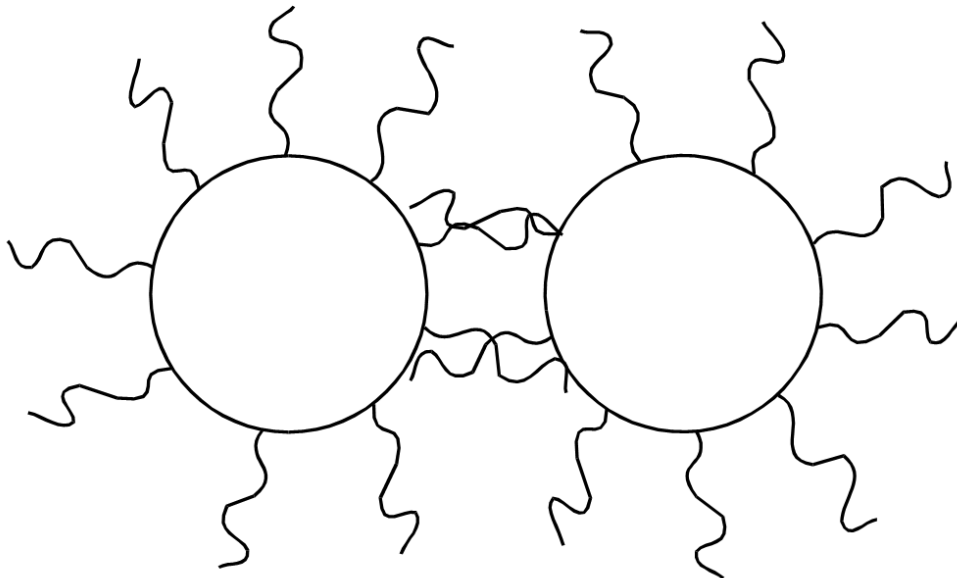


Fig. 4.2.1.3.3: Steric hindrance of the approach of powder particles in a suspension by long-chain molecules settled down (schematic).

The total repulsive potential energy is obtained then from

$$U_{\text{total}} = U_{\text{attracting}} + (U_{\text{repulsive electrostatic}} + U_{\text{repulsive steric}})$$

The steric repulsion is proportional to the thickness of the adsorbed layer and to the chemical composition respectively the concentration of the adsorbed molecules. A particle surface with long-chain molecules settled down on it will avoid the direct interaction between two neighbour particles especially when the surface charges are partly screened by the polymer chains so that the ion concentration around the particles decreases. This corresponds to an increase in thickness of the double layer  $\kappa^{-1}$ .

A good example is the coupling of oleates (that are often used to liquefy ceramic slurries) at  $\text{Al}_2\text{O}_3$  surfaces, which is to be seen from Fig. 4.2.1.3.4.

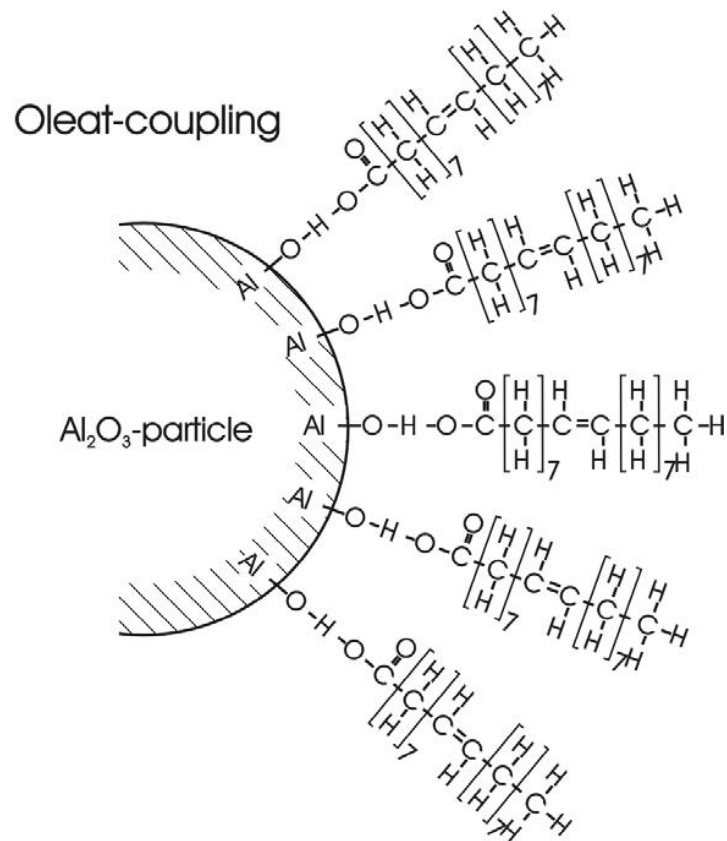


Fig. 4.2.1.3.4: Oleat coupling to a  $\text{Al}_2\text{O}_3$  surface (schematic).

Fig. 4.2.1.3.5 shows some dispersing agents often used in ceramic suspensions which may couple to powder particle surfaces in a similar way.



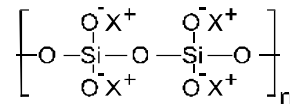
Videoclip: Coagulation

---

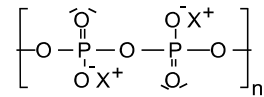
**Inorganic dispersing agents**X=Na, K, NH<sub>4</sub>

---

Polysilicates



Polyphosphates

Also used: sodium hydroxide, soda

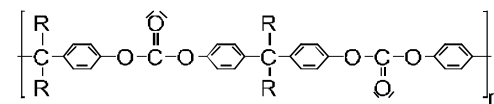
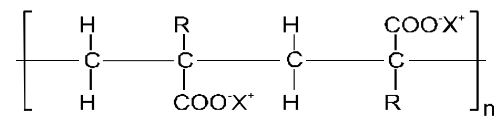
---

---

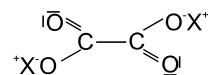
**Organic dispersing agents** X=Na, K, NH<sub>4</sub>; R=C<sub>k</sub>H<sub>2k+1</sub> mit k=0,1,2,3,...

---

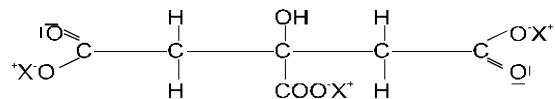
Polycarbonates

Polyacrylates (*k=0*) and methacrylates  
(*k=1,2,3,...*)

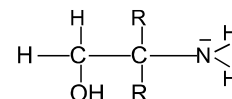
Oxalates



Citrates



Alcanolamines (Aminoalcohols)



Also used: Tartrates, phosphonates, styrolene maleics acid copolymerisates, cellulosics, ligno sulfonates.

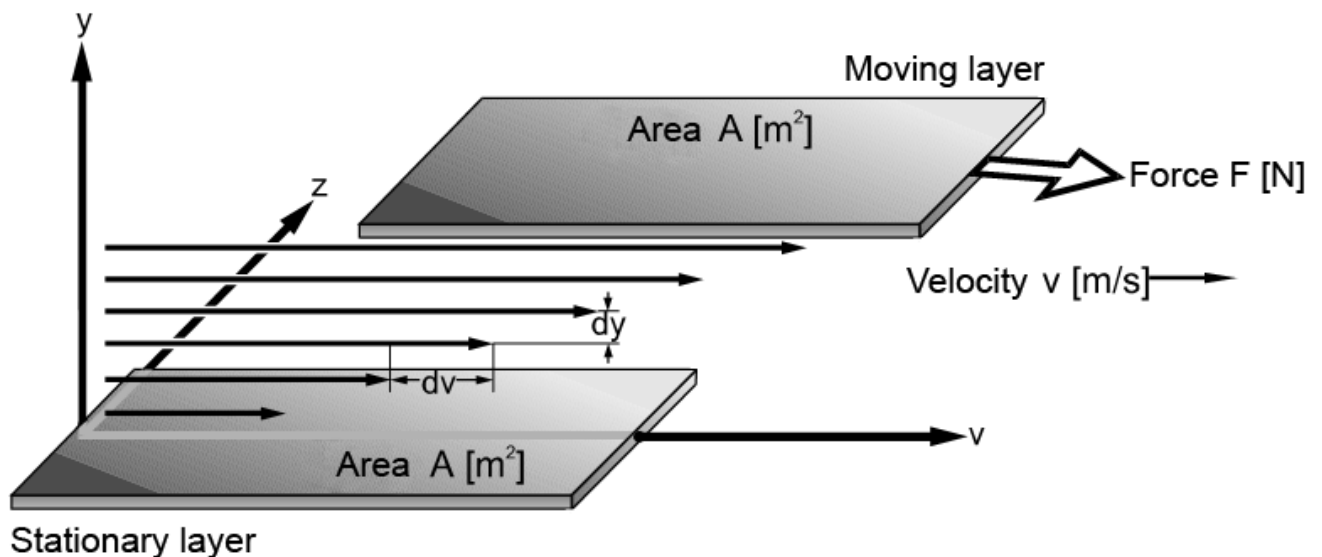
---

Fig. 4.2.1.3.5: Dispersing agents for ceramic suspensions.

#### 4.2.1.4 Rheological properties of ceramic suspensions

The knowledge of the rheological properties of ceramic suspensions is of essential importance for their preparation. To know how these slurries react against relatively weak outer forces allows understanding the structure of the suspension and the processing characteristics required.

In order to adjust laminar flow in a liquid it is necessary to apply a shear stress. Starting from a stationary layer (i.e. the wall of a slip pipe) a velocity gradient  $dv/dy$  (Fig. 4.2.1.4.1) will build up in the liquid when such a stress (for example pump pressure in a slip pipe) is applied.



$$\text{Shear stress } \tau = \frac{F}{A} \text{ [Pa]}$$

$$\text{Shear rate } D = \frac{dv}{dy} \text{ [s}^{-1}\text{]}$$

$$\text{Viscosity } \eta = \frac{\tau}{D} \text{ [Pa}\cdot\text{s]}$$

Fig. 4.2.1.4.1: Model of the viscous flow in a liquid and definition of shear stress, shear rate and coefficient of viscosity.

The velocity of the suspension is 0 at the wall of the slip pipe while it is at its maximum in the middle of the pipe. The size of the shear rate depends on the shear stress and on the material based proportionality factor viscosity  $\eta$ .

$$\frac{dv}{dy} = D = \frac{\tau}{\eta}$$

The viscosity is a measure for the internal friction of liquid molecules counteracting the flow of the liquid. If there is a linear relation between shear rate and shear stress we talk about Newton's liquids (fig. 4.2.1.4.2).

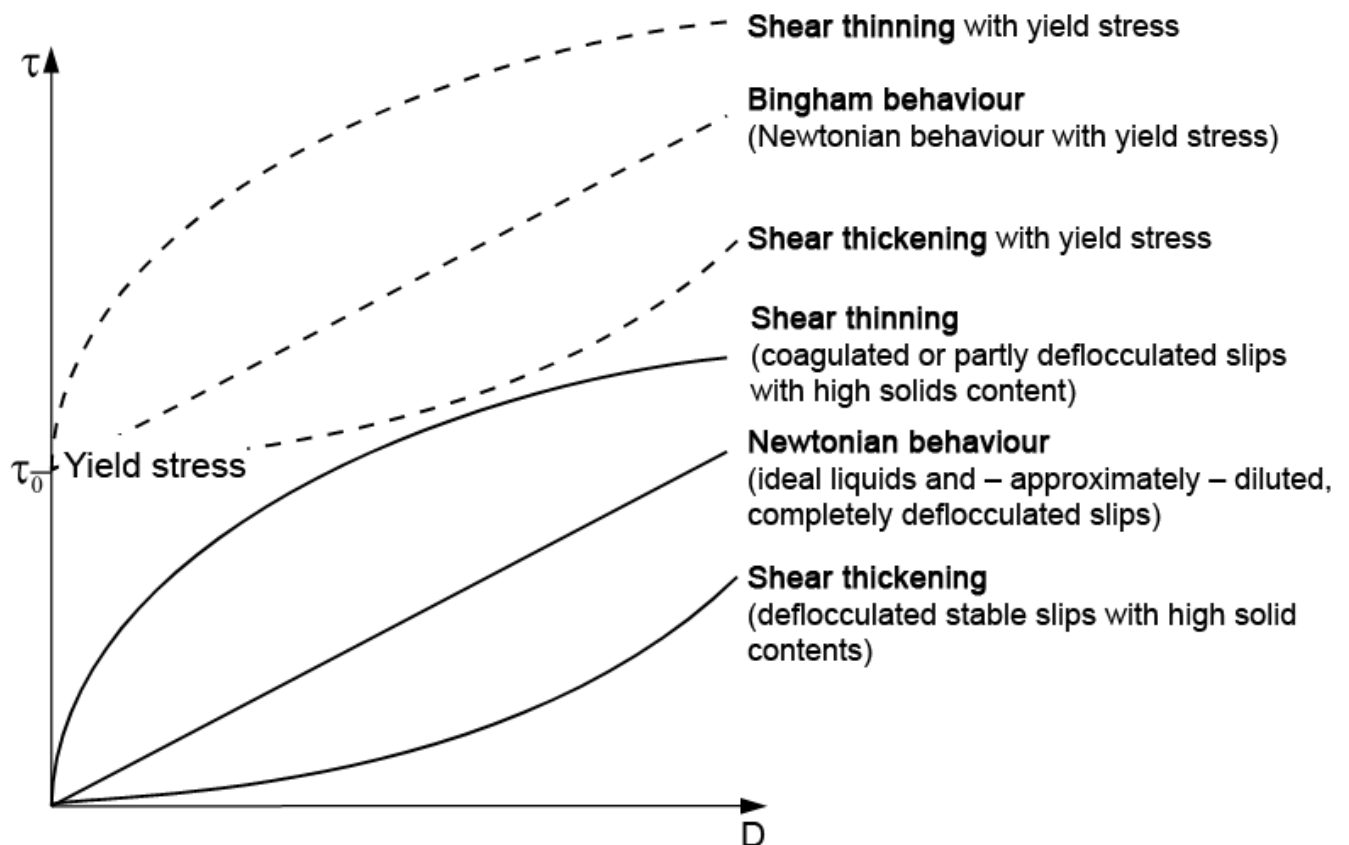


Fig. 4.2.1.4.2: Variation of shear stress with shear rate for different flow behaviour (schematic).

If there are large molecules contained in liquids or when suspensions contain lamellar particles which repulse each other (i.e. kaolin particles) they can direct themselves in a laminar flowing liquid. In addition, in coagulated slurries with high solid yield agglomerates may be destroyed when the shear stress increases. Both appearances reduce the flow resistance and the shear stress required to increase the shear rate by a certain amount will decrease. This behaviour is called shear thinning and may be described mathematically by the below mentioned empiric potential law

$$D = \frac{1}{\eta} \tau^n \quad .$$

$\eta$  is the apparent viscosity to change with increasing shear strain. In case of shear thinning  $n$  will be  $< 1$ .  $n > 1$  describes stable slurries with high solid yield where the interaction between the particles and also the apparent viscosity increases with increasing shear strain. This behaviour is called shear thickening.

In suspensions where molecules or particles build up super structures by mutual interactions (i.e. hydrogen bonds or electrostatic effects) they must be destroyed before starting the flow processes which is achieved at the yield stress  $\tau_o$ . This so-called Bingham behaviour may be described by

$$\tau = \tau_o + \eta \frac{dv}{dy}$$

The dependence on time of the rheological properties is of great practical importance. So for example shear thinning slurries show frequently a decrease in shear stress with time at constant shear rate. In other words the viscosity of the slip (slope of the curves in fig. 4.2.1.4.3) will decrease at constant shear rate with time, the slip becomes more fluid. This thixotropic behaviour is often observed for shear thinning suspensions, where super structures are decomposed in the course of time. This appearance is reversible, as a rule. But in case of a thixotropic slip with yield stress also this value increases sometimes when the slip was kept in neutral position because of further super structures that had been built up.

Some materials show an increase in shear stress at constant shear rate with time i.e. the slip becomes more viscous with increasing time (Fig. 4.2.1.4.3).

This rather rare behaviour is called rheopectic and is observed when due to the slip movement additional bonds between molecules and particles become possible.

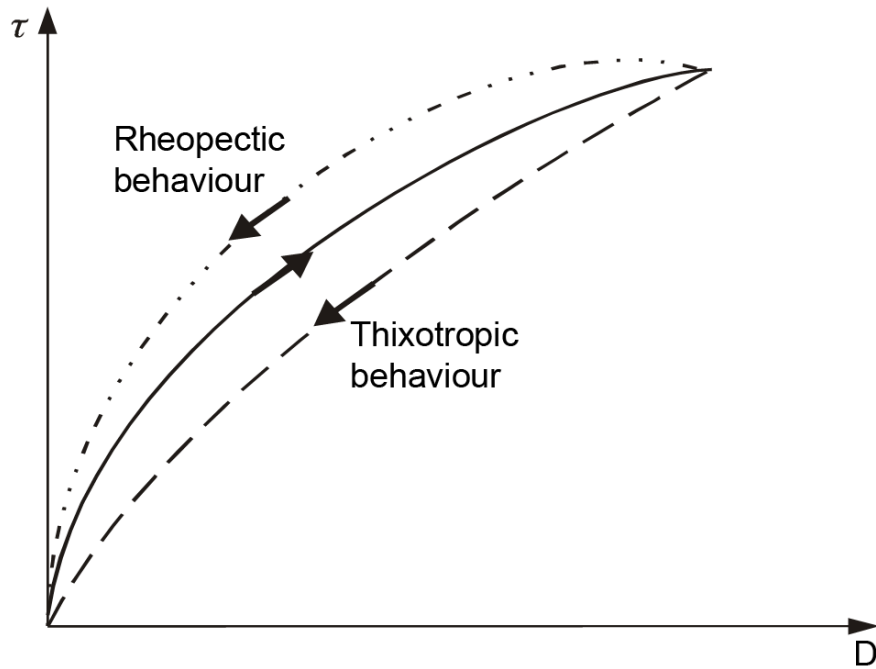


Fig. 4.2.1.4.3: Thixotropic and rheopectic behaviour of ceramic suspensions.

The addition of organic additives (binders, deflocculants) to ceramic suspensions may considerably change the flow curves. Due to the complicated interactions of the organic additives to each other the slip properties are normally empirically optimized in practical use.

With increasing temperature the viscosity of liquids may be reduced as follows

$$\eta = A \exp\left(\frac{Q}{RT}\right)$$

where A and Q = const. Normally ceramic slurries are processed at room temperature. But small thermal fluctuations may cause enormous changes in processing due to the exponential temperature dependence of the viscosity. Moreover, temperatures of 30 to 35°C will very quickly lead to the growth of bacteria cultures that may change the properties of the organic additives considerably and thus the rheological properties of the slurries. This appearance is avoided by adding so-called preservatives.

The viscosity of the suspensions is greater than the viscosity of the liquid. The relation of both to each other is called relative viscosity  $\eta_r$ . For a suspension with particles without any interaction in a Newton's liquid Einstein calculated the viscosity of a laminar flow as follows:

$$\eta_r = \frac{\eta_{Suspension}}{\eta_{Liquid}} = 1 + 2,5V_p \quad .$$

where  $V_p$  is the share in volume of the dispersed particles. An empiric enlargement for solids concentrations up to 74 vol.% is to be seen from Michaels [11]:

$$\eta = \eta_0 \left( 1 + \frac{1,25 V_p}{1 - \frac{V_p}{0,74}} \right)^2$$

In practical use the correlations between viscosity and solid yield are much more complex, but in principle the viscosity will increase with increasing solid yield of the suspension.

For processing ceramic slurries great effort is made to set high solid yields (low drying rate!) and to liquefy the slurries in the optimum way. Fig. 4.2.1.4.4 shows the correlation between the zeta potential respectively the formation of a diffuse electric double layer and the viscosity on the example of alumina. Graule et al. [12] determined a viscosity minimum in the acidic and basic range (Fig. 4.2.1.4.4) in  $Al_2O_3$  slurries. This correlates to a characteristic double layer respectively a high zeta potential in these pH ranges (fig. 4.2.1.4.4). In between is a viscosity maximum coinciding with the isoelectric point where the particles develop only low repulsive forces. The optimum double layer is built up by varying the deflocculant concentration and thus the viscosity minimum for the slip preparation is set.



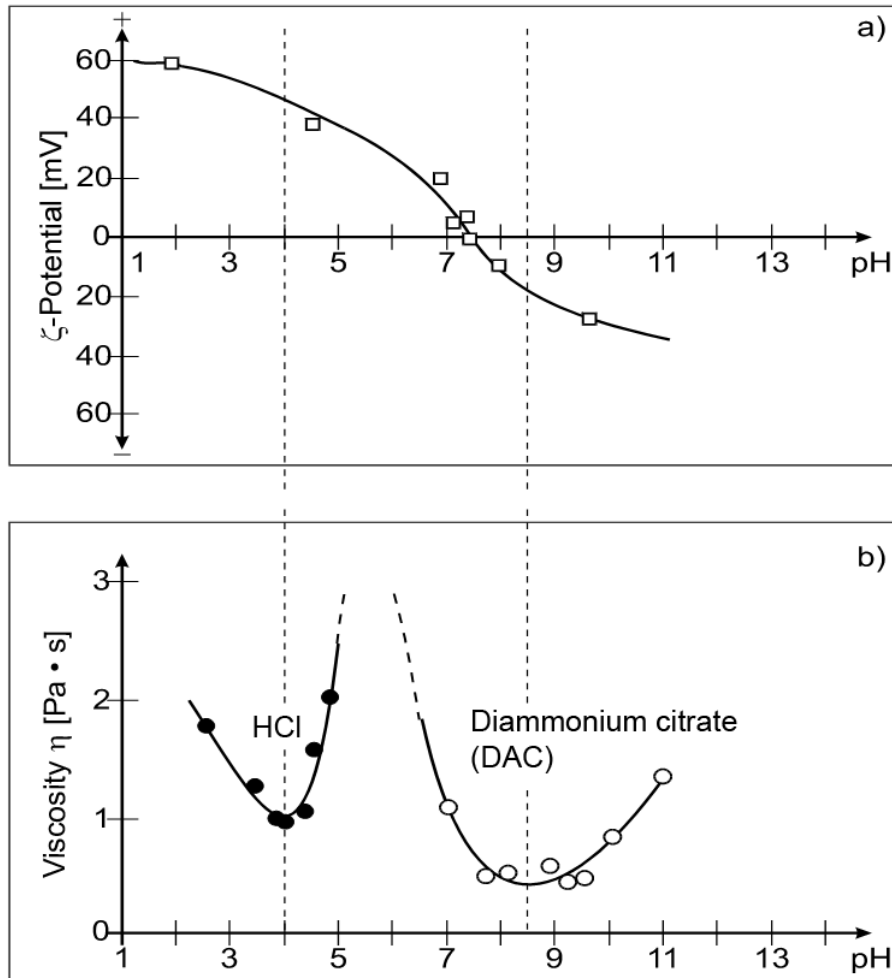


Fig. 4.2.1.4.4: Zeta potential and viscosity of  $\text{Al}_2\text{O}_3$  suspensions (from [12], [13]).

#### 4.2.2 Plasticity of ceramic systems

Plastic behaviour is normally understood as the plastic deformation of a material by means of dislocation movements, grain boundary sliding and diffusion processes. In the ceramics industry this term has been transferred to heterogeneous material mixtures with a liquid phase that show a permanent deformation after surpassing a yield stress without losing the unity of the body building particles [14]. That is why we also call it plasticity limited by crack formation for which maximum stresses and deformations may be specified.

Although a lot of trials have been run in order to define and mathematically determine the terms of plasticity respectively ductility, there is no uniform measuring study available up to this date to test this characteristic. The critical point for plasticity evaluation in the main the yield stress, measured as load under definite geometric conditions in the beginning of the forming process and the maximum achievable deformation up to crack formation.

The Pfefferkorn [15] method is still used in many industrial laboratories because of its simplicity. In this test, a disk falls on a cylinder manufactured out of a ceramic feed and the deformation obtained is the measure for the plasticity of the feed. According to Haase [16] in the Pfefferkorn test the kinetic energy of the falling disk is equated with the deformation work done. The yield stress  $\tau_f$  is calculated from the Pfefferkorn values as follows

$$\tau_f = \frac{m H}{2 V \ln (h_0 / h)}$$

m = mass of the Pfefferkorn disk

H = height of the falling disk

V = volume of the feed cylinder

$h_0, h$  = height of the feed cylinder before and after the compressive strain test

If the Pfefferkorn method is applied by considering the compressive strain until crack formation under slow and quick test conditions and by taking the penetration velocity of a pin under certain conditions as a basis for comparison reasons, you will obtain the plasticity figure according to Dietzel [17] with the respective water content.

In other processes the pressure required to extrude feeds through a die is determined as a function of the yield stress. These methods have been described among others by Macey [18], Linseis [19] and Czerch et al. [20].

The extruded body is characterized by its fracture strength. With increasing water content the fracture strength passes through its maximum while the deformation pressure decreases steadily (Fig. 4.2.2.1). According to Haase [14] the ratio of fracture strength to deformation pressure may be used as a criterion for plasticity, as shown in Fig. 4.2.2.2.

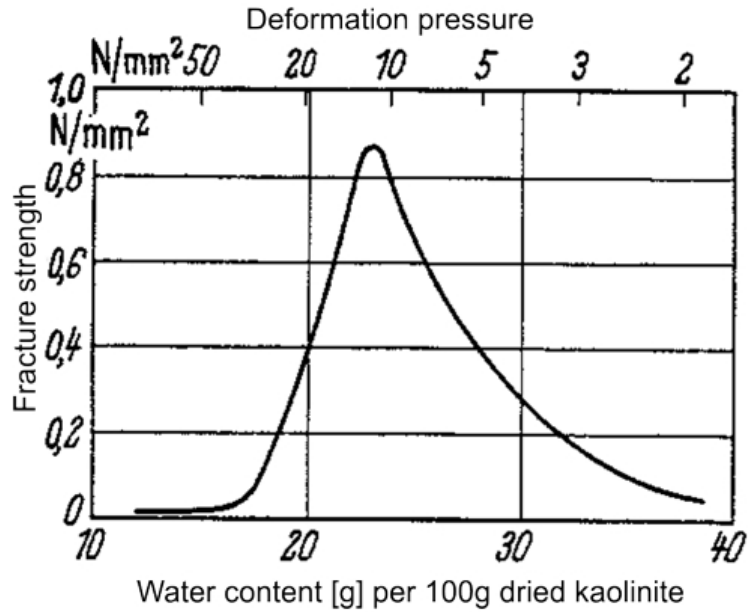


Fig. 4.2.2.1: Dependence of fracture strength and deformation pressure of a Ca kaolinite on the water content according to Czerch et al. [20].

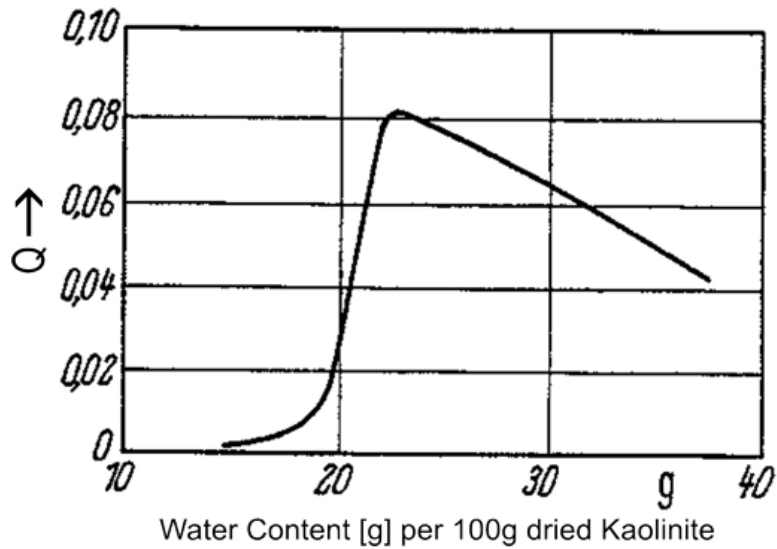
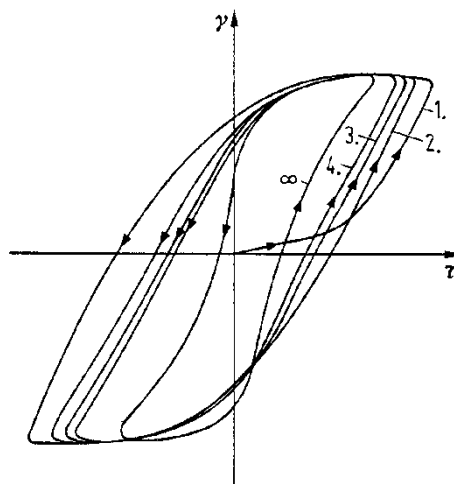


Fig. 4.2.2.2: Evaluation of the curve in Fig. 4.2.2.1 as per the ratio  $Q$  = fracture strength /deformation pressure.

Various authors, i.e. Händle [21], determine the characteristic of extrudable clay feeds from the torque of the Brabender equipment for blend preparation under steady water addition. This method is also used for feeds for injection molding whose liquid phase consists of molten thermoplastics.

According to Norton [22] the influence of the water content on the maximum deformation before crack formation may be developed to a function by forming a product with the counter-influence on the yield stress that passes through its maximum at a water content that is characteristic for the feed. But also by this method no hint on the suitability for a certain forming process will be obtained, either.

The behaviour of plastic ceramics feeds under a cyclic deformation standard and the observation of the stress-strain curves obtained have been discussed in detail by Astbury, Hennieke, Kersting, Kienow and Kobayashi [23-26]. By these torsional cyclic loading tests, where the torsional stress varies between  $+\tau$  and  $-\tau$  (in periods of about 1 min.), the elastic and plastic deformation is recorded. The area within the stress-strain hysteresis curves is a measure for the deformation energy that is converted into heat (Fig. 4.2.2.3).



**Fig. 4.2.2.3:** Stress-strain curves under cyclic torsion tests according to Astbury [23] (only the 1<sup>st</sup> to the 4<sup>th</sup> and the equilibrium cycles are shown).

Although the plasticity characteristics are not exactly defined their values of influence will briefly be discussed here.

The plastic behaviour of clay based feeds is determined by the quality and quantity of the liquid phase, the concentration of dissolved salts, the type of solid phases, their particle size distribution and morphology and by the ion concentration on the particles. These correlations are described in detail by Moore/Hennieke [27].

Water has a great adsorption tendency to oxide surfaces and clay minerals. Only 2 mg per gram of kaolin with a specific surface of  $13\text{m}^2/\text{g}$  are sufficient to obtain a mono-molecular covering and a particle unity by hydrogen bonds. Thicker layers of disoriented liquid water of

more than 10 nm (circa 30 H<sub>2</sub>O layers) lead to a mechanical movability of the particles with still efficient residual forces. The fine solids particles may also be unified by the influence of interfacial forces of the water in the small gaps and cavities. In case of still higher water contents the feed becomes liquid, usually showing the non-Newtonian behaviour of shear thinning and an intensified thixotropic appearance. Thus the water content is of great importance for the plasticity of clay minerals and must be optimized for the respective forming process.

With decreasing grain size of the inorganic powder particles both the number of nearest neighbours and the probability of a new adhesion after the deformation increase, so that plasticity will be improved. Platelets (i.e. kaolinite) show a favourable behaviour towards plasticity as they allow sliding over vast areas without losing their unity [28] when cohering in parallel to each other. According to Mostetzky [29] model observations of water layers between balls or plates show for the latter a lower shear stress to be overcome which explains the positive influence on plasticity.

The ion exchangeability of clay based raw materials leads to a limited bonding of the clay minerals to other solid constituents of the feed like feldspar particles. This bonding capacity increases with decreasing thickness of the platelets. According to Hofmann [30] for montmorillonite with its coating by Na<sup>+</sup> ions this capacity and thus the influence on plasticity may be intensified by swelling up the inner crystalline layers.

If clay based particles are missing in an inorganic powder mixture to make the feed plastic (i.e. in oxide or non-oxide ceramic masses), plasticity can be obtained by adding organic polymers. Such feeds are used for extrusion and injection molding. The additives used, their processability and their function are described in chapters 3.2.2 and 3.2.3.

#### 4.2.3 Granulation

Pressing techniques with powder mixtures being compressed in almost dry condition are preferred for forming ceramic products with appropriate geometries. Ceramic starting powders are normally milled down to the micrometer range in order to increase their sintering capacity. On the other hand, attractive forces arise at the particle surfaces and lead to uncontrolled agglomerations and a bad processability. In order to optimize the flowability and to increase both the bulk density and the storing capability of comminuted powders in silos and hoppers they are granulated before further processing.

#### 4.2.3.1 Production of granules

Spray drying is the most common thermal granulating process in ceramic production. Horizontal fluid bed granulation and spray freeze granulation are also thermal processes but have never approached the importance of spray drying.

Besides fluid bed granulation and compaction the layer agglomeration is quite suited to overtake the spray granulation for economic reasons. That is why this method will be explained here in detail. An explicit survey on the variety of granulating processes is to be seen from Capes [31].

#### Spray drying

In this thermal granulating process a ceramic slip is atomized to create fine spherical shaped drops which are dried in a hot gas stream. We have to distinguish in the main between rotary and nozzle atomization as they will lead to different distributions of the granule sizes (Fig. 4.2.3.1.1).

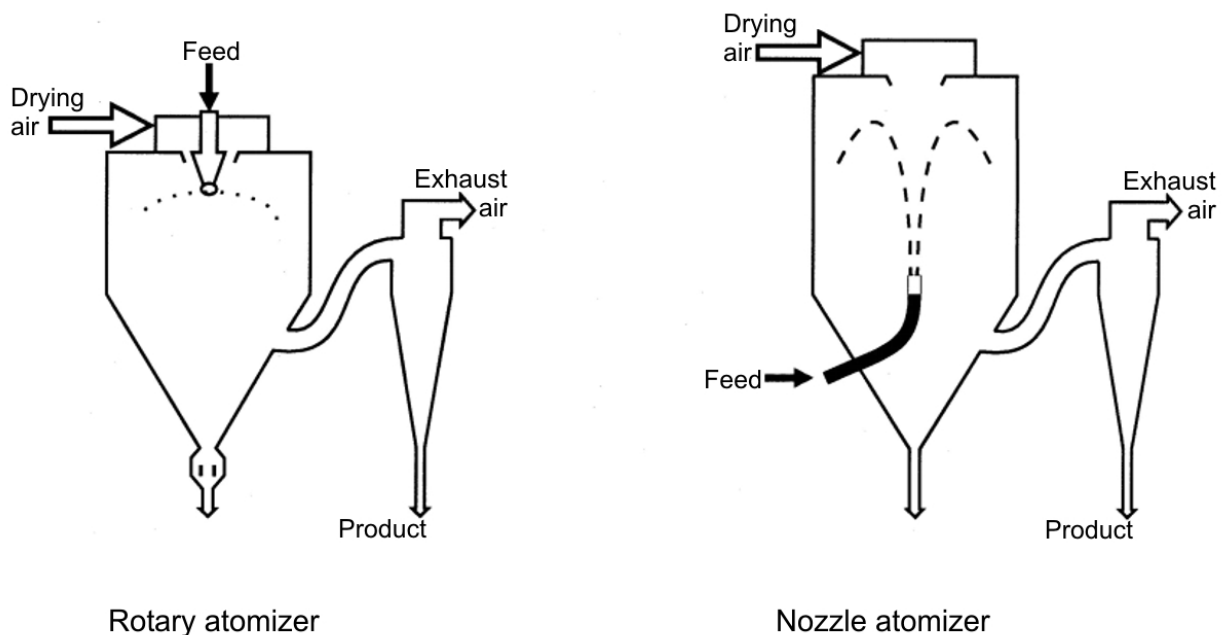


Fig.4.2.3.1.1: Spray driers with different atomizing modes (schematic).

In the case of rotary atomizing the suspension is partitioned into little drops by centrifugal and gravity forces when it leaves a rotating disk. In case of nozzle atomizing different suspensions may be atomized against the hot gas stream through multi-material nozzles. After drying in the hot gas stream, the primary particles are bonded by chemical bridging (Fig. 4.2.3.1.2), by attraction forces between solid particles and by interlocking as described by Rumpf [32, 33]. Due to interfacial and capillary forces of the free liquid surfaces in the chemical bridging, adhesion and cohesion forces in not free moving binder bridges play also a role. Granules present various amounts of liquid between the primary particles (Fig. 4.2.3.1.3) depending on their drying condition. By the free fall of the granules against the hot gas stream in the spray dryer, with a temperature of circa 300°C, the water in the hollow spheres evaporates so that shrinkage and hardening of the granules take place. In order to ensure uniform vapour diffusion from inside the granules to their surface, the temperature and the falling time in the spray dryer must be selected very carefully to avoid both that the granules incrust at their surfaces and that the vapour transport will be hindered.

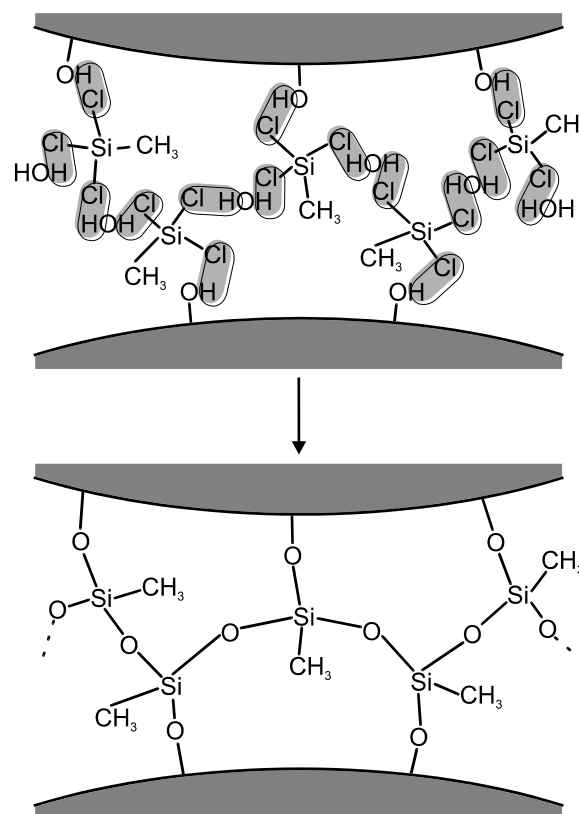


Fig. 4.2.3.1.2: Model of chemical solid-state bridges, due to the presence of Trichlormethylsilane during spray drying [34].

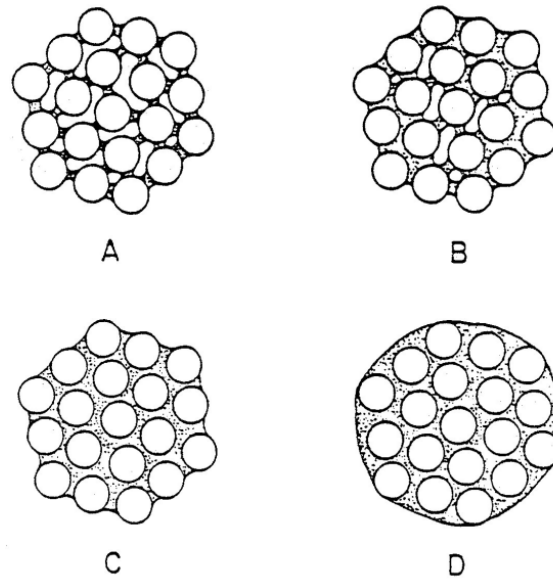


Fig. 4.2.3.1.3: Four stages of agglomerate structures depending on the water content [35].

In order to achieve sufficient green strength after the shaping process, mostly organic binders are added to the suspensions. They enrich at the surfaces on the granules during the drying process, due to their higher evaporation temperatures compared to pure water, so that further transport of water vapour is hindered and a uniform water transport is no longer possible. This leads to cavitation or, in case of high vapour pressure inside the granules, the thin granule wall may burst open (Fig. 4.2.3.1.4). Typical granulate shapes after spray drying are to be seen from Fig. 4.2.3.1.5. The humidity and binder content of the granules will affect their compressibility in the subsequent pressing process and has to be adapted to the respective requirements.



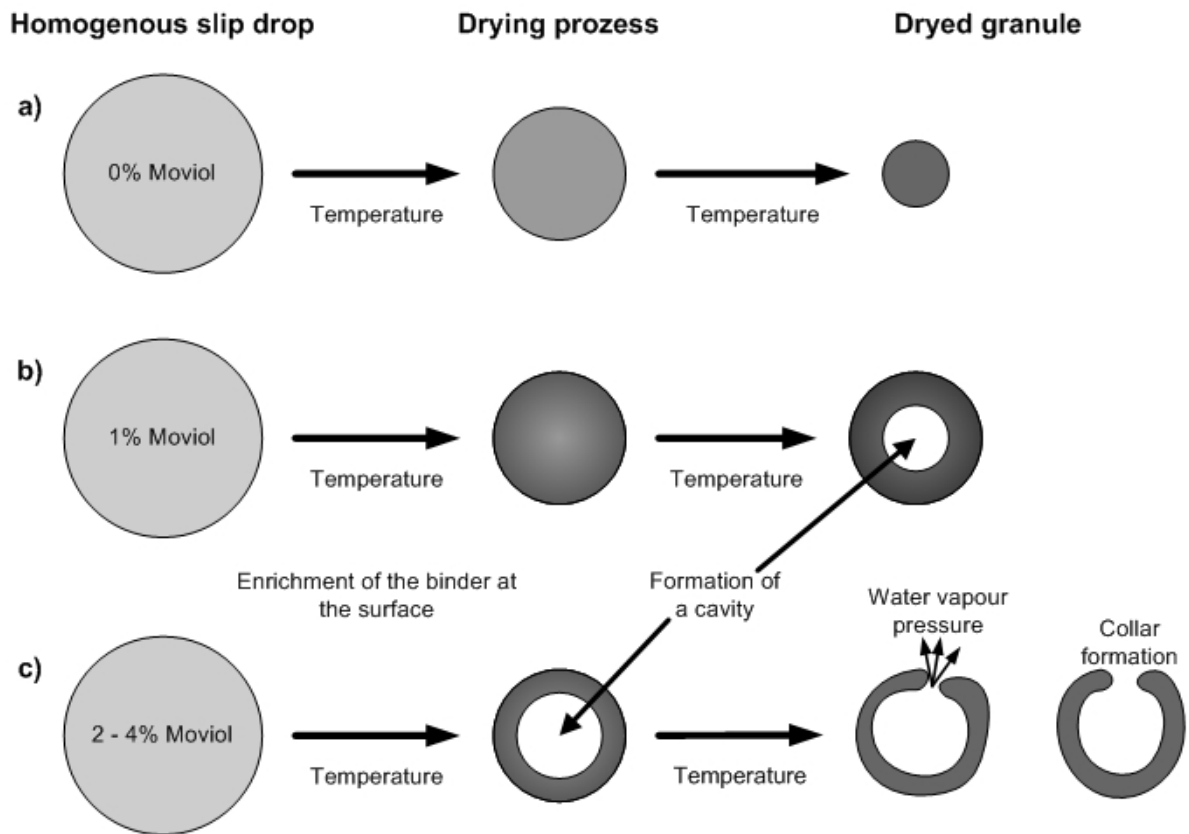


Fig. 4.2.3.1.4: Drying operation in the spray drying process with different binder contents [35] (schematic).

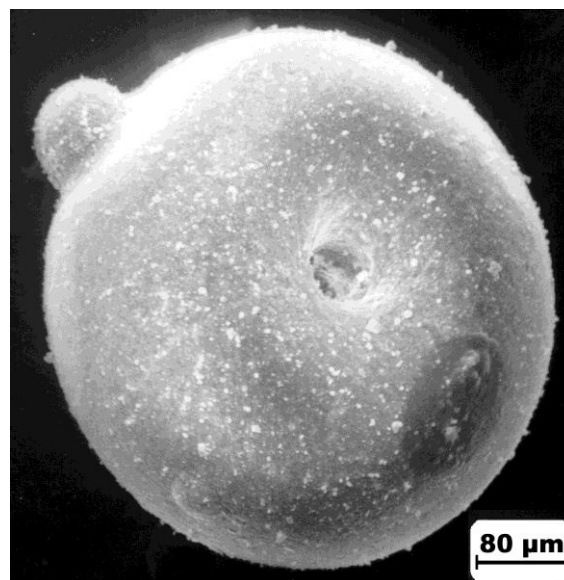


Fig.4.2.3.1.5: Alumina spray granule (SEM).



Videoclip: Granulation by spray drying

### Layer agglomeration

In the case of layer agglomeration fine-dispersed powder particles agglomerate to form granules upon addition of water and organic binders while moving in a powder bed. After nucleation, where secondary grains are created by the movement (mixing, stirring, fluid bed etc.) of the powder bed and by simultaneously adding water and after the agglomeration to bigger particles, agglomerates are formed by layer-wise growth of concentric rings (Fig. 4.2.3.1.6).

In the nucleation range, the growth rate of the granules increases considerably and achieves a maximum while forming bigger particles (Fig. 4.2.3.1.6). In [36] the following law is used to describe the growth rate of discontinuous drum granulation:

$$\frac{dD}{dt} = c_1 D^3 \exp(c_2 t)$$

- $c_i$  = constants
- $D$  = diameter of granules
- $t$  = time of rotation

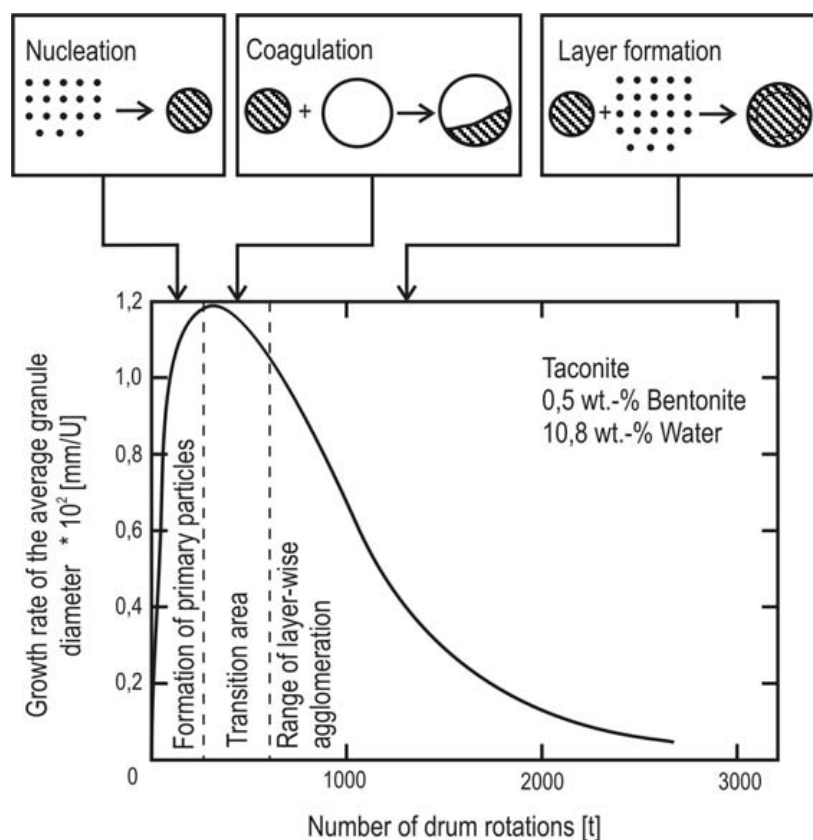


**Fig. 4.2.3.1.6:** Mechanisms of grain size modification and growth rate of granules at different revolutions of the pelletizing drum [36].

In the range of layerwise agglomeration the growth rate decreases again, the number of primary particles decreases and a further growth can be achieved only by agglomerating small secondary particles. A further movement of the granules may result in destruction by abrasion again.

The layer agglomeration of ceramic materials is done in pelletizing disks, mixers or in a fluid bed as shown in Fig 4.2.3.1.7. In all these processes the particles are moved in relative to each other and agglomerated by impact, provided that the sticking forces are greater than the always existing separating forces. The agglomeration may be affected by the initial grain size, the temperature, the drum revolution, the gas velocity, the liquid quantity and by the organic binder contents. These values influence the further processability of the granules like it is also the case for the spray granulation process.

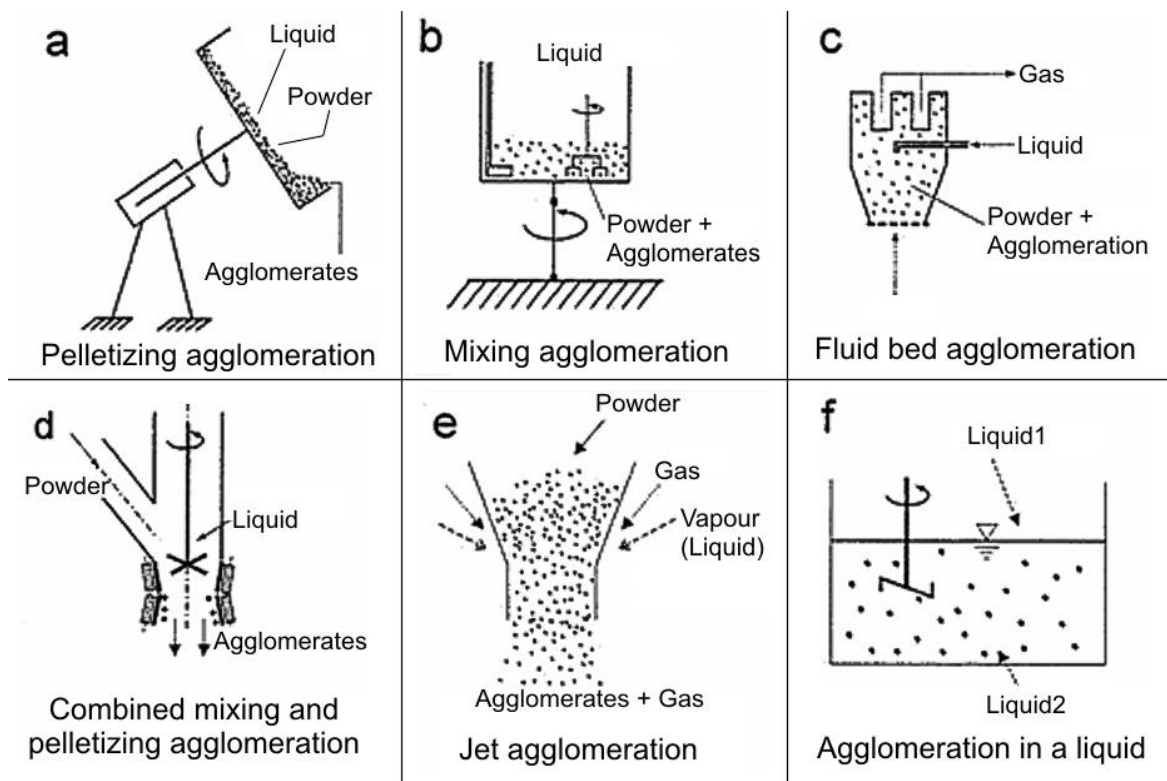


Fig. 4.2.3.1.7: Granulation by layer agglomeration [37].

### 4.2.3.2 Characterization of granules

#### Flowability

The two essential characteristics of granulates with regard to their processability are flowability and compressibility. For the filling of pressing molds and the behavior in silos and hoppers, mono-disperse spherical granules with smooth surfaces and high fracture strength would be favourable. Granules consisting of ceramic primary particles, agglomerated by spray drying or layer agglomeration however, have a relatively wide grain size distribution and rough and porous surfaces. Moreover, they contain residual humidity and interfacial active organic additives which affect their flowability. The flowability is often determined by measuring the time required to pour granules out of standardized vessels or by determining the angle of response when pouring out powders. The influence of adhesion forces on the flowability may be better understood when observing a granule rolling over an uneven surface, as described by Frisch et. al. [38], the uneven surface consisting of compressed granules of the same type.

According to fig. 4.2.3.2.1 a granulated grain rolls down if the moment  $M_I$  is somewhat greater than  $M_{II}$ . Under equilibrium conditions the following applies

$$K_H \cdot r_1 = (K_N + K_A) r_2$$

$$\text{resp. } G \sin \alpha r_1 = (G \cos \alpha r + \sigma_A A_A) r_2$$

where

$K_H$  = rolling force

$K_N$  = normal force

$K_A$  = adhesion force

$\sigma_A$  = adhesion stress

$G$  = mass of the granule

$\alpha$  = angle of inclination

$r_1$  = radius of the granule

$A_A$  = sliding surface

$r_2$  = radius of the sliding surface

According to Frisch et al.:

$$\sin \alpha = \frac{6 \cdot \sigma_A \sqrt{f^3}}{\rho} \frac{1}{r_2} + \sqrt{f \cos \alpha}$$

where  $\rho$  = density of granules and  $f = \frac{r_2^2}{4\pi r_1^2}$ .

Despite great deviations the relation between  $\sin \alpha$  and  $1/r_1$  can be seen from the results obtained from silicate ceramics granules (Fig. 4.2.3.2.2). For granules with a diameter of 200  $\mu\text{m}$  adhesion stresses were calculated between 0,2 and 0,02  $\text{N}/\text{mm}^2$  assuming adhesion forces of  $10^{-6}$  to  $10^{-7}\text{N}$ ,  $f$ -values of  $10^{-3}$  to  $10^{-5}$  and sliding surface radii of 2 to 3,4  $\mu\text{m}$ .

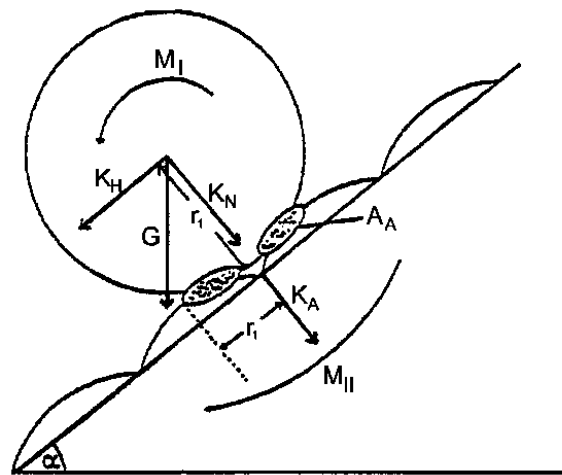


Fig. 4.2.3.2.1: Granule rolling on an uneven surface (explanations see text [38]).

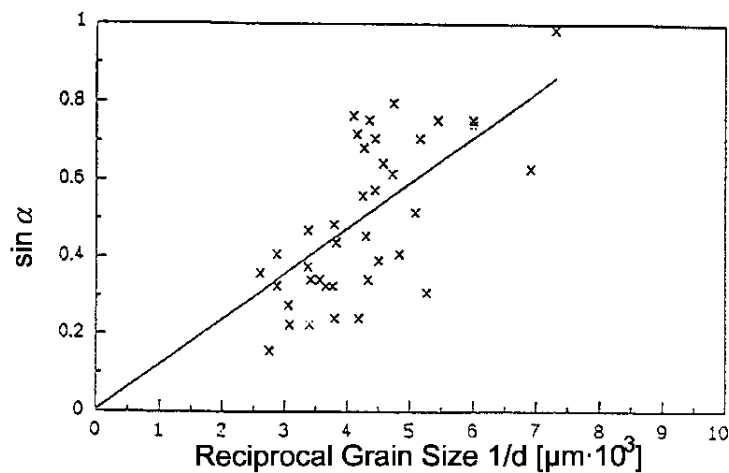


Fig. 4.2.3.2.2: Sinus of the angle of inclination on the surface of a pressed body as a function of the reciprocal grain size of the granules [38].

### Strength of individual granules

A further important characteristic of granules both with regard to their flowability and their compressibility is their strength. To determine the strength of individual granules they are fractured between two stamps in a compression test (Fig. 4.2.3.2.3).

Assuming the ideal spherical shape and referring the fracture stress to the meridional area of the sphere [31], the fracture strength of the granule  $\sigma_g$  is calculated as follows [40].

$$\sigma = \frac{4 F_B}{\pi \cdot d^2}$$

with

$F_B$  = fracture load

$d$  = granule diameter

In practical use the general correlation

$$F_B = \text{const} \cdot d^n$$

is observed with  $n$  varying between 1 and 2.

In [31] these variations are related to either the shell formation ( $n=1$ ) or to the homogeneous distribution of the contact forces between the primary particles over the whole granule cross section ( $n= 2$ ). That means that variations in the granule structure and size distribution result in a wide strength distribution of the granules. This can lead to problems during pressing and will be discussed in chapter 4.3.3.

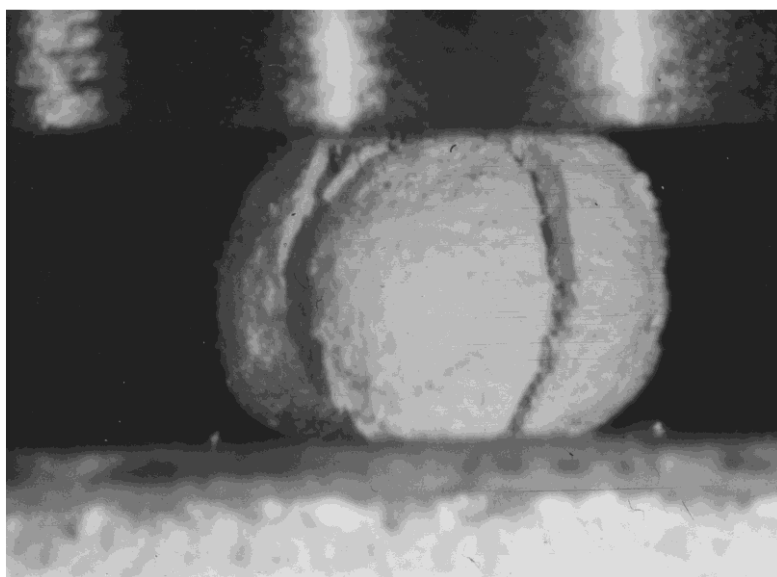


Fig. 4.2.3.2.3: Determination of the strength of individual granules in the pressure test (Courtesy of Dr. Rainer Oberacker, Karlsruhe University [39]).

### 4.3 Forming

During the forming, deflocculated slurries, plasticized materials or granules are transformed into green bodies with defined size, shape, density and reproducible tolerances. The geometric dimensions required and the quantities to be produced are decisive for determining the forming process to be applied. The shrinkage caused by the subsequent firing process is subject to the fluctuations of the green density and the dimensional tolerances. The reproducibility of these sizes and the avoidance of defects that can hardly be cured any longer in the subsequent sintering decide on the economy of the respective forming process apart from investment and personnel costs. In order to achieve a sufficient green strength for the transport of the parts, but also to optimize the processability characteristics of the initial materials for the respective forming process, organic additives are added to the ceramic feeds to fulfil different functions (Fig. 4.3.1).

<b>Additive</b>	<b>Function</b>
Ceramic powder	Matrix
Sintering additive	Densification aid
Solvent	Dispersion
Deflocculant	Control of surface charges and pH, dispersion
Dispersing agent	Deagglomeration
Wetting agent	Reduce of the surface tension of the solvent
Antifoaming agent	Avoidance of bubbles
Preservative	Avoidance of bacteria cultures
Binder	Green strength
Plasticizer	Flexibility
Softener	Flexibility
Lubricant	Reduce die and internal friction, mold release

Fig. 4.3.1: Functions of processing additives in ceramic feeds.

Depending on the forming process applied, either organic or inorganic additives with different molecular weights and chemical compositions are added to obtain the processing characteristics required. The interaction of the additives to each other is extremely complex so that the concentrations are mainly determined empirically in practical use. While ceramic products are dried and further sintered, the organic additives will decompose. During this step, extra care must be taken due of the partly critical decomposition products arising. The productivity of a forming process is in the main subject to the possibility of manufacturing as close to the final contours as possible, i.e. to the extension of finishing that may be required. Without any finishing the dimensional tolerances of the essential forming processes are within the values indicated in Fig. 4.3.2. Especially for structural ceramics often much closer dimensional tolerances are required which may be achieved only by expensive finishing of the sintered products with diamond tools. Such processing costs should be avoided as far as possible both in the green and in the sintered stage as they may multiply the other manufacturing charges of a ceramic component.

<b>Forming process</b>	<b>Tolerances in %</b>
Slip casting	±2,0 to ±3,0
Injection molding	±0,5 to ±1,0
Uniaxial dry pressing	±0,5 to ±1,0
Isostatic pressing	±0,2 to ±0,5
Extrusion	±1,5 to ±2,0

**Fig. 4.3.2:** Tolerances of ceramic components made from  $\text{Si}_3\text{N}_4$ ,  $\text{SiSiC}$  and  $\text{Al}_2\text{TiO}_5$  after sintering for different forming processes.



### 4.3.1 Casting processes

#### 4.3.1.1 Slip casting



In the slip casting process, a porous, water absorbing mold (mostly made of gypsum) will absorb water from an aqueous suspension so that a solid cast is formed.

In the drain casting process (Fig. 4.3.1.1.1) the cast copies the inner contour of the mold so that very complex component geometries can be manufactured that way.

In solid casting a slip is being refilled until the dewatered cast fills up the plaster mold completely. Both in the drain casting and in the solid casting process only small wall thicknesses can be realized as the cast formed will more and more hinder the water penetration.

Assuming a stationary condition without any sedimentation with non-compressible cast the increase of the cast thickness  $dx$  is calculated as follows:

$$dx = \frac{c}{x} dt$$

where the material constant  $c$  respects the permeability and the drain volume of the cast as well as the solid yield and the viscosity [41].

By integration with the initial conditions  $x = 0$  at  $t = 0$  the result is

$$x = \sqrt{2ct}$$

resp. the casting rate

$$\frac{x^2}{t} = \text{const} .$$

So in the slip casting process the cast thickness increases proportionally with the square root of time.

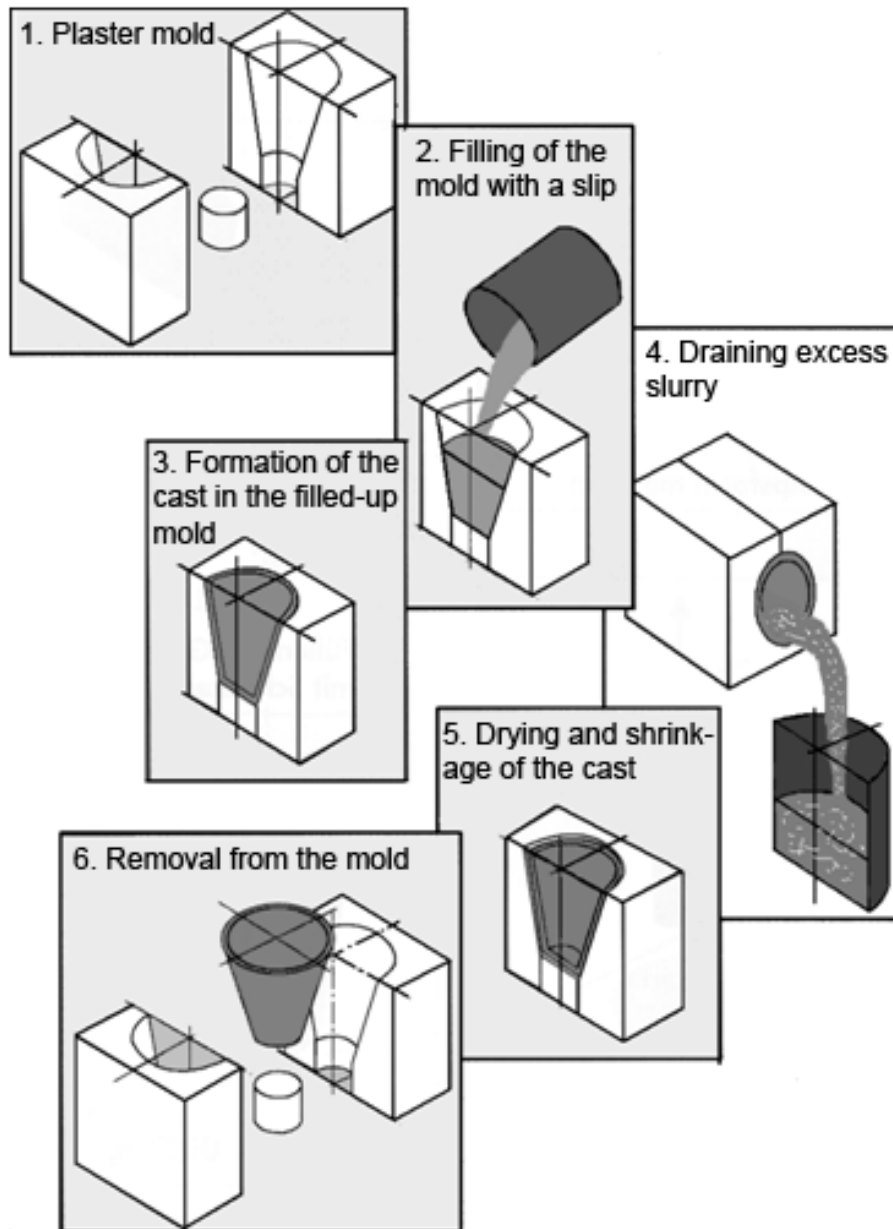


Fig. 4.3.1.1.1: The drain casting process (schematic) [42].

In order to minimize the drying effort the water content of a slip should be set as low as possible (25-35 wt.%). Moreover, the range of deflocculation with minimum viscosity shall be as wide as possible so that operational fluctuations will not cause too heavy changes. The correlations between the electrolyte content of the slip, the casting rate, the green density and the green strength are to be seen from Fig.4.3.1.1.2 on the example of an  $\text{Al}_2\text{O}_3$  slip. While the casting rate decreases with increasing electrolyte content, the dependence on  $\sqrt{t}$  of the cast thickness is valid for all concentrations. Optimum (low) viscosity leads to an exceeding green density and low shrinkage after subsequent sintering. Green strength increases with increasing deflocculant (binder) content.

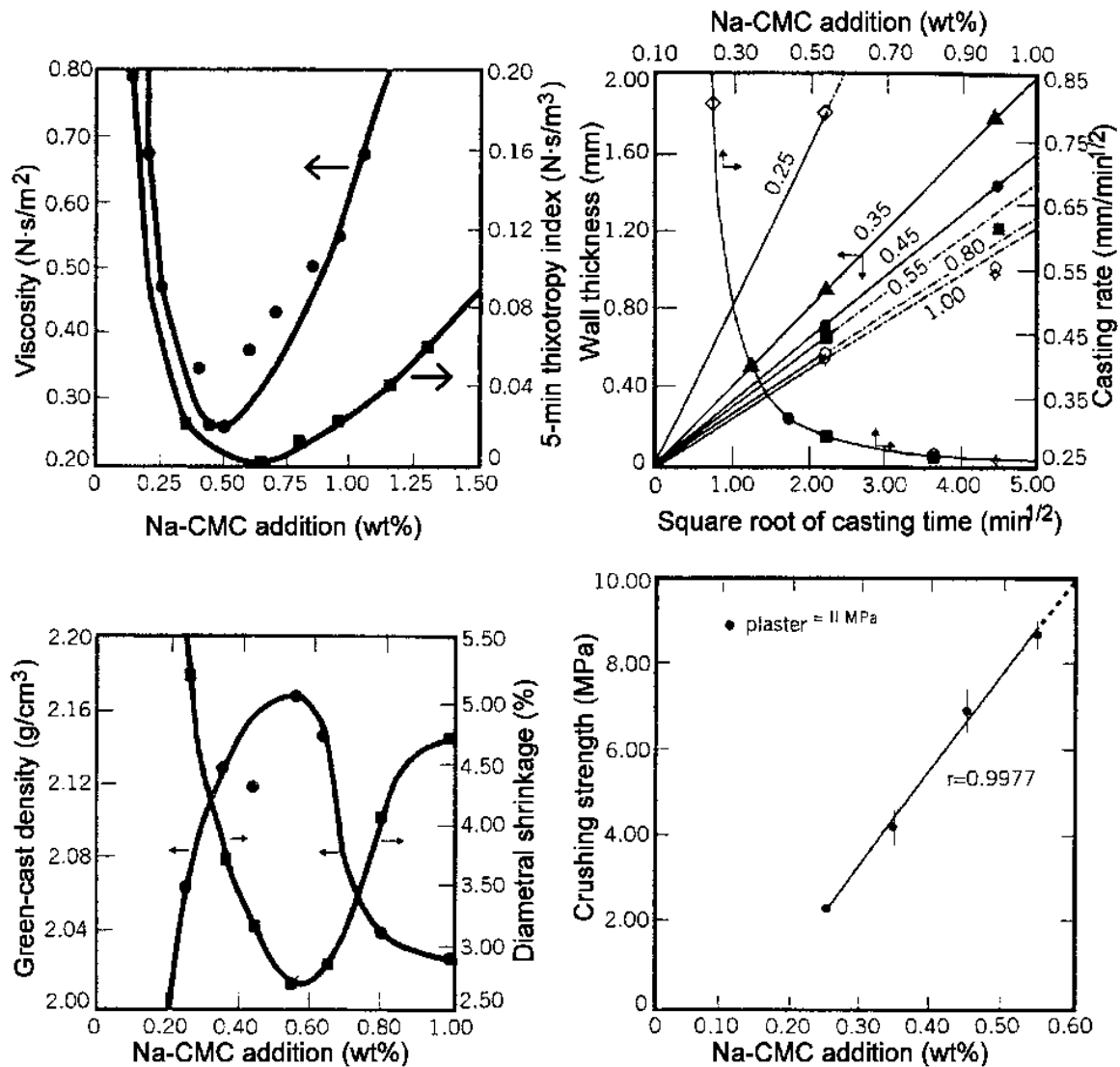


Fig. 4.3.1.1.2: Results obtained when casting an alumina slurry with varying concentrations of Na-carboxymethyl cellulose as deflocculant/binder: (top left) slip viscosity and thixotropy, (top right) casting rate, (bottom left) density and shrinkage of cast, (bottom right) strength of dried casts [43].

Apart from the time variations in the slip characteristics (thixotropy) the change of the organic additives under mechanical stress (i.e. destruction of the molecule chains during pumping) and the change in rheological characteristics involved are important for the processing in practical use. Bacterial proliferation on slurries after a too long storage or processing time will affect the viscosity and thus the casting rate of slurries, conducting to different end shrinkages respectively changes in the dimensional tolerances of the components. Conserving agents will avoid the growth of bacterial cultures but have to be changed in regular intervals as bacteria become resistant with time. Besides the variation of conserving agents through periodical cleaning of the whole pipe system is of special importance to avoid slip alterations, especially in the warmer seasons where bacteria grows quicker.

### 4.3.1.2 Pressure casting

Pressure casting has first been developed for manufacturing of voluminous thick-walled components in sanitary ceramics like for example sinks [44], but later-on this process has been transferred to other ceramic materials and components, as well. Applying pressure during the casting process will reduce the casting time required and allow for different wall thicknesses in the solid casting process (Fig. 4.3.1.2.1).

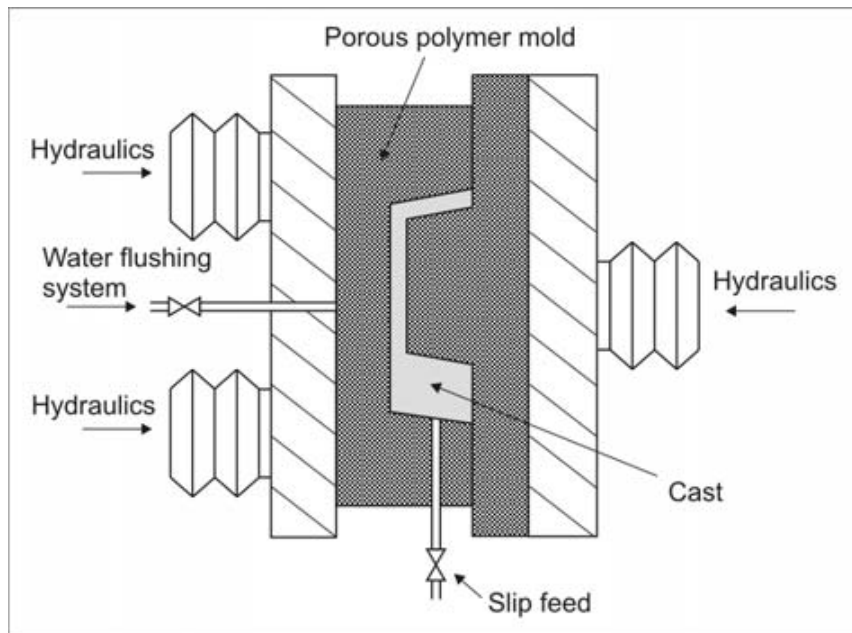


Fig. 4.3.1.2.1: Pressure casting (schematic).

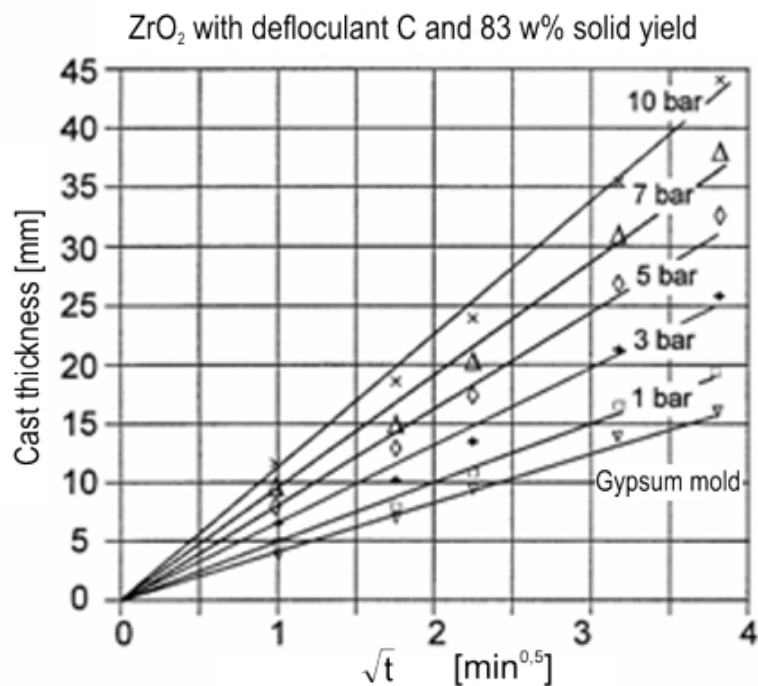


Fig. 4.3.1.2.2: Cast thickness as a function of  $\sqrt{t}$  and pressure [47].

Porous normally non sucking polymers are used as materials for the molds. Upon formation of the ceramic cast the porous polymer mold is opened and is rinsed with water from behind to release the cast. As the mold material must not be self-drawing it needs not to be dried. For pressures up to about 40 bars that are usually applied in pressure casting Frassek [45] describes the pressure dependence of the cast thickness  $x$  by the following function:

$$x = \sqrt{\frac{2 k_m P t}{\alpha \eta}}$$

with

$$\alpha = \frac{1 - n_s - c}{c}$$

where

$k_m$  = average permeability coefficient of the formed cast ( $\text{cm}^2$ )

$P$  = pressure difference (Pa)

$t$  = time (s)

$\eta$  = viscosity of the solvent (mPas)

$n_s$  = cavity factor of the cast ( $\text{cm}^3/\text{cm}^3$ )

$c$  = solid yield ( $\text{cm}^3/\text{cm}^3$ )

According to Akers und Ward [46] the average permeability coefficient is a function of the pressure as per the following equation

$$k_m \approx k_o \cdot P^{-s}$$

where  $s$  = compressibility coefficient and  $k_o$  = initial permeability. At  $s = 0$  the cast is incompressible, while at  $s = 1$  it is completely compressible.

From the two above equations the casting rate is calculated as follows:

$$\frac{x^2}{t} = \frac{2 k_o P^{1-s}}{\alpha \eta}$$

For compressible casts ( $s \rightarrow 1$ ) there is only a small increase of the casting rate with increasing pressure. For most of the systems  $s$  is between 0,1 and 0,3. Because of the varying compressibility of ceramic materials the pressure dependence of the casting rate must be determined for each system separately. For a  $ZrO_2$  slip with 83 wt.% solid yield the pressure dependence of the cast thickness is shown in Fig. 4.3.1.2.2.

In an up-to-date casting plant several polymer molds are connected to each other so that up to ten molds may be filled simultaneously according to the component geometry required. The polymer molds allow for up to 20.000 casts subject to the slip quality used. Besides closer dimensional tolerances and reduced casting times at variable and higher wall thicknesses the essentially increased durability of the molds offers considerable advantages compared to the conventional slip casting process at atmospheric conditions. The decision for the respective casting process is ultimately subject to the quantities to be produced and the economic contemplations involved. Further pressure-supported casting processes that are applied for special component and material groups are the pressure filtration (hard magnetic ferrites), the vacuum casting (fibre insulation) and the centrifugal casting (high tech ceramics).

#### 4.3.1.3 Tape casting



Videoclip: Tape casting

Tape casting is the process for manufacturing very thin ceramic substrates of large area. Tapes with thicknesses from 25  $\mu\text{m}$  to 1,5 mm are used to manufacture capacitors, piezoelectrical components, ferrites and substrates for electronic connections [48]. By laminating tapes with printed circuit tracks multilayer packages for integrated semiconductor circuits are obtained [49]. Catalyst carriers or heat exchangers are created by stacking and winding embossed or stamped tapes [49, 50].

To produce components from ceramic tapes ceramic powders have to be dispersed first of all with binders, deflocculants and plasticizers in organic or aqueous solutions. The homogenized and degassed slip is poured over a micro-adjustable gate (doctor blade) onto a continuous steel belt (partly equipped with carrier films like polyethylenterephthalate, bi-oriented polypropylene) that is conveyed horizontally over two rollers. During the transport to the other end of the casting belt warm air passes over the film in the opposite direction so that the solvents will evaporate. According to the binder content used a more or less flexible tape may be peeled off to be stamped, laminated or wound up (Fig. 4.3.1.3.1).

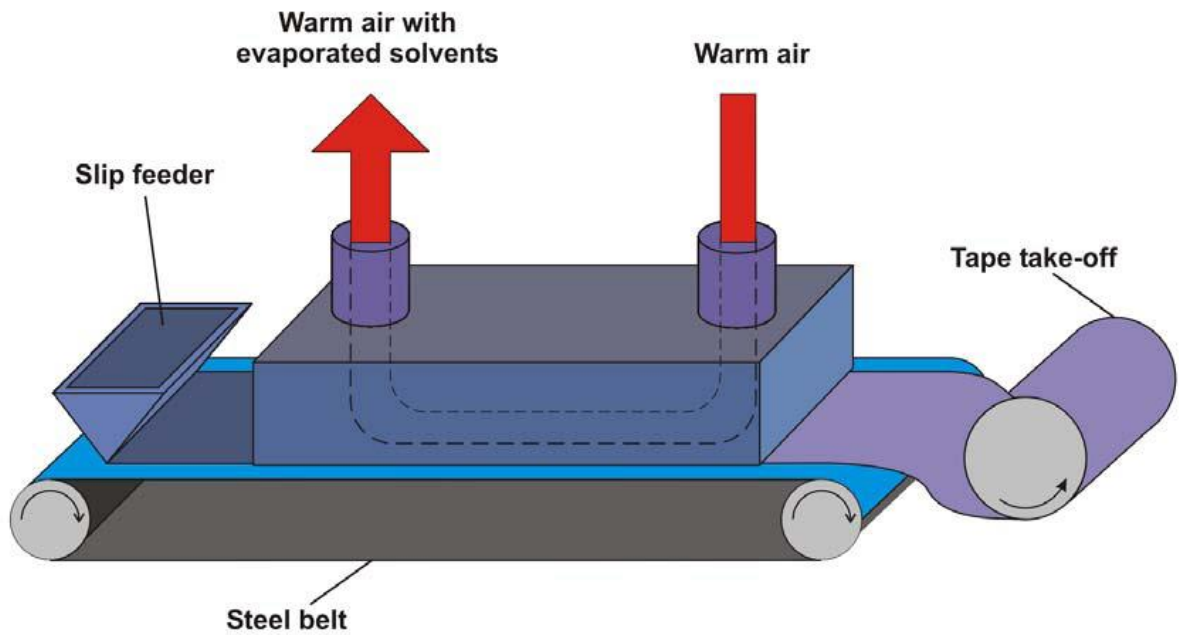


Fig. 4.3.1.3.1: The tape casting process (schematic).

The tape thickness is in the main subject to the geometric conditions of the doctor blade, the belt speed and the rheological characteristics of the slip to be cast. According to Chou, Ko and Yan [51] the height  $H$  of the sheet is calculated as follows:

$$H = A D_r h_0 (1 + h_0^2 \Delta P / 6\eta_s v L)$$

$A$  = constant, dependent on the geometric effects of the doctor blade

$D_r$  = ratio of the density of the slurry/density of the dried tape

$h_0$  = cast thickness at the blade

$L$  = length of the cast

$\Delta P$  = hydrostatic pressure under the blade

$\eta_s$  = viscosity of the slurry

$v$  = carrier velocity

The thinner the tape and the thicker the viscosity of the slurry ( $h_0/h_s$  is relatively low) the lower the influence of the carrier velocity (fig. 4.3.1.3.2).

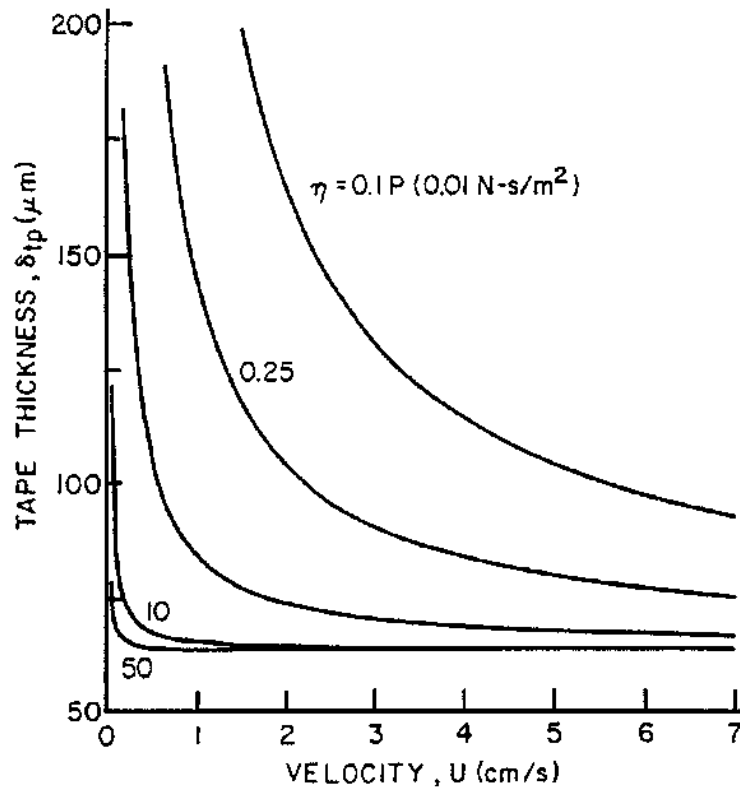


Fig. 4.3.1.3.2: Tape thickness as a function of the carrier velocity for slurries of varying viscosity (viscosity in  $\text{mPa}\cdot\text{s}$ ) [51].

According to the ceramic starting powder used either aqueous solutions or – in case of possible reactions between water and ceramic powder – organic solvents must be added. As binders, plasticizers, deflocculants and wetting agents may be solved by different agents the systems must be exactly adapted to each other. Fig. 4.3.1.3.3 gives a survey on the huge choice of possible systems for aqueous and non-aqueous solvents. A detailed view of the rheological characteristics and the structure of organic substances for the tape casting process are given in [52] and [53].



Solvents	Binders	Plasticizers	Deflocculants	Wetting agents
<u>Non-aqueous:</u>				
Acetone	Celluloseacetate butyrate resin	Butylbenzylphtalate	Fatty acids	Alkylarylpolyether alcohol
Ethyl alcohol	Nitrocellulose	Butylstearate	(Glyceryl-tri- oleate)	Polyethylenglycolethyl ether
Benzole	Petroleum resin	Dibutylphtalate	natural Fish oils (Menhaden)	Athylphenylglycol
Bromochlorometh ane	Polyethylene	Dimethylphtalate	Synthetics (Benzene sulfonic acids)	Polyoxyethylenacetate
Butanol	Polyacrylate ester	Methylabietate		Polyoxethylenester
Diacetone	Polymethylmethacryl ate	Mixed Phtalateesters (Hexal-, octyldecylalcohol)		
Ethanol	Polyvinylalcohol	Polyethylenglycol		
Isopropanol	Polyvinylbutyral resin	Polyalkylenglycol		
Methylic isobutylketone	Polyvinylchloride	Polyalkylenglycol derivates		
<u>Toluol</u>		(Triethylenglycolhexoat)		
Trichlorethylene		Trikresylphosphate		
Xylol				
<u>Aqueous:</u>				
Water (with antifoaming agents based on resigns)	Acrylic polymer	Butylbenzylphtalate	Complex vitreous phosphates	Non-ionic octylphenoxyethanol
	Acrylic polymer	Ethyltoluolsulfonamid		
	Emulsion	Glycerine	Condensed arylic sulfoic acid	
	Ethylenoxide polymer	Polyalcylenglycol		
	Hydroxyethylencellul ose	Triethylenglycol	Natural sodium salt	
	Methylcellulose	Tri-N-butylphosphate		
	Polyvinylalcohol			
	TRIS. Isocyanate			
Resign based sliding additives				

**Fig. 4.3.1.3.3:** Some additives for the tape casting processes with aqueous and non-aqueous slurries [52].

Criteria for the selection of constituents for the tape casting process are in the main a low vaporization point and low viscosity of the solvent. This solvent has to solve the binder and the plasticizer as well as the wetting agent and the deflocculant. Solving the ceramic powder or reactions with it are however not desired. A combination of solvents will mostly be advantageous, as the different organic additives will be solved by different solvents. It is true that organic solvents with low vaporization points will prevent the hydration of ceramic powders and may easily be burned out again, but they may often require also special safety measures with regard to toxicity and inflammability.

The ceramic powders are ground, mixed and degased together with the additives. Alumina, which is used for the production of substrates and multilayer packages for example, is not soluble in water nor does it react with it. Therefore an aqueous slip with water soluble binders, plasticizers, deflocculants and wetting agents may be produced in this case. A typical composition is shown in Fig. 4.3.1.3.4.

Material	Function	wt. %
Al <sub>2</sub> O <sub>3</sub> powder	Matrix	40 -50
MgO powder	grain growth inhibitor	0,5 - 3
Distilled water	solvent	30 - 50
Polyvinylacetate	binder	5 - 10
Polyethyleneglycol	plasticizer	0,5 - 3
Dibutylphthalate	plasticizer	0,5 - 3
Arylic sulphuric acid	deflocculant	0,1 - 0,3
Octylphenoxyethanol	wetting agent	0,1 - 0,3

Fig. 4.3.1.3.4: Composition of an aqueous-Al<sub>2</sub>O<sub>3</sub> slurry.

Material	Function	wt.%
SiC	Matrix	40 - 50
Trichlorethylen	solvent	15 - 25
Ethylalkohol	solvent	15 - 25
Polyvinylbutyral	binder	5 - 10
Polyethylenglykol	plasticizer	0,5 - 3
Octylphthalat	plasticizer	0,5 - 3
Menhaden fish oil	deflocculant	0,5 – 3

Fig. 4.3.1.3.5: Composition of a non-aqueous SiC slurry.

Many non-oxide ceramic materials cannot be processed in aqueous systems as they will frequently react with the separation of hydrogen, so that on the one hand the pH will change with time and such slurries have a tendency to form bubbles on the other. That is why stable slip characteristics cannot be guaranteed over a protracted period of time. Therefore organic solvents with accordingly adapted additives are used. Fig. 4.3.1.3.5 shows a typical slurry composition on the example of silicon carbide that is used in the heat exchanger production.

Especially when the ceramic powder consists of laminar or rod shaped crystallites, sedimentation during tape casting will cause texturing within the tapes that will even be intensified during sintering (fig. 4.3.1.3.6).

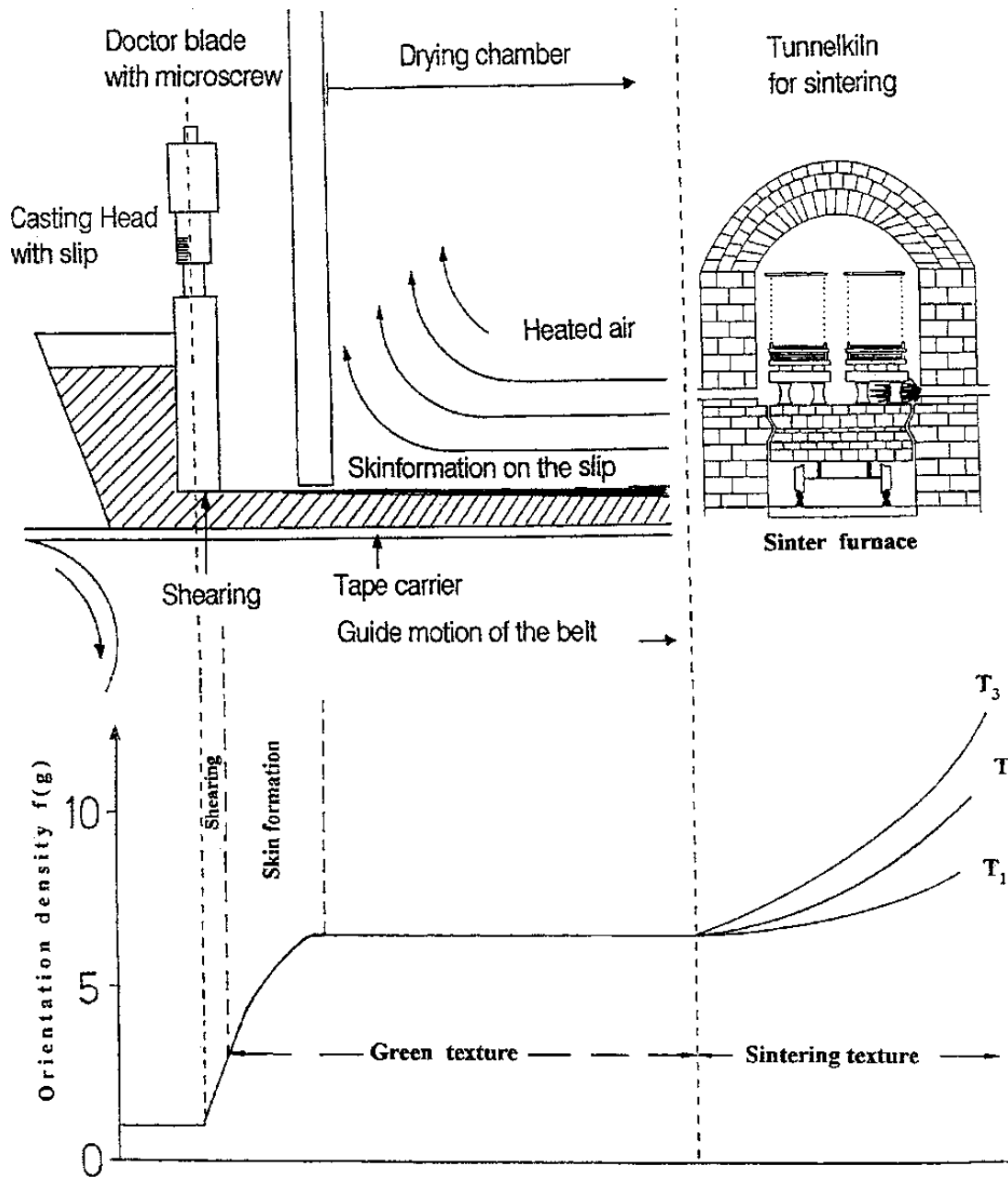


Fig. 4.3.1.3.6: Texturing upon the production of alumina substrates (schematic) [54].

Furthermore in multilayer components the laminated areas are often the weak points because of pore formation while the organic constituents are burned out. Both effects will lead to a directional dependence of the characteristics perpendicular and parallel to the laminates (fig. 4.3.1.3.7).

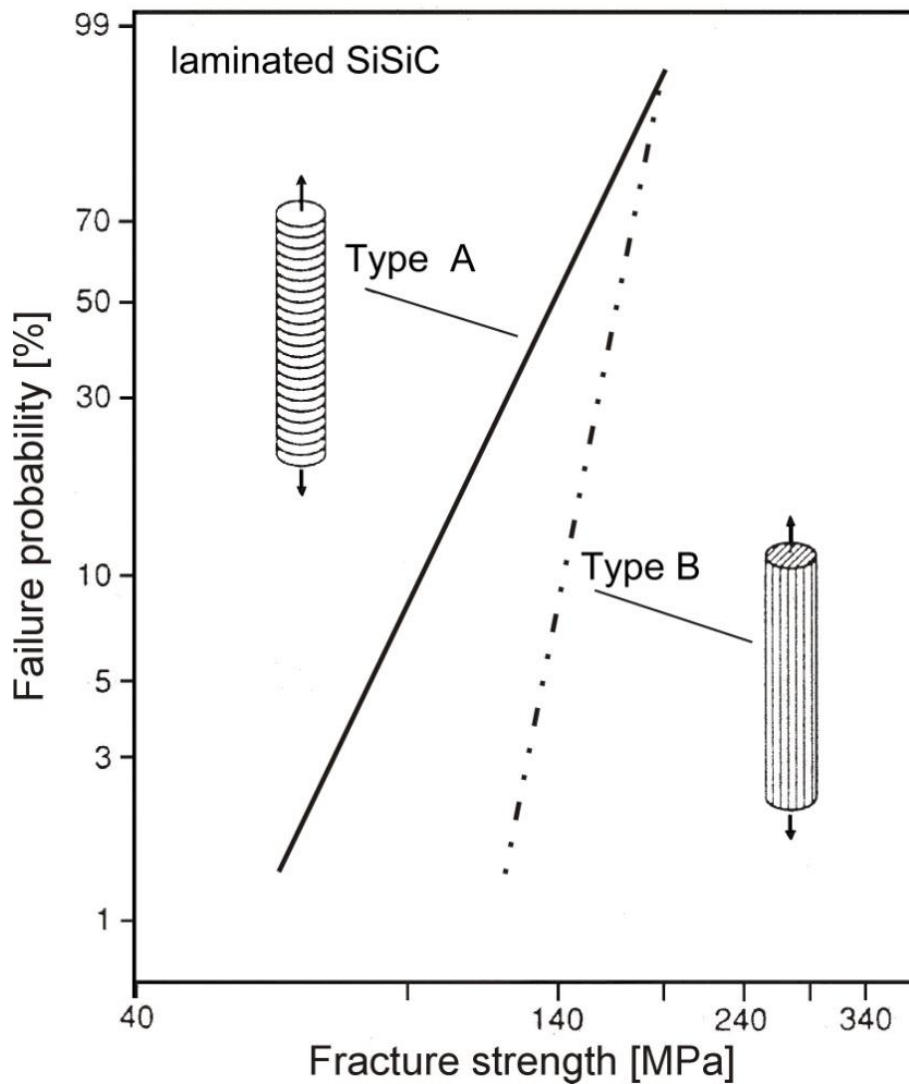
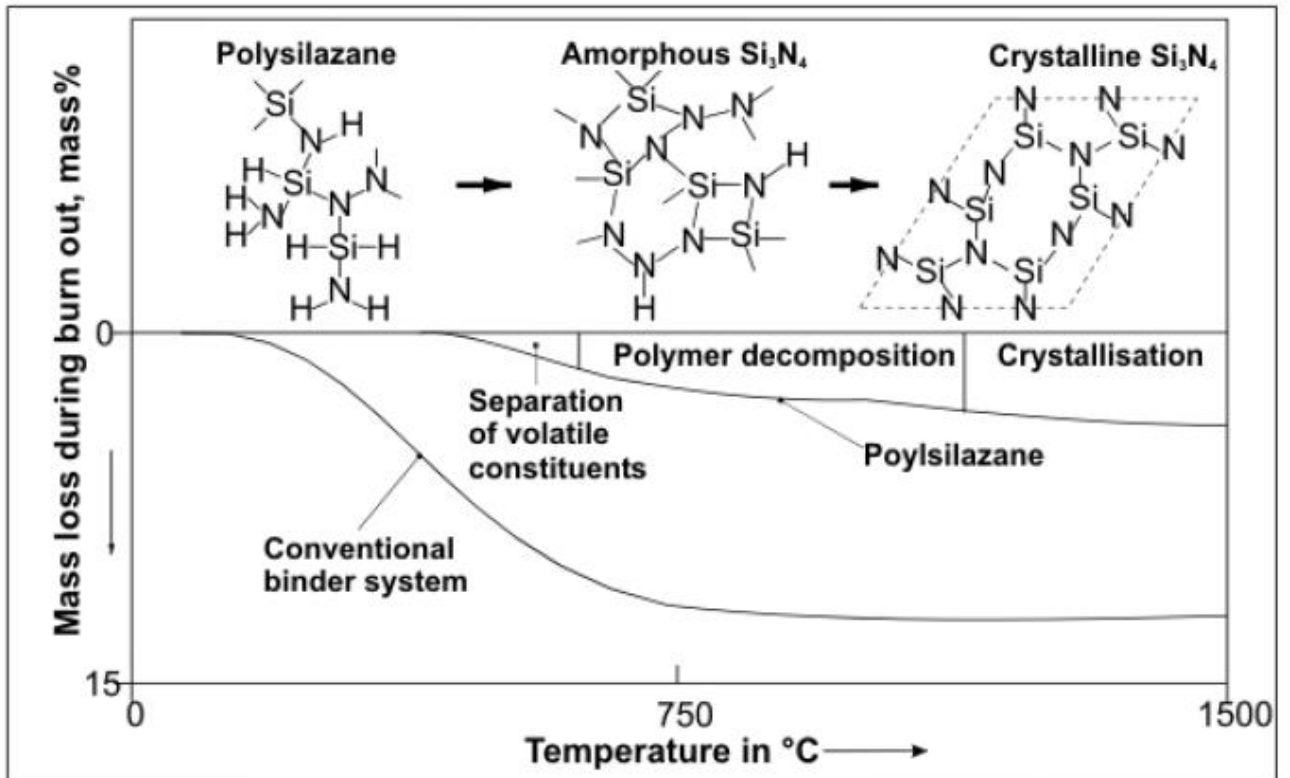
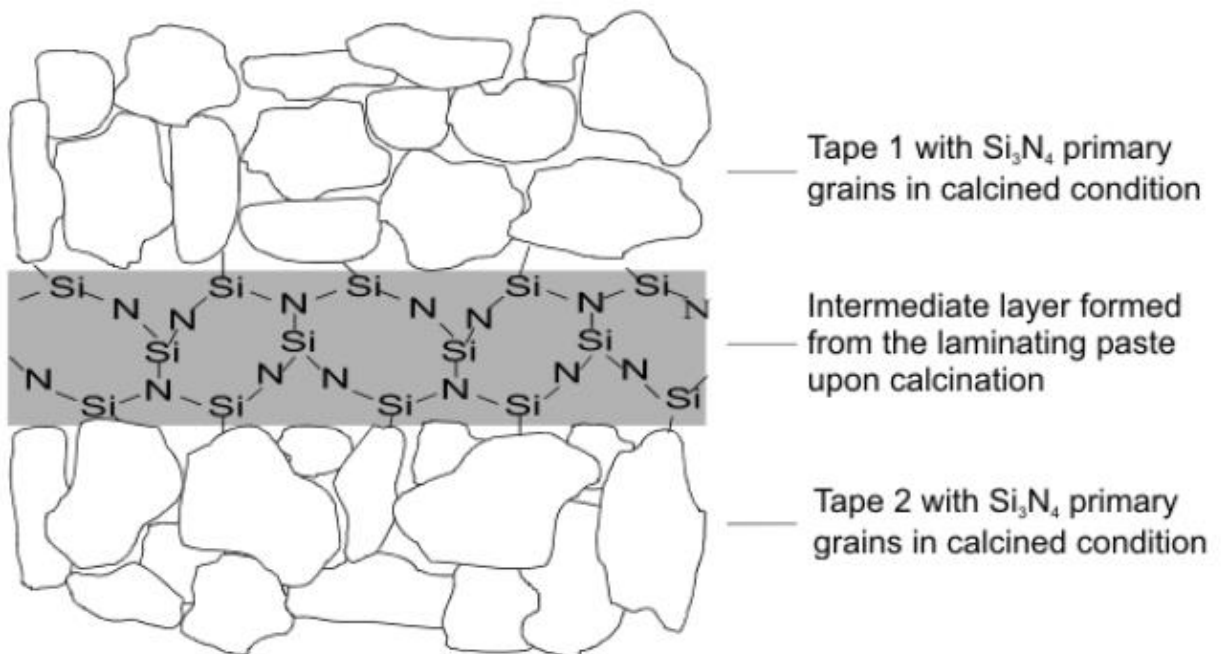


Fig. 4.3.1.3.7: Tensile strength perpendicular and in parallel to the laminating direction of SiSiC samples [55].

A new variation in laminating individual tapes is the use of preceramic polymers as laminating paste. Fig. 4.3.1.3.8 shows by the example of polysilazane that - compared to conventional binders - during thermal decomposition only a small amount leaves the laminating paste as volatile matters while more than 80% of the polymer remains as crystalline skeleton in the laminated areas. So in the laminates microstructures may be set that correspond to those of the tape in sintered condition or are even superior to them according to the characteristics required. Directional dependences are to be avoided by that.



(a)

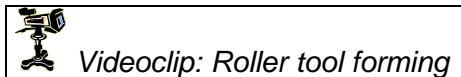


(b)

Fig. 4.3.1.3.8: a) Burn out behavior of polysilazane from laminating pastes, b) Transition area between two silicon nitride tapes in calcined condition (schematic).

## 4.3.2 Plastic deformation forming

### 4.3.2.1 Roller tool forming



For manufacturing axially symmetric table ware, roller tool forming is still an important process, despite the meanwhile introduced dry bag pressing (chapter 4.3.3.2). In the so-called jiggering process a metallic roller tool shapes a section of a de-aired extrudate over a mold (mostly made from plaster or polyurethane), while in the jollying process for manufacturing axially symmetric hollow ware the roller tool is inserted into the mold (Fig. 4.3.2.1.1). For example, the bottom of a plate is embossed by the profile of the roller tool while the top of the plate reflects the upper surface of the plaster mold. The outer contour of mugs or cups is shaped by the plaster mold, while the roller tool determines the inner contour and the wall thickness of the parts. As soon as the roller tool touches the extrudate its shape is changed by squeezing. A cut-off device removes the mass squeezed over the edge of the plaster mold. Roller tool forming is applied for plastic (ductile) feeds with yield stress, which is a precondition for permanent deformation, as otherwise green blanks would change their shape due to their own weight.

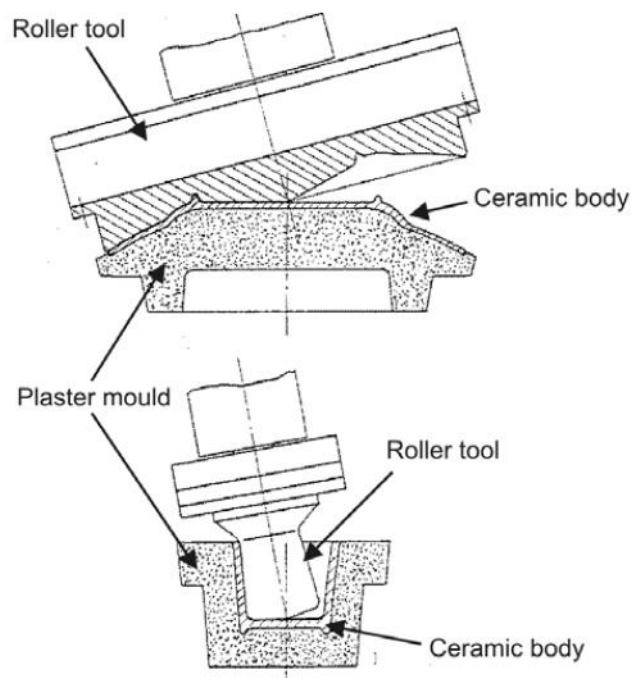
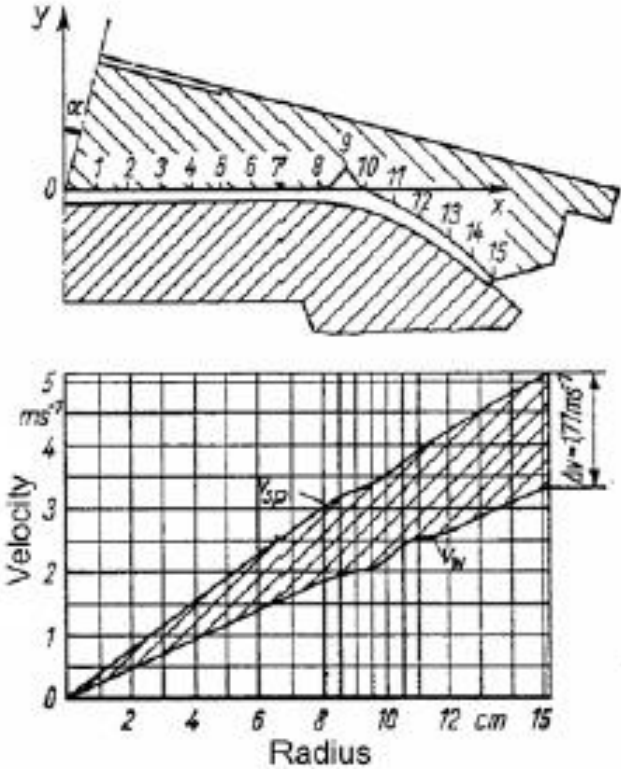


**Fig. 4.3.2.1.1:** Schematic of the jiggering process (the bottom of the plate is formed by the roller tool) and of the jollying process (the inside of the mug is formed by the roller tool) [56].

When processing plastic feeds, high deformation velocities are advantageous as porcelain pastes will behave like real liquids, so that texturing and crack formation can be avoided as far as possible [57]. For that reason, high velocity differences are desirable between the roller tool and the spindle supporting the plaster mold, while both turn in the same direction.

In the jiggering process this requirement is limited by centrifugal forces caused. Typical velocity differences of plates and bowls with diameters of 11 to 24 cm range between 80 and 180 min<sup>-1</sup> [57]. They cause tangential speed differences at the outside of the plate of max. 1,77 m/s (fig. 4.3.2.1.2). The requirement of processing plastic feeds with a high shear rate is realized in the best possible way in the jollying process where velocity differences use to range between 1000 and 1200 min<sup>-1</sup> [57].



$v_w$  = tangential velocity of the tool,  $v_{sp}$  = tangential velocity of the spindle (diameter of the tool = 278mm, dumping angle of the tool = 15°, r.p.m. of the tool = 272min<sup>-1</sup>, diameter of the mold = 272 mm, r.p.m. of the mold = 360min<sup>-1</sup>).

Fig. 4.3.2.1.2: Distribution of the tangential velocities on the bottom profile of the plate [58].



In order to avoid that the plastic feed sticks to the roller template the roller tools are heated so that a vapour film comes up between the roller tool and the extrudate that improves the flow behavior additionally.

In the jiggering process undercuts may be manufactured when a lateral lifting is achieved either by a roller tool or by a spindle displacement. A detailed description of machine parameters and factors influencing the forming process are described by Seegerer [56] and Hülseberg [57].

#### 4.3.2.2 Extrusion



Extrusion of plastic ceramic feeds is used for manufacturing components with defined cross sections whose length is determined by cutting an extruded rod. The plastic material is fed through a charging hopper and the metering screw into the press. In a vacuum chamber the feed is evacuated and fed by the auger to the die (Fig. 4.3.2.2.1). Basic literature on the function of auger extruders can be found in [59] and [60]. Depending on the die geometry, feeding extrudates are produced to be further process as starting material for the manufacturing of isolators and dinner ware or to extrude bricks, tiles, tubes, substrates or “honeycomb” structures for catalyst carriers by means of suitable inserts.

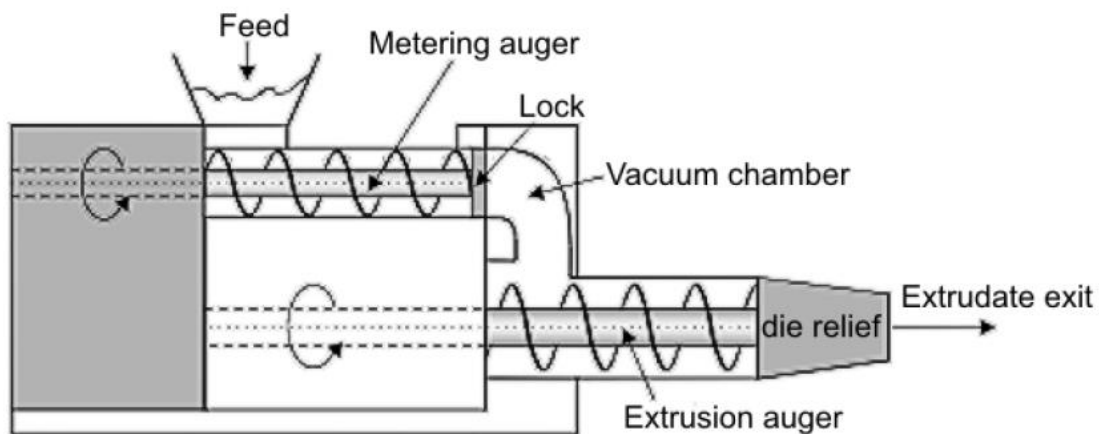


Fig. 4.3.2.2.1: Auger extruder (schematic).

In case of clay based feeds the raw materials are plasticized by water and very small quantities of deflocculants. Oxide and non-oxide ceramic raw materials are plasticized by aqueous and non-aqueous binder systems. Three typical examples of ceramic feeds that are suited for extrusion are shown in Fig. 4.3.2.2.2.

Silicon carbide		Alumina		Electrical porcelain	
SiC	50	Al <sub>2</sub> O <sub>3</sub>	46	Quartz	16
Hydroxyethyl cellulose	6	Ball Clay	4	Feldspar	16
Polyethylenglycol	2	Methylcellulose	2	Kaolin	16
H <sub>2</sub> O	42	H <sub>2</sub> O	48	Ball Clay	16
				CaCO <sub>3</sub>	<1
				H <sub>2</sub> O	36

Fig. 4.3.2.2.2: Composition of extrudable ceramic feeds in vol.% [2].

For the practical use the mass flow and the pressure course around the die of the extruder are important. According to Pels-Leusden [61] the theoretic flow of an auger extruder is

$$\dot{V}_{\max} = \frac{\pi^2 D_s^3}{4} \left(1 - \frac{d_k^2}{D_s^2}\right) n \sin \beta \cos \beta$$

Where

$\dot{V}_{\max}$  = max. theoretical flow

$D_s$  = auger diameter

$d_k$  = hub diameter

$\beta$  = average auger helix angle

$n$  = auger r.p.m.

The fact that in practical use only up to 40% of the theoretical flow are achieved is due to the apparent motions between feed and auger resp. cylinder wall and the so caused slip. According to Reed [2] the shear stress at the radial position  $r$  in the cylindrical part of the feed screw for steady state laminar flow is calculated as follows.

$$\tau = r (P_1 - P_2) / 2L$$

where  $\Delta P/L$  is the differential axial pressure for a cylinder segment of length  $L$ . The maximum shear stress occurs at the cylinder wall, when  $r = R$

$$\tau_{\text{Wall}} = R \cdot \Delta P / 2 L.$$

So the cross section velocity profile shown in Fig. 4.3.2.2.3 is achieved. In the middle of the plug, where the shear stress is lower than the yield strength of the plastic feed the plug flow is constant so that no plastic deformation appears.

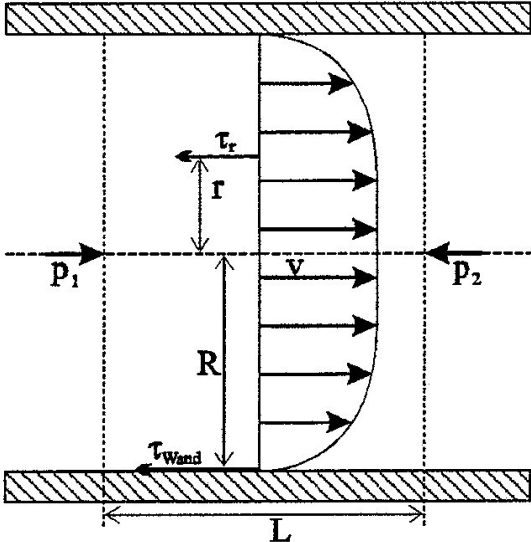


Fig. 4.3.2.2.3: Cross section velocity profile in the cylindrical part of the auger of an extruder.

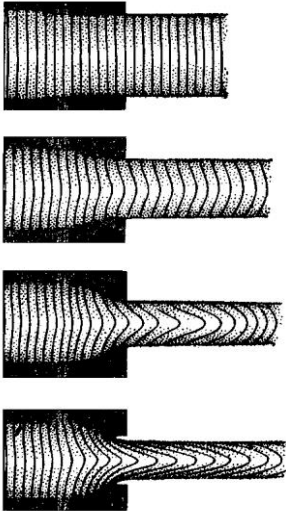


Fig. 4.3.2.2.4: Formation of flow textures when reducing the barrel diameter [62].

The velocity differences between cylinder wall and rod centre increase with reducing the rod diameter in the die.

A too sharp reduction of the die diameter will intensify the formation of textures in the feed rod (Fig. 4.3.2.2.4) [62].

For an exit speed  $v$  of the mass rod a pressure difference  $\Delta P$  is required that is calculated for a circle shaped section as in [2] as follows:

$$\Delta P = 2 \ln (D_0/D) [\tau_b + k'_b (v /D)^n] + (4L/D) [\tau_f + k_f v^m]$$

Where

- $D_0$  = barrel diameter
- $D$  = die-land diameter
- $\tau_b$  = internal yield strength of the plastic body
- $\tau_f$  = yield strength of the slippage film on the wall of the die-land
- $k'_b, k_f$  = velocity constants
- $n, m$  = shear thinning exponents for the body and the slippage film
- $L$  = length of the segment in question

At the transition between the auger cylinder and the die, a pressure drop is caused that reflects the energy required to deform the material towards the smaller diameter. The pressure drop in the die reflects the stress required to overcome the friction forces so that the material glides. The pressure drop depends on the rheological behaviour of the feed and on the geometric conditions of the extruder. Fig. 4.3.2.2.5 shows an example of the axial pressure drop for different  $L/D$  ratios of a die.

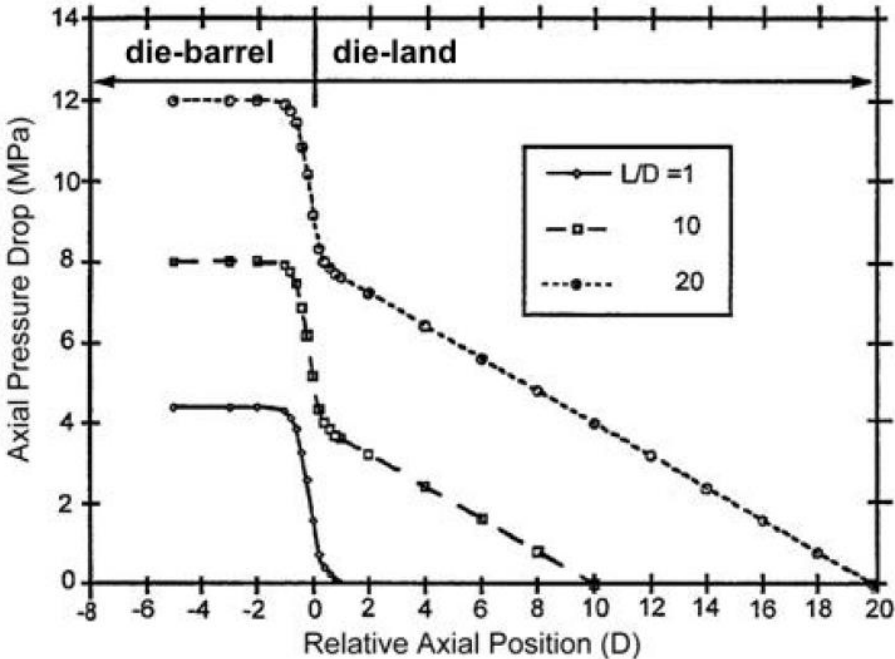


Fig. 4.3.2.2.5: Variation of extrusion pressure for different length/diameter ratios of the die [2].

The complex pressure conditions and relative motions inside the extruder cause textures in the extruded parts. Especially in clay based feeds micro-textures are built up due to the particle alignment. S-shaped macro-textures that warp like a corkscrew (Fig. 4.3.2.2.6) are due to the screw rotation and will destroy the components completely in most of the cases during the subsequent drying process. That is why for every composition an exact tuning between rheological characteristics of the feed and the machine parameters is necessary in order to avoid defects of fabrication.

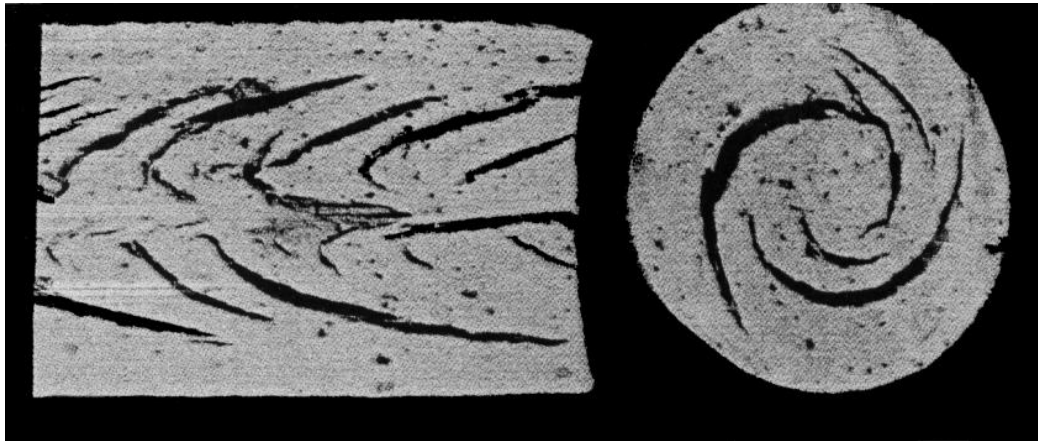
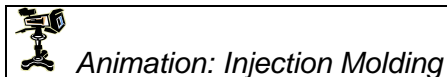


Fig. 4.3.2.2.6: Typical longitudinal (left) and transversal (right) extrusion faults in an extruded rod [63].

#### 4.3.2.3 Injection molding



Injection molding is a process to manufacture small components of complex geometries and low wall thicknesses in large quantities. Typical injection molded components are cores for metal casting, thread guides, cutting tools, welding nozzles and turbocharger rotors. Ceramic powders with binders, plasticizers and lubricants are homogenized to plastify the feeds, which is done in heatable mixers or kneaders above the melting point of the organic additives. The high shear stresses required for mixing and for the dispersion of agglomerates will result in high torques in the mixer and often in considerable abrasion of metallic components. Typical binder systems for injection molded ceramic feeds are to be seen from fig. 4.3.2.3.1. Detailed information on the injection molding process is given in [63-68].

<b>Binders</b>	<b>Plasticizers</b>	<b>Lubricants</b>
<u>Thermoplastics:</u> Polyethylen Polypropylen Polystyrene	Methylethylketone Ethylenvinylacetat Ethylenacrylic acid	Stearic acid Oleic acid Butylstearat
<u>Waxes:</u> Paraffine Epoxy Microcrystalline		

Fig. 4.3.2.3.1: Binder systems for the injection molding process.

The homogenized feed with up to 50 vol.% of organic additives is cooled and granulated simultaneously through the screws or sigma rotors. This granulate is fed through the filling hopper to the heatable injection molding machine (Fig. 4.3.2.3.2).

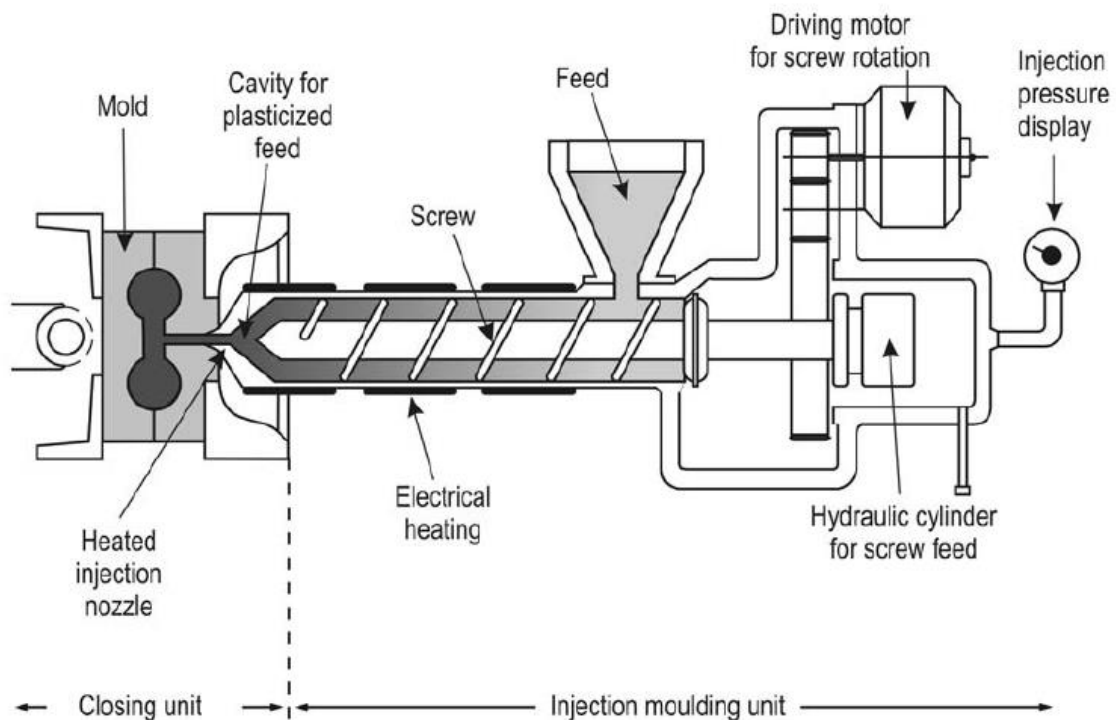
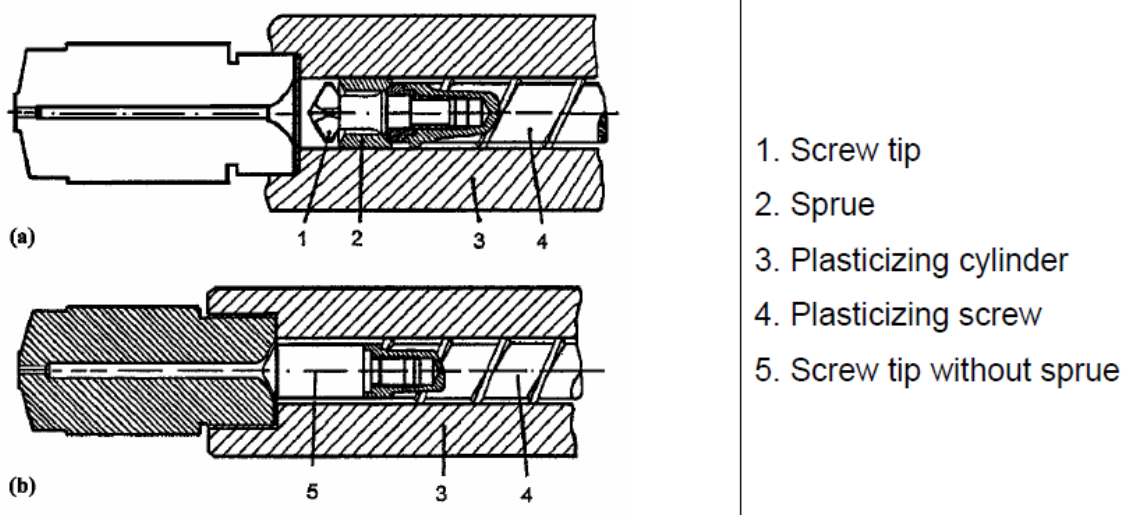


Fig. 4.3.2.3.2: Schematic diagram of a screw type injection molding machine.

The feed is plasticized in the heated cylinder and injected into the mold by the screw which acts both as feeding and pressing device. The temperature zones of the heatable plasticizing cylinder are subject to the melting points and the viscosity course of the organic constituents used. They range between 440 and 510 K depending on the flow behaviour of the powders and the content of organic components.

The mold temperature is lower than the melting points of the organic materials used so that the plastic feed solidifies and may be removed from the mold. It should be adjusted so as to maintain the flowability of the feed till the mold is completely filled. High mold temperatures may thus avoid press cones and inhomogenities in the sample cross section. On the other hand this temperature must be far enough below the melting point of the lowest-melting organic constituent so that the formation of bubbles at the sample surfaces will be avoided upon removal from the mold. In order to meet this compromise the mold temperatures normally range between 310 and 330 K.



**Fig. 4.3.2.3.3:** (a) Screw tip with sprue, cylinder with open nozzle; (b) Screw top without sprue, cylinder with open nozzle.

According to the flow behaviour of the feed screws with different geometries are used. For a high organic content and powders with a wide grain size distribution conventional screws for thermoplastics with compression zone and sprue may be used because of the good flowability of the mixtures (Fig. 4.3.2.3.3 at the top). In the compression zone in the front part of the screw the core diameter increases so that an additional homogenizing effect is obtained. The sprue prevents back flowing material during the injection process.

When using powders with a very narrow grain size distribution, or in case of very low organic contents in the feed, duromer screws without compression zone and sprue are used because

of the bad flowability of the mixtures (Fig. 4.3.2.3.3 down). Thanks to the larger gap between screw core resp. screw tip and cylinder wall also bad flowing powders can be injection molded.

Moreover, for feeds with bad rheological behaviour, the injection into the mold will not be done perpendicular to the split level of the mold as shown in Fig. 4.3.2.3.2, but the feed will be injected directly into the parting line through a vertically installed plasticizing cylinder. This arrangement will avoid unnecessary by-pass channels in the mold where the feed may tend to separate out. The homogeneity of the injection molded samples may in addition be improved by optimizing the injection velocity and the injection pressure.

The torque, the r.p.m. and the geometry of the screw affect the material transport and determine the shear stresses required to homogenize the feed. The torque  $T_x$  for a special screw diameter  $D_x$  can be calculated from a known torque  $T_o$  at a given velocity  $D_o$  [64].

$$T_x = T_o (D_x / D_o)^{2.7}$$

The mass flow is in the main subject to the flight depth  $h$  of a screw, the flight angle  $\theta$ , the cylinder diameter  $D$  and the r.p.m.  $N$  of the screw.

$$Q = \frac{\pi^2}{2} D^2 N h \sin\theta \cos\theta$$

while a pressure dependent reverse transport of the feed in the screw cylinder and a certain material leakage must be deducted from this flow.

On the other hand the shear rate, which is important for homogenizing, increases within the feed area of the screw according to [64] as follows:

$$\dot{\gamma} = \frac{D N}{h}$$

Where

$\dot{\gamma}$  = shear rate

$D$  = screw diameter

$N$  = screw r.p.m.

$h$  = flight depth



For materials of low viscosity, as already mentioned, low flight depths (compression zone) are selected, while for feeds of higher viscosity higher flight depths (duroplastics screws) are required. The influence of the screw geometry on the flow and the homogeneity of the injection molded components is described in detail in [64]. Moreover, the homogeneity of the injection molded components may be improved by optimizing the injection speed and the injection pressure. Fig. 4.3.2.3.4 shows the parameters influencing the injection molding process.

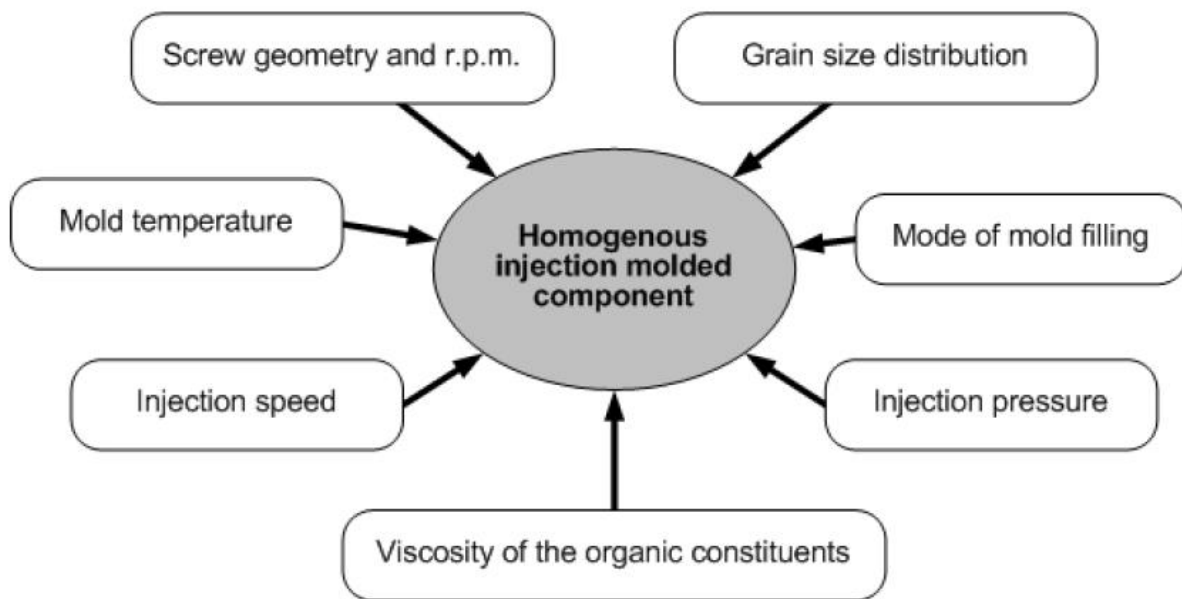


Fig. 4.3.2.3.4: Optimization parameters for injection molding.

A very decisive process step in manufacturing injection molded ceramic components is burning out the organic additives. Up to 50 vol.% of binders, plasticizers and lubricants have to be expelled from the green body before sintering. According to the wall thickness involved burning out of the additives may take from some hours to several weeks. Under vacuum (preferred in the main for nonoxide ceramics) the burn out time is estimated by German [65] as follows:

$$t = \frac{22,5 H^2 (1 - E^2) P G}{[ E^3 D^2 F ( P^2 - P_0^2 ) ]}$$

where

H = wall thickness of the component

E = porosity

- P = pressure at the binder/vapour interface
- G = vapour viscosity
- D = particle diameter
- F = ratio of the binder volume in solid and gaseous condition under a pressure P
- P<sub>o</sub> = external gas pressure

This equation includes several simplifications, but shows clearly that the burn out time t increases parabolically with the wall thickness H of the component.

When burning out liquid organic constituents in a powder bed the velocity of binder loss depends on capillary forces. This process is recommendable when low-viscous waxes are used, for example. The driving force for expelling the liquid additives is the gravity and capillary forces as per [2]

$$\Delta P = 2 \gamma_{LV} \left( \cos \theta_1 / R_1 - \cos \theta_2 / R_2 \right)$$

where

- $\gamma_{LV}$  = surface tension of the organic liquid
- $\theta_1, \theta_2$  = wetting angle of the liquid in the component and in the powder bed
- $R_1, R_2$  = pore radius in the component and in the powder bed

The burn out time according to this process has been evaluated by German [65] again as follows:

$$t = 4,5 \left[ \frac{(1 - E_c)^2 G H^2 D_w}{E_c^3 W D_c (D_c - D_w)} \right]$$

where

- E<sub>c</sub> = porosity of the component
- G = viscosity of the organic liquid
- H = wall thickness of the component
- D<sub>w</sub> = particle diameter of the powder bed
- W = binder-vapour surface energy
- D<sub>c</sub> = particle diameter in the component

By this method the decomposition of the organics increases faster with increasing porosity in the component, and while decreasing viscosity of the binder and wall thickness of the components and with increasing difference in the particle sizes of component and powder bed. For oxidation sensitive materials the thermal and oxidative decomposition is used to expel the organic additives. Here, evaporation, diffusion and flow play a similar part as in the ceramics drying process. Mutsuddy [64] describes the oxidation of the polymers as a series of chemical reactions according to Fig. 4.3.2.3.5.

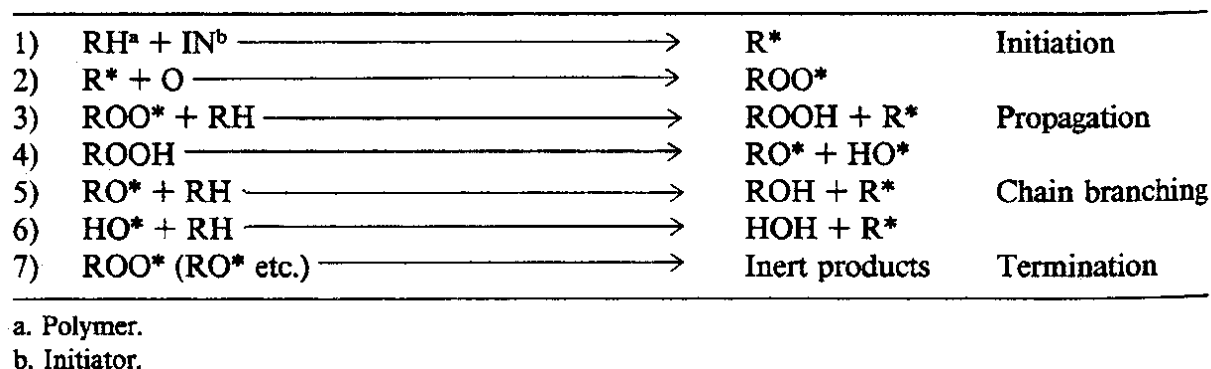


Fig. 4.3.2.3.5: Oxidation course of polymers [64].

In a first reaction, radicals are formed within the polymer by annealing (equation 1) which later-on react with oxygen to a peroxide radical (2). This radical in turn forms hydroperoxide and an additional radical with hydrogen from other polymer molecules (3). This second radical reacts again as per equation (2) and (3). This chain reaction may be repeated consecutively. Hydroperoxide is unstable and decomposes into radicales (4) forming new branched chains with hydrogen from other molecules (5) and (6). The process is at its end when the radicals are consumed by forming inert products.

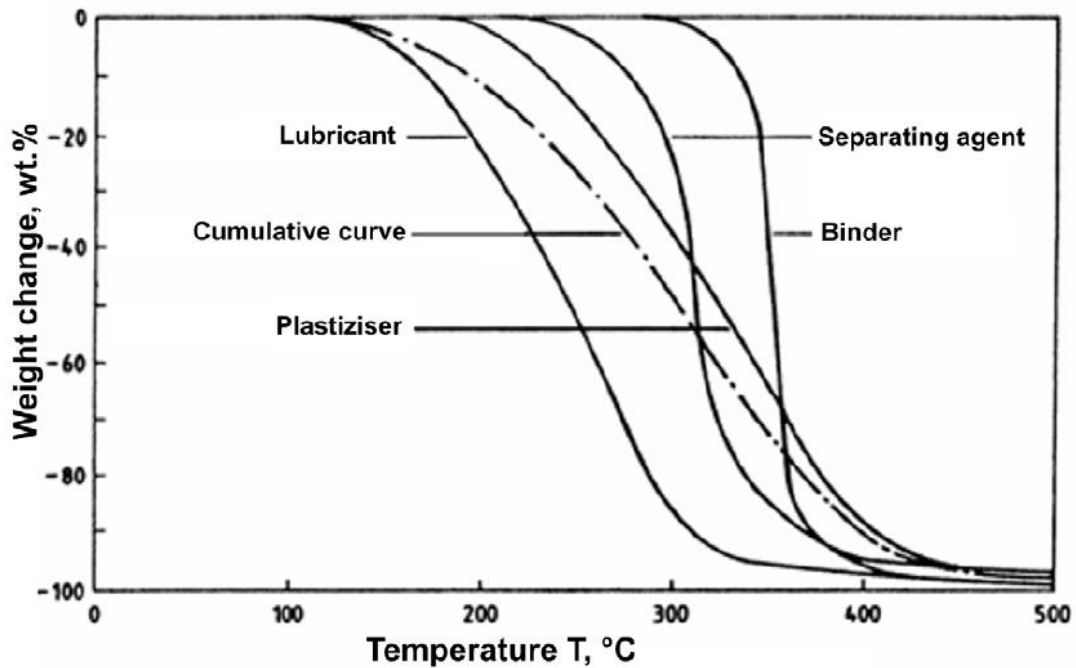


Fig. 4.3.2.3.6: Burn out behaviour of organic constituents from injection molded components.

Part of the binder leaves the porous component through the liquid phase while the residual quantity as a gaseous product. Driving forces are pressure differences for burning out a liquid binder. For burning out through the gaseous phase driving forces are concentration resp. vapour pressure differences which lead to diffusion processes. In this case the Knudsen diffusion in capillaries is the rate controlling step for the amount of gaseous reaction products emerging from the porous component.

Experimental investigations have shown that the pore diameter  $D$  obtained after the burning out the binder depends on the particle diameter  $R$  of the injection molded powders: According to Wada und Oyama [66]

$$D = (0,3 - 0,4) R \quad \text{for silicon nitride}$$

$$D = (0,2 - 0,3) R \quad \text{for silicon carbide.}$$

In order to avoid defects during burning out it is essential in practical use that oxidation and decomposition of binders, plasticizers and lubricants will not start at the same temperature. The weight loss should bridge over a widest possible temperature range.

### 4.3.3 Pressing

#### 4.3.3.1 Uniaxial dry pressing



The term of dry pressing generally describes the densification of powders or granules in axial direction between two stamps in hardened metal molds (Fig. 4.3.3.1.1).

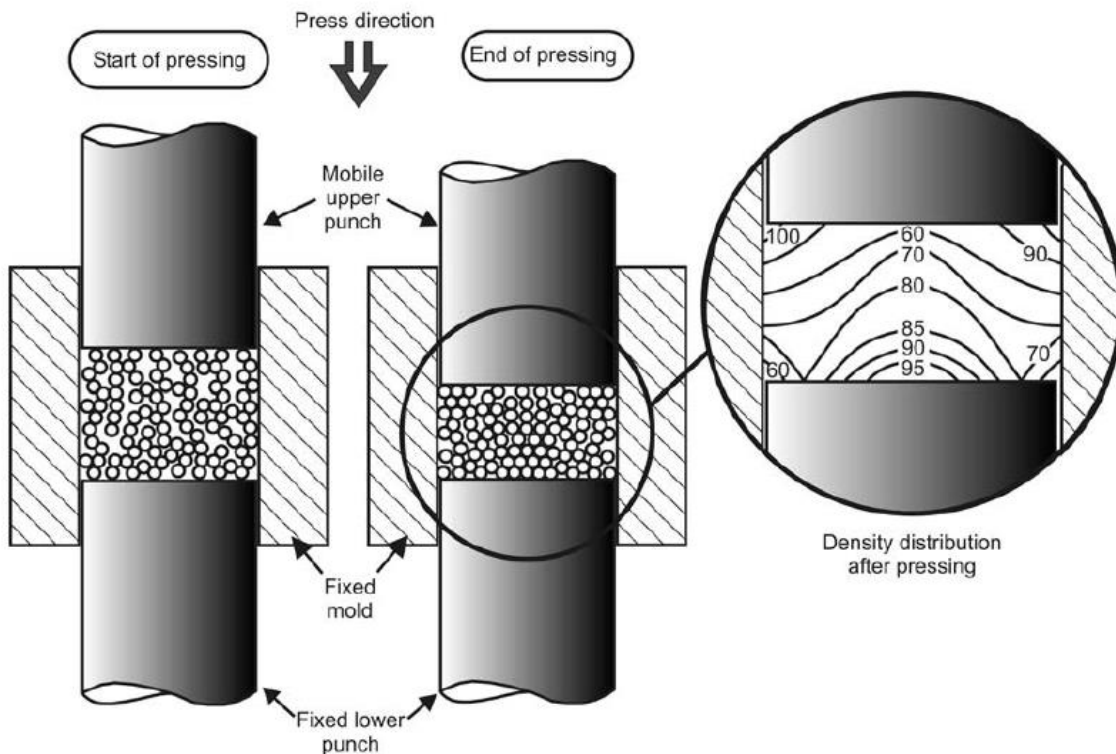


Fig. 4.3.3.1.1: Schematic diagram of the uniaxial dry pressing process.

This process allows only comparatively simple geometries to be manufactured like magnetic and dielectric components, alumina substrates, cutting tools, sensors, refractories, grinding disks, steatite isolators and tiles. After filling the mold the parts are densified and ejected. The densification is generally described by a pressure-density curve and is divided into three ranges [69]. In the first range of densification the particles are displaced in the pressing direction and densified by sliding and orienting. The sliding processes are favoured by organic additives that are normally added to the powders before or during the granulation (fig. 4.3.3.1.2).

Additive	Concentration (wt.%)
Polyvinyl alcohol	83,1
Glycerole	8,3
Ethylene glycol	4,1
Deflocculant	4,1
Wetting agent	0,2
Anti-foaming agent	0,2

Fig. 4.3.3.1.2: Organic additives for a spray-dried ceramic granulate [2].

The total concentration of densification aids ranges between 1 and 5wt.%, as a rule. In the second range agglomerates are destroyed, in the third plastic deformation is partly obtained. The density after pressing increases in the first range almost linear with the operating pressure, but shows a highly progression after all. Based on the models of Fischmeister and Arzt [70] and Helle, Easterling and Ashby [71], Oberacker et al. [40] describing the pressing pressure-density curve as follow, taking into account the determination of the individual granulate strength:

$$P = 3D^2 \frac{(D - D_o)}{(1 - D_o)} \frac{1}{20} [5 + 6(5D - 6D_B)^2] \sigma_{yg} \quad \text{for } [D_o < D < 0,9]$$

$$P = \frac{2}{3} \ln \frac{(1)}{(1 - D)} \frac{1}{20} [5 + 6(5D - 6D_B)] \sigma_{yg} \quad \text{for } [0,9 < D < 1]$$

where

P = Operating pressure

D<sub>o</sub> = starting density of the powder bed referred to the starting density of the individual granules

D = actual density of the pressed body at pressure P referred to the starting density of the individual granules

σ<sub>yg</sub> = pressure dependent yield strength of the granulate obtained from the individual granule test

D<sub>B</sub> = equivalent density at break of the granule

For  $\text{Al}_2\text{O}_3$  fluid bed sprayed granules with polyvinyl alcohol (PVA) and polyethyleneglycol (PEG) as lubricant they showed (once determined with the granule strength  $\sigma_g$ , once with the yield strength  $\sigma_{yg}$  of the individual granules) that the compressibility curve may be pre-calculated very well from the characteristics of the individual granules assuming certain simplifications like for example incompressibility of the individual granules (Fig. 4.3.3.1.3).

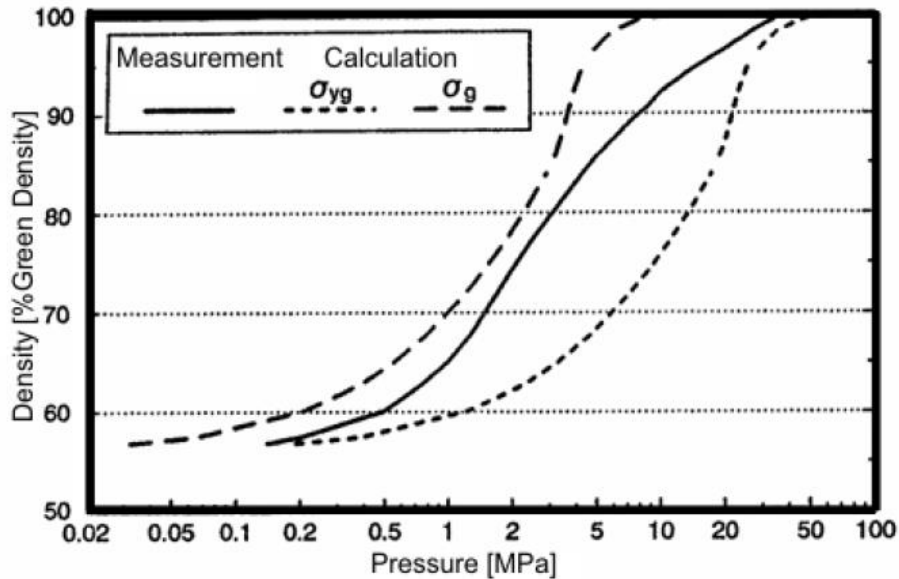


Fig. 4.3.3.1.3: Comparison of experimental data with calculations based on the granule strength resp. yield strength of individual grains (PVA/PEG = 40/60) [40].

All these contemplations start from a uniform densification of the component cross section. Subject to the diameter/height ratio, however, the obtained density distributions (Fig. 4.3.3.1.2) cause a deformation of the components during sintering. This non-uniform densification is caused by friction between the grains, friction between powder particles and mold as well as by the different displacements of the individual granules. In practical use these factors are opposed by changing the organic additives and by tuning the movement of the upper and the lower punch. Drumm et al. [72] have determined in suitably equipped pressing molds with sensors for pressure and displacement both the radial pressures and the hub of upper and lower punches. In addition, the elastic relaxation of dry pressed articles in axial and radial direction must be taken into account for the mold design.

In order to accelerate the mold design today the component fabrication is simulated [73] by means of the finite element method combined with suitable material laws for pressing and sintering. The knowledge of the green density distribution allows the calculation of the distortion during sintering (Figs. 4.3.3.1.4 and 4.3.3.1.5), taking into account the mathematical description of the sintering kinetics. The high time requirement and the high costs of the trial and error methods can be significantly reduced by these techniques.

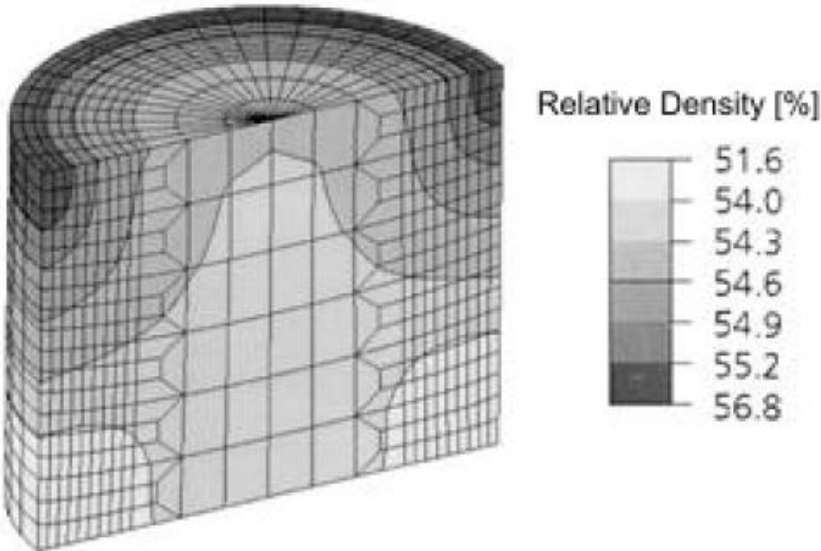


Fig. 4.3.3.1.4: Density distribution in the upper half of a dry pressed cylinder (axial cross section through the middle of the cylinder) [72].

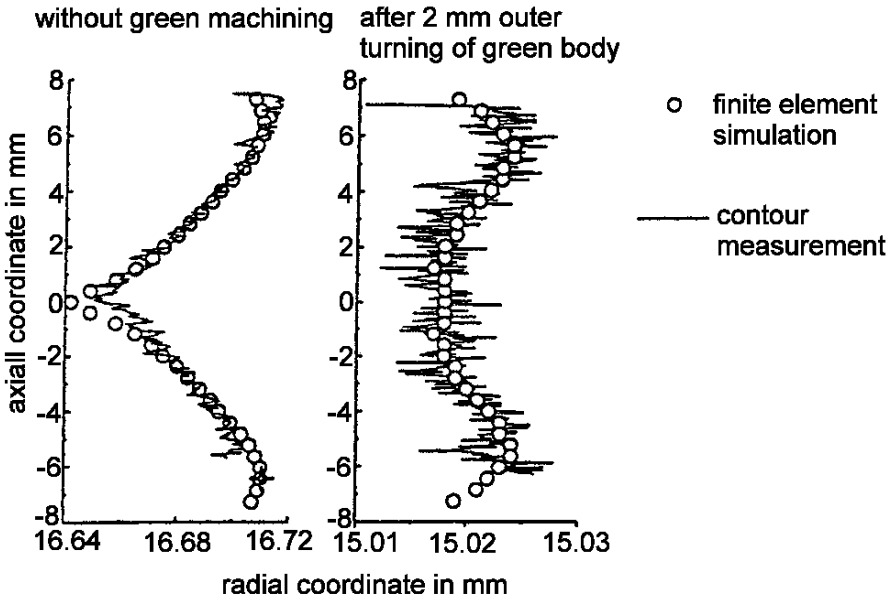





Fig. 4.3.3.1.5: Comparison of the predicted contour of a machined and an unmachined dry pressed and sintered cylinder with experimental results [72].



### 4.3.3.2 Isostatic Pressing

 *Animation: Isostatic wet bag pressing*

 *Animation: Isostatic dry bag pressing*

 *Videoclip: Isostatic plate pressing*

Products with a large length/diameter ratio of complicated or voluminous kind often cannot be dry pressed and have therefore to be isostatically densified. In this process the pressure is applied uniformly from all sides on to the granules to be densified. Pressure media are liquids, the granules to be densified being separated from the pressure medium by an elastic wrap. This wrap (mostly rubber or flexible polymer) must transfer the pressure as uniformly as possible.

In wet bag pressing (Fig. 4.3.3.2.1) flexible molds are filled with granules on vibrating tables, frequently evacuated and sealed. Then these molds are densified in a pressure vessel filled with liquid under pressures of up to 400 MPa. After the pressure relief the densified parts may be removed from the mold. In order to manufacture hollow bodies the granules are pressed on round metal rods. Due to the elastic relaxation upon pressure relief the metal part shaping the inner contour of the hollow body can be pulled out.

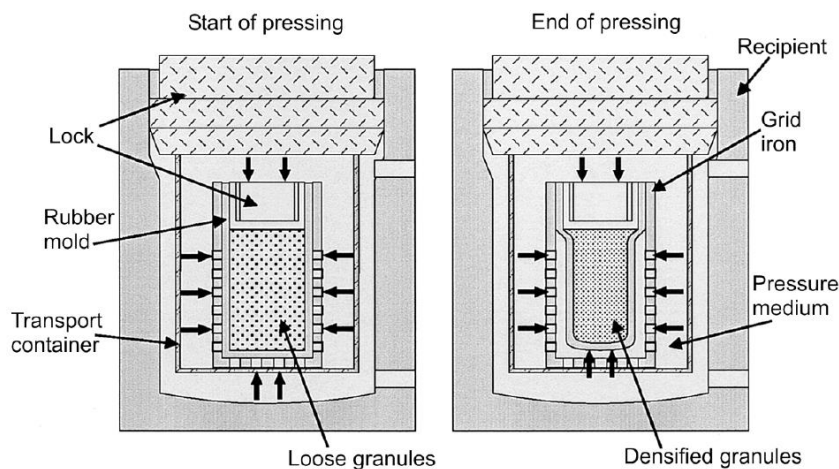


Fig. 4.3.3.2.1: Schematic diagram of wet bag isopressing.

In dry bag pressing (Fig. 4.3.3.2.2) the flexible mold is firmly connected with the pressure vessel. Thus, the mold is filled by granules within the press, while the pressure of up to 50 MPa is transferred by the pressure medium and the flexible mold onto the granules to be densified. In particular for flat table ware of larger sizes this pressing method approaches the dry pressing process very closely. For small articles like spark plugs, grinding balls or fuse bodies the isostatic principle is rather realized. A detailed description of the isostatic pressing techniques and their variations as well as of the basic densifying mechanisms and technological solutions is given by Schulle [74] and Hülsenberg [57].

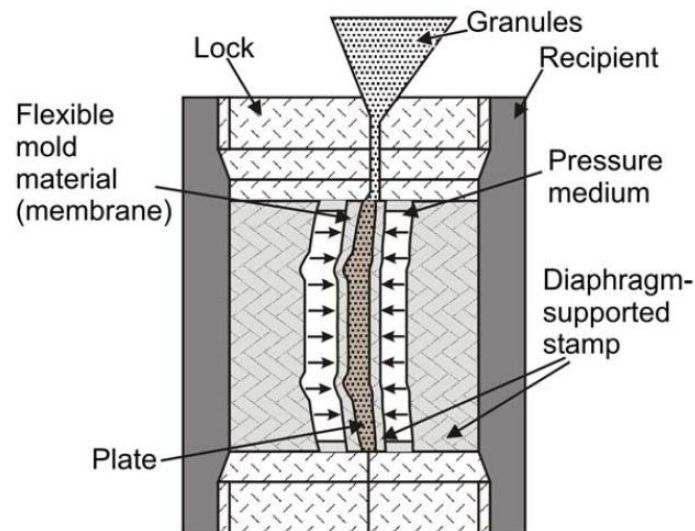


Fig. 4.3.3.2.2: Schematic diagram of dry bag isopressing.

For pressures of > 20 MPa the pressure depending densification according to Hechel [75] is described for the wet bag process as follows:

$$\ln \left( \frac{v_p}{v_p - v_\infty} \right) = c_1 p + c_2$$

where

$v_p$  = Volume of the pressed body at pressure  $p$

$v_\infty$  = Volume of the test sample at infinite pressure

$c_1, c_2$  = Constants

$p$  = Operating pressure

For the dry bag process Ulrich [76] has modified the Kawakita equation [77], which describes the relation between pressure and densification:

$$\frac{P}{c_v} = \frac{1}{c_3 c_4} + \frac{P}{c_3}$$

with  $c_v = \frac{V_o - V_p}{V_o}$

$V_o$  = Volume of the unpressed body

$c_3, c_4$  = constants

$p$  = pressure

On the example of porcelain feeds this relation could be confirmed up to a pressure of 50 MPa (Fig. 4.3.3.2.3). Although the pressure distribution is not quite isostatic because of the fixing of the mold in the dry bag process it has succeeded in mass production of spark plugs, fuses and flat table ware.

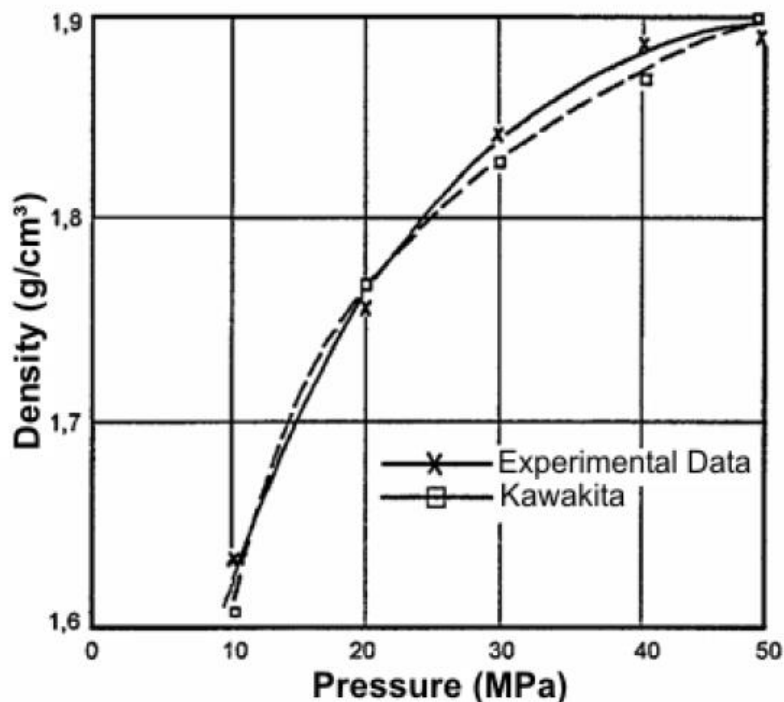


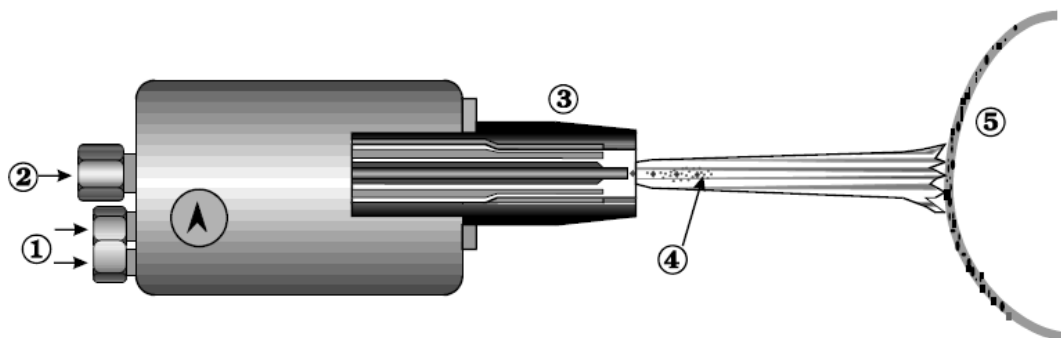
Fig. 4.3.3.2.3: Density of porcelain molds as a function of pressure for measured and calculated values according to the modified Kawakita equation [76].

#### 4.3.4 New developments

In the past some forming processes have been developed that show significant advantages compared to conventional processes. But nobody knows yet whether they will succeed in practical use.

Thermal spray coating processes have originally been developed to apply ceramic coatings on metals in order to protect them against temperature and corrosion. But recently new techniques have been developed to manufacture complex components by this process too. In the flame spraying process ceramic powders or rods are melted with acetylene, oxygen or other combustion mixtures and sprayed onto the cold or slightly preheated roughened substrate (Fig. 4.3.4.1). The spray torche works according to the balanced pressure principle inserting the spray materials by injection from the reservoir into the burner flame.

Plasma spraying is applied where materials with very high melting points are used so that the temperatures of the flame spraying process are too low to melt the particles. A plasma is created between an automatically following rod type carbon cathode and a rotating disk type anode, i.e. a dissociated and high-ionised electrically conducting gas that is in case of the water plasma burner stabilized in its centre by water rotations.



- 1) gas / oxygen
- 2) powder + feed gas
- 3) burner nozzle with or without water cooling
- 4) gas- / oxygen flame and spray particles
- 5) work piece

Fig. 4.3.4.1: Schematic diagram of the flame spraying process.

A small portion of the water is evaporated and decomposes into hydrogen-oxygen plasma while the main part of the water keeps cooling the plasma. The water plasma burner excels by high powder flow and accordingly high spray coating rates. For manufacturing components the molten powders are sprayed onto preheated metallic bodies. As the coefficient of thermal expansion of metals is normally higher than that of ceramics, they will shrink more when they cool down so that at least for simple-shaped components the spray coat may be taken off after the cooling process and the parts may be sintered [78]. In order to increase the particle velocity and to optimize the yield of energy in the powder to be processed the detonation and laser spraying processes have been developed [79, 80].

In the Gelcasting process a ceramic slip is used that contains reactive monomers as organic additives. Monofunctional acrylamid ( $C_2H_3CONH_2$ ) is dissolved in deionised water together with difunctional methylenebisacrylamid ( $(C_2H_3CONH)_2 CH_2$ ). Under presence of an initiator like ammonium persulfate ( $(NH_4)_2 S_2O_8$ ) and a catalyst like tetramethylethylendiamide a vinyl polymerisation is caused that results in an elastic hydrogel and thus in a component to be easily manipulated. Suitable materials for the molds are glass or simple metal containers [81]. After gel formation and removal of the parts from the mold the binder is burned out like for conventionally cast components and the products may be sintered.

Coagulation casting is a process for slurries with solid yields exceeding 60 vol.%. Upon feeding the slip into a more or less optional mold material the repulsive forces at the particle surface are eliminated in order to coagulate the suspension and to produce a viscoelastic solid-state body. In order to minimize the repulsive forces the pH is approached to the isoelectric point with the consequences described in chapter 2.1, thus creating a coagulation of the particles and forming a viscoelastic solid-state body [82]. The pH may be changed by the enzymatical decomposition of a substrate or by the slow self-decomposition of organic reagents (Fig. 4.3.4.2). The pH may thus be varied from the acidic to the basic range or vice-versa. Moreover, the repulsive forces may be influenced by increasing the salt concentration which will affect the double-layer thickness at the particle surface. The influence of the pH and the salt concentration on the transformation into a viscoelastic body is to be seen from Fig. 4.3.4.3.

Reaction	PH Change
Autocatalytic	
Hydrolysis of urea (>80°C)	3 -7
Hydrolysis of formamide (>60°C)	3-7 or 12-7
Hydrolysis of esters	11-7
Hydrolysis of lactones	9-4
Enzymatic	
Hydrolysis of urea by unreuse	4-9 or 12-9
Hydrolysis amides by amidase	3-7 or 11-7
Hydrolysis of esters by esterase	10-5
Oxidation of glucose by glucosoe oxidase	10 4

Table 4.3.4.2: Some reactions to change the pH of a suspension [82].

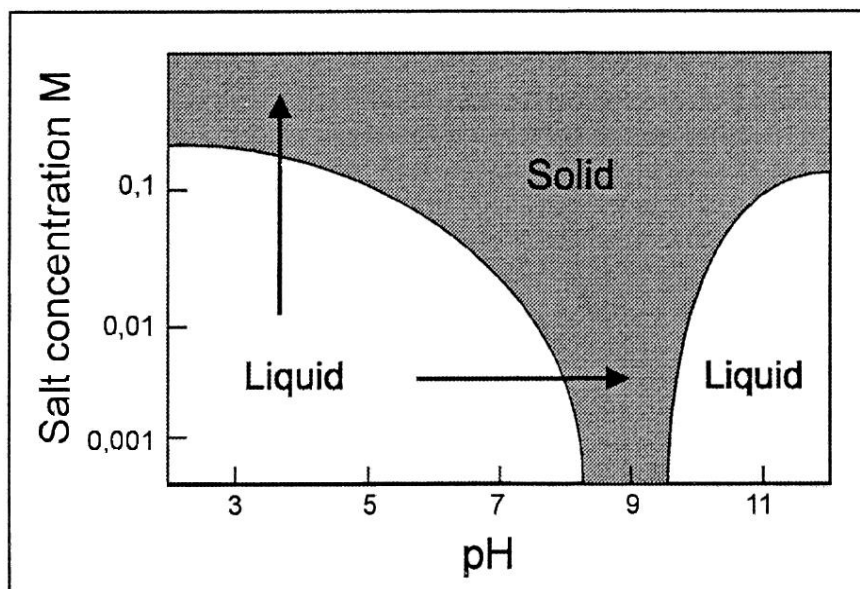


Fig. 4.3.4.3: Coagulation of slurries realized with pH near the isoelectric point and at increased salt concentrations (reduction in thickness of the electric double layer at the particle surfaces) [82].

In this process, too, complicated shaped components may be produced in simple metal, rubber or glass containers without the necessity of self-absorbing porous mold materials or higher pressure, even for components with higher wall thicknesses.

Pre-ceramic polymers are under discussion as starting materials for the production of non-oxide ceramic materials in the main. When creating silicon carbide from polycarbosilane (Fig. 4.3.4.4) shrinkage in volume of more than 50% will be obtained by the polymer-ceramics conversion.

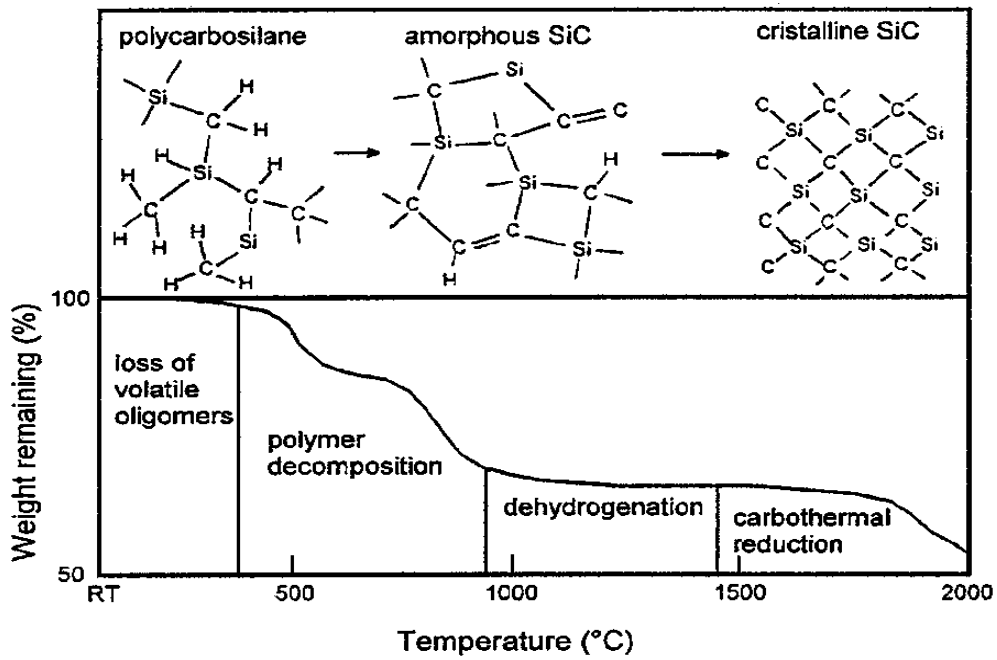


Fig. 4.3.4.4: Structural changes upon the thermal decomposition of a pre-ceramic polymer (polycarbosilane) [83].

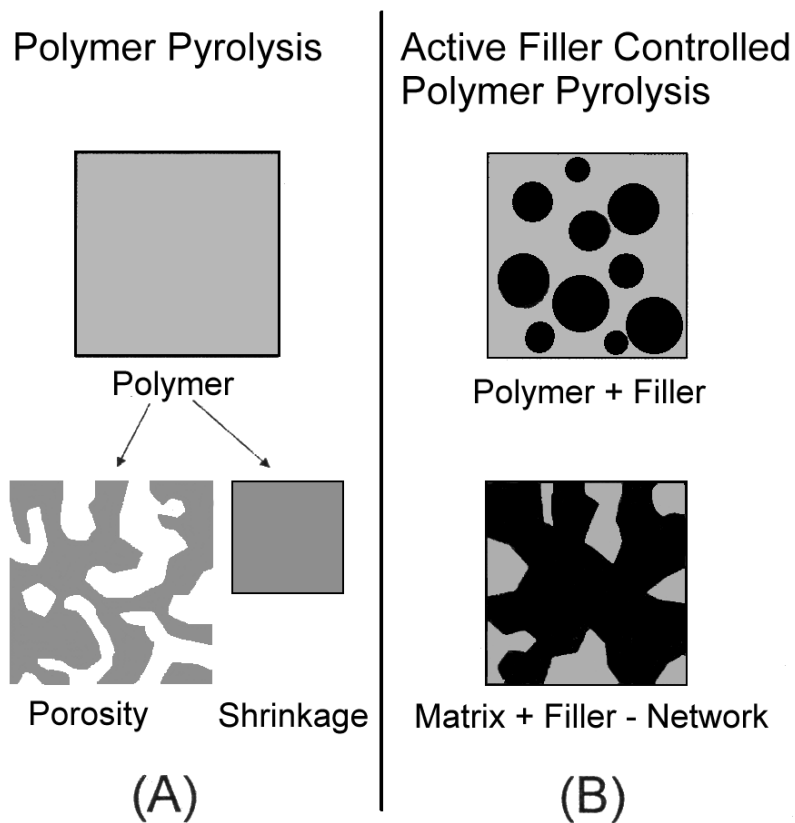


Fig. 4.3.4.5: Microstructural changes caused by the polymer-ceramics conversion: (A) Polymer pyrolysis without filler showing porosity and shrinkage and (B) Polymer pyrolysis with active fillers that compensates the shrinkage by reacting with decomposition products of the polymer [83].

Normally, this will lead to micro cracks or porosity formation respectively destroys the component. Shrinkage may be reduced by filling the polymer matrix with reactive filler particles that expand during the reaction with decomposition products of the polymer to compensate the original shrinkage. These conditions are shown in fig. 4.3.4.5 schematically.

Even if this process is far from being applied in mass production it is expected that characteristics profiles of ceramic components may be set starting from pre-ceramic polymers that cannot be achieved by other shaping processes. For special applications, the polymer pyrolysis will certainly be taken into account in the future.

For manufacturing prototypes several methods are under development. All those processes combine the construction and laminar sectioning of components by a CAD equipment, while they vary in the way of constructing the layer and in the way of constructing components from these layers.

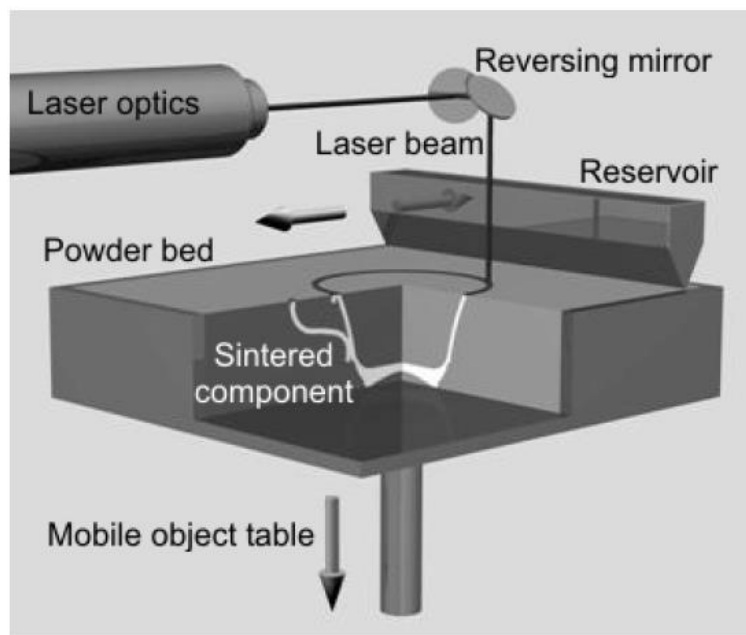


Fig. 4.3.4.6: Schematic diagram of a laser sintering equipment.

Derived from stereolithography where light-sensitive polymers are polymerized and thus stabilized by a laser beam, 3D printing has been enveloped [84]. In this process a component is designed layer by layer by gelling aqueous ceramic suspensions. The layer manufacturing technique (LMT) uses ceramic tapes [85] to construct components. This process is known for decades already in the technical ceramics industry and is the elementary production process for ceramic multilayer packages for electronic applications. This technique is the only mold-free manufacturing method that has been developed up to mass production.



The layerwise construction of ceramic components by extrusion (Shape Deposition Manufacturing, SDM) is used to manufacture prototypes from a mixture of ceramic powders and organic polymers as they are used in the injection molding process [86]. All the above-mentioned methods are handicapped by the fact that the organic additives have to be burned out before sintering. A very promising promising way for manufacturing complex shaped prototypes without adding organic additives to the starting powders has been offered by the laser assisted sintering (LAS) [87]. A laser beam controlled by a CAD device is used to sinter individual layers in a ceramic powder bed and to construct the component successively that way (Fig. 4.3.4.6). This process is best suited for the manufacture of porcelain prototypes as it is simulating a biscuit fired body. Components manufactured that way may be conventionally decorated and glazed.



Videoclip: Rapid Prototyping LSD

#### 4.4 Literature list of chapter "Forming"

1. Parks, G.A.; de Bruyn, P.L.: „The Zero Point of Charge of Oxides“, J. Phys. Chem. 66 (1962) 967-973
2. Reed, J.: Introduction to the Principles of Ceramic Processing. John Wiley & Sons, New York (1988)
3. Thiessen, P.A.: Wechsel seitige Adsorption von Kolloiden. Z. Elektrochem. 48 (1942) 675-681
4. Helmholtz, H.: Studien über elektrische Grenzschichten. Annalen der Physik und Chemie 7 (1879) 337-382
5. Stern, O: Zur Theorie der elektrischen Doppelschicht. Z. Elektrochem. 30 (1924) 508-516
6. Gouy, G.: Sur la Constitution de la Charge Électrique a la Surface d'un Électrolyte. J. Physique 9 (1910) Nr 4; 457-469
7. Chapman, D.L.: A Contribution to the Theory of Electrocapillarity. Phil. Mag. 25 (1913) 475-481
8. Horn, R.G.: Particle Interactions in Suspensions: In: R.A. Terpstra, P.P.A.C. Pex, A.H. de Vries: Ceramic Processing. Chapman & Hall, London (1995)
9. Derjaguin, B.; Landau, L.: Theory of the Stability of Strongly Charged Lyophobic Sols and of the Adhesion of Strongly Charged Particles in Solutions of Electrolytes. Acta. Physicochim., 14 (1941) 633

10. Verwey, E; Overbeck, Th.G.: Theory of the Stability of Lyophobic Colloids., Elsevier Amsterdam (1948)
11. Michaels, A.S. Rheological Properties of Aqueous Clay Systems. In: Kingery, W.D.: Ceramic Fabrication Processes. John Wiley & Sons, Inc., New York, Chapman & Hall, Limited, London,(1958).
12. Graule, T.F; Baader, F.H.; Gauckler, L.J.: Enzyme Catalysis of Ceramic Forming., J. Mat. Educ. 16 (1994) 243-267
13. Heinrich, J.: Herstellung von keramischen Portlinern für Kolbenmotoren im Schlickergießverfahren. Keram. Z. 44 (1992) 822-826
14. Haase, T.H.: Untersuchungen zur Bildsamkeit keramischer Massen. Silikattechnik 3 (1952) 265-267
15. Pfefferkorn, K.: Ein Beitrag zur Bestimmung der Plastizität in Tonen und Kaolinen. Sprechsaal 57 (1924) 297-299
16. Haase, Th.: Der Pfefferkorn-Apparat als absolutes Meßgerät. Ber. Dtsch. Keram. Ges. 43 (1966) 593-594
17. Dietzel, A.: Messung der Plastizität. Ber. Dtsch. Keram. Ges. 45 (1968) 63-66
18. Macey, H.H.: Experiments on plasticity. Trans. Brit. Ceram. Soc. 43 (1944) 5-28; 47 (1948) 183-190, 259-267, 291-326
19. Linseis, M.: Beiträge zur Plastizitätsmessung unter Berücksichtigung praktischer Erfordernisse. Ber. Dtsch. Keram. Ges. 29 (1952) 35-37
20. Czerch; W.: Frühauf, K.; Hofmann, U.: Über die Ursachen der Verflüssigung des Kaolins. Ber. Dtsch. Keram. Ges. 37 (1960) 255-265
21. Händle, F.: Beitrag zur sogenannten Plastizität von Ton-Wasser-Systemen. Ziegelindustrie 31 (1978) 472-476
22. Norton, F.H.: An instrument for measuring the workability of clays. J. Amer. Ceram. Soc. 21 (1938) 33-36
23. Astbury, N.F; Moore, F.; Lockett, J.A.: A cyclic torsion test for the study of plasticity. Trans. Brit. Ceram. Soc. 65 (1966) 435-462
24. Hennicke, H.W.; Kersting, R.: Electronic analogue models for the mechanical behaviour of heterogeneous materials in ceramics. Science of Ceramics 5 (1970) 263-280
25. Hennicke, H.W.; Kienow, E.: Organische Plastifizierungsmittel für feinkeramische Werkstoffe. Ber. Dtsch. Keram. Ges. 56 (1979) 67-71, 95-102
26. Kobayashi, T.: u.a.: Rheological properties of plastic clay body: An examination on the Astbury's cyclic torsion test method. J. Ceram. Soc. Japan 80 (1972) 64-74

27. Moore, F.; Hennicke, H.W.: Rheologie in der Keramik, Goslar: Hübner 1967
28. Wilson, E.O.: The plasticity of finely ground minerals with water. J. Amer. Ceram. Soc. 19 (1936) 115-120
29. Mostetzky, H.: Zwei Modellelemente für die Bildsamkeit keramischer Massen. Tonind.-Ztg. 98 (1974) 287-288
30. Hofmann, U.: Über die Grundlagen der Plastizität der Kaoline und Tone. Ber. Dtsch. Keram. Ges. 26 (1949) 21-32
31. Capes, C.E.: Particle Size Enlargement. In: J.C. Williams; T. Allen (Editor): Handbook of Powder Technology Volume 1 Elsevier Scientific Publishing Comp. (1980)
32. Rumpf, H.: Grundlagen und Methoden des Granulierens. Chemie-Ing. Techn. 30 (1958) Nr. 3, 144-158
33. Rumpf, H.: Particle Adhesion. In: K.V.S. Sastry (Editor): Agglomeration 77, AIME New York (1977) 97-129
34. Frisch; B.; Thiele, W.-R.: Adhesion Effects of Intermediate Layers on the Densification of Ceramic Powders. Journal Adhesion, 22 (1987) 81-95
35. Schulz, P.; Pfaff, E.; Zografon, C.: Der Einfluß des Bindergehaltes auf Bildung und Eigenschaften von Sprühgranulat. Keram. Z. 34 (1982) 561-564
36. Claussen, N.; Petzow, G.: Wachstum und Festigkeit kugeliger Agglomerate aus Pulvern hochschmelzender Werkstoffe, High Temperatures - High Pressures., Vol. 3 (1971) 467-485
37. Schubert, H.: Grundlagen des Instantisierens und Dispergierens von Pulvern. cfi Beiheft: Granulate in der Keramik (1995) 55-74
38. Frisch, B.; Hör, Th.; Thiele, W.R.; Klemm, U.; Soback, D.; Stolle, W.: Characterization of Ceramic Dry Pressed Bodies - Measurement Techniques and Evaluation. cfi/Ber. Dtsch. Keram. Ges. (1994) 24-33
39. Oberacker, R.: Persönliche Mitteilung
40. Oberacker, R.; Agniel, Y.; Thümmeler, F.: Bedeutung der Einzelgranulateigenschaften beim Verpressen von aufbaugranulierten Feinpulvern. In: H. Kolaska: Fortschritte bei der Formgebung in Pulvermetallurgie und Keramik. VDI Verlag (1991) 185-208
41. Mostetzky, H.: Formgebung in der Keramik. Handbuch der Keramik, Gruppe I D1, Verlag Schmid GmbH Freiburg i. Brg. (1978) 1-12
42. Kolaska, H.; Schulz, P.: Pulvermetallurgie der Hartmetalle. Vorlesungsreihe Fachverband Pulvermetallurgie, Hagen (1992)

43. Ruys, A.J.; Sorrel, C.C.: Slip Casting of High-Purity Alumina Using Sodium Carboxymethylcellulose as Deflocculant/Binder. *Am. Ceram. Soc. Bull.* 69 (5), (1990) 828-832
44. Nürnberger, G.: Entwicklung und Einführung des Druckgießverfahrens in der Sanitärkeramik. *Keram. Z.* 40 (1988) 227-232
45. Frassek, L.; Hennicke, H.W.: Einige Aspekte zum Schlickerdruckgießen von tonfreien Suspensionen. *cfi Beiheft: Moderne Formgebungsverfahren in der Keramik* (1989) 61-72
46. Akers, R.J.; Ward, A.S.: Liquid filtration theory and filtration pretreatment Filtration; Principles and Practices. Part I ed. by Orr e.a. *Chem. Proc. Eng. Vol. 10* Marcel Dekker Inc. New York, Basel (1979) 169 ff.
47. Frassek, L.: Formgebung über tonfreie Schlicker in der Keramik. Dissertation TU Clausthal (1988)
48. Mistler, R.E.; Shanefield, D.J.; Runk, R.B.: Tape Casting of Ceramics In: G.Y. Onada, Jr.; L.L. Hench: *Ceramic Processing Before Firing*. John Wiley and Sons, Inc. New York, Chichester, Brisbane, Toronto (1978) 411-448
49. Heinrich, J.: Foliengießen oxidischer und nichtoxidischer keramischer Pulver. *Keram. Z.* 38 (1986) 79-82
50. Richerson, D.W.: *Modern Ceramic Engineering*. Marcel Dekker, Inc. New York, Basel 1982
51. Chou, Y.T.; Ko, Y.T.; Yan, M.F.: Fluid Flow Model for Ceramic Tape Casting. *J. Am. Ceram. Soc.* 70 (10), C280-C282 (1987)
52. Williams, J.C.: Doctor-Blade Process. In: F.F.Y. Wang: *Treatise on Materials Science and Technology*. Vol. 9, Academic Press., New York, San Francisco, London (1976) 173-197
53. Onada, G.Y., Jr.: The Rheology of Organic Binder Solutions. In: G.Y. Onada, Jr.; L.L. Hench: *Ceramic Processing before Firing*. John Wiley and Sons, Inc. New York, Chichester, Brisbane, Toronto (1978) 236-251
54. Böcker, A.; Bunge, H.J.; Huber, J.; Krahn, W.; Ruska, J.: Texture and of  $\alpha$ -Al<sub>2</sub>O<sub>3</sub> Substrates. *Textures and Microstructures* Vol. 24 (1995) pp. 167
55. Kleer, G.; Goller, R.; Döll, W.; Heinrich, J.; Rosenfelder, O.: Strength and Crack Propagation Behaviour of Anisotropic Laminated SiC. *Proc. Euro-Ceramics II*, ed. by Ziegler, G.; Hauser, H.: *Dtsch. Keram. Ges. e.V. Köln* (1991) 1067-1071
56. Segerer, H.: Rollerformgebung. *Handbuch der Keramik, Gruppe I D2.3*. Verlag Schmidt GmbH. Freiburg i.Brg. (1985) 1-6
57. Hülsenberg, D.; Krüger, H.-G.; Steiner, W.: *Keramikformgebung*. VE Deutscher Verlag für Grundstoffindustrie Leipzig (1987)

58. Bayer, B.: Untersuchung eines neuen Formgebungswerkzeugs zur Herstellung von Flachgeschirr. Silikattechnik 19 (1968) 386-392
59. Hallmann, E.: Strangpressenberechnung für keramische Stoffe. Sprechsaal 116 (1983) 1, 25-27; 8, 653-662; 10, 895-898; 12, 1075-1077
60. Pels-Leusden, C.O.: Ablauf und Beeinflussung der Texturbildung während der Formgebung. Ziegelindustrie 38 (1985) 7, 390-405
61. Pels-Leusden, C.O.: Über die Betriebsweise der Arbeitszone einer Schneckenpresse bei der Förderung einiger grobkeramischer Rohstoffe. Dissertation TH München (1965)
62. Händle, F.: Formgebung, Sonderdruck aus Ziegelindustrie International Nr. 1/82 14-22
63. Janney, M.A.: Plastic forming of ceramics: Extrusion and injection moulding. In: R.A. Terpstra, P.P.A.C. Pex, A.H. de Vries: Ceramic Processing, Chapman & Hall London (1995)
64. Mutsuddy, B.C., Ford, R.G.: Ceramic Injection Molding. Chapman & Hall, London (1995)
65. German, R.M.: Theory of Thermal Debinding. J. Powder Med., Am Powder Met. Inst. 23 (4) (1987) 237-245
66. Wada, S.; Oyama, Y.: Thermal Extraction of Binder Components from Injection Molded Bodies, Toyota Central Res. and Dev. Labs., Nagakute, Aichi Japan (1989) 480-11
67. Edirisinghe, M.J.; Evans, J.R.G.: Review: fabrication of engineering ceramics by injection molding. I. Materials selection. Int. J. High Technol. Ceram. (1986) 2, 1-31
68. Edirisinghe, M.J.; Evans, J.R.G.: Review: fabrication of engineering ceramics by injection molding. II. Materials selection. Int. J. High Technol. Ceram. (1986) 2, 249-78
69. Frisch, E.; Thiele, W.R.; Peter, M.: Zum Einfluß von Zwischenschichten auf Preßverdichtung und Scherbeneigenschaften feinkeramischer Massen. Ber. Dtsch. Keram. Ges. 54 (1977) 7, 224-229 und 8, 259-263
70. Fischmeister, H.F.; Arzt, E.: Densification of Powders by Particle Deformation, Powder Met. 26 (1983) 82-88
71. Helle, A.S.; Easterling, M.F.; Ashby, K.E.: Hot-Isostatic Pressing Diagrams: New Developments. Acta Metall. 33 (1985) 2163-2174
72. Zipse, H.: Finite-Element Simulation of the Die Pressing and Sintering of a Ceramic Component. J. Europ. Cer. Soc. 17 (1997) 1707-1713
73. Drumm, R.; Frisch, B.; Hör, T.; Martin, J.; Thiele, W.R.: Mechanische Eigenschaften von Einzelsekundärkörnern und das Axial-Radialdruckverhalten von keramischen Preßkörpern. cfi Ber. DKG 68 (1991) 332-337

74. Schulle, W.: Die halbisostatische Preßformgebung in der Keramik. Handbuch der Keramik, Gruppe I D3.3. Verlag Schmid GmbH Freiburg i.Brg. (1991) 1-16
75. Heckel, R.W.: Density-pressure relationship in powder compaction. Trans. of Mat. Soc. AIME 221 (1961) 8, 671-675
76. Ullrich, R.: Untersuchungen zum Preß- und Verdichtungsverhalten dünnwandiger feinkeramischer Formlinge nach dem isostatischen Trockenmatrizenverfahren. Dissertation Bergakademie Freiberg (1985)
77. Kawakita, K.; Lüdde, K.-H.: Some Considerations on Powder Compression Equations. Powder Technol 4 (1970/71) 61-68
78. Schindler, S.; Schultze, W.: Plasma Generated Oxide Ceramic Components. Interceram 37 (1988) (2) 39-42
79. Borisow, S.Yu., Astakhov, E.A., Klimenko, V.S.: Detonationsspritzen: Anlagen, Werkstoffe, Anwendungen, DVS-Berichte Band 130 (1990), ISBN
80. Herziger, G., Loosen, P.: Werkstoffbearbeitung mit Laserstrahlung. Carl Hanser Verlag, München, Wien, 1993.
81. Young, A.C.; Omatete, O.O.; Janney, M.A.; Menchhofer, P.A.: Gelcasting of Alumina. J. Am. Ceram. Soc. 24 (1991) 612-18
82. Graule, T.J.; Baader, F.H.; Gauckler, L.J.: Casting uniform ceramics with direct coagulation. Am. Chem. Soc. (1995) 31-37
83. Greil, P.: Active-Filler-Controlled Pyrolysis of Preceramic Polymers. J. Am. Ceram. Soc. 78 [4] (1995) 835-48
84. Teng, W.D.; Edirisinghe, M.J.: Development of continuous direct ink jet printing of ceramics. Brit. Ceram. Trans. 97 [4], 1998, 169-173.
85. Cawley, J.D.; Heuer, A.H.; Newman, W.S.; Mathewson, B.B.: Computer-aided manufacturing of laminated engineering materials. Am. Ceram. Soc. Bull. 75, 1996, 75-
86. Argawala, M.K.; Jamalabad; V.R.; Langrana, N.A.; Safari, A.; Whalen, P.J.; Danforth, S.C.: Structural Quality of Parts Processed by Fused Deposition. Rapid Prototyping Journal 2, 1996, 4-19.
87. Heinrich, J.G.; Ries, C.; Görke, R.; Krause, T.: Lasersintern keramischer Werkstoffe. In: J. Heinrich, G. Ziegler, W. Hermel, H. Riedel (Hrsg.): Keramik. Werkstoffwoche 1998, DGM Informationsgesellschaft mbH, Verlag der Deutschen Gesellschaft für Materialkunde e.V., Frankfurt.

## 5. Thermal processes

### 5.1 Drying

After shaping of the ceramic parts, the parts follow to drying. During drying, the particles that have been surrounded by more or less water, depending on the forming techniques get closer and the green body smaller, what is called shrinkage (Fig. 5.1.1). Shrinkage is finished as soon as the powder particles touch each other. The remaining water now has to leave the system through the small pore or channels. In the Bourry diagram (Fig. 5.1.2) the water content is plotted versus the drying time. Water content diminishes at the beginning of the drying process and the part shrinks. After about 72 hours, water can only be found in the pores. Water content further decreases, but shrinkage does not change any more. The dry bending strength increases as the green bodies' water content decreases (Fig. 5.1.3). As a result the particles can be handled and, for example, be set on conveyor bands mechanically or by hand.

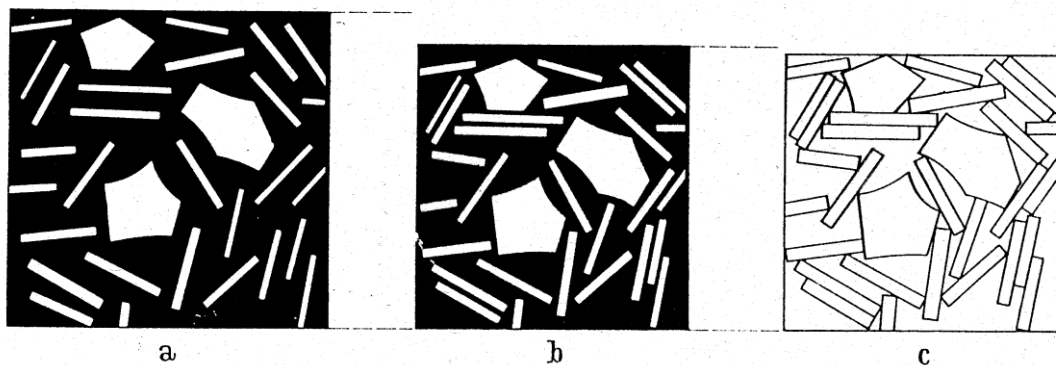


Fig. 5.1.1: Illustration of the drying stages in ceramic compounds [1].

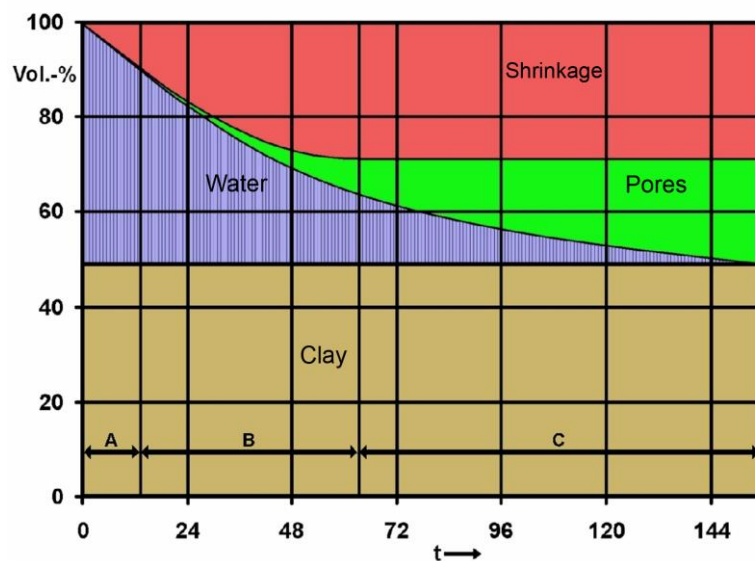


Fig. 5.1.2: Bourry drying diagram for clay components.

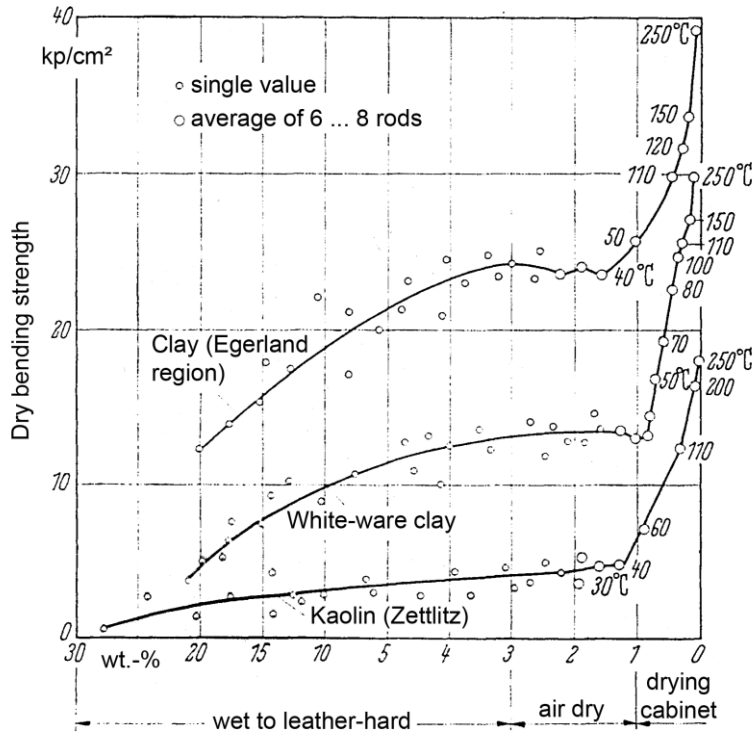


Fig. 5.1.3: Dry bending strength as a function of the drying temperature [1].

The graphic of the mass loss (Fig. 5.1.4) shows the moisture content as a function of the drying time. At the beginning, the reduction on the moisture content is linear. In this case, the water has direct access to the surface of the tested pieces. When the water is trapped into the pores, the curve deviates from the straight line. The differentiated mass loss graph (Fig. 5.1.4b) shows the area of constant drying rates even clearer. Drying speed decreases with the water's retraction into the pores. The drying speed in dependence of the moisture content (Fig. 5.1.4c) is also a standard presentation in the literature. The diagram has to be read from right to the left. If the moisture content is high, the drying speed at first is constant, and decreases as the water is trapped into the pores.

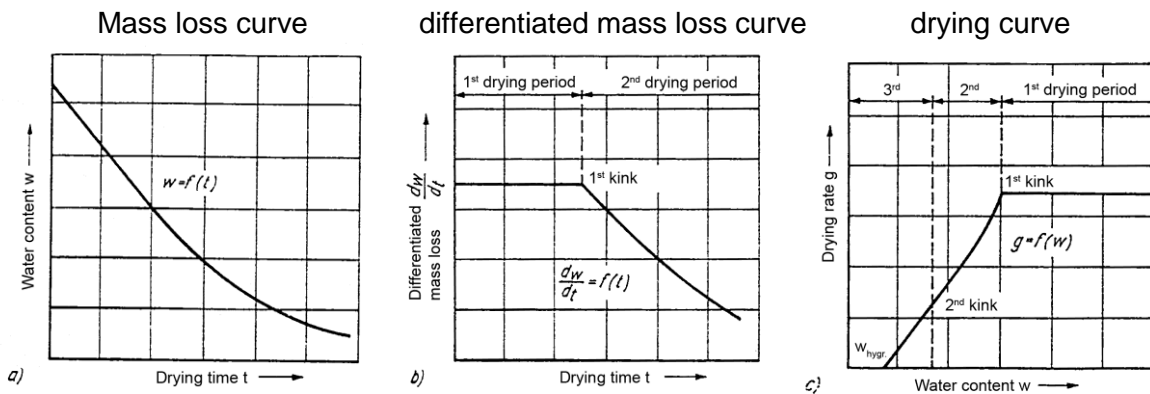


Fig. 5.1.4: Drying diagram according to Scholz.



Drying rate can be increased by raising drying air speed (Fig. 5.1.5) and temperature (Fig. 5.1.6). Furthermore, the drying speed is affected by specimen geometry and density of the components (Fig. 5.1.7). If the total porosity is high (decreasing density), the water can leave the system relatively quickly. At very low moisture degrees we see again a deviation in the curve. This is the point at which only OH groups are found at the surface. Now, if temperature is further increased, drying speed is again reduced and the OH groups leave the surface of the test sample. This is the third drying stage which, however, is not relevant in practice.

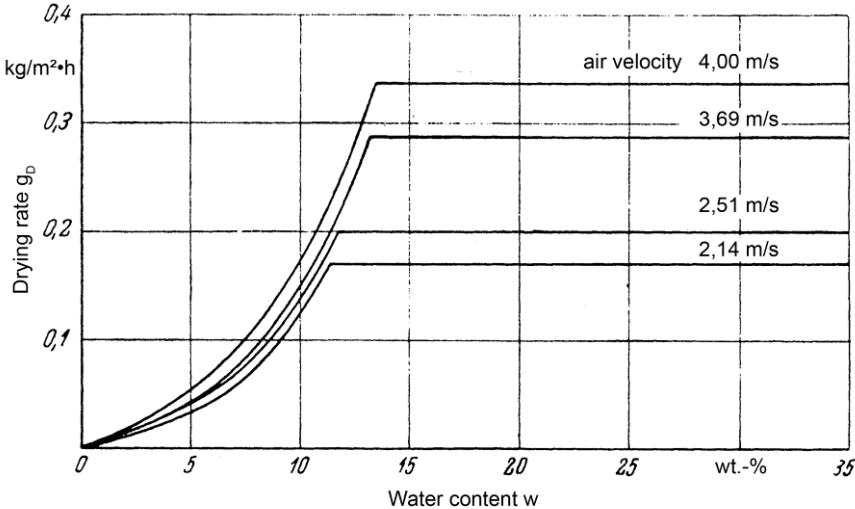


Fig. 5.1.5: Drying curve for clay minerals, two-stage drying of samples with thickness of 3 cm, in a air humidity of 53.7% and temperature of 25°C according to Kamei.

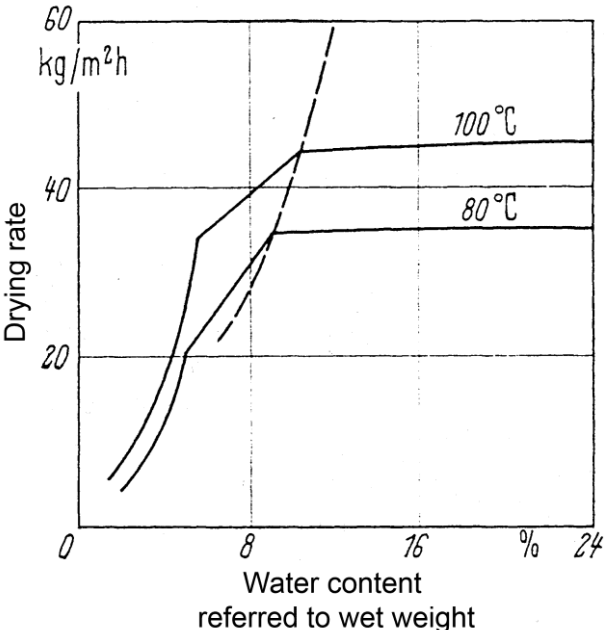


Fig. 5.1.6: Drying velocity of granulates used for floor-ware tile compounds according to Schrader.

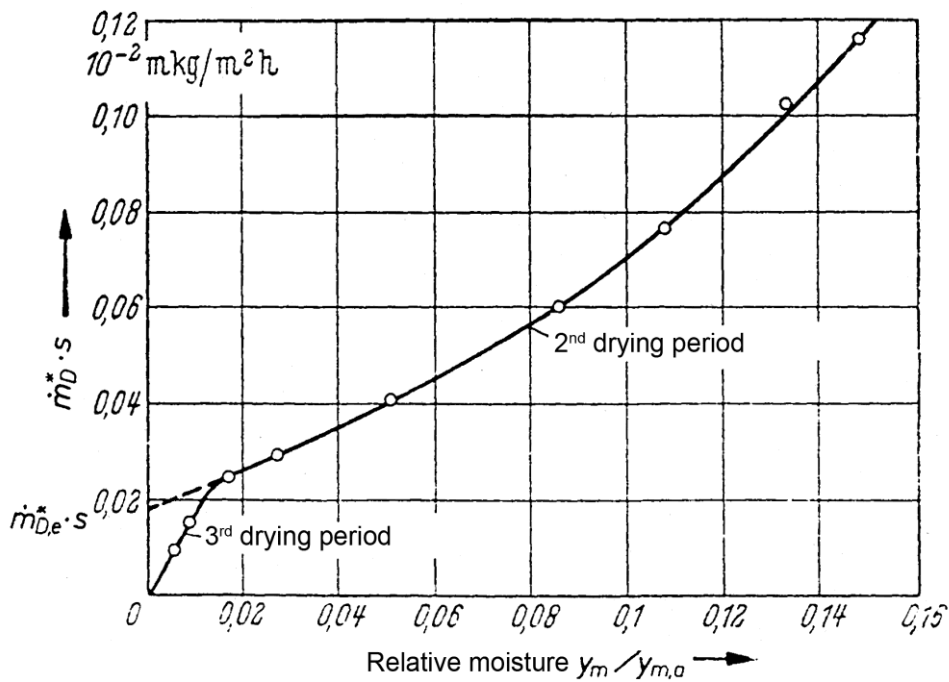
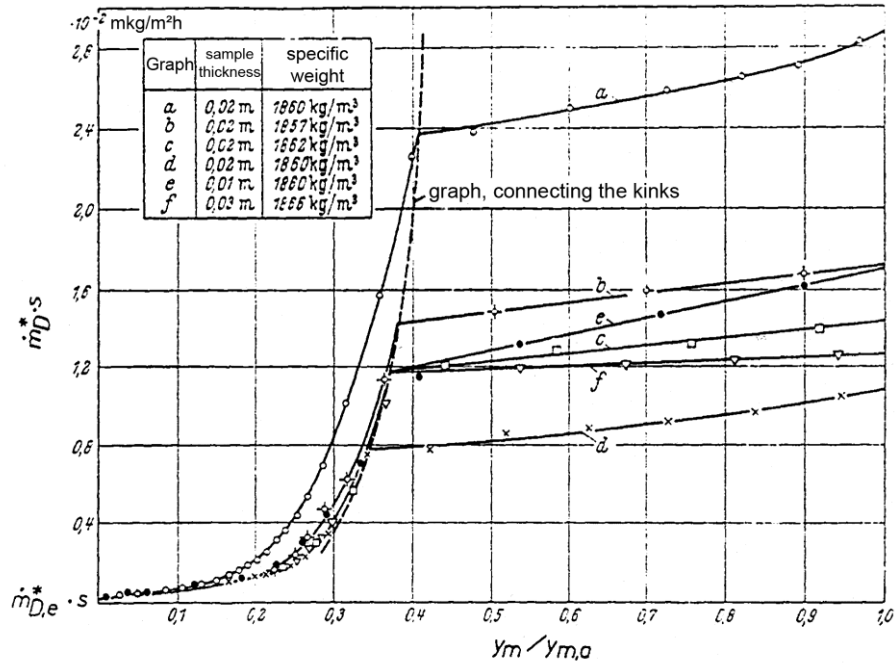


Fig. 5.1.7: Drying curves of different samples of brick tiles according to Schmidt.

Several drying plants will be presented in the following. When the drying process begins the relative moisture is high. As the drying process proceeds and water starts to get trapped into the pores, temperature is increased and humidity reduced (Fig. 5.1.8). These complex correlations are discussed in detail in other lectures and shall not be further explained in this one.

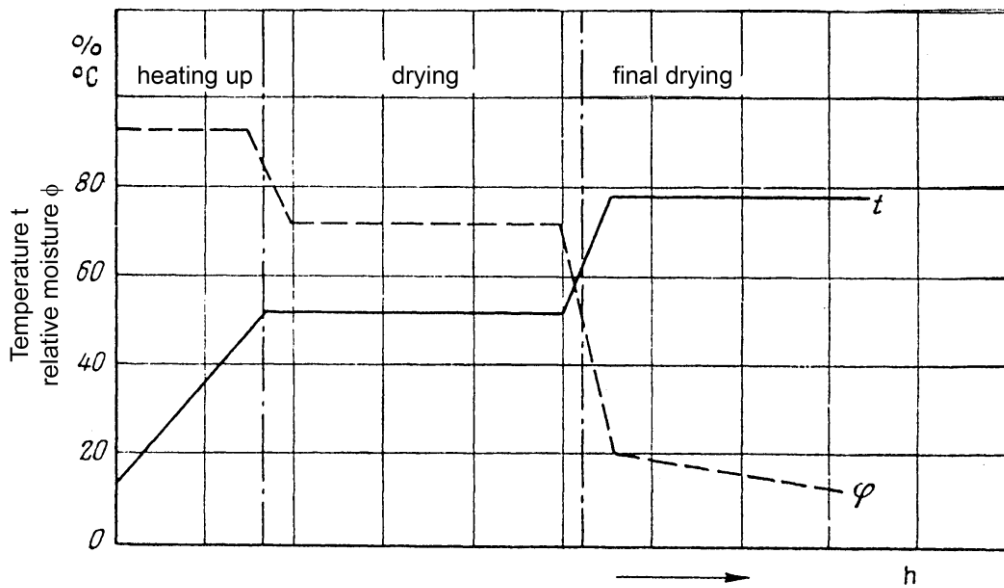


Fig. 5.1.8: Variation of the air humidity and temperature in a drying chamber according to Krause.

Transitions in a real furnace aggregate are more sliding (Fig. 5.1.9). In a progressive tunnel dryer, the ware is brought in from the right side. Temperature is relatively low at the beginning while humidity is high. In the course through the furnace, temperature increases and humidity decreases. Therefore, an almost constant drying speed can be adjusted for the complete drying process.

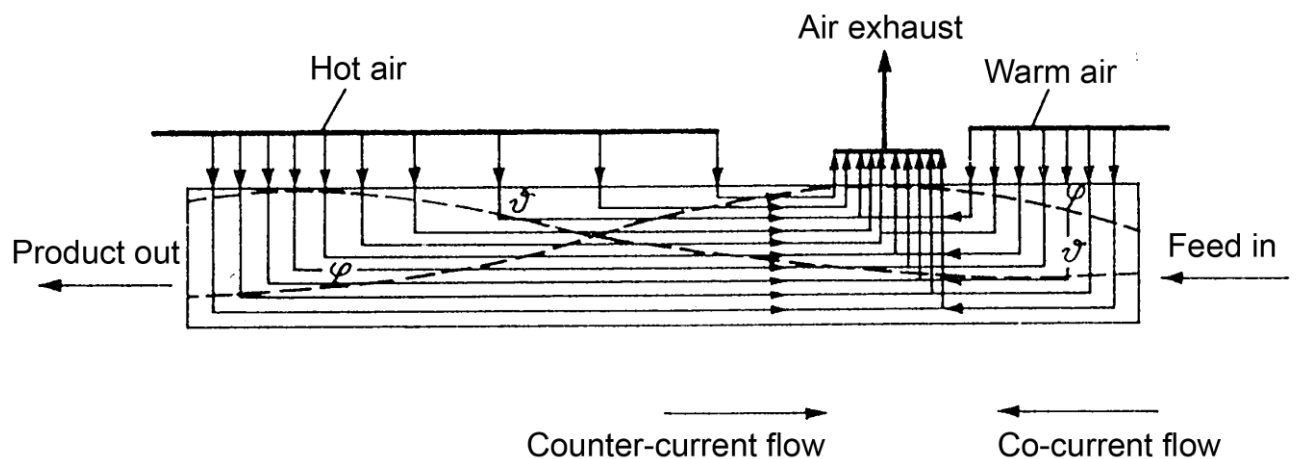


Fig. 5.1.9: Combined contra and parallel air current in a tunnel dryer according to Krause.

Porcelain articles are sometimes dried together with the plaster form used for shaping. Plates, cups or bowls still lying on their plaster forms are, for example, directly blown on and dried at the same time (Fig. 5.1.10).

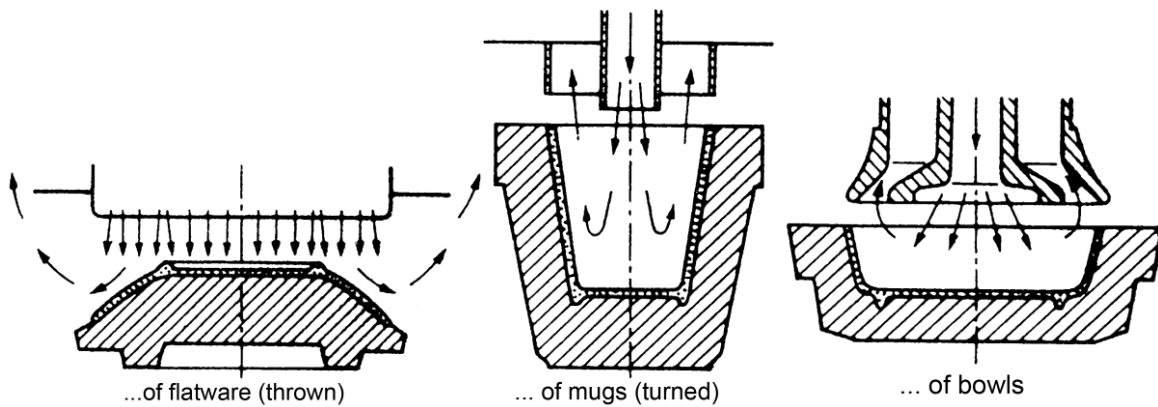


Fig. 5.1.10: Principle of the blowing dryer.

Bricks are dried in big chamber dryers by blowing the air directly between the bricks (Fig. 5.1.11). Chamber dryers are discontinuous aggregates.

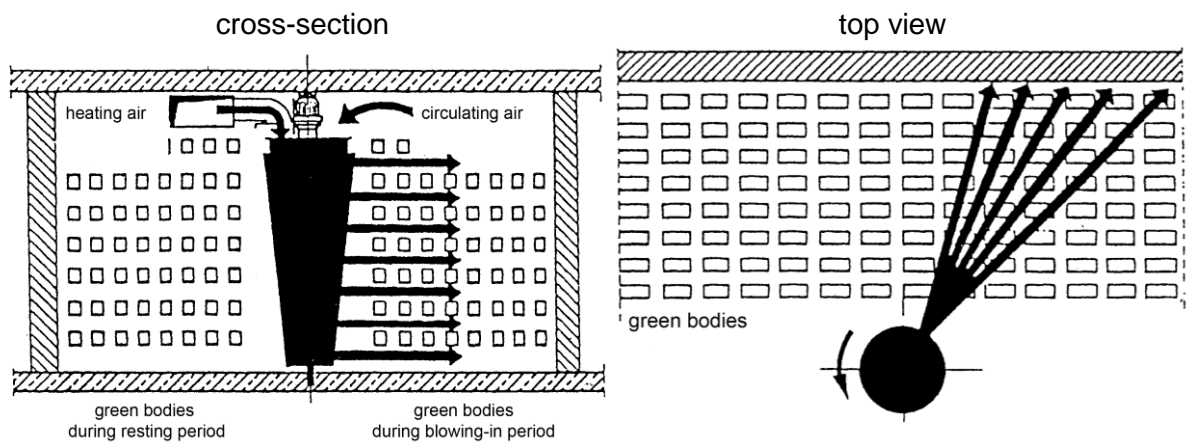


Fig. 5.1.11: Rotomixair (according to Thoma).

A roller dryer (Fig. 5.1.12) can perform the drying continuously. In a flat chamber, the temperature across the whole channel can be maintained constant. For example, tiles are transported on the rollers without firing support. This drying process is particularly qualified for mass production.

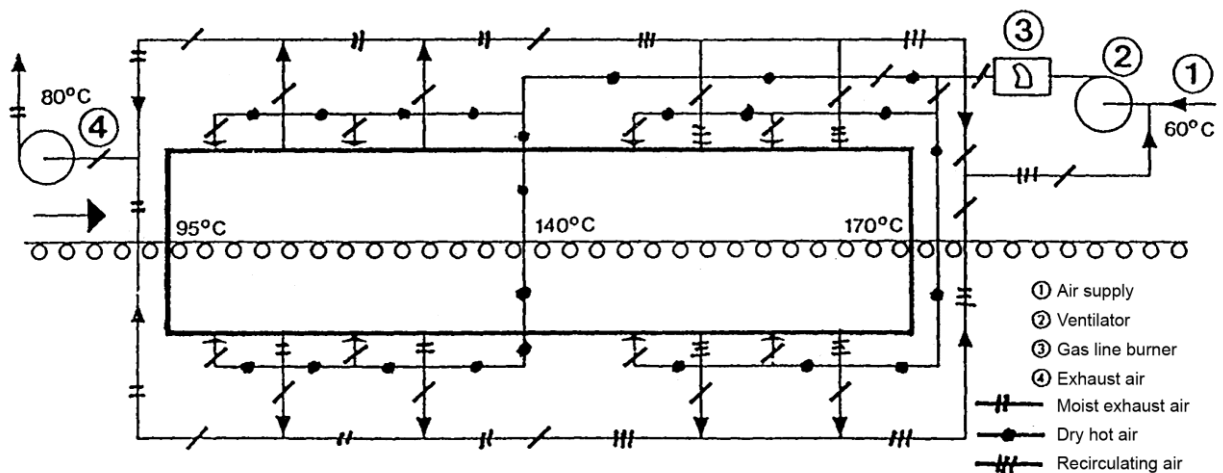


Fig. 5.1.12: Roller dryer (Heimsoth).

## 5.2 Sintering

Drying is followed by a further thermal treatment, considerably below melting point of the ceramics, the so-called sintering. Sintering promotes consolidation combined with further shrinkage. Now the ceramic products get their typical structure and their characteristics.

### 5.2.1 Sintering of porcelain, silicate and oxide ceramics

Porcelain is made from the natural raw materials kaolin, feldspar and quartz (50:25:25 weight-%). Before chemical reactions between these raw materials take place, some physical and chemically bonded water is dehydrated (Fig. 5.2.1). Furthermore, some phase transformation can happen, which is in most of the cases related to volume changes. This may cause stresses during cooling and, if the temperature is inappropriately adjusted, lead to cracks in the components.

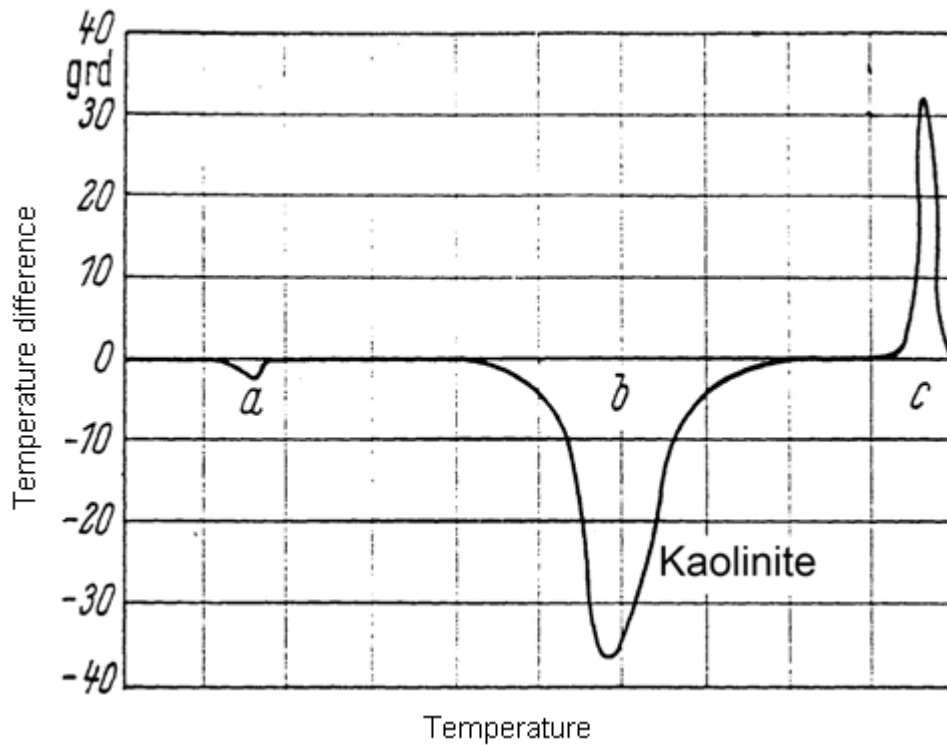


Fig. 5.2.1.1: DTA analysis of a kaolin [1].

When quartz is used as raw material, at 573°C there is the low to high quartz temperature modification. This is combined with a volume expansion. At 870°C the formation of tridymite which at 1470°C is transformed into cristobalite. Both transformations are combined with volume changes. Tridymite can be transformed during cooling into its low temperature modification, as well as cristobalite (Fig. 5.2.1.2). To avoid stresses or crack formation, threshold times are adjusted in the T-t program during cooling.

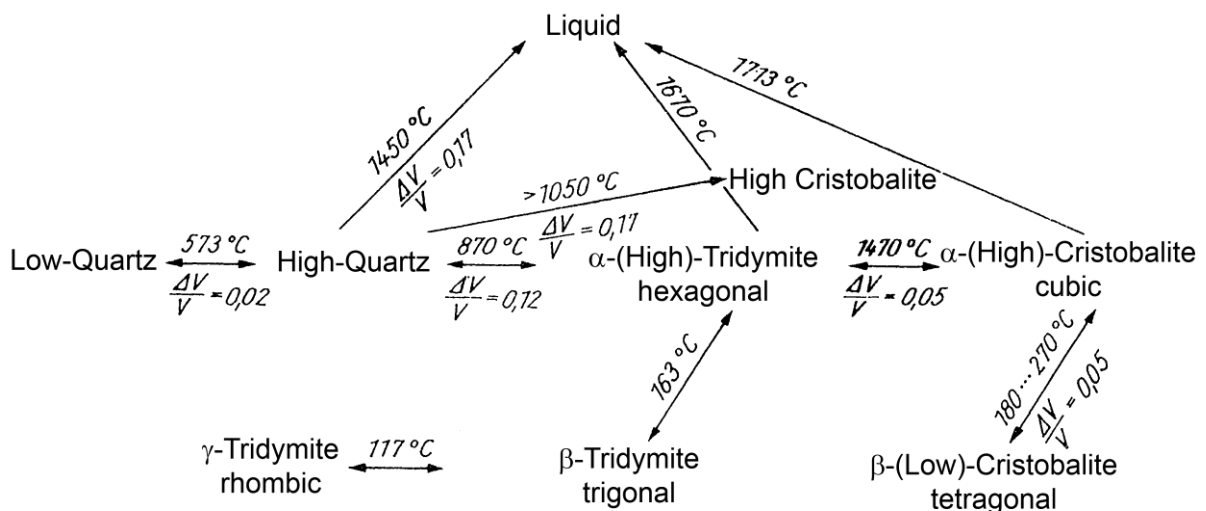
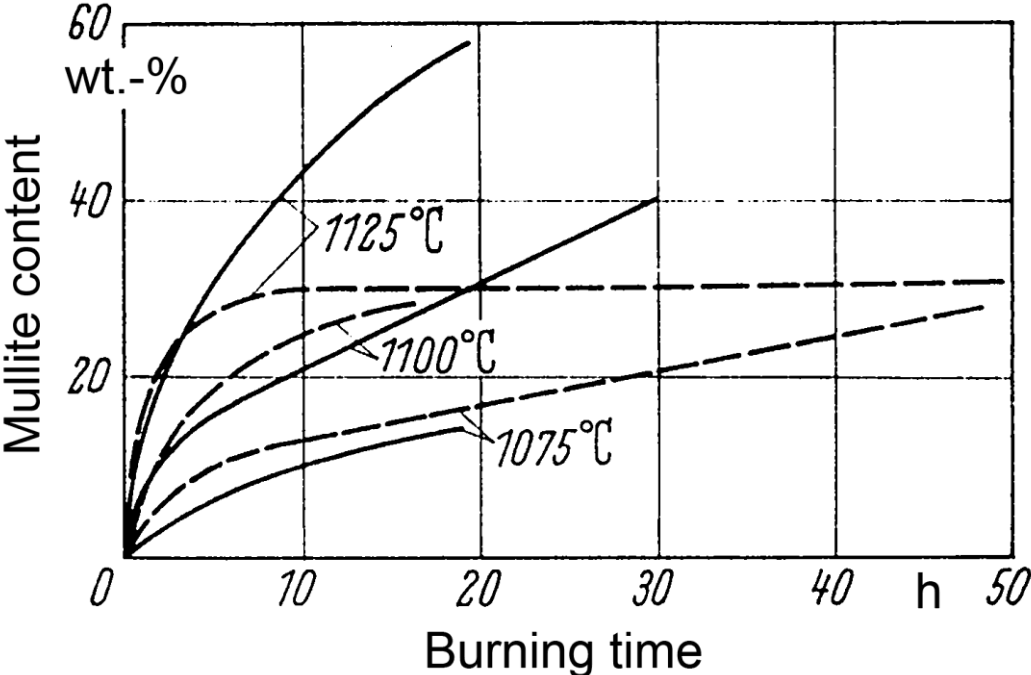


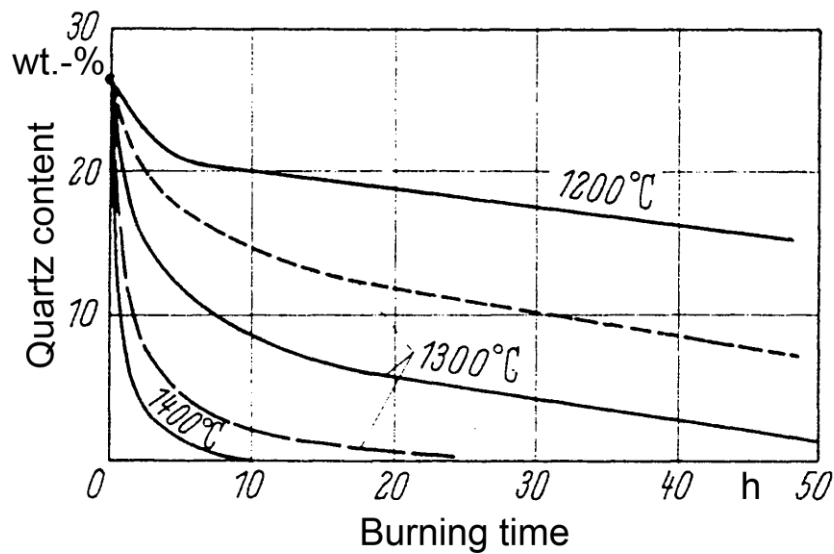
Fig. 5.2.1.2: Phase transformation diagram in the SiO<sub>2</sub>-system with the temperature.

Crystal transformations and also chemical reactions may occur during the sintering of porcelain. After the water dehydration, kaolin reacts with quartz to build mullite. The mullite content grows as the temperature increases (Fig. 5.2.1.3). Part of the quartz disperses in the melted feldspar, therefore the quartz content of the structure decreases as the temperature is increased (Fig. 5.2.1.4). Depending on the sintering temperature, different contents of feldspar, quartz, mullite and rest glass phase can be found in the structure of porcelain (Fig. 5.2.1.5).



———— kaolin  
 - - - - - kaolin-feldspar mixture (2:1 in weight)

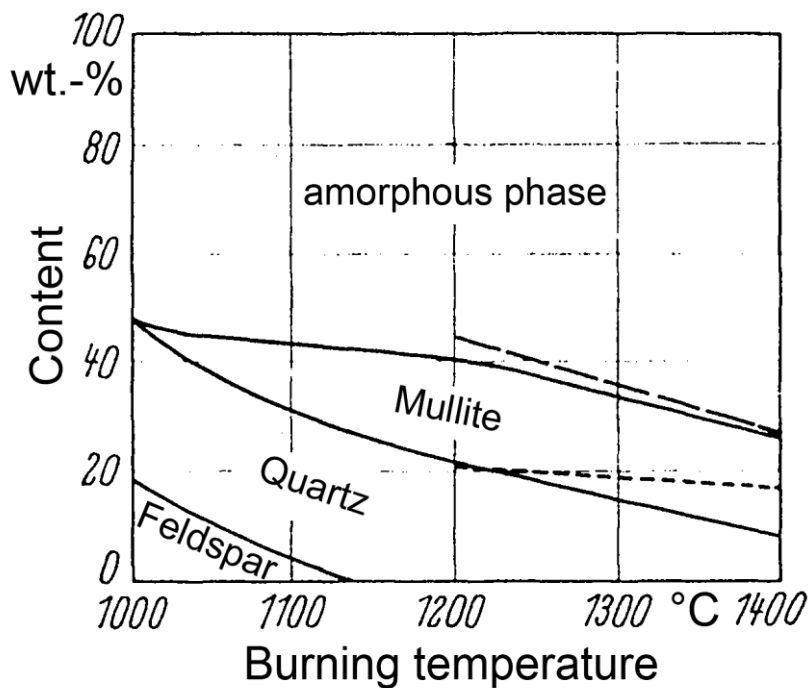
Fig. 5.2.1.3: Dependence of the final mullite content in different kaolin mixtures on the time and temperature of sintering [1].



Medium quartz grain size:

- 13,2 μm
- 6,42 μm
- 27,5 μm

Fig. 5.2.1.4: Dependence of the final quartz solubility in different mixtures on the time and temperature of sintering [1] (Kaolin: Feldspar : Quartz ratio = 50 : 25 : 25).



- measured
- calculated
- calculated

Fig. 5.2.1.5: Phase composition of a porcelain after sintering at different temperatures (Kaolin:Feldspar:Quartz ratio = 40:30:30 wt.%) [1].



Porcelain is sintered normally at about 900°C – 1400°C in gas-heated furnaces with reducing atmosphere, but also with CO excess. The reason is simple: natural raw materials contain certain portions of iron oxide. When  $\text{Fe}_2\text{O}_3$  is sintered at oxidizing atmospheres and at high temperatures,  $\text{Fe}_3\text{O}_4$  is built. Contrary to  $\text{Fe}_2\text{O}_3$  which appears white, greenish or blue,  $\text{Fe}_3\text{O}_4$  leaves brown or black spots. Therefore, at temperatures over 900°C a carbon monoxide atmosphere is adjusted to avoid iron transformation (Fig. 5.2.1.6). If, by mistake, there is CO excess already at temperatures slightly below 900°C, carbon monoxide according to the Boudouard equilibrium transforms to  $\text{CO}_2$  and carbonate (Fig. 5.2.1.7). This has to be avoided, since carbonate also produces black spots in the porcelain. The same may happen if silicon monoxide appears. It can develop if firing supports made of  $\text{SiO}_2$  are used.  $\text{SiO}$  can react to  $\text{SiO}_2$  and Si, developing black spots, too.

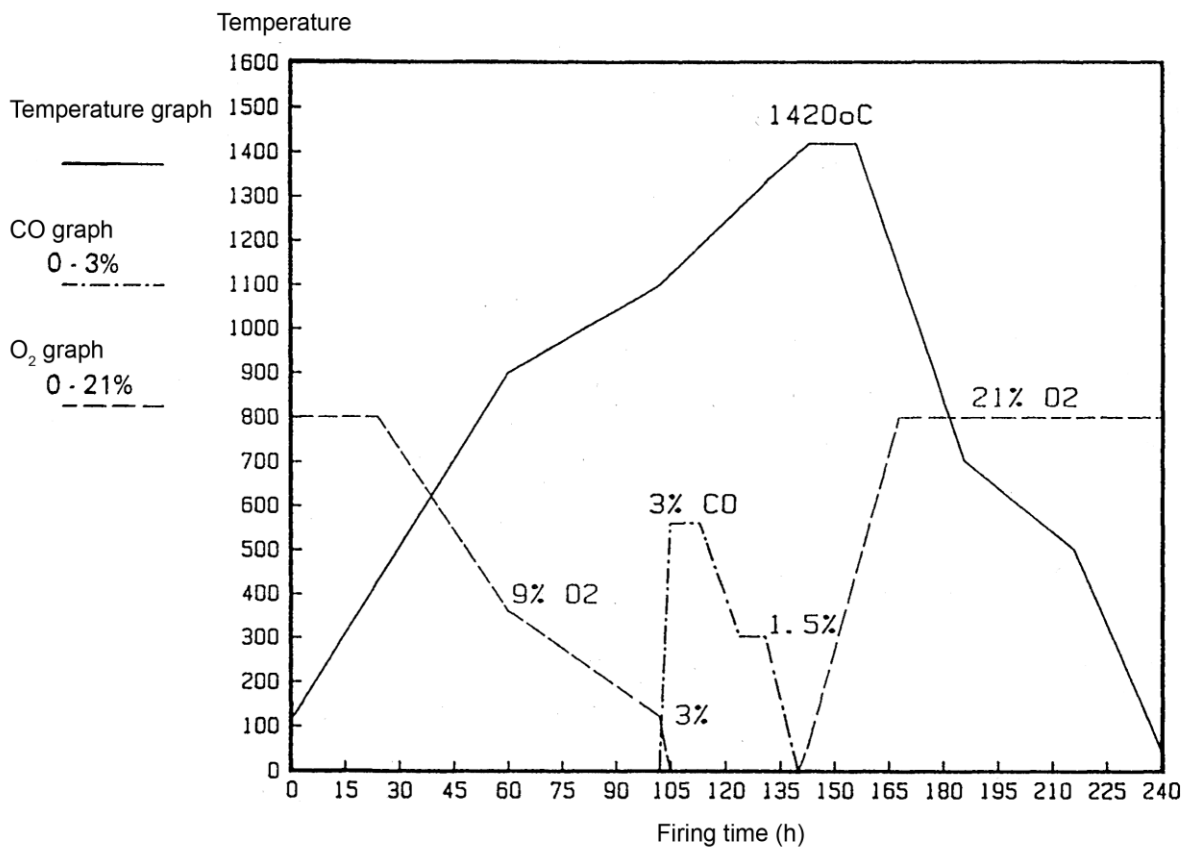


Fig. 5.2.1.6: Glost firing of porcelain.

Boudouard equilibrium  $\text{CO}_2 + \text{C} \leftrightarrow 2 \text{CO}$

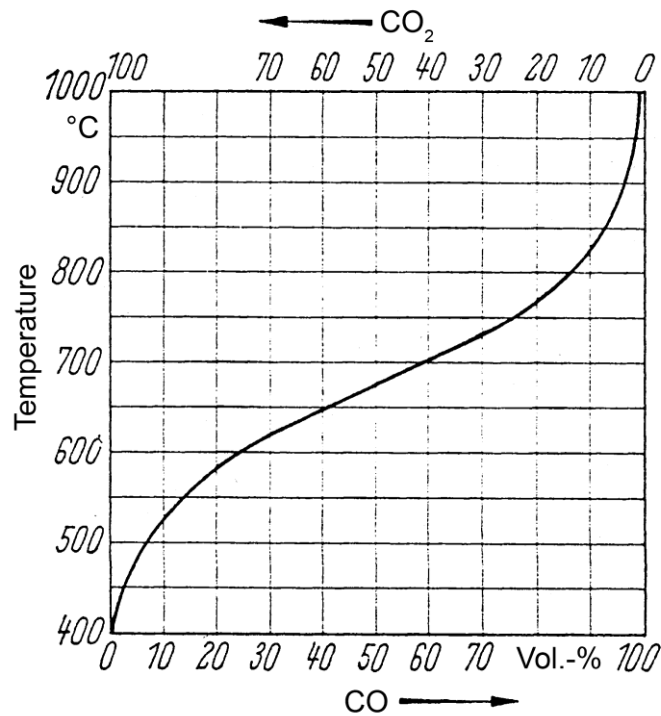
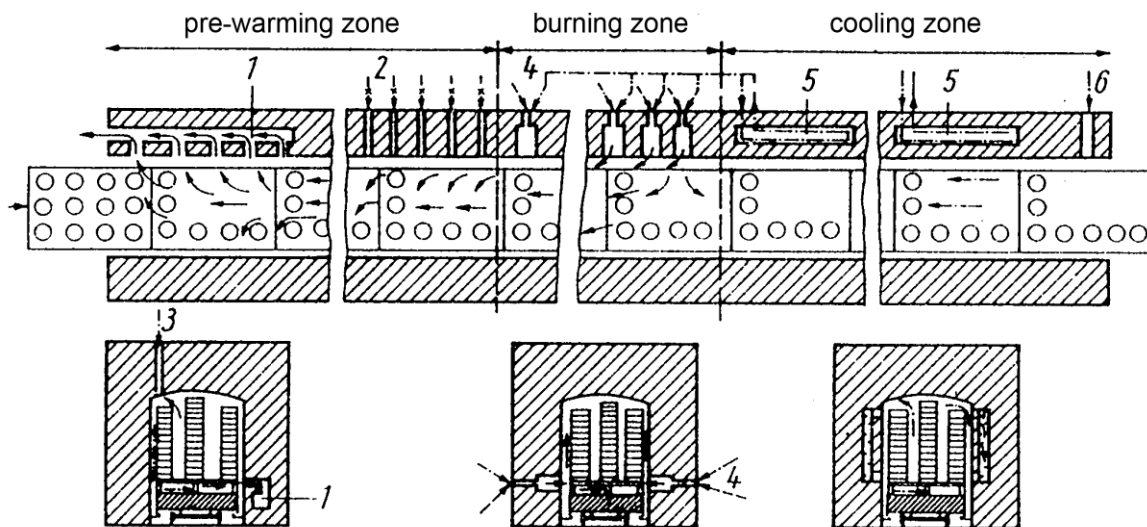


Fig. 5.2.1.7: Temperature dependence at the Boudouard equilibrium.

Porcelain is continuously fired in tunnel kilns (Fig. 5.2.1.8 and Fig. 5.2.1.9) or discontinuously in bogie hearth kilns (Fig. 5.2.1.10). In a tunnel kiln the ware is continuously shifted through preheating zone, firing zone and cooling down zone. This furnace aggregate is particularly qualified for mass production. Today, burning time in modern firing aggregates is below 10 hours (Fig. 5.2.1.11).



1 exhaust linear, 2 burner, 3 injector, 4 main burner, 5 recuperator, 6 air duct

Fig. 5.2.1.8: Illustration of a tunnel kiln with preheating, sintering and cooling zones.



Fig. 5.2.1.9: Kiln aggregate in a sanitary ceramic industry. Tunnel aggregate with long sintering times.



Fig. 5.2.1.10: Kiln aggregate in a sanitary ceramic industry. Bogie hearth kilns with shortened sintering times.

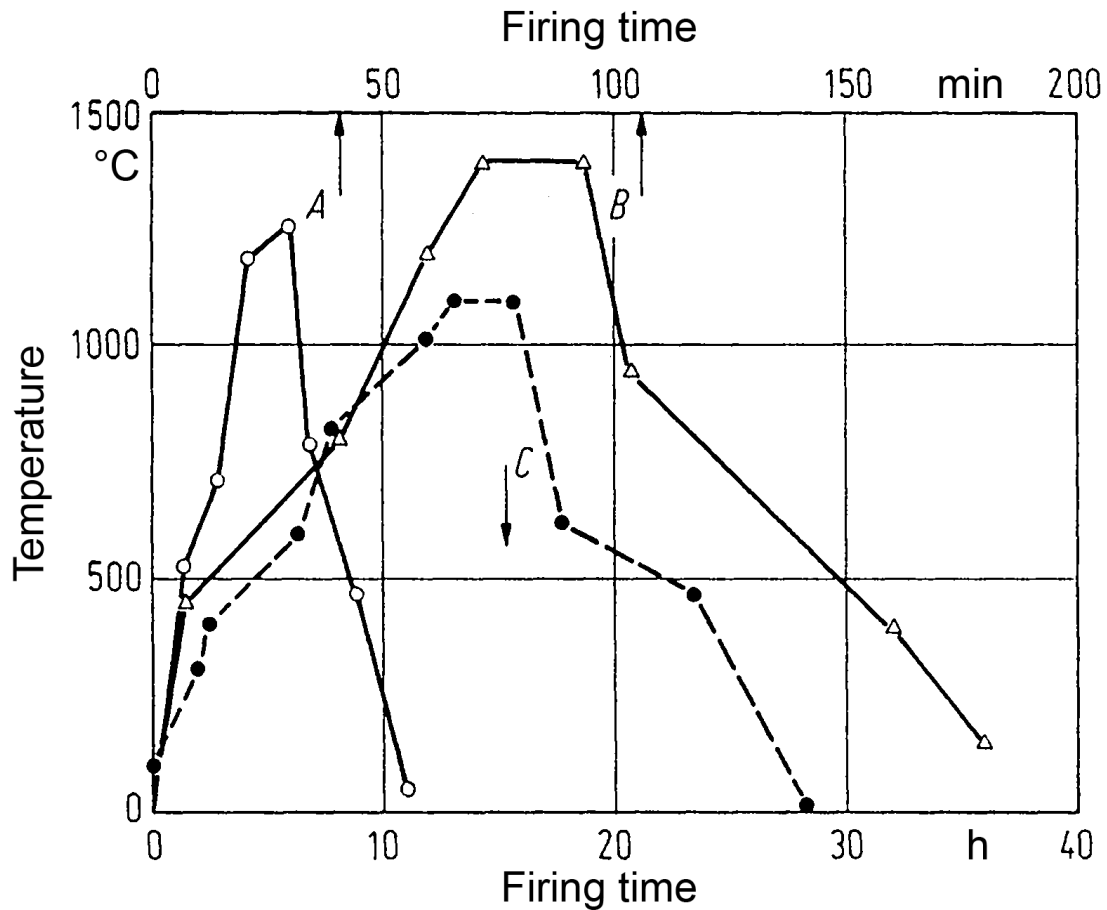


Fig. 5.2.1.11: Optimized sintering program for porcelain (A) and (B) bricks (C) according to Mörtel (A), Holmström (B) and Schmidt (C),

Due of the high number of influencing factors, the control of the temperature with thermal elements or pyrometers is supported by observation of Seger cones. Seger cones soften according to their chemical composition at different temperatures (Fig. 5.2.1.12). Contrary to thermal elements and pyrometers, Seger cones also consider the influences of the gas atmosphere and time. By now, it represents a reasonable completion for temperature measurement.

Average bending temperatures of Cones (°C)

Heating rate grad/h	Seger Cone				Orton Cone			
	large		small		20	100	150	600
	20	150	20	150				
No.	20	150	20	150	20	100	150	600
06a <sup>1</sup>	970	990	980	995	1005		1015	
05a	990	1000	1010	1010	1030		1040	
04a	1015	1025	1035	1055	1050		1060	
03a	1040	1055	1055	1070	1080		1115	
02a	1070	1085	1090	1100	1095		1125	
01a	1090	1105	1105	1125	1110		1145	
1a	1105	1125	1120	1145	1125		1160	
2a	1125	1150	1135	1165	1135		1165	
3a	1140	1170	1150	1185	1145		1170	
4a	1160	1195	1170	1220	1165		1190	
5a	1175	1215	1185	1230	1180		1205	
6a	1195	1240	1210	1260	1190		1240	
7	1215	1260	1230	1270	1210		1250	
8	1240	1280	1255	1295	1225		1260	
9	1255	1300	1270	1315	1250		1285	
10	1280	1320	1290	1330	1260		1305	
11	1300	1340	1315	1350	1285		1325	
12	1330	1360	1340	1375	1310		1335	
13	1360	1380	1375	1395	1350		1350	
14	1380	1400	1395	1410	1390		1400	
15	1400	1425	1420	1440	1410		1435	
16	1425	1445	1445	1470	1450		1465	
17	1445	1480	1465	1490	1465		1475	
18	1470	1500	1480	1520	1485		1490	
19	1495	1515	1505	1530	1515		1520	
20	1515	1530	1530	1540	1520		1530	
23		1540		1560		1580		
26		1560		1585		1595		
27		1595		1605		1605		
28		1605		1635		1615		
29		1635		1655		1640		
30		1655		1680		1650		
31		1680		1695		1680		
32		1695		1710		1700		
33		1710		1730		1745		
34		1725		1755		1760		
35		1765		1780		1785		
36		1790		1805		1810		
37		1815		1830		1820		
38		1840		1855		1835		
39				1875				1865
40				1900				1885
41				1940				1970
42				1980				2015



<sup>1</sup> The letter 'a' (0,6 to 6) is not being used for Orton Cones

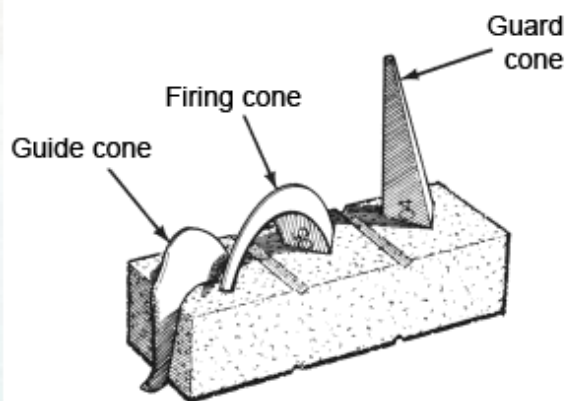


Fig. 5.2.1.12: Average softening temperature of Seger cones (in °C).



Videoclip: Roller furnace

In the roller kiln, the charge is transported on rollers through this continuous furnace. The gas feed lines supply gas to the burners. The reducing gas atmosphere is adjusted with these burners. With this adjustment you may realize that more firing ware is heated than can be sold. Therefore the energy input is very high. The rollers are made from recrystallized silicon carbide and continuously transport the ware through the furnace. As already mentioned, it is qualified for mass ware to be transported through the kilns in big quantities and, if possible, with always the same geometries. If different masses are processed which need various T-t curves, flexible bogie hearth kilns are frequently used to sinter the ware.



*Videoclip: Bogie hearth kiln*



*Videoclip: Elevator kiln*

Here at the Riedhammer technical center we see a bogie hearth kiln in a small scale and in an elevator kiln.

Oxide ceramic catalyst carriers are sintered for the automobile industry. The relatively complicated gas feeder system also allows for adjustment of different gas atmospheres. The next chart shows an electrically heated elevator kiln for ferrite sintering.

### 5.2.2 Sintering of non-oxide ceramics

To avoid oxidation, non-oxide ceramic materials have to be heat treated in vacuum or in inert gas atmosphere. Fig. 5.2.2.1 shows one example of infiltration of SiC with liquid Si at 1600°C. Silicon carbide powder is first mixed with carbonate and a carbon-containing binder. This mixture is homogenized and then shaped with different techniques. After debinding, the porous pre-product is infiltrated in vacuum with liquid silicon. The inert gas furnace is equipped with graphite heating elements and graphite isolation. The components are set on boards equipped with silicon powder. Silicon is sucked through the pores above the Si melting point, because the wetting behaviour for SiC by silicon is very good. Carbon reacts with liquid silicon to secondary SiC and we get a product consisting of 80% SiC and 20% silicon.

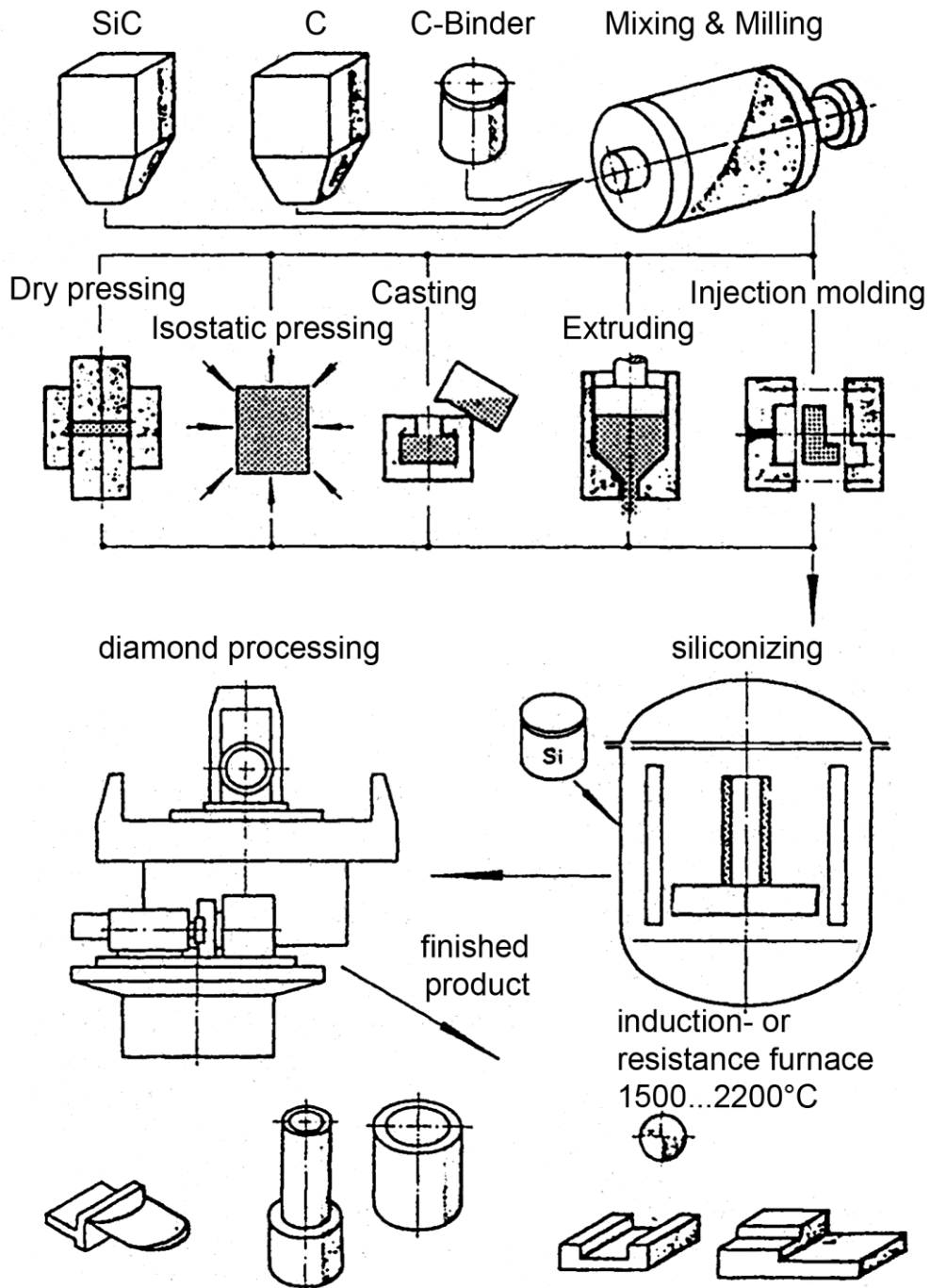


Fig. 5.2.2.1: Process route for infiltrated Si-SiC according to Gugel.



Videoclip: Silicon infiltration  
Break discs from Porsche (SGL)

### 5.2.3 Pressure sintering

Silicon nitride is often sintered at higher nitrogen pressure. The higher the nitrogen pressure, the higher the decomposition temperature and the higher the sintering temperature must be reached in order to increase diffusion activities. In this case, sintering is carried out in pressure sintering ovens (Fig. 5.2.3.1). The gas in the furnace chamber is increased by compressors to pressures up to 200 MPa, allowing that the temperature can be increased from 1800°C to 2100°C.



Fig. 5.2.3.1: Pressure sintering oven.



### 5.2.4 Microwave sintering

During conventional sintering in electrically or gas heated furnaces, ceramic components are slowly heated from the outer region to the interior. In large components, the sintering process sometimes have been already initiated at the surface, while in the middle parts nothing has happened. This leads to stresses up to crack formation. Conditions during microwave sintering are completely different (fig. 5.2.4.1). There is no heating in materials which are transparent for microwaves. If the material is opaque and the microwave cannot enter, the material is also not heated. However, the material gets heated, if microwaves are absorbed and the electrons are stimulated and brought to oscillation. Heating is carried out evenly throughout the complete cross-section of the component.

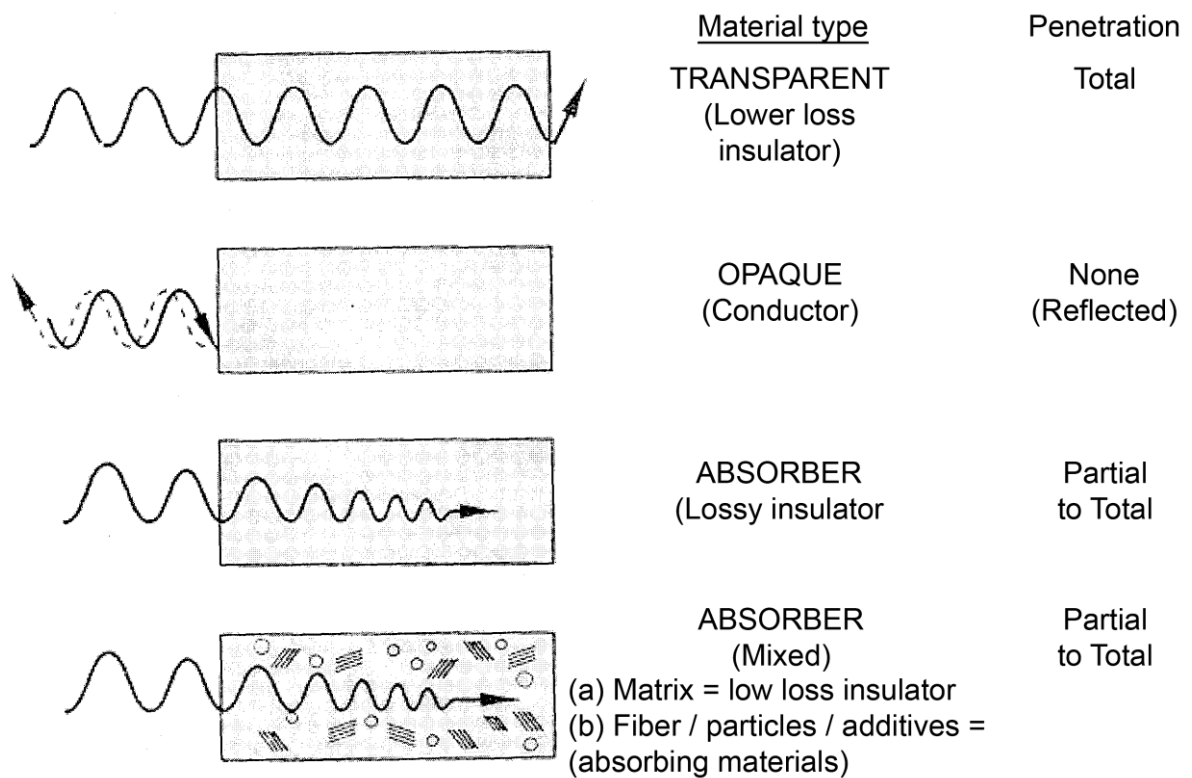


Fig. 5.2.4.1: Interaction of the microwave with different materials [8].

Fig. 5.2.4.2 shows schematically the difference between conventional and microwave heating.

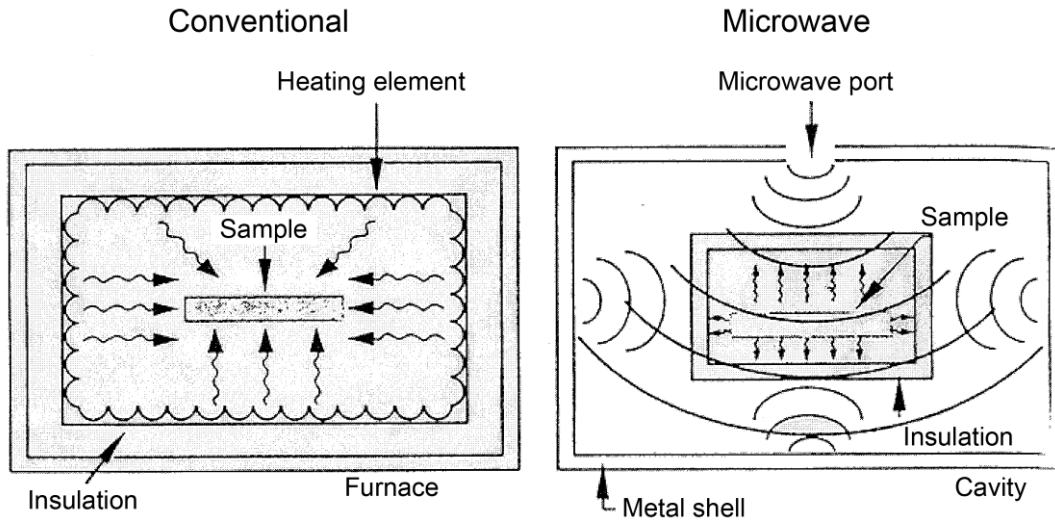


Fig. 5.2.4.2: Heating patterns in conventional and microwaves furnaces [8].

Consistent application of energy produced by stimulation of the electrons is followed by significant increase of the sintering speed at the same temperature (Fig. 5.2.4.3). Therefore, by microwave sintering, densification of a material at constant temperature can be reached considerably faster as by conventional sintering (Fig. 5.2.4.4).

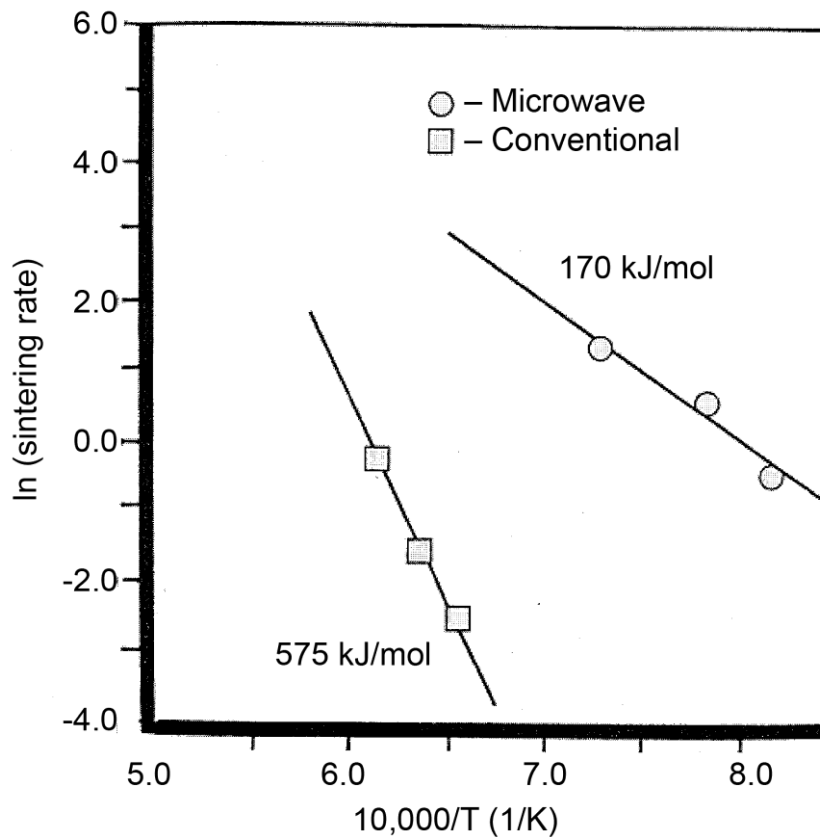


Fig. 5.2.4.3: Apparent activation energy for  $\text{Al}_2\text{O}_3$  sintered by microwave and conventional processes [9].

Despite these advantages, microwave sintering, for economic reasons, could not be established for large-scale production yet. However, microwave drying is state of the technology for mass productions like the porcelain industry.

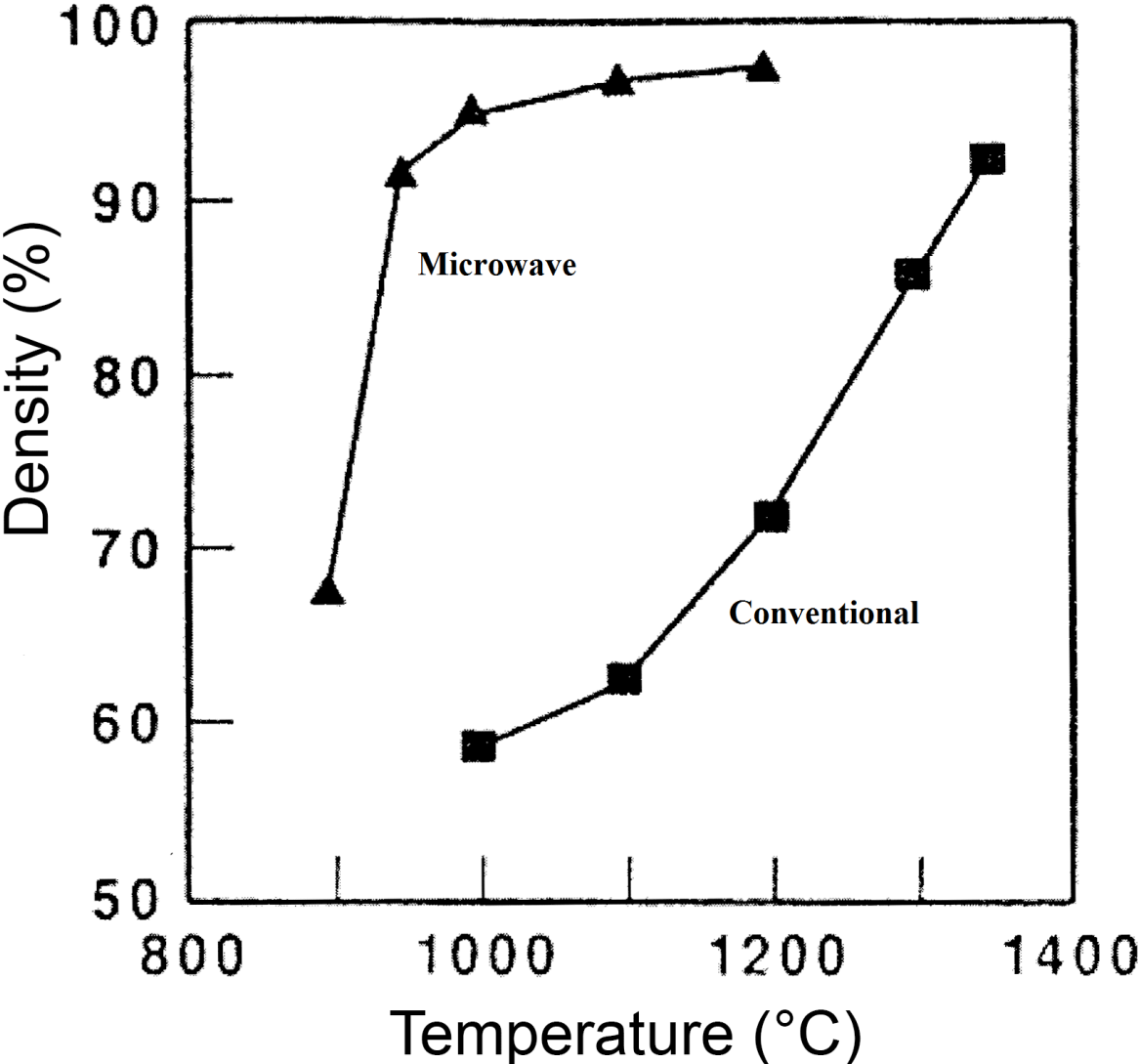


Fig. 5.2.4.4: Density versus temperature of microwave (28 GHz) and conventionally sintered  $Al_2O_3$  [9].

## **6. Finishing and post processing**

### **6.1 Glazing**

Unglazed porcelain surfaces are relatively mat and rough which, for example, is very unpleasant at drinking. Therefore, porcelain is glazed to seal the surface. After glazing the articles are often decorated and color prints are applied on the surface.

During glazing, the articles, first fired at 900°C (biscuit firing), are dipped in a glass powder suspension. The glaze can be applied either by immersion or by spraying. For small amounts of parts, glazing is performed manually (Fig. 6.1.1), while for large amounts automatically (Fig. 6.1.2). After drying, sintering occurs at about 1450°C to consolidate and seal the surface.

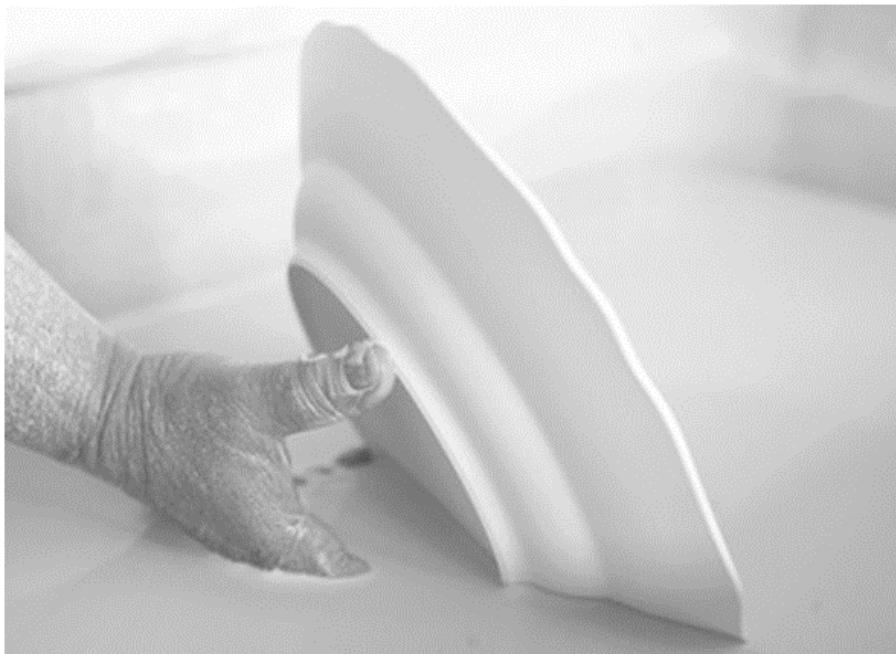


**Fig. 6.1.1:** Manual glazing by immersion of the porcelain in a glazing tank.

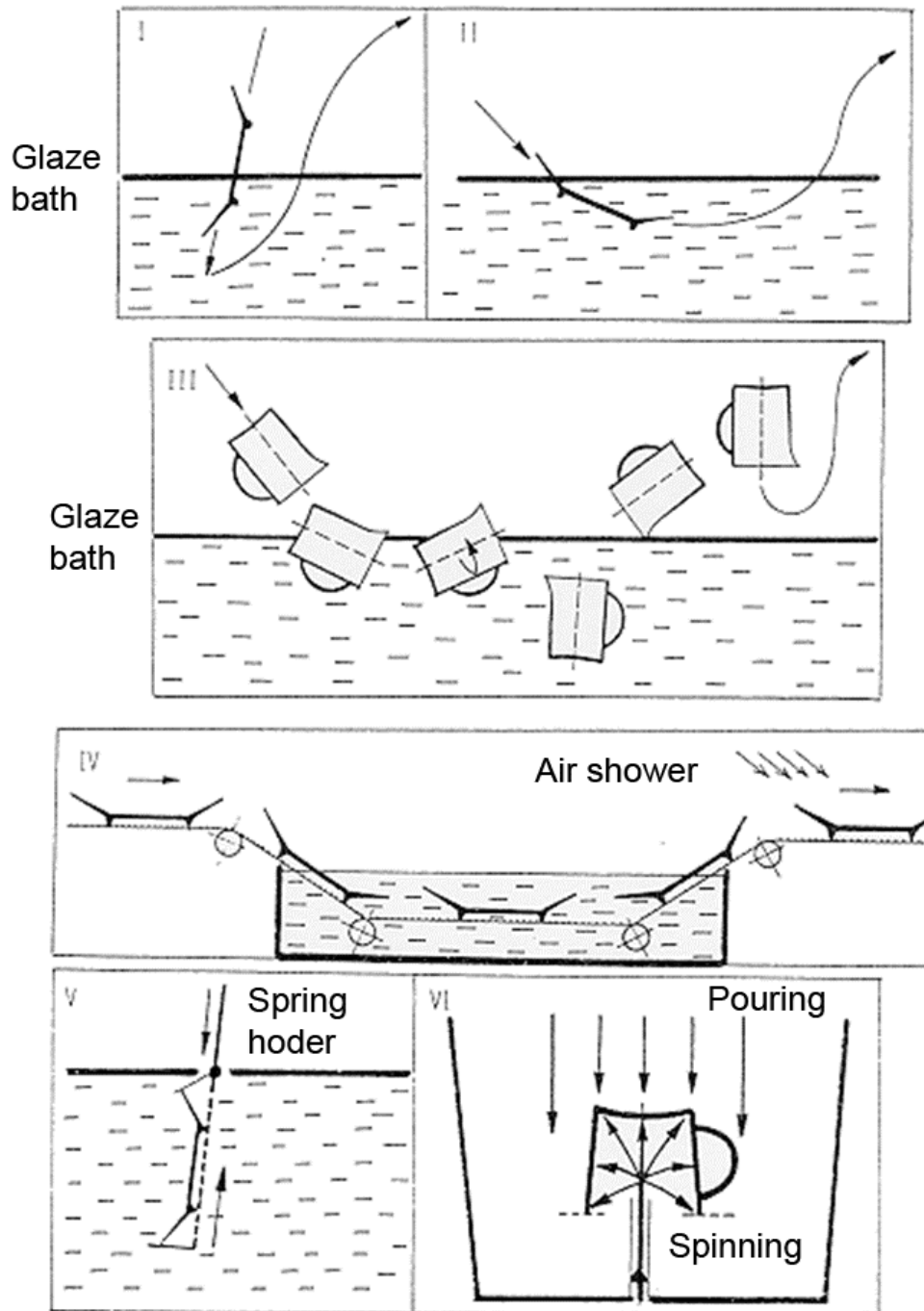


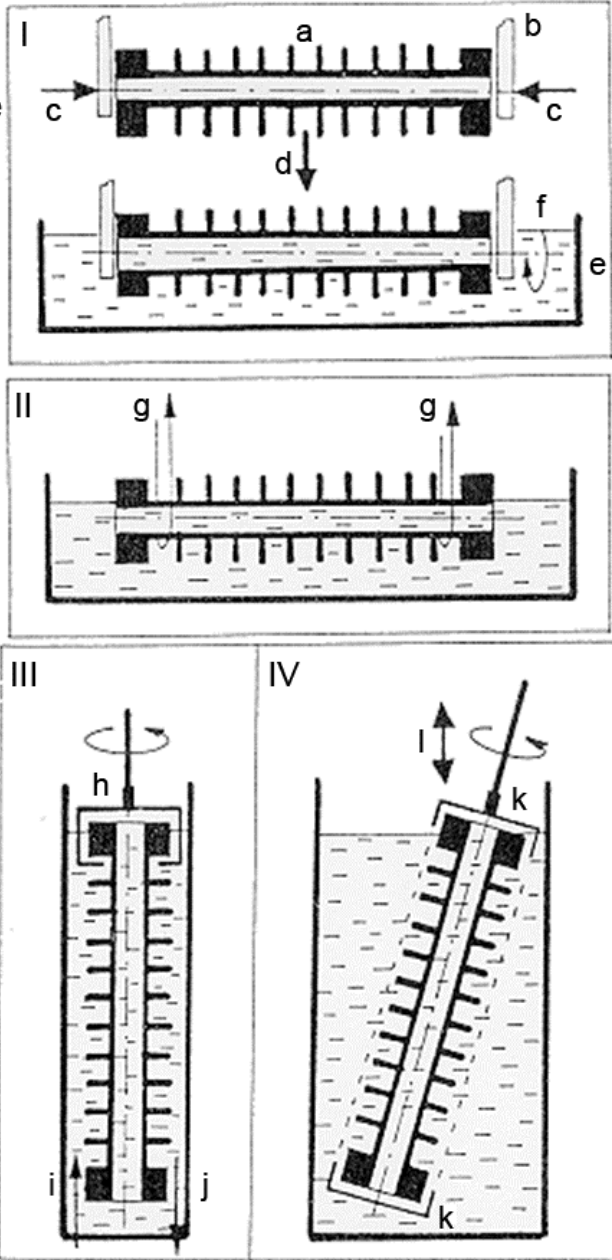
Fig. 6.1.2: Glazing process for dishes (schematic).



Videoclip: Glazing

Large-sized components, like for example high-voltage insulators or stoneware pipes, are turned in big glaze tubs, attached to carrier belts (Fig. 6.1.3), or dipped (Fig. 6.1.4) and then sintered. In case the parts are very complicated, spray robots are used to apply the glaze (Fig. 6.1.5).

- a = Insulator
- b = Chucks
- c = Compressive force
- d = Lowering device
- e = Glaze bath
- f = Rotating device
- g = Rope loops



- h = Holding device
- i = Flooding with
- j = glaze
- k = Outlet of glaze
- Chucks
- l = Immersing- / Lift-
- ing device

Fig. 6.1.3: Glazing procedure for insulators (schematic).

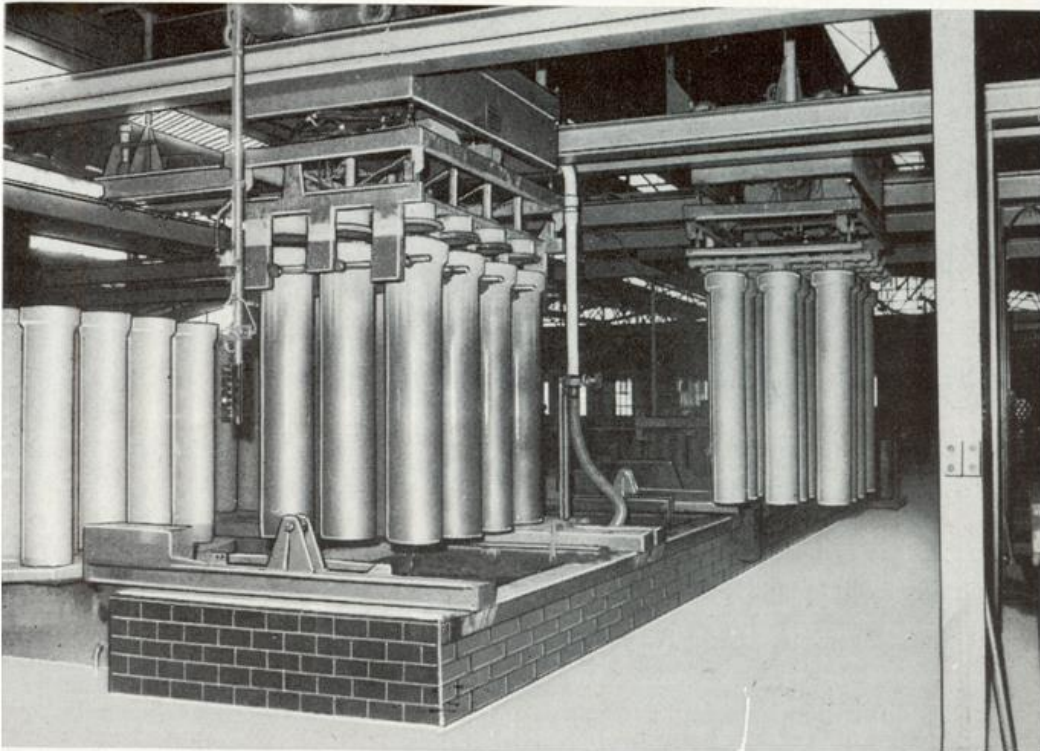


Fig. 6.1.4: Automatic immersion glazing tank for pipelines.

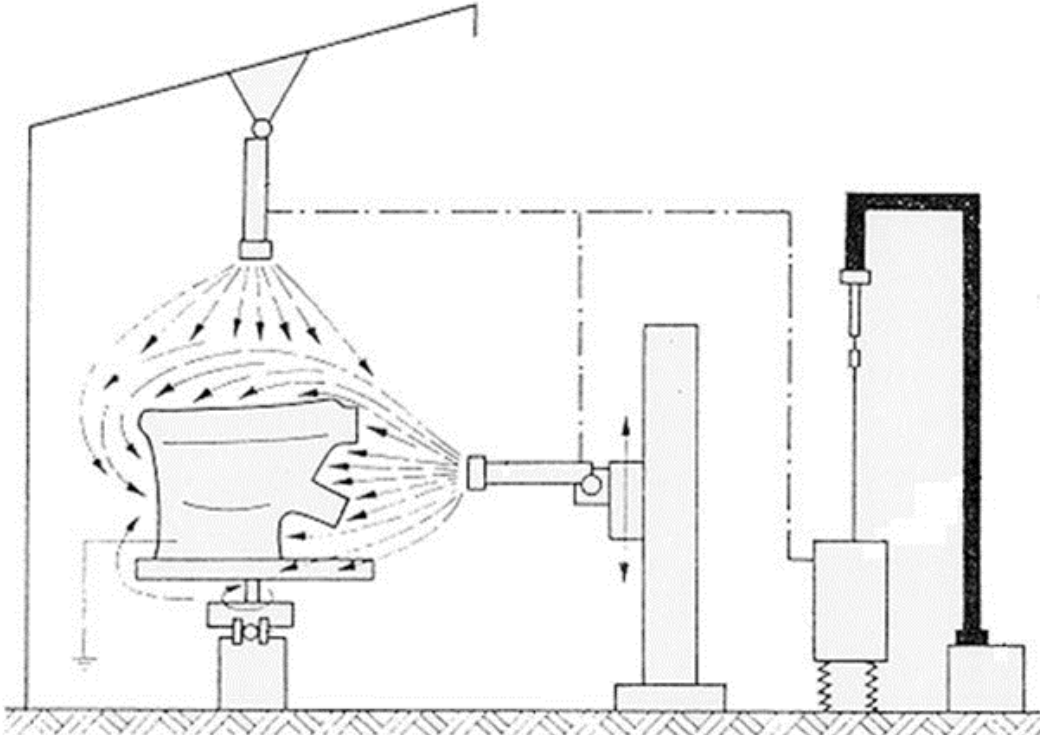


Fig. 6.1.5: Illustration of a spray robot (schematic).

Melting temperatures and coefficients of expansion are adjusted between the clay bodies and the glaze by varying the chemical composition (Fig. 6.1.6). Details referring to the formation of glass by network formers and modifiers are discussed in lecture “Principles of Glass”.

950 °C e.g. for earthen ware	}	0.3 Al <sub>2</sub> O <sub>3</sub>	}	2.1 SiO <sub>2</sub> 0.5 B <sub>2</sub> O <sub>3</sub>
0.2 K <sub>2</sub> O				
0.2 Na <sub>2</sub> O				
0.3 CaO				
0.3 PbO				
1200 °C e.g. for stone ware	}	0.4 Al <sub>2</sub> O <sub>3</sub>		3.5 SiO <sub>2</sub>
0.3 K <sub>2</sub> O				
0.1 MgO				
0.5 CaO				
0.1 ZnO				
and 1430 °C for hard porcelain	}	1.1 Al <sub>2</sub> O <sub>3</sub>		10.0 SiO <sub>2</sub>
0.2 K <sub>2</sub> O				
0.2 MgO				
0.6 CaO				

Fig. 6.1.6: Chemical composition of glazes presenting different melting temperatures [1].

If the coefficient of expansion of the glaze is too small (Fig. 6.1.7), the ceramic body shrinks more than the glaze during cooling. This may sometimes be the intention, since compression stress may occur in the glaze and glasses resist much better to compression stresses than to tensile stresses. If the stress becomes far too strong, parts of the surface may chip off.

The thermal extension coefficient of the glazing is too low

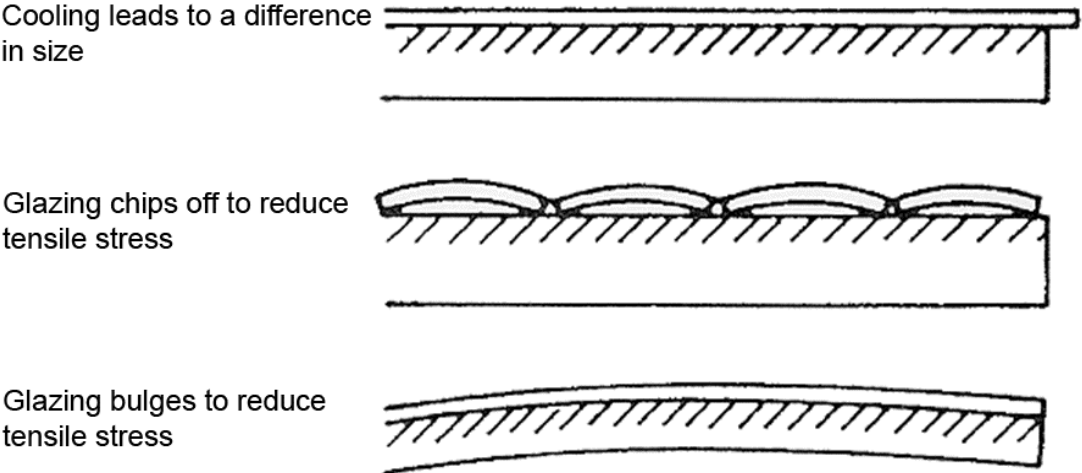


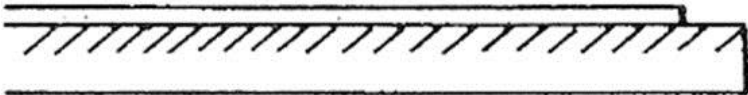
Fig. 6.1.7: Illustration of the coefficient of expansion from the glaze smaller than the one from the ceramic body (schematic).



In case the glaze's coefficient of expansion is too big, the glaze shrinks quicker than the clay body during cooling and crack formation may appear in the glaze coat (Fig. 6.1.8). Modification of the coefficient of expansion caused by crystal transformations in the ceramic body may suddenly lead to compression stress instead of the expected tensile stress, and vice versa (Fig. 6.1.9). Therefore, knowledge about temperature-dependent modifications in the structure is of significant importance for the evaluation of crack formations.

The thermal extension coefficient of the glazing is too high

Cooling leads to a difference in size



Glazing crazes to reduce tensile stress



Porcelain bulges to reduce tensile stress

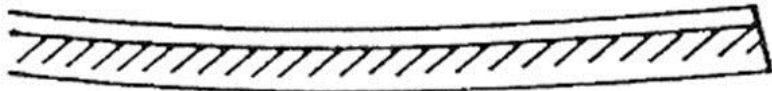
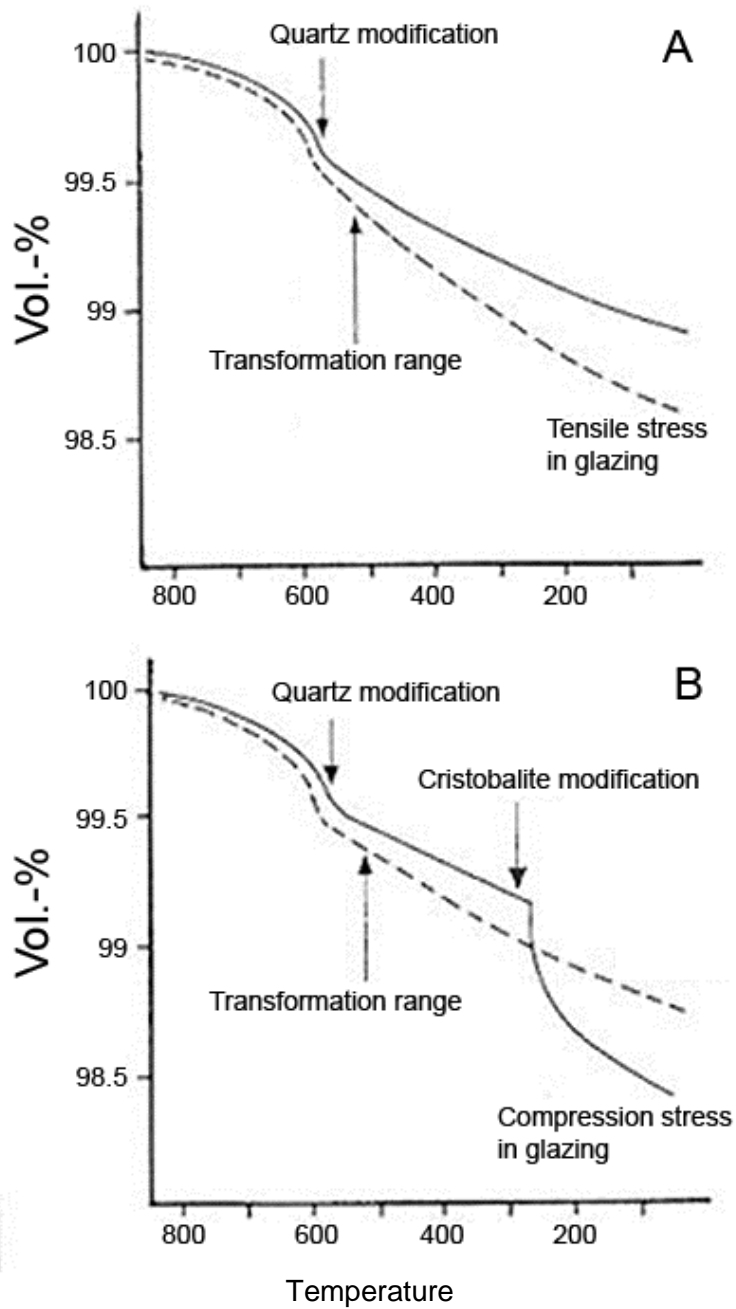


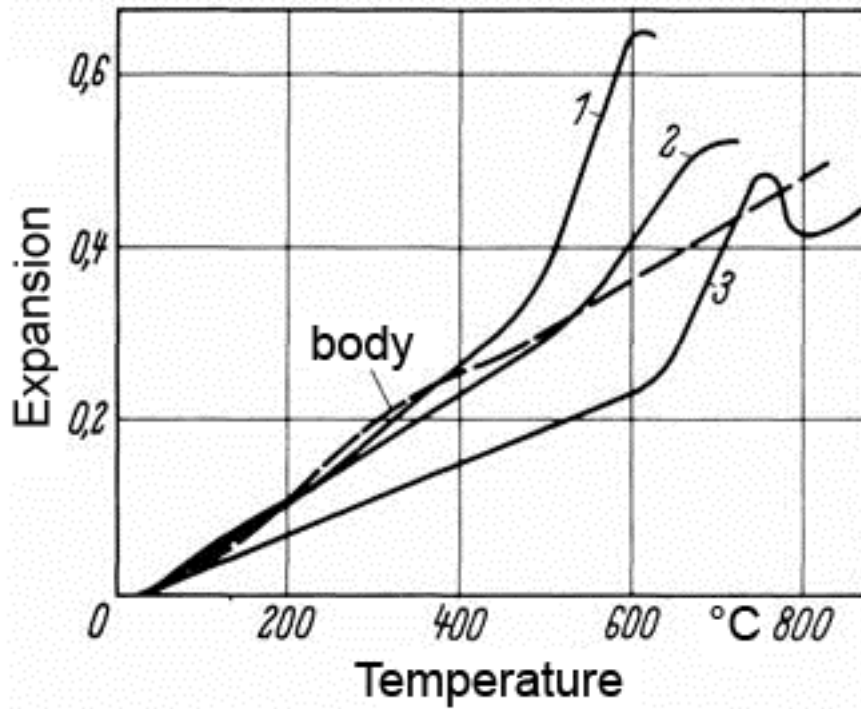
**Fig. 6.1.8:** Illustration of the coefficient of expansion from the glaze bigger than the one from the ceramic body (schematic).



————— Contraction of the body glazing  
 - - - - - Contraction of the glazing

**Fig. 6.1.9:** Illustration of the volumetric changes in a glazed quartz containing body (A) and in one cristobalite containing body (B) during the cooling.

As already mentioned, the expansion properties of glazes can be influenced by variation of the chemical composition (Fig. 6.1.10).



Glazing 1	0.25 K <sub>2</sub> O 0.25 Na <sub>2</sub> O 0.25 CaO 0.25 PbO	}	0.35 Al <sub>2</sub> O <sub>3</sub>	}	2.5 SiO <sub>2</sub> 0.5 B <sub>2</sub> O <sub>3</sub>
Glazing 2	0.095 K <sub>2</sub> O 0.095 Na <sub>2</sub> O 0.545 CaO 0.265 PbO		0.376 Al <sub>2</sub> O <sub>3</sub>		2.74 SiO <sub>2</sub> 0.19 B <sub>2</sub> O <sub>3</sub>
Glazing 3	1.0 CaO		0.2 Al <sub>2</sub> O <sub>3</sub>		2.0 SiO <sub>2</sub> 0.6 B <sub>2</sub> O <sub>3</sub>

**Fig. 6.1.10:** Expansion curve of a stoneware body (Clay: Feldspar: Quartz = 50: 8,5: 41,5 wt.%) and three distinct glazes [1].

Fig. 6.1.11 shows the amplitude of tested glazed parts with glazes 1, 2 and 3. The Steger voltmeter presents a positive amplitude for the glazes 2 and 3 (Fig. 6.1.11) which have a smaller CTE than the clay body. The glazes show compression stresses in the surface.

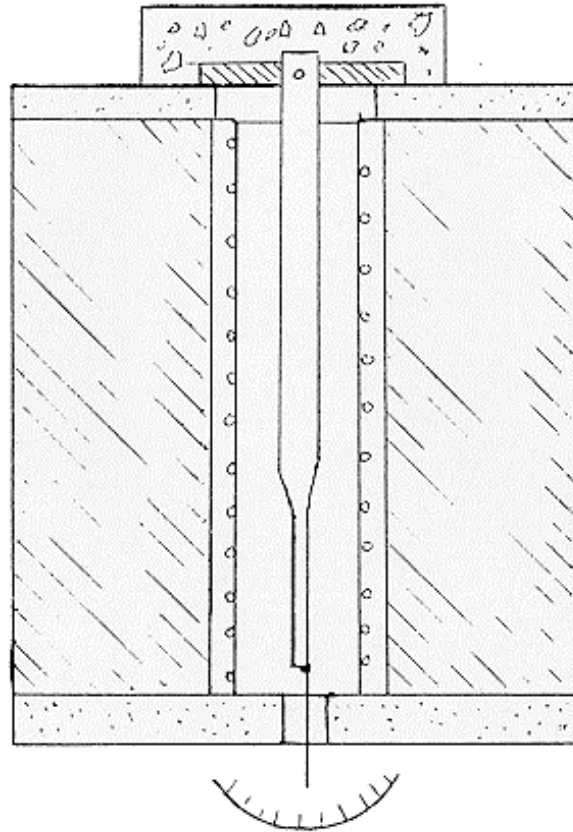


Fig. 6.1.11: Steger voltmeter (schematic).

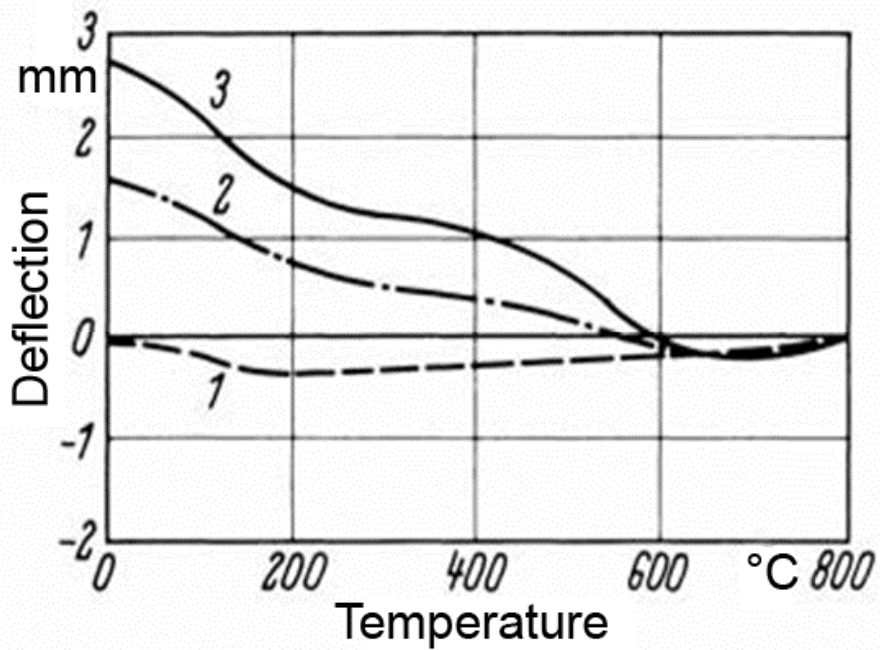


Fig. 6.1.12: Voltage tests according the Steger method in the glaze and the body [1].

These stresses can be calculated by means of the equation shown in Fig. 6.1.13. We know today from empirical experience that the difference of the CTE of body and glaze must not be higher than  $0.3 \cdot 10^{-6}$ . If the difference is higher, the stresses increase and then cracks occur.

$$\sigma_g = \frac{(\alpha_s - \alpha_g) \Delta T}{\frac{1 - \mu_g}{E_g} + \frac{1 - \mu_s}{E_s} \cdot \frac{d_g}{d_s}} \quad \text{and} \quad \sigma_s = \frac{(\alpha_g - \alpha_s) \Delta T}{\frac{1 - \mu_s}{E_s} + \frac{1 - \mu_g}{E_g} \cdot \frac{d_s}{d_g}}$$

$\Delta T$  : temperature difference;  $T_g$ : glass transition temperature;  $\mu$ : Poisson constant; E: young modul; d: layer thickness.

Fig. 6.1.13: Calculations of the stresses in glazes and body.

## 6.2 Decoration

Colors can be applied in the porcelain by different application techniques. Direct techniques include, for example, a rubber tampon dipped in a color. Following, the tampon presses the color on the surface of the plate. Colors may also be spayed on the base of the body or directly applied by screen printing. Concerning indirect print methods the colors are first processed as pictures and then applied on the porcelain article (Fig. 6.2.1).

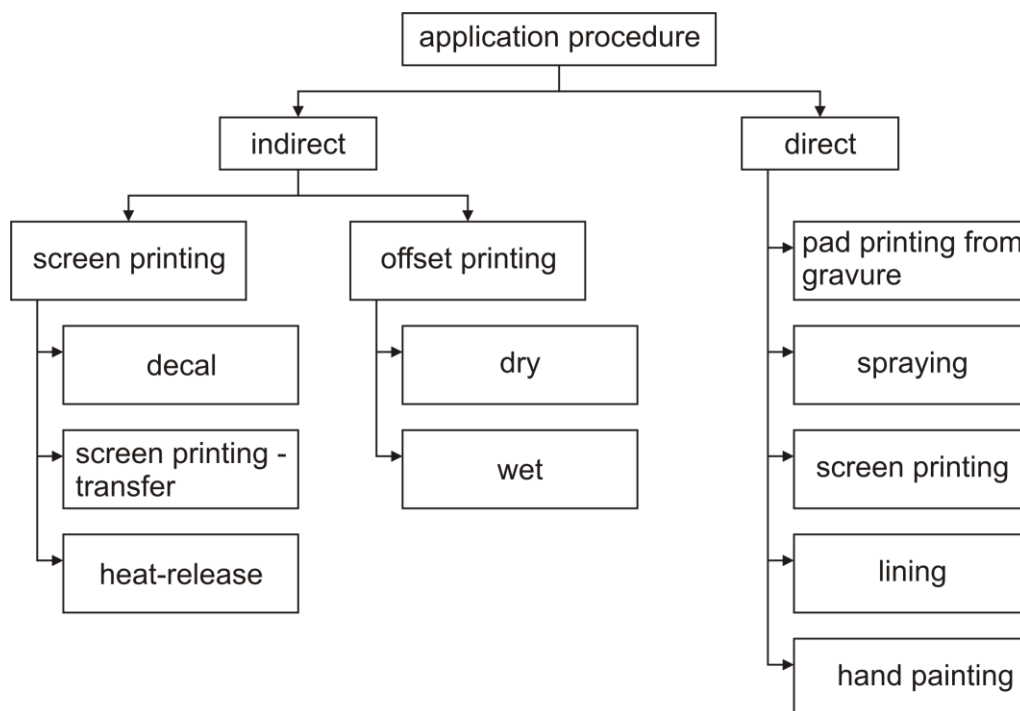


Fig. 6.2.1: Overview of the different decoration processes in ceramic (according to Huber).

If the decoration is applied on the clay body right after biscuit firing, followed by glazing and sintering afterwards, we talk about under-glaze decoration. The colours must resist a glaze firing temperature of about 1450°C which limits the range of colour possibilities.

It called on-glaze or in-glaze decoration, if the colours are applied after the glaze firing being heat treated by moderate temperatures (Fig. 6.2.2).

<b>Firing</b>	<b>Porcelain</b>	<b>Bone China</b>	<b>Stoneware</b>
Overglaze	800...840°C	750...820°C	750-820°C
Inglaze	1150...1250°C		
Underglaze	1350...1450°C		

Fig. 6.2.2: Range of firing temperatures for different decoration techniques for glaze and body (according to Huber).

Fig. 6.2.3 shows some decoration tools for manual decoration. Decals consist of a support paper, a dextrin layer, the real colour body and a coating solution (Fig. 6.2.4). The method to produce this decal is screen printing. Such pictures are applied on the article to be decorated either by hand (Fig. 6.2.5) or fully automatically (Fig. 6.2.6). With regard to automatization, a rubber tampon picks up the complete picture from a printed screen, moves downwards on the plate, applies the print and moves back to the screen which in the meantime received again the colours. This is followed by decoration firing (Fig. 6.2.7).



Fig. 6.2.3: Decoration tools.

## decal

film solution
colour
dextrin layer
release paper

## thermal decal

film solution
colour
wax
release paper

Fig. 6.2.4: Decal methods.

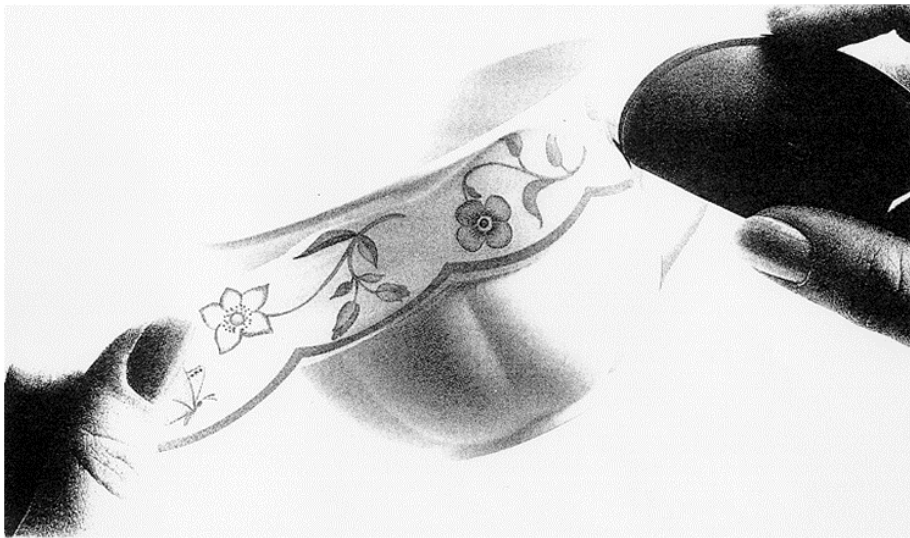


Fig. 6.2.5: Manual application of a decal.



Fig. 6.2.6: Decoration machine for thermal decal application.



Fig. 6.2.7: Firing of ceramic decoration.

Caution should be taken if multi-coloured on-glaze decoration is applied. Lead or cadmium oxides are frequently used to lower the firing temperature and therefore amplify the colour spectrum. When vinegar is used (for example in salad bowls), the heavy metals are dissolved and can be brought into the human body (Fig. 6.2.8).

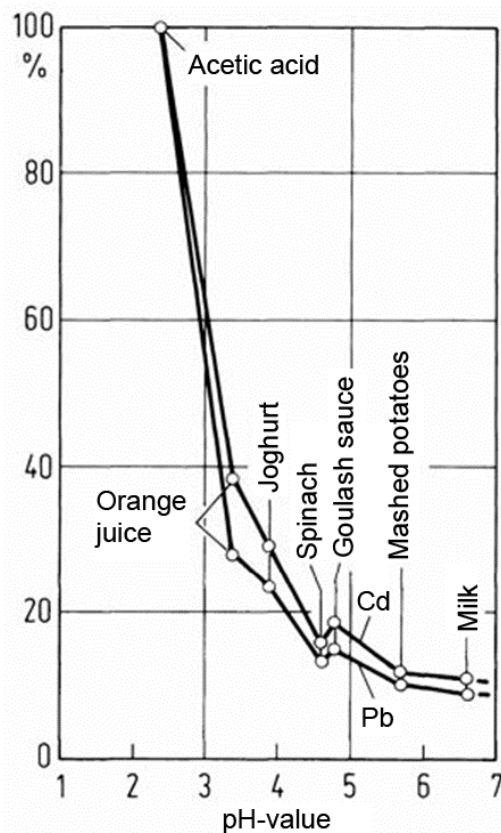


Fig. 6.2.8: Average values of the release of Pb and Cd from the glaze and from decoration colours in dependence of the pH for different aliments.



## **7. Special technologies**

Using the examples of porcelain, clay brick, silicon carbide and piezoceramic production, the common characteristics and differences of production techniques shall finally be pointed out.

### **7.1 Porcelain production**

The raw material kaolin is dissolved in water. Quartz and feldspar must be normally grinded (Fig. 7.1.1). The suspensions made of kaolin and grinded feldspar and quartz have to be mixed, sieved, cleaned and transported to a filter press. The filter cakes are evacuated in a de-airing pug mill and with this consistency used to shape the plates or cups (today, to a large extent this method has been replaced by compression moulding techniques). Such suspensions can also be used for casting.

After shaping the articles are fired at about 900°C (biscuit firing). Decoration of the pieces made after this firing and before glazing is called under-glaze decoration. Decoration made after glaze firing at about 1400°C is called on-glaze decoration. Those parts of the porcelain pieces which had been in contact with firing auxiliaries are polished after firing.

The Production Process of Porcelain Tableware

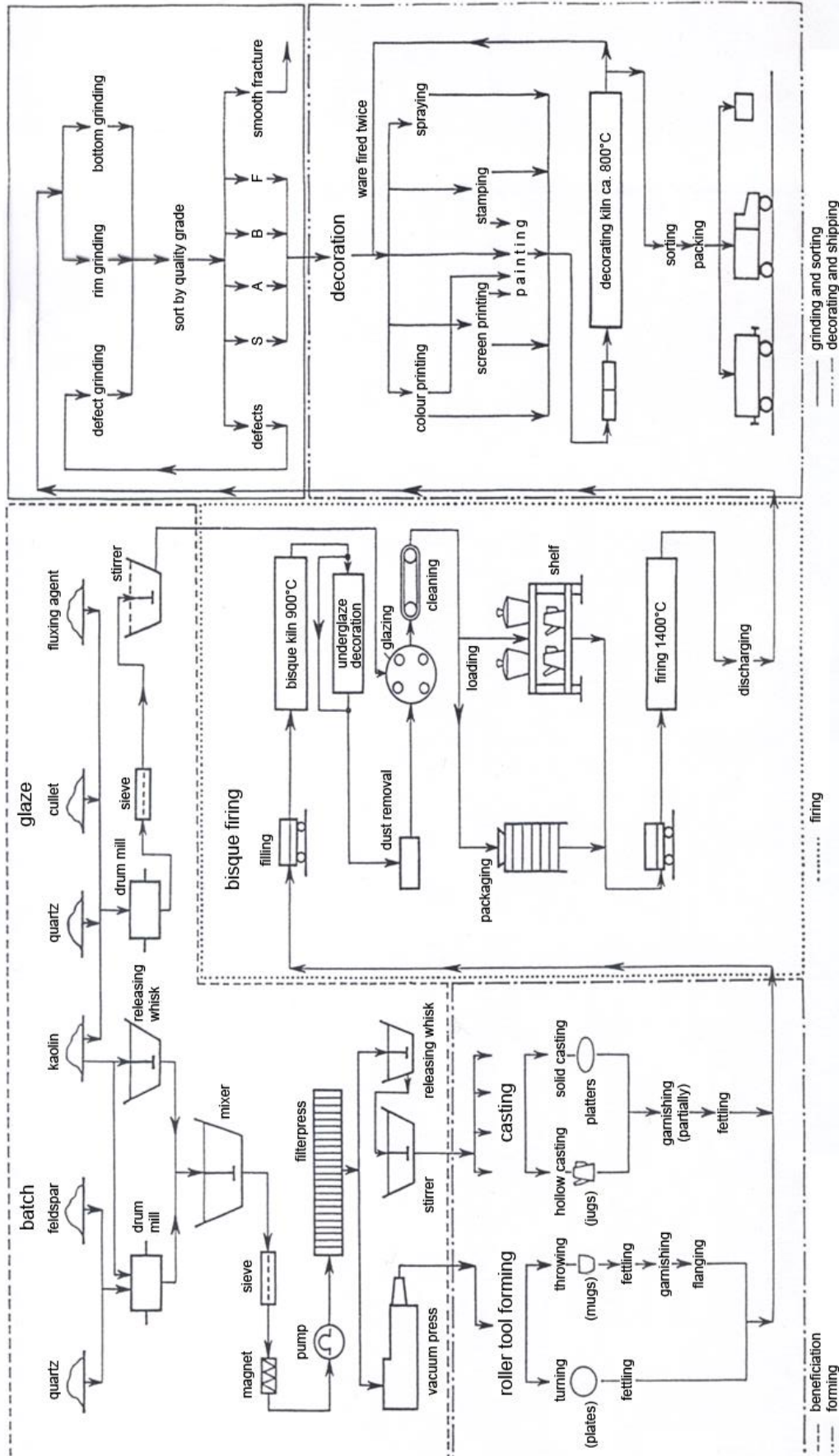


Fig. 7.1.1: Illustration of the processing route for porcelain (schematic).

## 7.2 Brick production

Today, bricks are to a large extent produced in fully automated processes (Fig. 7.2.1). Preparation of the mass (homogenization of the raw materials) is followed by extrusion shaping. The extruded parts are brought to a dryer and then set on kiln cars, which are transported through the tunnel kiln. The kiln cars are automatically discharged, the bricks fully automatically stacked and carried away. Modern brick factories produce about 300t/day.

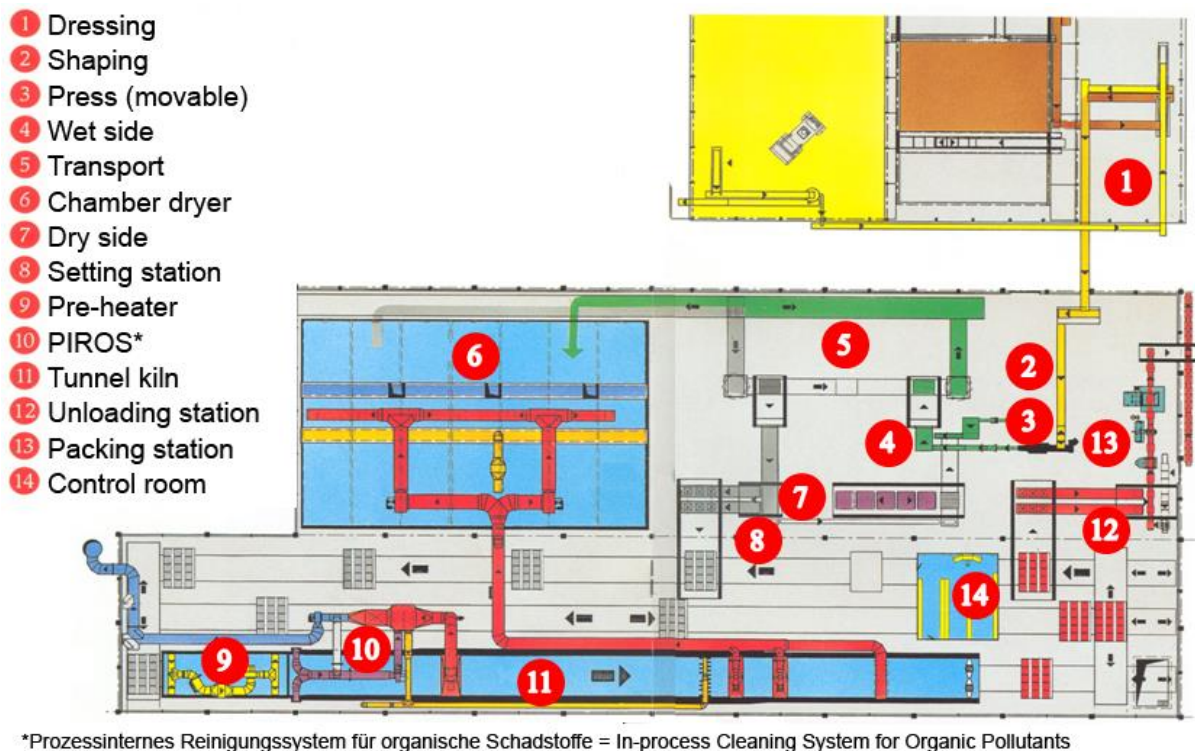


Fig. 7.2.1: Brick production (courtesy Keller).

## 7.3 SiC production

Non-oxide ceramic materials are sintered in vacuum or inert gas atmosphere, partly at increased pressure (fig. 7.3.1). This is normally made in discontinuously working furnace aggregates. For hot pressing of silicon carbide SiC powder is mixed with sinter additives and densified at high temperatures and increased pressure in a hot press machine consisting of a graphite cylinder and graphite dies. In a resistance heated hot press densification happens at over 2000°C and pressures of about 30 MPa. However, only relatively simply shaped components can be produced with this method.

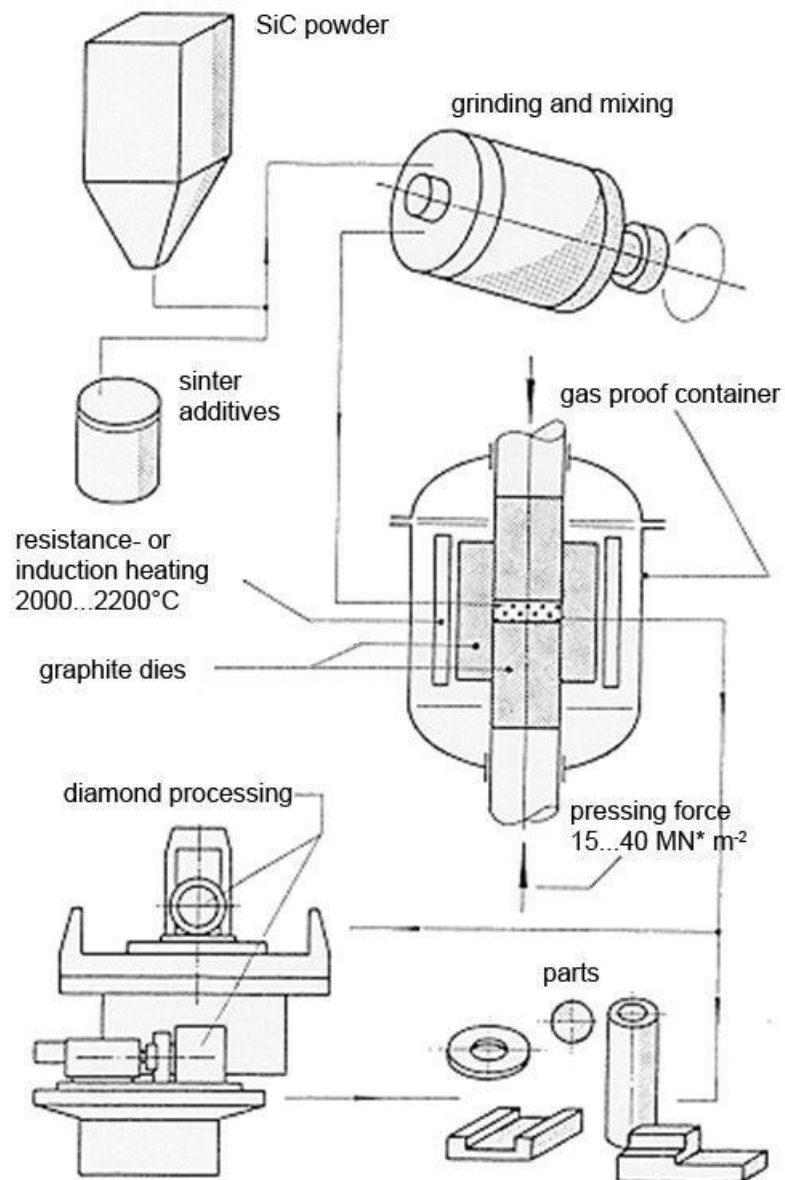


Abb. 7.3.1: Process route for notpressed silicon carbide.

#### 7.4 Piezoceramics production

Fig. 7.4.1 shows the production of piezoceramic materials. Again, the raw materials are first mixed, homogenized and shaped. The components are metallized after sintering. High voltage is applied for polarization of the parts. Ferroelectric domains adjust to the electric field providing the polycrystalline component with piezoelectric properties.

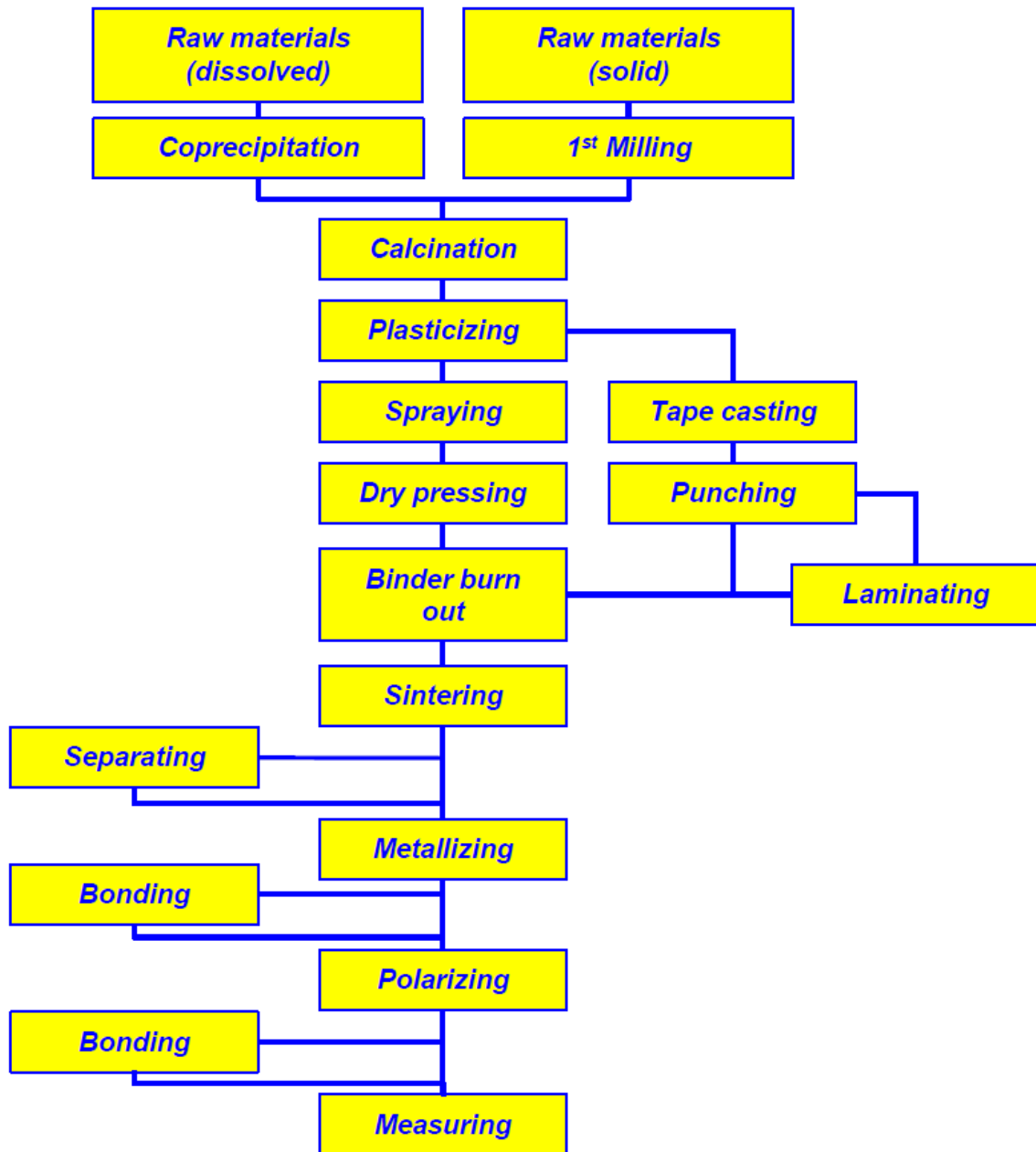


Abb. 7.4.1: Processing route for piezo ceramics.

## 7.5 Laser sintering



Videoclip: Laser sintering of SiO<sub>2</sub> crucibles

Ultra pure SiO<sub>2</sub> crucibles for waver processing in the semiconductor industry can be sintered without any impurities by a laser beam.

## **8. Literature**

1. H. Salmang, H. Scholze: Keramik, 5.-7. Auflage, Springer Verlag, Berlin-Heidelberg, 1968-2007.
2. Handbuch der Keramik, W. Bilke (Hrsg.), Verlag Schmid GmbH, Freiburg i.Br.
3. F. Harders, S. Kienow: Feuerfestkunde. Springer Verlag, Berlin-Göttingen-Heidelberg, 1960.
4. J.G. Heinrich: Introduction to the Principles of Ceramic Forming, Göller Verlag, Baden-Baden, 2004, CD, ISBN 3-87264-016-X.
5. R.A. Terpstra, P.P.A.C. Pex, A.H. de Vries: Ceramic Processing, Chapman & Hall, London, 1992.
6. W.D. Kingery: Ceramic Fabrication Processes. John Wiley & Sons Inc., New York, 1975.
7. E. Krause et.al.: Technologie der Keramik, Band 1-4, VEB Verlag für Bauwesen, Berlin, 1980-1986.
8. D.E. Clark, F.D. Gac, W.H. Sutton: Microwaves: Theory and Application in Materials Processing. In: Ceramic Transactions, Vol. 2, Am. Ceram. Soc. Inc., 1991.
9. R.L. Beatty, W.H. Sutton, N.F. Iskander: Microwaves: Processing of Materials III, Mat. Res. Soc., Pittsburgh, 1992.
10. W.E. Matthes, Keramische Glasuren, Grundlagen, Eigenschaften, Rezepte, Anwendungen, Verlagsgesellschaft Rudolf Müller GmbH, Köln, 1985.
11. A. Huber: Dekoration von Porzellan, Steingut und Bone China, Cfi/Ber. DKG 73, 1996, 16-22.
12. O.E. Radczewski: Die Rohstoffe der Keramik, Springer Verlag, Berlin-Heidelberg-New York, 1968.
13. J. Reed: Introduction to the Principles of Ceramic Processing. John Wiley & Sons, New York, 1988.
14. H. Schubert: Aufbereitung fester mineralischer Rohstoffe, Band I-III, VEB Dt. Verlag für Grundstoffindustrie, Leipzig 1972, 1975, 1978.